

**DEVELOPMENT OF PNEUMATIC BRAILLE DISPLAY
SYSTEM USING HIGH-ASPECT-RATIO
MICROSTRUCTURE**

Rungrueang Phatthanakun

**A Thesis Submitted in Partial Fulfillment of the Requirements for the
Degree of Doctor of Philosophy in Electrical Engineering
Suranaree University of Technology
Academic Year 2009**

การพัฒนาระบบแสดงผลอักษรเบรลล์แบบนิวมเมติก
ด้วยโครงสร้างจุดภาคตัดส่วนสูง

นายรุ่งเรือง พัฒนากุล

วิทยานิพนธ์นี้เป็นส่วนหนึ่งของการศึกษาตามหลักสูตรปริญญาวิศวกรรมศาสตรดุษฎีบัณฑิต
สาขาวิชาวิศวกรรมไฟฟ้า
มหาวิทยาลัยเทคโนโลยีสุรนารี
ปีการศึกษา 2552

**DEVELOPMENT OF PNEUMATIC BRAILLE DISPLAY SYSTEM
USING HIGH-ASPECT-RATIO MICROSTRUCTURE**

Suranaree University of Technology has approved this thesis submitted in partial fulfillment of the requirement for the Degree of Doctor of Philosophy.

Thesis Examining Committee

(Assoc. Prof. Dr. Kittit Attakitmongcol)

Chairperson

(Dr. Nimit Chomnawang)

Member (Thesis advisor)

(Dr. Prapong Klysubun)

Member

(Assoc. Prof. Dr. Thanatchai Kulworawanichpong)

Member

(Assoc. Prof. Dr. Arthit Srikaew)

Member

(Prof. Dr. Sukit Limpijumnong)
Vice Rector for Academic Affairs

(Assoc. Prof. Gp. Capt. Dr. Vorapot Khompis)
Dean of Institute of Engineering

รุ่งเรือง พัฒนากุล : การพัฒนาระบบแสดงผลอักษรเบรลล์แบบนิวแมติกด้วยโครงสร้างจุลภาค
สัดส่วนสูง (DEVELOPMENT OF PNEUMATIC BRAILLE DISPLAY SYSTEM
USING HIGH-ASPECT-RATIO MICROSTRUCTURE) อาจารย์ที่ปรึกษา : อาจารย์
ดร.นิมิต ชมนาวัง, 221 หน้า.

อักษรเบรลล์คือการแสดงผลทางการสัมผัสรูปแบบหนึ่งที่ถูกพัฒนาขึ้นมาเพื่อให้การช่วยเหลือ
ทางด้าน การอ่านและการเขียนกับผู้พิการทางสายตา โดยมี การนำไปประยุกต์ใช้กับทุกภาษาเพื่อการ
สื่อสาร อักษรเบรลล์ถูกพัฒนาขึ้นมาจากการใช้เครื่องมือเฉพาะทางที่เรียกว่าแสตมป์และดินสอ มาสู่การใช้
เครื่องพิมพ์ จนกระทั่งเข้าสู่ระบบแสดงผลอักษรเบรลล์ที่มีการเชื่อมต่อกับระบบคอมพิวเตอร์ โดยใช้
หลักการขับเร้าจุดแสดงผลให้ทะลุผ่านขึ้นมาจากรูบนพื้นผิวที่ราบเรียบเพื่อลดข้อจำกัดการเข้าถึงข้อมูล
ความโดดเด่นนี้ ส่งผลให้ความต้องการของอุปกรณ์เพิ่มขึ้นอย่างต่อเนื่อง ขณะที่ประสิทธิภาพในการใช้
งานและต้นทุนที่ต่ำกำลังเป็นตัวผลักดันให้เกิดการพัฒนาเทคนิคต่างๆในการนำมาใช้งาน แต่ถึงกระนั้น
เครื่องแสดงผลอักษรเบรลล์ยังคงต้องอาศัยเทคนิคและวิธีการผลิตที่ซับซ้อน เป็นผลต่อเนื่องถึงต้นทุนที่
ยังคงอยู่ในระดับที่ผู้พิการไม่สามารถเข้าถึงได้ ท่ามกลางการพัฒนาของระบบแสดงผลอักษรเบรลล์ที่
หลากหลาย ระบบกลไฟฟ้าจุลภาคได้เข้ามาสร้างการปฏิวัติการพัฒนาด้วยเทคนิคการผลิตโครงสร้าง
จุลภาคที่สนับสนุนให้เข้าถึงสิ่งที่ต้องการ แต่ข้อจำกัดหลายอย่างของวิธีการนี้ ทำให้งานวิจัยส่วนใหญ่อยู่
เพียงในห้องปฏิบัติการ ซึ่งในจุดนี้ส่งผลให้เทคโนโลยีโครงสร้างจุลภาคสัดส่วนสูงเข้ามามีบทบาทสำคัญ
ในการผลิตชิ้นงาน ด้วยความสามารถในการผลิตโครงสร้างจุลภาคที่แม่นยำและละเอียด ร่วมกับ
กระบวนการหล่อแบบ ซุปเปอร์คอนดักตีฟไฟไฟและการพิมพ์นาโน ชิ้นส่วนจำนวนมากสามารถสร้างขึ้นได้อย่าง
รวดเร็ว ส่งผลให้ต้นทุนในการผลิตกลไกของระบบแสดงผลอักษรเบรลล์มีแนวโน้มลดลง งานวิจัยนี้
มุ่งเน้นการพัฒนาของระบบแสดงผลอักษรเบรลล์แบบนิวแมติกโดยใช้เทคโนโลยีโครงสร้างจุลภาคสัดส่วนสูง
ด้วยรังสีเอ็กซ์จากเครื่องกำเนิดแสงซินโครตรอน การพัฒนาจะมุ่งเน้นการศึกษาถึงโครงสร้างระบบ
แสดงผลอักษรเบรลล์พื้นฐานและความสามารถในการผลิตโครงสร้างจุลภาคสัดส่วนสูงของสารไวแสง
SU-8 ที่มีความซับซ้อน เพื่อให้บรรลุผลดังกล่าวเทคนิคการอบรังสีเอ็กซ์บนสารไวแสงหนาผ่านหน้าฉาก
ดูดซับรังสีที่โปร่งแสงจึงถูกพัฒนาขึ้น โครงสร้าง 3 มิติที่มีความแม่นยำสร้างจากเทคนิคการหลอมรวมผง
สารไวแสง SU-8 และควบคุมความหนาของชั้นฟิล์มด้วยสมการทางคณิตศาสตร์ถูกพัฒนาขึ้น โครงสร้าง
ได้ผ่านการทดสอบมาเพื่อเป็นต้นแบบสำหรับการทดสอบโครงสร้างระบบแสดงผลอักษรเบรลล์ที่
ต้องการ กลไกการแสดงผลแบบซ้ำเติมของจุดสัมผัส ถูกพัฒนาขึ้นเป็น 2 รูปแบบ รูปแบบแรกคือการ
แสดงผลด้วยจุดขนาดตัวของวัสดุพอลิเมอร์ PDMS ที่มีกลไกดึงตัวกลับจากคุณสมบัติความยืดหยุ่นของพอลิ
เมอร์ แต่เนื่องจากวัสดุ PDMS เป็นวัสดุที่มีความยืดหยุ่นสูง ทำให้การสัมผัสไม่ชัดเจน อีกทั้งเกิดความ
สึกปรกได้ง่าย นอกจากนี้การนำตัวของจุดสัมผัสภายใต้แรงดันระดับต่างๆ ไม่มีกลไกจำกัดระยะของจุด
ส่งผลให้วัสดุ PDMS เกิดความเสียหายเนื่องจากแรงดันที่มากเกินไป รูปแบบที่สอง เป็นการแสดงจุด
สัมผัสแบบแข็งด้วยวัสดุสารไวแสง SU-8 ที่พัฒนาขึ้นมาจากโครงสร้างชั้นสารไวแสงหนา 2 ชั้น จุดสัมผัส

จะวางกลไกเป็นลูกสูบเคลื่อนที่ขึ้น-ลงในหน้าจอสัมผัสที่ทำหน้าที่เป็นกระบอกสูบ แต่อย่างไรก็ตาม โครงสร้างนี้ แม้จะให้ความรู้สึกในการสัมผัสที่เด่นชัดและทนทานต่อการใช้งาน แต่กลไกการดึงตัวกลับ ไม่ได้ถูกสร้างร่วมขึ้นมาด้วย เพื่อให้การขยับเร้าจุดสัมผัสสามารถทำงานแบบซ้ำเดิมภายใต้การขยับเร้าแบบ นิวแมติก จุดสัมผัสแบบแข็งที่สร้างจากวัสดุ SU-8 ด้วยกลไกลูกสูบ จึงถูกนำไปเพิ่มกลไกการดึงตัวกลับ มุ่งเน้นที่ระดับการแสดงผลด้วยแรงกระทำอ้างอิงขั้นต่ำที่ระดับ 1.5 gf โดยแบ่งได้เป็น 2 รูปแบบคือ แบบแรกคือจุดสัมผัสด้วยการดึงตัวกลับของแผ่นพอลิเมอร์ ที่ใช้ความยืดหยุ่นของ PDMS มาเป็นโครงสร้าง สปริง โดยวางจุดสัมผัสไว้ด้านบนและครอบด้วยหน้าจอสัมผัส ภายหลังจากขยับเร้าด้วยแรงดันแก๊ส จะสามารถเคลื่อนที่ขึ้นเพื่อแสดงผลด้วยแรงกระทำ 76.71 gf ที่แรงดันขยับเร้า 16.87 kPa รูปแบบที่สองคือตัว แสดงจุดสัมผัสด้วยกลไกสปริงโลหะโค้ง ซึ่งถูกติดตั้งกลไกการดึงตัวกลับที่ด้านล่างของจุดสัมผัส โดยสามารถรองรับน้ำหนักขนาด 10 g ด้วยแรงดันขยับเร้า 109.48 kPa การควบคุมการขึ้น-ลงของจุดแสดงผล ใช้วาล์วชนิดขดลวดแม่เหล็กไฟฟ้าและปรับขนาดของแรงดันแก๊สด้วยตัวคุมแรงดัน นอกจากนี้ การพัฒนา ให้ระบบแสดงผลอักษรเบรลล์ทำงานร่วมกับตัวคุมแรงดันแก๊สด้วยไมโครวาล์วได้ถูกทดสอบ ไมโคร วาล์วชนิดแผ่นคานโค้งที่ขยับเร้าด้วยไฟฟ้าสถิตย์สามารถขยับเร้าการเคลื่อนที่ขึ้น-ลงของจุดสัมผัสเป็นระยะ 120 μm โดยมีการรั่วไหลเกิดขึ้นระหว่างการปิดช่องทางไหลของแก๊ส ส่งผลให้จุดสัมผัสไม่สามารถ ทำงานได้อย่างบูรณ อย่างไรก็ตาม การพัฒนานี้ ส่งผลให้เกิดต้นแบบของระบบแสดงจุดสัมผัส ที่สามารถ นำไปประยุกต์ใช้เป็นเซลล์อักษรเบรลล์ที่เชื่อมต่อกับอุปกรณ์อิเล็กทรอนิกส์ที่ส่งผ่านข้อมูลมาแสดงผลบน หน้าจอสัมผัสสำหรับผู้พิการทางสายตาได้ในอนาคต

RUNGRUEANG PHATTHANAKUN : DEVELOPMENT OF PNEUMATIC
BRAILLE DISPLAY SYSTEM USING HIGH-ASPECT-RATIO
MICROSTRUCTURE. THESIS ADVISOR : NIMIT CHOMNAWANG, Ph.D.,
221 PP.

BRAILLE DISPLAY/TACTILE DISPLAY/SYNCHROTRON/ MICROVALVE/X-RAY
LITHOGRAPHY/MEMS/RBDS/HIGH-ASPECT-RATIO

Braille characters have been devised to assist blind people in reading and writing. The system has been adopted in almost all languages. Conventional Braille characters have been recorded by hand using a slate and stylus, or by a Braille type writer. Moreover, Refreshable Braille Display System (RBDS) has also been recently developed. RBDS is a human-computer interface utilized to create refreshable raised dots in order to present information. Demand for this device has been dramatically increasing in consumer markets and other tangible applications, while the requirements in terms of reliabilities have been driving forces adapting its various mechanisms. However, commercial products are currently expensive due to their complex mechanisms and special fabrication techniques. Among numerous Braille displays, Micro-Electro-Mechanical Systems have been utilized to revolutionize these product categories. Nevertheless, its applications in tactile display have been limited due to several factors. Based on repeated fabrication by micro-molding of polymer and electroforming used in Lithographic Galvanoformung Abformung (LIGA) technologies, RBDS with lower cost and better performance can be achieved. This thesis concentrates on realization of tactile dots for RBDS utilizing X-ray LIGA process which is performed at the beamline BL-6 of the Synchrotron Light Research Institute (Public Organization), Ministry of Science and Technology, Thailand. Two specific tactile display mechanisms were formulated regarding the design of X-ray LIGA based on the pneumatic

RBDS. The first mechanism that the tactile display can actively raise the tangible dot up with a thin PDMS membrane has been evaluated through the strength of suspended PDMS membrane on the X-ray LIGA structure. The second mechanism that the single tactile dot can perform similar to the conventional tangible dot has been considered through a complicated X-ray LIGA structure. The tactile dot as a piston inside a cylinder has been successfully fabricated, resulting in the robust and obvious perception under the applied pressure. Consequently, the refreshable tactile displays improved from these mechanisms were realized by combining them together for the first X-ray LIGA tactile display. The tactile dot was placed on the suspended PDMS membrane to create the spring element. It can operate as the rigid tactile display with the maximum applied pressure of 16.87 kPa resulting in the actuated force of 76.71 gf. Furthermore, the second X-ray LIGA tactile display was improved by adding two curved segments of metal under the tactile dot. It is operated as the refreshable tactile display with the maximum load of 10 g required the applied pressure of 109.48 kPa. To increase the performance of the refreshable tactile display systems, the curled-up closure plate microvalve was combined instead of the conventional valve. The microvalve was positioned under the tactile display with PDMS spring element and controlled by high dc voltage. In the repeat operation as the RBDS, the tactile dot can be move upward and downward at the actuated voltage of 150 V with maximum distance of 120 μm and 42.98 kPa applied pressure. This innovation is demonstrated the possibility to bring out a new system that invents tactile display device as a new interface for visually impaired people.

School of Electrical Engineering

Academic Year 2009

Student's Signature _____

Advisor's Signature _____

Co-advisor's Signature _____

ACKNOWLEDGMENTS

This thesis would have not been possible without the support of many people. I would like to express my deepest gratitude and appreciation to my advisor Dr.Nimit Chomnawang who was abundantly helpful and offered invaluable assistance, support and guidance. I am deeply grateful to my co-advisor, Dr.Prapong Klysubun, Head of the Accelerator Division, Synchrotron Light Research Institute (Public Organization), for his detailed and constructive comments, and for his important support throughout this work.

Very special thanks go out to Assoc. Prof. Dr.Kitti Attakitmongcol who is the chairman of my advisory committee, Assoc. Prof. Dr.Thanatchai Kulworawanichpong, and Assoc. Prof. Dr.Arthit Srikaew who serve as my advisory committees for their help throughout graduate program procedures and revision of this thesis.

I would like to thank many graduate and undergraduate students I have worked with in SUT MEMS group including Satit Seemungkoon, Winai Wanburee, Suppakit Promwikorn, Manot Mapato, Pittaya Deekla, Pradit Kaewsarn, Kamonrat Boonprakong, Chalermchai Pantong, Sompong Sukprasong, Arisara Leenaphet, Watcharapon Pummara, and Sittisak Khosinklang.

There are people to whom I would like express my special thanks including SLRI staffs, Chanwut Sriphung, and Pakaporn Wattanakul, and EE SUT staffs Unchulee Rakdanklang, and Pattarawan Kenpanan for their generous help. My warm thanks are due to my elder sister, Sununntha Siripaiboonsup who is SLRI staffs for her valuable advice and kindly help.

I would also like to thank my family for the support provided to me throughout my entire life. I must acknowledge Wilailuk Khitsang, without her encouragement, I would have not finished this thesis.

Finally, I would also like to convey thanks to the Synchrotron Light Research Institute (Public Organization) and Beamline 6: X-Ray Lithography Laboratory of SLRI for providing research facilities, financial supports and all kinds of help throughout my studies.

Rungrueang Phatthanakun

TABLE OF CONTENTS

	PAGE
ABSTRACT (THAI).....	I
ABSTRACT (ENGLISH).....	III
ACKNOWLEDGMENTS.....	V
TABLE OF CONTENTS.....	VII
LIST OF TABLES.....	XIII
LIST OF FIGURES	XIV
LIST OF SYMBOLS AND ABBREVIATIONS.....	XXVII
CHAPTER	
I INTRODUCTION.....	1
1.1 Problems and rationale.....	1
1.2 Research objectives	3
1.3 Scope and limitation of the study.....	3
1.4 Benefits of the study	3
1.5 Thesis organization	4
II LITERATURE REVIEW	6
2.1	
Introduction.....	6
2.2 Properties of cutaneous mechanoreceptors in the fingertips.....	6
2.3 Tactile display applications	8
2.4 Braille display modalities.....	10
2.5 Refreshable Braille display system	12

TABLE OF CONTENTS (Continued)

	PAGE
2.5.1 History of refreshable Braille display system.....	12
2.5.2 State-of-the-art Braille displays	15
2.5.2.1 Piezoelectric.....	15
2.5.2.2 Piezoelectric polymer.....	17
2.5.2.3 Microstep motor	20
2.5.2.4 Phase change materials (PCMs).....	20
2.5.2.5 Electrostatic actuator	22
2.5.2.6 Electromagnetic solenoid	24
2.5.2.7 Electrorheological (ER) fluid.....	26
2.5.2.8 Pneumatic Braille display.....	28
2.5.2.9 Shape memory alloy (SMA).....	29
2.5.2.10 Lateral skin deformation	31
2.5.2.11 Servo motor	33
2.5.2.12 Bimetallic strip.....	34
2.5.2.13 Electrocutaneous	35
2.5.2.14 Air jet tactile display.....	37
2.6 The Braille display utilizing MEMS technology.....	37
2.7 Motivations for LIGA Braille display.....	39
2.8 Chapter summary.....	40
III DEVELOPMENT OF 3D X-RAY LIGA PROCESS.....	42
3.1 Introduction.....	42
3.2 X-ray masks on a transparent substrate.....	42

TABLE OF CONTENTS (Continued)

	PAGE
3.2.1 Power spectrum through various filters	43
3.2.2 X-ray mask fabrication.....	45
3.2.3 X-ray lithography experiments.....	47
3.3 Three-dimensional X-ray lithography.....	48
3.3.1 SU-8 powder preparation.....	49
3.3.2 Single-layer reflow casting.....	51
3.3.3 X-ray lithography of single-layer reflow casted SU-8 film.....	53
3.3.4 Multilayer reflow casting.....	54
3.3.5 Experimental results.....	58
3.4 Bonding of PDMS and SU-8 for tactile dot stimulation.....	64
3.4.1 Thin PDMS films using sacrificial photoresist.....	65
3.4.2 PDMS-SU-8 bonding for construction of tactile dot.....	67
3.5 Fabrication of micro-piston based on release etching of a conformal sacrificial layer.....	71
3.5.1 PDMS molding.....	73
3.5.2 PDMS-conductive substrate bonding.....	73
3.5.3 Nickel electroplating.....	76
3.5.4 The piston releasing.....	78
3.6 X-ray LIGA application.....	79
3.7 Chapter summary.....	87

TABLE OF CONTENTS (Continued)

	PAGE
IV ELECTROSTATIC ACTUATOR FOR MICROVALVE	
APPLICATION	88
4.1 Introduction.....	88
4.2 Curled-up SU-8/metal closure plate actuator.....	90
4.3 Design and fabrication processes.....	91
4.4 Experimental setup and results.....	96
4.5 Mathematical models.....	104
4.5.1 Mathematic models of the curled-up closure plate.....	104
4.5.2 Modeling results.....	110
4.6 Chapter summary.....	115
V DEVELOPMENT OF PNEUMATIC TACTILE DISPLAY	116
5.1 Introduction.....	116
5.2 Tactile dot display with a PDMS membrane.....	117
5.2.1 PDMS-SU-8 bonding.....	117
5.2.1.1 PDMS-PDMS/SU-8 plasma bonding.....	119
5.2.1.2 PDMS-SU-8 wet bonding.....	124
5.2.1.3 PDMS tactile display by using SU-8 sacrificial material	127
5.2.2 Load-deflection of circular PDMS membrane with an uniform pressure.....	130
5.2.3 Load- deflection experimental setup.....	134

TABLE OF CONTENTS (Continued)

	PAGE
5.3 SU-8 tactile display.....	136
5.3.1 Assembled SU-8 tactile display.....	137
5.3.2 SU-8 tactile display by releasing of sacrificial layer.....	140
5.4 Refreshable tactile display.....	147
5.4.1 PDMS spring element for the SU-8 refreshable tactile display.....	148
5.4.2 Curved spring segments for the SU-8 refreshable tactile display.....	150
5.4.3 Deflection of curved segments with one support.....	154
5.5 Chapter summary.....	159
 VI EXPERIMENTAL OF REFRESHABLE TACTILE	
DISPLAY.....	160
6.1 Introduction.....	160
6.2 Experimental setup of the refreshable tactile display.....	160
6.3 Force-pressure characteristics of the refreshable tactile display.....	164
6.3.1 Force-pressure of the tactile display with PDMS spring element.....	164
6.3.2 Force-pressure of the tactile display with curved spring segments.....	167
6.4 Refreshable tactile display by controlling of curled-up closure plate microvalve.....	171
6.5 Chapter summary.....	174

TABLE OF CONTENTS (Continued)

	PAGE
VII CONCLUSIONS AND FUTURE STUDIES	175
7.1 Conclusions.....	174
7.2 Future studies.....	177
REFERENCES.....	183
APPENDICES	
APPENDIX A. FABRICATION PROCESSES OF CHAPTER III.....	191
APPENDIX B. FABRICATION PROCESSES OF CHAPTER IV.....	201
APPENDIX C. FABRICATION PROCESSES OF CHAPTER V.....	206
APPENDIX D. PUBLICATIONS RELATED TO THE	
PhD RESEARCH.....	214
BIOGRAPHY.....	221

LIST OF TABLES

TABLE	PAGE
2.1 Summary of mechanoreceptor properties	8
3.1 The suitable correction factor for reflow casting process.....	61
4.1 Design and constant values of the curled-up closure plate microvalve.....	91
5.1 Calculated of residual stress and Young's modulus values for PDMS membranes.....	133
5.2 The dimensions and the nickel properties of the curved spring segment.....	151

LIST OF FIGURES

FIGURE	PAGE
2.1	Mechanoreceptors of the glabrous skin 7
2.2	Braille code 10
2.3	Refreshable Braille display system 12
2.4	Piezoelectric bimorph reed mounted for use as a tactile simulator..... 13
2.5	Commercially available refreshable Braille display (a) with cell piezoelectric actuation mechanism and (b) the NIST rotating-wheel Braille display..... 15
2.6	Piezoelectric material application (a) exaggerated motion of piezoelectric material and (b) a cantilever piezoelectric bimorph for tactile display..... 16
2.7	Piezoelectric linear motor (a) downward actuation and (b) upward actuation..... 17
2.8	Piezoelectric PVDF bending sheets (a) with top and bottom electrodes and (b) with planar comb electrodes..... 18
2.9	A rectangular fluid-tight housing of piezoelectric bending element (a) structural view (b) ON state and (c) OFF state elements..... 19
2.10	A microstep motor Braille dot (a) structural view and (b) conversion of a rotation in to a linear movement through a lead-screw mechanism..... 20
2.11	Braille dot actuations based on PCMs (a) with thermo-pneumatic actuation and (b) with electro-thermal actuation..... 22
2.12	Electrostatic display (a) cross-sectional view and (b) a group of three displays on a 4-inch wafer..... 23
2.13	Deformation of an elastic dielectric film under electric pressure..... 23

LIST OF FIGURES (Continued)

FIGURE	PAGE
2.14 Electrostatic tactile stimulator with elastic dielectric.....	24
2.15 Electromagnetic solenoid (a) cross-sectional schematic and (b) the field and flux lines that form closed loops around the coil resulting in a different polarity	25
2.16 The Braille dot using electromagnetic solenoid (a) cross-sectional view and (b) the commercial miniature dc solenoids actuator for Braille display.....	26
2.17 Forming of electrorheological fluid (a) without applied electrical field and (b) with applied electrical field	27
2.18 A tactile display utilized ER fluid (a) cross-sectional view and (b) another actuator with a spring-load pin inside the uppermost plate.....	28
2.19 Pneumatic Braille displays (a) using raising individual pins in the early principle and (b) using an array of actuators and an elastic membrane.....	29
2.20 Microscopic diagram of the shape memory effect.....	30
2.21 SMA based Braille display (a) structured view and (b) extension and contraction energizing of the SMA coil.....	31
2.22 Braille display based on lateral skin deformation (a) reading the Braille dot by skin sensation and (b) a lateral displacement to the load of piezoelectric bimorph	32
2.23 Thick piezoelectric bender plates (a) assembly of the virtual Braille display and (b) strain applied during finger contact.....	33
2.24 Driving mechanism of servo motor based Braille dots.....	34

LIST OF FIGURES (Continued)

FIGURE	PAGE
2.25	A Braille dot based on a principle of bimetallic strip
	(a) unheated and (b) heated with raised rod..... 35
2.26	A Braille dot based on electrocutaneous stimulation (a) anodic-current stimulation for SAI mode (b) cathodic-current stimulation for RAI mode and (c) deeper-region stimulation or RAI mode..... 36
2.27	Stimulation modes of an electrocutaneous Braille dot in a 2D case 36
2.28	Air jet tactile display (a) the air pressure stimulation (b) the vibration stimulation and (c) schematic diagram of air jets stimulator..... 37
2.29	Schematic of the commercial refreshable Braille display of the iACTIV corporation 38
2.30	LIGA fabrication sequences..... 41
3.1	Components of X-ray mask.....43
3.2	Power spectrum of lithography beamline BL-6 through various filters44
3.3	Fabrication sequences of the transparent X-ray mask.....46
3.4	X-ray mask with silver absorber (a) on copier transparency and (b) on PI sheet.....47
3.5	Samples of X-ray microstructures (a) The SU-8 300 μm -thick photoresist and (b) nickel microstructures with thickness of 150 μm47
3.6	A model of multilayer powder casting of SU-8 thick film.....49
3.7	Duration time for soft bake of SU-8 powder preparation50
3.8	Sequence process for SU-8 powder preparation (a) SU-8 liquid content on PI tape laminated on aluminum disc (b) soft bake to reduce solvent content and (c) dried SU-8 photoresist into powders 51

LIST OF FIGURES (Continued)

FIGURE	PAGE
3.9	Fabrication sequences of single layer reflowed casting of SU-8 photoresist..... 52
3.10	X-ray lithography of single-layer reflow casted SU-8 film (a) transparent x-ray masks used in synchrotron X-ray and (b) the first microstructure after development..... 54
3.11	X-ray lithography of the second layer reflowed casted SU-8 film (a) SU-8 microstructures from previous layer enclosed by PDMS frame for next reflow casting (b) X-ray lithography steps for formation of multilayer complicated microstructures (c) the second X-ray mask and (d) the second microstructure..... 55
3.12	X-ray lithography of the third layer reflowed casted SU-8 film (a) the third X-ray mask and (b) SU-8 multi-layer..... 58
3.13	A flow chart for realization of multi-step microstructures by using SU-8 powder reflow casting technique..... 59
3.14	Relationship between correction factor and film thickness (a) the first layer (b) the second layer and (c) the third layer..... 60
3.15	Casted SU-8 thick film (a) after polishing surface and (b) after reflow at low temperature to regain film transparency..... 62
3.16	Average surface roughness of casted SU-8 thick film (a) before reflow treatment and (b) reflowed surface..... 63
3.17	SEM images of a three-layer SU-8 mirostructure..... 64
3.18	Preparation of thin PDMS films by spin coating (a) SYLGARD 184 Silicone Elastomer Kit and (b) PDMS film spin coated on a glass substrate..... 65

LIST OF FIGURES (Continued)

FIGURE	PAGE
3.19 Thickness of film spin coated at various spinning rate.....	66
3.20 Preparation of thin PDMS film (a) AZ 1512 photoresist for sacrificial layer and (b) release of PDMS film.....	67
3.21 Preparation of an SU-8 frame of the tactile dot array (a) X-ray mask and SU-8 thick film for X-ray lithography (b) the sample development and (c) the tactile dot.....	68
3.22 Peeling of the PDMS membrane after release of AZ photoresist sacrificial layer.....	69
3.23 Bonding of SU-8 frame and PDMS thin membrane for tactile dot cells (a) compress with the pressure of mass 1 kg weights (b) SU-8/PDMS bonding before released from the substrate and (c) the result of interface bonding.....	70
3.24 Testing of SU-8/PDMS dot cell by applying a gas pressure (a) non-deflected PDMS membrane and (b) deflected of PDMS membrane under nitrogen gas pressure.....	70
3.25 Optical micrographs of a Ni master mold (a) top view and (b) bird's eye view.....	71
3.26 Fabrication processes of micro-pistons and complementary cylinders by using a conformal and conductive sacrificial spacer layer.....	72
3.27 PDMS molding (a) a nickel master mold placed inside a PDMS frame (b) cutting around the casted PDMS and (c) peeling off from the master	73
3.28 (a) Touch and paste bonding and (b) stick with PI tape	74

LIST OF FIGURES (Continued)

FIGURE	PAGE
3.29 (a) The bonding of the photoresist to the substrate and (b) cumulative photoresist around circumference of the base mold	74
3.30 (a) Bonding with AZ photoresist and (b) sticking on the substrate with PI tape.....	75
3.31 The result of PDMS-substrate bonding	75
3.32 The seed layer exposing by oxygen plasma	76
3.33 Gas bubbles trapping inside the structure	76
3.34 (a) Current ramping rate of nickel electroplating and (b) the piston without any gas bubbles	77
3.35 Fabrication sequences of piston (a) The SU-8 mold for the cylinder Electroplating (b) growing of silver sacrificial layer (c) the cylinder electroplating and (d) the mechanical polishing to expose the silver ring.....	78
3.36 Releasing of sacrificial layer (a) small hole around the piston between wet etching and (b) the piston releasing from the cylinder	79
3.37 Gear structure (a) 3D model (b) top view and (c) cross-section view.....	80
3.38 X-ray masks for the multi-layer gear.....	81
3.39 Three master molds of SU-8 photoresist.....	81
3.40 Molding of PDMS (a) PDMS loaded into the SU-8 master mold and (b) the PDMS mold removed from the mold.....	82
3.41 Fabrication sequences of the first gear structure	83
3.42 Fabrication sequences of the second gear structure.....	84
3.43 Fabrication sequences of the third gear structure.....	85

LIST OF FIGURES (Continued)

FIGURE	PAGE
3.44 SEM image of gear structure (a) finished structure (b) the connection area between layer 2 and 3 and (c) between layer 1 and 2.....	86
3.45 Problems of PDMS molding (a) Remained PDMS on the SU-8 master mold and (b) the peeling partially of PDMS mold between electroplating.....	86
4.1 Application of electrostatic microvalve in tactile display systems.....	89
4.2 Structure of curled-up closure plate for electrostatic microvalves.....	90
4.3 Schematic of operation principle of SU-8/metal electrostatic microvalve (a) microvalve in open configuration and (b) microvalve closed by applying voltage	91
4.4 Characteristics of microvalve (a) cross-section view and (b) schematic layout.....	92
4.5 Fabrication sequences of the nickel substrate with an inlet orifice.....	94
4.6 Fabrication process of the curled-up closure plate of microvalve.....	95
4.7 The finished curled-up closure plate microvalve compared to ant.....	96
4.8 Bird's eye view optical micrographs of the curled-up closure plate microvalve.....	97
4.9 Experimental testing of the curled-up plate of microvalve.....	97
4.10 (a) Microvalve setup inside the acrylic package and (b) cross-section of microvalve setup	98
4.11 Experimental setup for the microvalve.....	99
4.12 Experimental testing the microvalve (a) no voltage potential (b) applied gas pressure and (c) applied closing voltage	100
4.13 Volume flow rate as a function of the applied voltage.....	101

LIST OF FIGURES (Continued)

FIGURE	PAGE
4.14 The characteristics of curled-up electrostatic microvalve.....	102
4.15 (a) Top view of the polished nickel substrate and (b) bird eye view.....	103
4.16 The distorted curve on the closure plate of microvalve.....	104
4.17 Dimensions of the curled-up closure plate.....	105
4.18 Structure parameter in a nozzle of microvalve.....	107
4.19 The fixed-end cantilever free body diagram.....	109
4.20 Simulation results (a) moving of closure plate and (b) deflection-voltage behavior.....	111
4.21 The modelling results of the SU-8 curled-up closure plate microvalve.....	113
4.22 The actuated voltage simulation compare with the experimental results.....	114
5.1 The nominal Braille specifications as set by the National Library Service for the Blind and Physically Handicapped (NLS).....	116
5.2 Plasma bonding (a) PDMS membrane fixing on the SU-8 tactile structure and (b) peeling of PDMS membrane under the applied pressure of 16.38 kPa.....	118
5.3 (a) Hydrophobic state before oxygen plasma (b) oxygen plasma treatment on the PDMS surface and (c) hydrophilic state after oxygen plasma.....	119
5.4 Chemical structure of PDMS-PDMS bonding by oxygen plasma.....	120
5.5 Fabrication sequences of the tactile dot by using PDMS-PDMS/SU-8 plasma bonding.....	121
5.6 Peel-off damages of the PDMS membrane after testing.....	122

LIST OF FIGURES (Continued)

FIGURE	PAGE
5.7	Optical micrograph of the PDMS dot (a) OFF position and (b) ON position with deflected membrane under 27.6 kPa differential pressures..... 123
5.8	Measured deflections of PDMS membranes prepared by various spin coating speeds..... 123
5.9	Fabrication sequences of PDMS tactile dot by wet bonding (a) spin-coating PDMS on AZ photoresist sacrificial layer (b) placed SU-8 frame and press with a mass of 1 kg (c) release from the substrate and (d) test under an applied pressure..... 125
5.10	The PDMS dot display resulting from wet bonding (a) bottom view and (b) side view with deflected membrane under applied pressure..... 126
5.11	Measured deflection of the PDMS membrane in PDMS-SU-8 wet bonding Braille dot..... 127
5.12	Damaged PDMS membrane under an applied pressure 127
5.13	Fabrication sequences of a PDMS tactile dot by using SU-8 sacrificial material (a) planarized with SU-8 photoresist sacrificial (b) spin-coated PDMS membrane (c) released sacrificial (d) cover with SU-8 tactile panel and (e) test under an applied pressure 128
5.14	(a) The PDMS membrane covering the SU-8 orifice and (b) SU-8 tactile panel placing on the membrane 129

LIST OF FIGURES (Continued)

FIGURE	PAGE
5.15	Load-deflection characterizations according to PDMS spin speed coating130
5.16	Deflection of a suspended PDMS membrane in reaction to an applied pressure130
5.17	The relationship between P/d and d^2 for the calculation of Young's modulus and residual stress of the membrane132
5.18	Load-deflection curve for membranes with different thickness compare with the analytical model..... 134
5.19	Load deflection experimental setup 135
5.20	Schematic diagram of a SU-8 tactile display (a) OFF and (b) ON position..... 136
5.21	Fabrication sequences of an assembled SU-8 tactile display.....138
5.22	Photographs of a two layers of SU-8 tactile display 139
5.23	The assembled SU-8 tactile dot display on the PDMS membrane for actuation (a) OFF position and (b) ON position140
5.24	Fabrication sequences of the released tactile dot display (a) conformally coat with sacrificial layer (b) reflow SU-8 photoresist (c) polish top surface (d) polish bottom surface (e) remove sacrificial layer and (f) polish the tactile panel and insert SU-8 pin.....141
5.25	Fabrication process of the tactile display by releasing of the sputtered sacrificial material (a) construct two layers of SU-8 tactile dot (b) conformally coat Al sacrificial layer (c) polish top surface to open Al layer and (d) remove sacrificial layer143

LIST OF FIGURES (Continued)

FIGURE	PAGE
5.26	The cracked structure when the tactile dot is forced to release form the panel 144
5.27	Fabrication process of the released tactile dot by silver sacrificial material (a) construct 300 μm -tick SU-8 photoresist (b) construct 800 μm -thick SU-8 photoresist (c) coat Ag seed layer by sputtering (d) increase Ag thickness by using electroplating (e) polish top surface (f) polish bottom surface (g) remove Ag sacrificial layer and (h) polish SU-8 tactile panel and insert SU-8 tactile dot 145
5.28	The assembly of the released tactile dot display (a) prepare a supporter of SU-8 tactile dot (b) place SU-8 tactile dot inside the supporter (c) cover with SU-8 tactile panel and (d) test under an applied pressure 147
5.29	Fabrication sequences of the PDMS/SU-8 refreshable tactile display (a) paint glue at the center of suspended PDMS membrane (b) place SU-8 tactile dot on the membrane (c) cover with SU-8 tactile panel and (d) test under an applied pressure 148
5.30	(a) The SU-8 tactile dot attaching on the PDMS membrane and (b) covering the tactile dot with the SU-8 panel 149
5.31	(a) The normal state and (b) the actuated state of the SU-8 refreshable tactile display with PDMS spring element 150
5.32	Schematic layout of the curved spring segment with one support 151

LIST OF FIGURES (Continued)

FIGURE	PAGE
5.33	Fabrication sequences of the spring SU-8 tactile dot display 152
5.34	(a) The display panel with the tactile dot on the substrate and (b) two layers of the display panel 153
5.35	(a) The SU-8/spring tactile dot and (b) the assembly of the tactile dot display 154
5.36	(a) Moving of the dot resulting from the mechanical force and (b) the rising of the tactile dot on the display panel 154
5.37	Curved segment of span angle loaded by force to the plan of the curve 155
5.38	Comparison of analytic curved spring segment (solid line) with the experimental results (points)..... 158
6.1	Chamber pressure with the tactile display holder 161
6.2	Assembled sequences of the tactile display with pressure chamber 162
6.3	Experimental diagram of the tactile display 163
6.4	(a) Force sensor placing over the tactile display and (b) force-pressure experimental setup 164
6.5	Portable tactile display 165
6.6	Experimental setup for the tactile display with PDMS spring element 166
6.7	(a) The normal state and (b) the actuation state of the tactile display with PDMS spring element 166
6.8	Force-pressure characteristic of the tactile display with PDMS spring element 167

LIST OF FIGURES (Continued)

FIGURE	PAGE
6.9 (a) The normal state and (b) the actuation state of the tactile display with curved spring segments.....	168
6.10 Force-pressure characteristics of the tactile display with curved spring segments.....	169
6.11 Weight - pressure experimental setup	170
6.12 Weight-pressure characteristics of the tactile display with curved spring segments	170
6.13 Assemble sequences of the refreshable tactile display with microvalve	172
6.14 The experimental setup for the refreshable tactile display	173
6.15 (a) The raising of tactile dot under the applied pressure and (b) the maximum downward distance after the closing of microvalve.....	174
7.1 (a) Braille display by combining of 6 LIGA tactile dots and (b) the tactile display controlled by microvalve	178
7.2 The schematic tactile display with the pressure supplier	179
7.3 Braille display drive circuit with microcontroller	180
7.4 Drive circuits of (a) solenoid valve and (b) microvalve.....	181
7.5 Vertical actuator for microvalve application	182

LIST OF SYMBOLS AND ABBREVIATIONS

a	=	Radius of PDMS membrane
A	=	Ampere
A	=	PDMS frame area
A_{eff}	=	Effective valve area
A_n	=	Area of X-ray exposed SU-8 pattern layer n calculated from LayoutEditor™ Program
A_{nm}	=	Overlapping X-ray projection areas calculated from LayoutEditor™ Program
AF	=	Activating Function
Ag	=	Silver
Al	=	Aluminum
Au	=	Gold
AZ 1512	=	Positive photoresist (Microchemicals)
AZ P4620	=	Positive photoresist (Microchemicals)
Be	=	Beryllium
C	=	Carbon, graphite
°C	=	Degree Celsius
CF ₄	=	Carbon Tetrafluoride
CH ₃	=	Methyl group
C_i	=	Discharge coefficient
CTE	=	Coefficient of thermal expansion
CTE_{metal}	=	Coefficient of thermal expansion of metal electrode

LIST OF SYMBOLS AND ABBREVIATIONS (Continued)

CTE_{SU-8}	=	Coefficient of thermal expansion of SU-8 photoresist
Cu	=	Copper
d	=	SU-8 density = 1.2 g/cm ³ , center deflection of PDMS membrane
E_1	=	Young's modulus of nickel (205 GPa)
E_2	=	Young's modulus of SU-8 photoresist (4.5 GPa)
\tilde{E}_1	=	Effective modulus of material one
\tilde{E}_2	=	Effective modulus of material two
$(\tilde{E}I)_{eqv}$	=	Equivalent beam strength
ER	=	Electrorheological
F	=	Direction of force
F_b	=	Force under the closure plate
f_c	=	Correction factor in SU-8 powder reflow casting
F_p	=	Net load applied pressure
g	=	Height of beam from substrate
g_0	=	Initial gap of beam from substrate
gf.	=	Gram-force
h_{max}	=	Gap height
h_0	=	Initial gap height
h_p	=	Deflection of the beam under the applied pressure
H ₂ O ₂	=	Hydrogen peroxide
I	=	Moment of inertia (= $wt^3/12$)
I_1	=	Moment of inertia of material one
I_2	=	Moment of inertia of material one
J	=	Polar second moment of rectangular section

LIST OF SYMBOLS AND ABBREVIATIONS (Continued)

k	=	Spring constant
K	=	Unit of absolute temperature (Kelvin)
k_t	=	Total spring constant
LIGA	=	<u>L</u> ithographic <u>G</u> alvano <u>f</u> ormung <u>A</u> bformung
L	=	Length of beam
L_{metal}	=	Length of metal electrode
L_{SU-8}	=	Length of SU-8 beam
m	=	Mass flow rate through the microvalve
m_{gap}	=	Mass flow rate through the gap
m_0	=	Mass flow rate through the orifice
M	=	Moment
M_1	=	Moment of material one
M_2	=	Moment of material two
MEMS	=	Micro-Electro-Mechanical Systems
Mylar [®]	=	Transparent sheet of polyester
NH ₄ OH	=	Ammonium hydroxide
Ni	=	Nickel
NIST	=	National Institute of Standard and Technology
O	=	Oxygen
O ₂	=	Oxygen gas
OH	=	Hydroxyl group
P	=	Axial force, applied pressure
P_1	=	Axial force inside material one
P_2	=	Axial force inside material two

LIST OF SYMBOLS AND ABBREVIATIONS (Continued)

Pa	=	Unit of pressure (Pascal)
Pb	=	Lead
PCMs	=	Phase change materials
PCR	=	Polymerase Chain Reaction
p_e	=	Absolute outlet pressure
PI	=	Polyamine
PDMS	=	Polydimethylsiloxane
PET	=	Polyester
PMMA	=	Poly (methyl methacrylate)
p_s	=	Absolute inlet pressure
PVDF	=	Polyvinylidene fluoride
PZT	=	Lead zirconate titanate
Q	=	Volume flow rate through the microvalve
R	=	Universal gas constant/molecular weight $\left(0.2869 \frac{k - m^2}{K - sec^2}\right)$
	=	Radius of curved spring segment
r_a	=	Radius of the closure plate
RA	=	Rapidly Adapting
RAI	=	Meissner corpuscles
RAII	=	Pacinian corpuscles
RBDS	=	Refreshable Braille Display Systems
r_e	=	Radius of the orifice
SA	=	Slowly Adapting
SAI	=	Merkel cells

LIST OF SYMBOLS AND ABBREVIATIONS (Continued)

SAII	=	Ruffini ending
Si	=	Silicon
SiC	=	Silicon carbide
SiN	=	Silicon nitride
Si-OH	=	Silanol group
SiO ₂	=	Silicon dioxide
SMA	=	Shape memory alloy
SU-8	=	Negative photoresist (MicroChem corp.)
SU-8 2100	=	Negative photoresist (MicroChem corp.)
t	=	Total thickness of beam, thickness of PDMS membrane
T	=	Temperature (Kelvin)
T	=	Torque
t_1	=	Thickness of material one
t_2	=	Thickness of material two
Ta	=	Tantalum
t_g	=	Thickness of Al sacrificial layer of microvalve
Ti	=	Titanium
t_{metal}	=	Thickness of metal electrode
t_n	=	Thickness of SU-8 reflowed casting layer n
t_{SU-8}	=	Thickness of SU-8 beam
U	=	Total strain energy
UV	=	Ultra-violet
V	=	Applied voltage
V_n	=	Volume of SU-8 photoresist for reflowed casting for layer n

LIST OF SYMBOLS AND ABBREVIATIONS (Continued)

$V_{PR(n)}$	=	Volume of exposed SU-8 photoresist layer n
w	=	Width of beam
w_1	=	Width of material one
w_2	=	Width of material two
W	=	Tungsten
W_{final}	=	Weight of SU-8 photoresist monitored in SU-8 powder preparation
$W_{initial}$	=	Weight of wet SU-8 photoresist in SU-8 powder preparation
w_{metals}	=	Width of metal electrode
W_n	=	Weight of SU-8 powder for layer n
w_{SU-8}	=	Width of SU-8 beam
x	=	Distance along the length of the beam
XOP	=	X-ray Oriented Programs
z	=	Deflection of beam
$z(x)$	=	Deflection of the closure plate along the length
Å	=	Angstrom (10^{-10})
ρ	=	Radius of curvature of the closure plate
ρ_0	=	Initial radius of curvature of closure plate
σ_0	=	Residual stress
σ_1	=	Residual stress of material one
σ_2	=	Residual stress of material two
α_1	=	Coefficient of thermal expansion of SU-8 photoresist (50 ppm/K)
α_2	=	Coefficient of thermal expansion of nickel (13.3 ppm/K)
T	=	Temperature
ΔT	=	Change in temperature

LIST OF SYMBOLS AND ABBREVIATIONS (Continued)

δ	=	Deflection of the end of the beam or closure plate, displacement of the applied point of force in the direction of force
ν_1	=	Poisson's ratio of material one
ν_2	=	Poisson's ratio of material two
γ	=	Ratio of specific heats of air (1.4)
θ	=	Span angle (radian)

CHAPTER I

INTRODUCTION

1.1 Problems and Rationale

After globalization era, people can communicate with each other easily via their own personal computer. Not only ordinary people, but also people with disabilities have gained a lot of benefit from technological advancements. Many assistive technologies such as audiphone, handtalk glove, speaker, and haptic display have enhanced abilities of impaired people up to the same level of ordinary people. Particularly for visual impaired people, haptic interface technologies have been combined with computer applications to help them to perceive simple electronic information as a form of texts and images via sense of touch, e.g. palpation, which is called tactile display system.

Braille characters which are text base information for the blinds have been developed in forms of electronic data that can be displayed on a tactile screen through computer programming. New real-time reading and writing model called Refreshable Braille Display System (RBDS) assists the blinds more conveniently to communicate with global network. It becomes a necessary tool for visual impaired people who need to work and communicate with other via the internet. However, its fabrication with special techniques and complex structure, such as piezoelectric and electromagnetic solenoid, are limitations of RBDS system. The unit price should be decreased so that the RBDS can be more affordable.

Among numerous Braille displays, Micro-Electro-Mechanical System (MEMS) have been revolutionized by micromachining techniques to support the realization of the complement system for development of smart products. As a batch fabrication, the

technique is similar to the integrated circuit process. MEMS can be used to make a large number of miniaturized devices at a time, reduce the weight of the display and lower the cost per actuator. Integration of actuators and electronic circuits on the same substrate are the way to increase the display resolution (Yobas et al., 2003). Nevertheless, MEMS applications for tactile display have encountered four main limitations. Firstly, microstructures may be damaged by mechanical load touch. Secondly, there is insufficient linear motion and force to stimulate touch sensation. Thirdly, the models must survive reliability testing before they can be launched to market. Finally, tactile devices must batch fabricated to lower the unit cost down to a reasonable market price. To overcome these limitations, Lithographic Galvanoformung Abformung (LIGA) technology was proposed to mass-produce microcomponents at a low-cost because of its special process including X-ray lithography, electroforming, and plastic molding.

This research concentrates on a tactile display for the refreshable Braille display systems utilizing X-ray LIGA process which was performed using the BL-6 beamline at the Synchrotron Light Research Institute (Public Organization), Ministry of Science and Technology, Thailand. The tactile display consists of a tactile dot and a tactile panel which were constructed by the complicated SU-8 microstructure by X-ray LIGA process. Tactile displays for RBDS that can be obviously sensed through a rigid tangible dot were designed and fabricated in two models. The first one was the tactile display with PDMS spring element which was generated from applying a different pressure inside the cavity across the tactile screen to deform the membrane by controlling of a solenoid valve. The second one was the tactile display with curved spring segments which was also controlled by a solenoid valve to drive the moving part of rigid element against the fingertip. All of them were based on X-ray LIGA technology to enable mass production and non-complicated processing to lower the cost of tactile display for visually impaired people.

1.2 Research Objectives

The main objectives of this study are as below:

- Design and implement a pneumatic Braille dot based on X-ray LIGA fabrication.
- Develop a new method for X-ray mask fabrication and photoresist deposition for multilayer thick film construction.
- Develop X-ray LIGA processes of complicated microstructures that is necessary for Braille display development.

1.3 Scope and Limitation of the Study

The scope and limitation of this study are described as following:

- The patterns of X-ray LIGA microstructures are designed by using an open-source layout drawing CAD tool (LayoutEditor™), then transferred to X-ray mask using UV lithography, and electroplated silver is used as X-ray absorber material.
- Three-dimensional X-ray lithography are performed by multi-alignment technique through transparent X-ray mask.
- Thick photoresist films of complicated microstructures are deposited by reflow casting process using a mathematical model to control the final film thickness.
- The preliminary models of pneumatic Braille dot stimulation are the polymer Braille dot and the piston Braille dot based on X-ray LIGA fabrications.

1.4 Benefits of the Study

The benefits of the study are presented as follows:

- A new method for X-ray mask fabrication using silver absorber on transparent membrane has been achieved.
- A new method to control thickness of photoresist film by using a minimum weight of SU-8 powder in reflow casting process has been obtained.

- Capability of 3D X-ray lithography for complicated microstructures has been developed.

- Prototype models of Braille dot stimulation systems based on X-ray LIGA fabrication have been demonstrated.

1.5 Thesis Organization

This dissertation is organized as follows. In the next chapter, Chapter 2, the overview of tactile display modalities and applications are investigated. The state of the art of the tactile mechanisms are described with the principle of raising individual pin or dot in presenting of text and graphics. Moreover, the MEMS and LIGA technologies are proposed to deliver the performance of the repeated fabrication for RBDS implementation.

Chapter 3 of this dissertation will discuss the development of basic micromachining processes which have been developed in order to realize the Braille dot model. Transparent X-ray mask was proved to create the complicated microstructures which were generated by using a SU-8 powder reflowed casting process. At the same time, two processes which are the fundamental technique for the tactile development are introduced. First, the tactile dot stimulation which is presented by using PDMS membrane can be achieved from the simply bonding. Second, the novel technique for releasing the piston is presented to delivers moving part of the dot display. Furthermore, the LIGA application for complicated gear structure is also introduced in capability of the repeated process.

In chapter 4, electrostatic actuator for microvalve application is presented to perform as a shutter of the tactile controller. The actuator based on composite SU-8/metal closure plate is presented on the basis of UV lithography process. In addition, the simulation models of the microvalve behavior based on electrostatic-fluidic-mechanical domains are proposed to estimate the microvalve characteristics. The experimental results show possibility in realizing moving mechanism for microvalve application.

Chapter 5 introduces the pneumatic tactile display mechanism based on LIGA technology. Its advantages are brought to implement the tactile structure combined with the repeated mechanism. Suspended PDMS membrane combined with the complicated SU-8 LIGA structure is first presented to utilize as a refreshable tactile display. Then, the SU-8 tactile structure with curved spring segments is proposed the novel mechanism to repeat the tactile dot. The mathematical models are also demonstrated to estimate the deflection behavior under a pneumatic applied pressure.

Chapter 6, the testing of the tactile display is proposed. The experimental setup is designed and employed in the tactile display characteristics. Load-pressure curve characteristics are experimented to estimate the tactile display force against a force pressure. Moreover, the curled-up closure plate microvalve is combined with the tactile display with PDMS spring element to play significant role in the refreshable Braille display system.

The last chapter, chapter 7, provides conclusions of the research work and suggestion for future studies.

CHAPTER II

LITERATURE REVIEW

2.1 Introduction

In order to understand Refreshable Braille Display Systems (RBDS), basic information related to tactile display must be investigated. Overall knowledge for realization of Braille display is surveyed in this chapter. Section 2.2 describes properties of cutaneous mechanoreceptors in the fingertips. This basic understanding is required in design of tactile displays. Section 2.3 discusses applications of tactile display. This shows performance of tactile system that can be applied to human life in several ways. Section 2.4 describes the modalities of Braille displays by explaining to the developments of tactile stimulator for Braille display from traditional to modern forms. Section 2.5 provides history and state of the art of RBDS. Various Braille dots actuation mechanisms from the past to present are given. Section 2.6 describes tactile displays utilizing MEMS technology which enables miniaturization of microstructures, devices and systems through batch fabrications and demonstrates many advantages of integrated circuit (IC) fabrication technology. Section 2.7 describes motivations of using LIGA technique in fabrication of Braille display based on synchrotron radiation. This is significant in realization of tactile dot actuation for this research using micromachining processes. Finally, the chapter summary is presented.

2.2 Properties of Cutaneous Mechanoreceptors in the Fingertips

Basic understanding of human glabrous skin is required for design of tactile displays. As shown in Figure 2.1, the sensing and encoding tactile information from outside sources are performed through the mechanoreceptors in skin tissue and sent to the brain by

natural impulses. There are four kinds of human glabrous skin (Johansson, 1978) including Meissner corpuscles (RAI), Merkel cells (SAI), Ruffini ending (SAII), and Pacinian corpuscles (RAII). They have specific responses to various stimuli that can be employed in tactile displays.

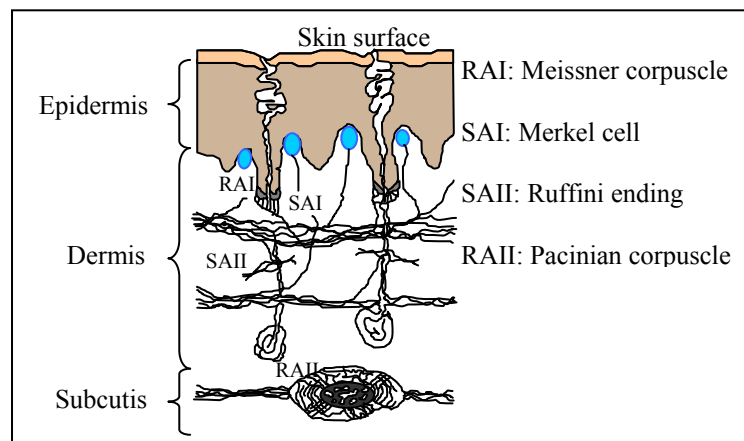


Figure 2.1 Mechanoreceptors of the glabrous skin.

Skin sensitivity occurs at the fingertips by stimulations in each kind of mechanoreceptors. The key feature as shown in Figure 2.1 can be categorized into two characteristics. First is their adaptation rate to a stimulus (Rapidly Adapting [RA] vs. Slowly Adapting [SA]). Second is their placement beneath the surface of the skin (type I receptors are located near the surface of the skin between the epidermis and dermis on the papillary ridges while type II receptors are located deeper beneath the skin in the dermis). Moreover, it is possible to classify them by the most important stimulus which they respond. This is usually considered that: RAI units (Meissner corpuscle) sense most to vibration at low frequencies (5-50 Hz), RAII units (Pacinian corpuscle) respond most to mechanical vibrations at high frequencies (50-1000 Hz), SAI units (Merkel cell) respond most to perpendicular skin indentation, and SAII units (Ruffini ending) react most to lateral stretch. A summary of mechanoreceptor properties is shown in Table 2.1.

Table 2.1 Summary of mechanoreceptor properties (Pasquero, 2003).

Mechanoreceptors	Type	Most important stimulus	Type of response	Principle functions
Meissner corpuscle	RAI	Low frequency vibration (5-50 Hz)	Transient	Detect low frequency motion and discriminate spatial localization
Pacinian corpuscle	RAII	High frequency vibration (50-1000 Hz)	Transient	Detect high frequency motion and detect traveling of mechanical vibrations
Merkel cell	SAI	Perpendicular indentation (0-30 Hz)	Sustained	Distinguish pressure magnitude and rates of change in pressure
Ruffini ending	SAIL	Tangential displacement (0-15 Hz)	Sustained	Perceive skin stretch and discriminate spatial localization

2.3 Tactile Display Applications

Over recent years, many applications are developed to support both blinds and ordinary people. Especially tactile display, they has played significant role on universal information communicated via human-computer interactions. Applications for tactile displays can be found in various forms including:

Text and Graphics: Text based information using refreshable Braille display that allows user to read through the screen display. By computer programming, matrix of Braille or graphic cells can be generated in specific formats to present information.

Medical applications: Tactile application with sensor array can be used to sense information from inside a patient's body and transmitted to the surgeon's fingertip during invasive procedures (Howe et al., 1999).

Entertainment and Education applications: It can be applied for simulate sensations to any action as a part of a 3D movie or gaming simulation such as electric shock or bullet impacts. Some application is designed for blinds and visually impaired children to play computer game through tactile boards with moving detectors as a part of game interface. The approach of tactile techniques can also be adapted to education software by providing a description of software in a specially generated tactile language on the devices.

Military application: Tactile displays are used to improve situation awareness on operation of high performance weapon platform, and increase human ability to work in critical situation.

Engineering applications: Engineering has play important role in design of equipment for assisting visually impaired people, for instance the tactile can be implemented within the blind walking cane (ultracane) (<http://www.qinetiq.com>). Ultrasonic transducers in the cane will sense and feedback information surroundings the user to tactile display.

Virtual environment application: Tactile interface devices can be cooperated with haptic display that provides both tactile and force feedback display to the hand. By tele-operation, tactile display will be operated as virtual environment in varieties situation by attached to each fingertip and the user's palm to present pulses or sustained vibration (Virtual Technologies, Inc.).

Electronics and wearable devices: Tactile display can also be embedded within consumer devices for communication with miniature handheld or wearable devices. The user will experience more effective, comfortable, and enjoyable interaction, for instance a tactile device is embedded within a PDA touch screen enhancing its basic GUI elements with tactile feedback.

2.4 Braille Display Modalities

Since Braille characters system have been devised for blind people in reading and writing in 1821 by Frenchman Louis Braille, the world-wide system used by visually impaired people are greatly adapted Braille to almost every known language. Braille character consists of 6-8 dot positions which formed in a rectangular shape containing two columns of three dots each, or 3×2 dots as shown in Figure 2.2. At any of the six positions, dots will be raised on the flat surface to excite the fingertip in order to interpreted and described in text form. Methods of transferring a desired pattern of Braille onto planar surface which have been further developed and utilized to impaired people will be described as follows.

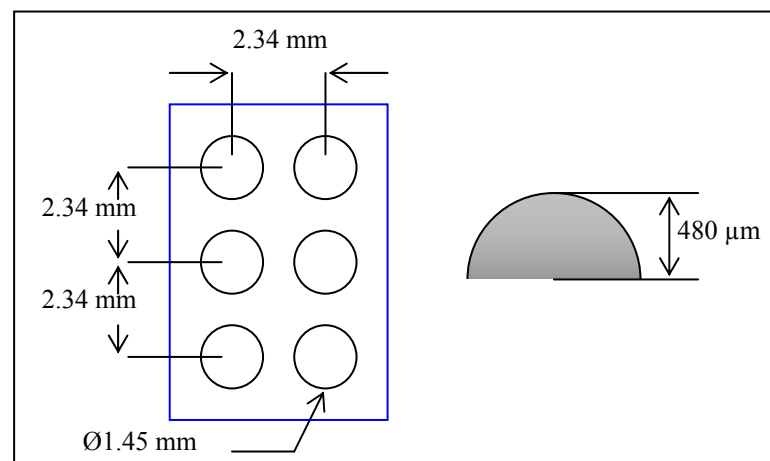


Figure 2.2 Braille code.

Firstly, Braille dots have been produced by hand through a slate and stylus. Each dot is created by writing in mirror images from the back of a paper, just as Louis Braille did. This method is a beginning of the Braille display, and each Braille paper can be combined into a book. In addition, economical drawing papers are employed in Braille characters recording, and the writing is also improved on literacy skills and familiar with Braille for novice.

Secondly, Braille dots have been produced by a Braille typewriter or Perkins Braillers which was first made in 1951 by David Abraham (<http://www.perkins.org>) who is a woodworking teacher at Perkins School for the Blind. This is a machine to speed up the writing process, and they are reliable, robust, and easier to use than the hand writing. Although new technology and special software are produced and made Braille printing very fast and comfortable with a Braille embosser connected to a computer, the old-fashioned mechanical Perkins Braille are still wanted by many people especially in classrooms all over the world where without electricity or computer.

Finally, Braille dots are produced by mean of raising dots through holes in the flat surface by controlling of electro-mechanical device. This method is called Refreshable Braille Display System or Braille terminal which is revolutionary reading device for a Braille reader. It consists of the refreshable Braille display unit with housing and the personal computer as shown in Figure 2.3. Each Braille cell can be arranged in the display or a screen reader of one line or multi-line as monitors in a computer system. There are actuator mechanisms inside each Braille module to raise the dots by controlling via a computer system that converts text information in to Braille character and sends to the display.

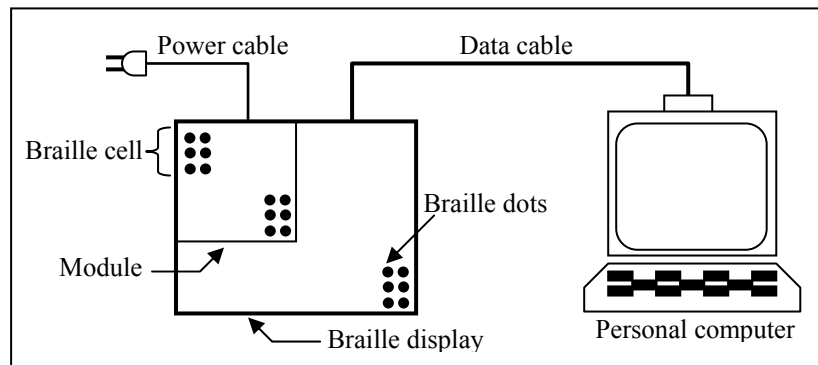


Figure 2.3 Refreshable Braille display system.

2.5 Refreshable Braille Display Systems

As described in the previous section, RBDS is the tactile reading aid of the Braille character unit which has electro-mechanical to raise dots through the flat surface. For Braille writing, the electromechanical drivers are applied to drive the pins and held in position. An erasing mechanism is provided to certainly drive the pin downward. Generally, the system of refreshable Braille display must be interfaced to the personal computer to translate display information into command for the Braille display system via data cable as shown in Figure 2.3. Braille cells are organized in modules of multi rows and columns. For electricity actuation, the power cable provides electrical power to the Braille display which can be plugged into standard voltage or separate batteries.

2.5.1 History of refreshable Braille display systems

Conventional tactile displays have used various mechanisms to produce dots. At first, the tactile display with a softening display panel was the main purpose of the invention. The display results were presented in the form of visual image in a window based on the tactile system. The first mechanism for the Braille character cell was introduced in the 1966 using piezoelectric bimorph actuators which were mounted as cantilever to vibrate individual pins (Linvill et al., 1966; Linvill, 1969; Bliss et al., 1970). Each Braille dot was raised up by piezo-effect of some crystals which expand when a

voltage was applied to them as shown in Figure 2.4. However, there were many drawbacks of the unit's ware that was very expensive to assemble. Moreover, the actuators required very large "volume overhead" to fit in Braille cell, and the footprint of cell was much larger than the display surface. This mechanism has been developed continuously to overcome their limitation until a company in Cambridge, Massachusetts was able to produce the display with two rows of Braille cell (Prince et al., 2004). It could be produced as a prototype of 4 lines by 40 columns. Nevertheless it was not commercially available due to the costs and difficulty of integrating large number of actuators in manufacturing.

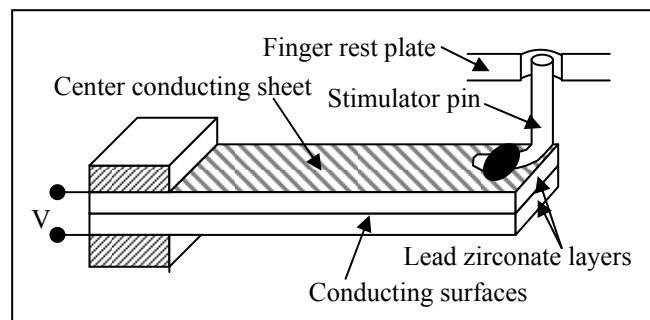


Figure 2.4 Piezoelectric bimorph reed mounted for use as a tactile simulator.

In 1970s, an optical-to-tactile image converter which was produced by the Optcon became first commercially available from TeleSensory Corporation (Sunnyvale, CA) (Linville et al., 1966; Linville, 1969; Bliss et al., 1970). It enabled the blinds to read normal printed material via an integrated array of photocell while the user was reading continuously with a stationary finger on a tactile plate. The tactile screen consisted of plate with 144 pinholes through a 6 by 24 array of pins which can be made to vibrate against the fingertip of users. This device had many user friendly features integrated into its device such as the screen display and a cursor locator. The Optacon still supported to optimum the size and cost of the tactile display, but the cost was still higher than a personal computer (Yobas et al., 2003).

Meanwhile, the quest for other actuating mechanisms of the Braille pin had been created with the various techniques and materials. The dot actuators can be controlled by electromagnetic solenoid which latches the pin in an up or down position (Frisken-Gibson et al., 1987), as well as shape memory alloy (SMA) wires (Taylor et al., 1988) which remember the alloy shape to drive the pin up. Alternative actuator types such as audio transducer (Kovach, 1985) and electrorheologic fluid (Taylor et al., 1998; Garner, 1996) were introduced. The actuation of electric shock to the finger tip was also performed as the tactile display without mechanical actuator (Strong et al., 1970). However, most of them were not commercially produced.

Nowadays, commercially available refreshable Braille displays do not differ significantly from what was described by Tretiakoff in 1977. The cantilever bimorph piezo-actuators still play significant role in the mechanism to support vertical pin at their free end. Figure 2.5 (a) shows the mechanism inside a cell package which is assembled with six or eight dots in the rectangular array of 3×2 or 4×2 . It is a common type of refreshable Braille cells and commercially available because it has relatively lightweight and small size (BrailleNote, <http://www.humanware.com>). In contrast, it is still limited primarily by cost which is often in a range of 10000-15000 USD for a conventional 80-characters refreshable linear Braille display. The annual maintenance cost can be around 500 USD (Roberts et al., 2000). A new Braille display development with a rotating wheel concept has been proposed in 2000 by National Institute of Standard and Technology (NIST). The NIST Braille Reader puts the Braille text on a rotating wheel or disc which allows the user to read continuously with a stationary finger instead of moving fingers over the screen display as shown in Figure 2.5 (b). The Braille dots are latched by the electromagnetic force from permanent magnet ring inside the wheel. It allows an infinite text line with the wheel spins at a selected speed. However, it is still in the process of commercialization with the expectation to be much less expensive than traditional Braille display.

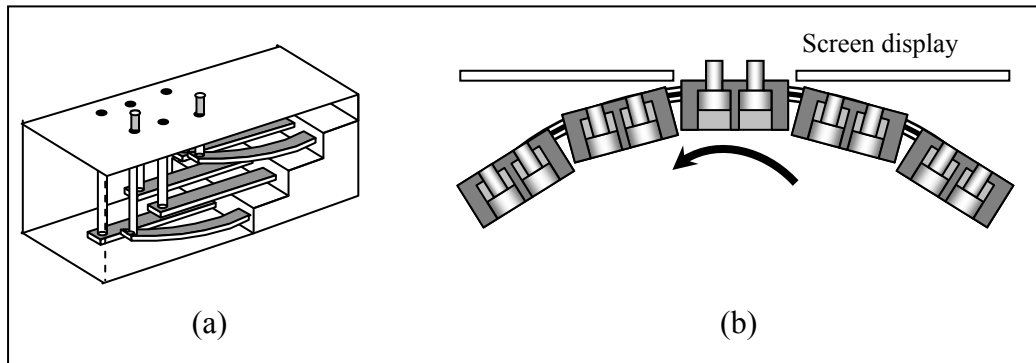


Figure 2.5 Commercially available refreshable Braille display (a) with cell piezoelectric actuation mechanism and (b) the NIST rotating-wheel Braille display.

2.5.2 State-of-the-art Braille displays

Various mechanisms to actuate the Braille dots and refresh the text were invented to find the new approach that would significantly lower cost and improve reliability. The tactile dots can be performed with the principles of actuation including raising individual pins, pressurized dome shape membrane, piezoelectric beam, piezoelectric polymer, microstep motor, Phase Change Materials, electrostatic actuators, electromagnetic solenoid, electrorheological fluid, shape memory alloy, lateral skin deformation, servo motor, bimetallic strip, electrocutaneous, and air jet tactile display. These tactile dot driving mechanisms and actuations are described in potential applications in following subsections.

2.5.2.1 Piezoelectricity

Piezoelectricity is the property of specific materials in which their shape can be changed under influence of electric field. Piezoelectric materials such as lead zirconate titanate (PZT) expand and contract when an electric field is applied as shown in Figure 2.6 (a). Two mechanisms based on these materials were proposed for the Braille dot actuation. The first is piezoelectric bimorph which consists of two active layers. It can be flexed under application of a voltage to change the shape of solid and produce a small

displacement with high force ability under properly designed mechanism. This technique was the earlier actuation, and it has been still played important function in the mechanism to support vertical pin in the Braille display (Linville et al., 1966; Bliss et al., 1970). The piezoelectric bimorph and the pin were combined in a cantilever manner as illustrated in Figure 2.6 (b). The upper and lower surfaces of the shim layer were coated with piezoelectric material. When the upper layer was connected to a driving voltage, it contracted longitudinally and the pin moved upward when the lower layer was driven by a voltage, the pin moved downward to ensure its normal position.

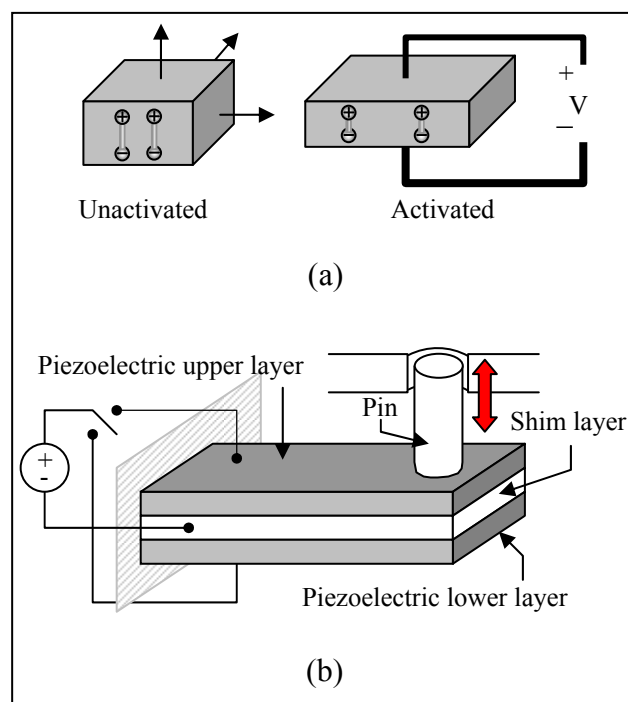


Figure 2.6 Piezoelectric material application (a) exaggerated motion of piezoelectric material and (b) a cantilever piezoelectric bimorph for tactile display.

Another mechanism was the piezoelectric linear motor which converted an electrical power to a deflection of material in motor mode (Cho et al., 2006). The piezoelectric linear motor was composed of piezoelectric material, elastic material, a shaft, and a pre-presser as shown in Figure 2.7. The elastic material was attached to the

lower surface of piezoelectric material, while the shaft was connected to the upper surface. The pre-presser which was contacted with the shaft applied pressure on the shaft and created a friction force between them. In the downward actuation as shown in Figure 2.7 (a), the deformation force, which was created between the shaft and pre-presser by small beading of the piezoelectric material in the first actuation but not generate any motion, was accumulated for the restoration force grater than the friction force. When the reverse polarity voltage was applied, the restoration force created a downward displacement combined with a reverse piezoelectric effect for the downward motion. The upward motion was attained by a similar way as shown in Figure 2.7 (b).

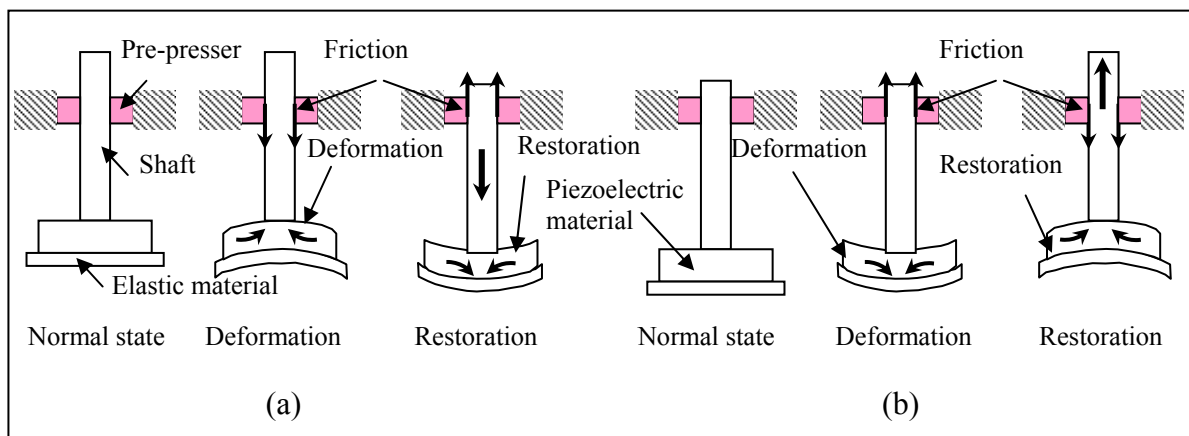


Figure 2.7 Piezoelectric linear motor (a) downward actuation and (b) upward actuation.

2.5.2.2 Piezoelectric polymer

Piezoelectric polymer or electroactive polymer for Braille display was reported in Linvill (1986). The author utilized transduction behavior of polyvinylidene fluoride (PVDF) to make arrays of electrodes using a sheet of material. For application of PVDF in motor mode, the transducer drove a mechanical load by input from an electrical source, hence the upper and lower surface of the PVDF sheet have to be coated with conductive material. By mechanically fixed at the left end of the strip as shown in Figure 2.8 (a),

the mechanical part at the right end generated a Coulomb force (F) with a deflection (y) when the electric field was applied from the voltage (V) across upper and lower electrodes. The Braille dots were performed by folding of PVDF sheet as a cylindrical tube and placed in 2×3 configurations of Braille cell, and driven by a 250 Hz square wave of 800 V to vibrate surfaces against fingertips of the blind reader. However, preparations of the piezo-sheets have to be done by hand cutting to isolate the electrical contacts for the applied voltage inside the folded sheet. Therefore, the cylindrical piezoelectric arrays using these methods are limited for large numbers construction.

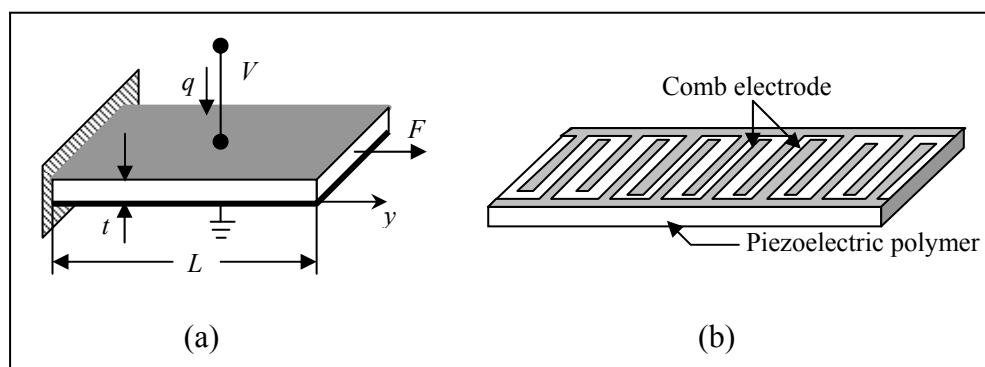


Figure 2.8 Piezoelectric PVDF bending sheets (a) with top and bottom electrodes and (b) with planar comb electrodes.

In addition, comb electrodes as shown in Figure 2.8 (b) were placed on one side of a piezoelectric polymer. Coulomb forces driven by applied electric field were generated resulting in bending of the polymer sheet. This mechanism was presented by Yang (2004) based on bending characteristic of piezoelectric polymers to provide hydraulic actuation for the tactile dots. The piezo-polymers with comb electrode were assembled to fluid-tight housing at top and bottom apertures for each window side which was connected together by support strips as shown in Figure 2.9 (a). The housing which contains appropriate fluid or gas to serve as the medium pressure was used to adapt

configuration when an electric voltage was applied. The bending of the piezo-polymer that displaces the fluid volume within the housing was sufficient to latch the Braille dot. In an actuation state as illustrated in Figure 2.9 (b), the actuator rod which was attached to the flexible diaphragm was raised up by a stabilizer block, while the supporting blocks were moved to support this stabilizer block at the center by pushing of rubber membranes. The height of the supporting blocks was sufficient to create a tactile dot. When the power to the bending elements is switched off, the four piezo-polymers will bend toward outside of the housing, and the negative pressure is generated inside the housing. The supporting blocks are moved away from the center and the actuator rod drops back to its rest position as shown in Figure 2.9 (c). The tactile dot is erased and the next cycle will be repeated when the voltage is applied again.

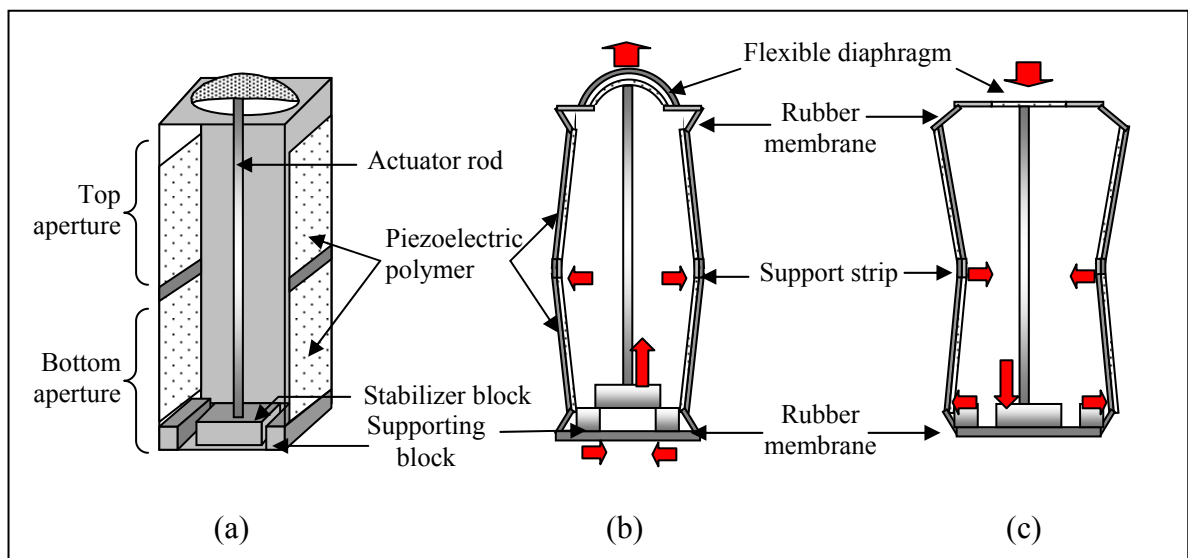


Figure 2.9 A rectangular fluid-tight housing of piezoelectric bending element

(a) structural view (b) ON state and (c) OFF state.

2.5.2.3 Microstep Motor

Microstep Motor was a rotary type actuation device. The Braille dot was performed by converting rotation to linear movement via a lead-screw mechanism (Shinohara et al., 1998). The purpose of this system was to create three-dimensional high spatial resolution tactile graphic display in large screen format. Based on a principle of electromagnetic actuation, a bipolar structure was adopted to generate a rotation which was controlled by an electric current as shown in Figure 2.10 (a). The motor-shaft rotation was converted into vertical movement through the lead-screw mechanism in 0.1 mm step, and adjusted the tactile-pin tip above the display board up or down as shown in Figure 2.10 (b).

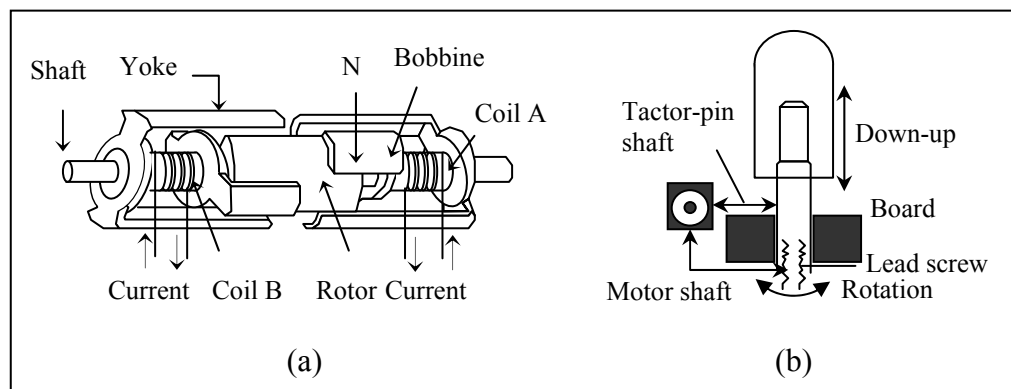


Figure 2.10 A microstep motor Braille dot (a) structural view and (b) conversion of a rotation in to a linear movement through a lead-screw mechanism.

2.5.2.4 Phase change materials (PCMs)

Phase change materials are substances that can change their phase from solid to liquid or from liquid to gas by external conditions such as temperature or pressure (Lee and Lucyszyn, 2005). Their volume expands or shrinks when they are energized, and the hydraulic force during phase transformation can be employed to actualize microactuators. Generally, when the hydraulic force of PCMs based on the expanded volume due to the distance between its atoms is increased, appropriate PCMs in

an actuator should have a certain transformation point suitable for the application and can produce a very large hydraulic force under this expansion. For the Braille dot actuation, thermopneumatic and electrothermal actuation were proposed for actuating mechanism based on PCMs.

The thermo-pneumatic actuation is a method to change the phase of a low boiling point liquid (for instance methyl chloride or acetone) to gas causing by the heating (Vidal Verdú et al., 2003). This was operated in a sealed metal cavity that has a flexible membrane attached on the upper cylindrical surface. A resistive heater was built inside. When the heater was energized to heat the liquid in the cavity, a gas volume resulting from the liquid-gas phase transition was generated. The flexible side of the cavity was displaced by the gas and the tactile dot was created as shown in Figure 2.11 (a). The electro-thermal actuation is a method to transfers electrical power to thermal actuation for PCMs materials. This requires the PCMs substances that change its phase from solid to liquid via external temperature. Paraffinic hydrocarbon or paraffin wax was chosen with the properties of the volumetric expansion during melting to generate very large hydraulic pressure that can perform actuation for tactile dots (Lee and Lucyszyn, 2005). Figure 2.11 (b) shows a micromachined cell designed for this mechanism. Paraffin wax was filled into bulk micromachined silicon containers with integrated microheaters on a bottom glass substrate, and elastomer diaphragms of silicone rubber were sealed on the top of the containers. After the tactile cells which consist of four layers were bonded together, a direct current (dc) actuation voltage was applied to the microheater. The paraffin wax was heated continuously expand the cavity volume, resulting in large hydraulic forces inside the containers. The flexible diaphragm was displaced and the tactile dot was raised up for display. The tactile dot was erased when applied current was eliminated.

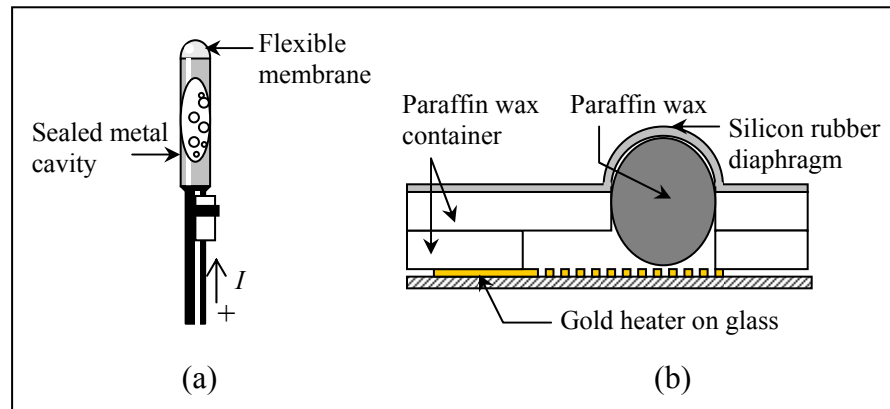


Figure 2.11 Braille dot actuations based on PCMs (a) with thermo-pneumatic actuation and (b) with electro-thermal actuation.

2.5.2.5 Electrostatic actuator

Electrostatic actuator for tactile display was based on an electrostatic attraction between the skin and the electrode (Beebe et al., 1995). The existence of the electrostatic force was generated when the voltage potential was applied across any two conductors that were separated by an insulator similar to capacitor. The conducting fluid in the fingertip acted as one plate of capacitor where an electric field was created in the insulation layer coated on external electrodes which acted as the other plate as shown in Figure 2.12 (a). Only electrostatic force alone, however, did not give a sensation. For an obvious sensation, the fingertip must be sliding across the surface of the electrode to create a shear force that was perceived as texture at the interface. Three of 49-point arrays which are tactile displays had been fabricated on a 4-inch wafer as shown in Figure 2.12 (b). By using 200-600 V pulse excitation, the preliminary experiments gave sufficient perceptions.

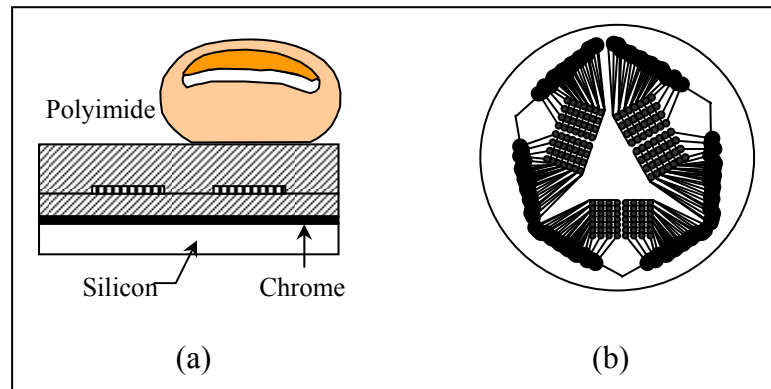


Figure 2.12 Electrostatic display (a) cross-sectional view and (b) a group of three displays on a 4-inch wafer.

Another electrostatic actuator with elastic dielectric was reported by Pelrine et al. (2000). It was elastic dielectric film which was sandwiched between compliant electrodes. Under electrostatic pressure between the electrodes, the dielectric could be contracted in thickness and expanded its area in direct result of the attracting charge on the electrodes. The mechanism of electrostatic Braille dot actuation with elastic dielectric is shown in Figure 2.13.

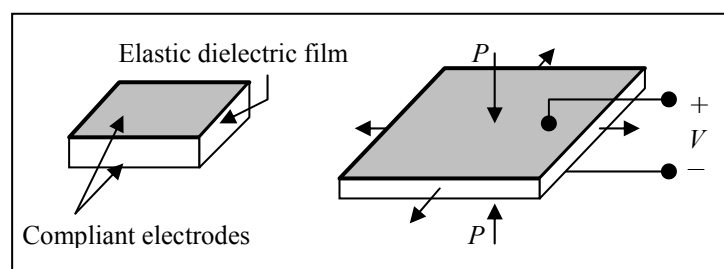


Figure 2.13 Deformation of an elastic dielectric film under electric pressure.

Since the linear motion of dielectric under electrostatic field was limited in the range of a few microns, it was necessary to stack many layers of dielectric film to increase actuation displacement. Compliant electrodes which could expand its area

due to the dielectric effect were inserted between each dielectric layer as shown in Figure 2.14, and the stimulator tip was attached on the upper surface. The actuator containers provided a gap around the actuator stack to ensure the area expansion. In normal mode, the actuator was always pressed against the fingertip. If the voltage was applied between neighboring electrode layer for text display, the dot was disappeared by shrinking of the dielectric stack. However, this actuator was limited from a very large number of the dielectric layer that requires more than 1000 layers with 10 μm thickness.

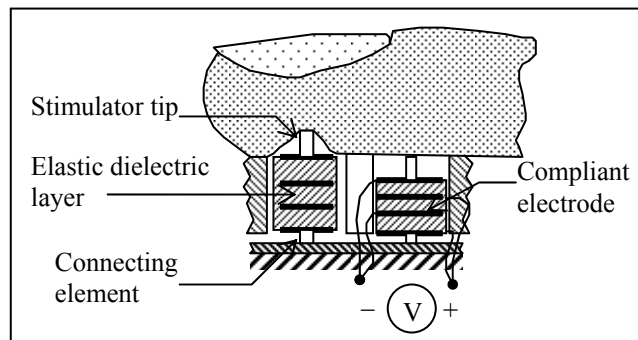


Figure 2.14 Electrostatic tactile stimulator with elastic dielectric.

2.5.2.6 Electromagnetic solenoid

Electromagnetic solenoid was a transducer device which converts electrical energy into linear motion based on electromagnetic fields. It consisted of two interacting parts, an electromagnetically inductive coil wound around a movable steel or iron slug (termed the armature) as shown in Figure 2.15 (a). When current was applied to the coil, based on right hand rule as shown in Figure 2.15 (b), it generated a magnetic field and flux lines that formed close loops around the coil which induce a north pole on the flux emerging and terminating on a south pole.

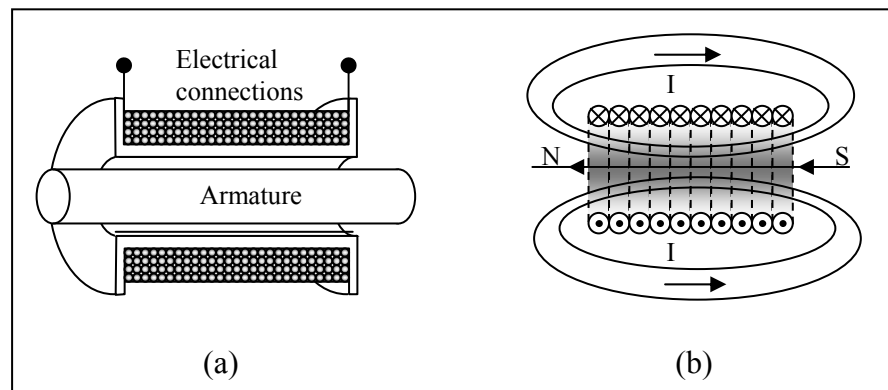


Figure 2.15 Electromagnetic solenoid (a) cross-sectional schematic and (b) the field and flux lines form closed loops around the coil resulting in a different polarity.

The armature like a short rod of iron which was placed at the center of the coil can be moved in and out by the electromagnetic force. This force occurred due to the coil magnetized the armature by created two separate magnets to the rod resulted in an attractive force to the different polarity and a repulsion force to the same polarity. The armature which was free from friction can be used to provide a mechanical force to some mechanism by controlling the current flowing through the coil. The Braille dot actuation based on this method provided a solenoid having a permanent magnetic rod to reduce the amount of current required to drive the dot upward, while the downward direction used a spring force or a heavy physical load. As shown in Figure 2.16 (a), the inductive coil winding of solenoid had permanently magnetized actuating rod in order to provide an opposite flux for tactile dot driving (Thompson, 1995). A flanged stop was located at the bottom end of the rod and passed through the hole of the tactile board. In this manner, when current was applied into the coil, the amount of electromagnetic force increased in the strength of the permanent magnetic rod. The dot pin in its lower position was raised up above the reading surface. By stopping the applied current, the pin dot dropped to the normal state with the total weight of the actuating rod. Another technique for Braille display was performed with the commercial miniature dc solenoids actuator as shown in Figure 2.16

(b) (Frisken-Gibson et al., 1987). The dot was driven up by dc current of 80, 100, or 120 mA, and the downward force of a non-linear spring were provided for this system.

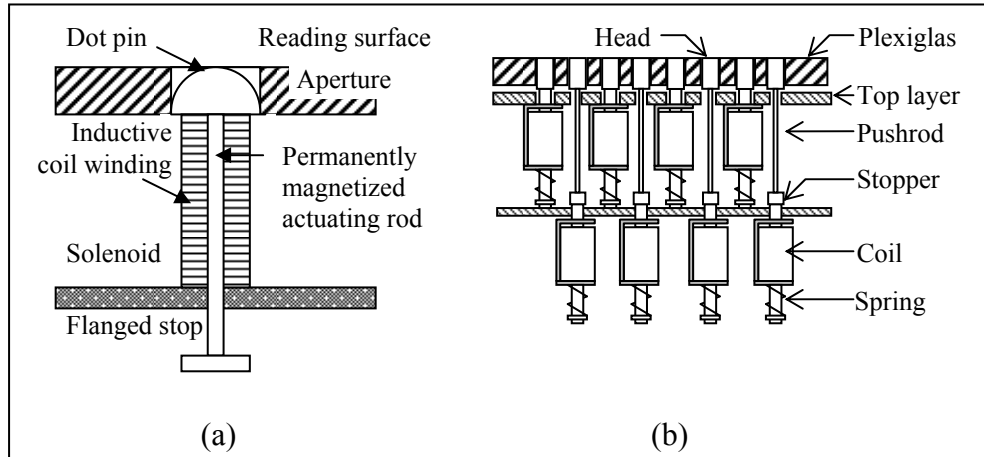


Figure 2.16 The Braille dot using electromagnetic solenoid (a) cross-sectional view and (b) the commercial miniature dc solenoids actuator for Braille display.

A flanged stop was located at the bottom end of the rod and passed through the hole of the tactile board. In this manner, when current was applied into the coil, the amount of electromagnetic force increased in the strength of the permanent magnetic rod. The dot pin in its lower position was raised up above the reading surface. By stopping the applied current, the pin dot dropped to the normal state with the total weight of the actuating rod. Another technique for Braille display was performed with the commercial miniature dc solenoids actuator as shown in Figure 2.16 (b) (Frisken-Gibson et al., 1987). The dot was driven up by dc current of 80, 100, or 120 mA, and the downward force of a non-linear spring were provided for this system.

2.5.2.7 Electrorheological (ER) fluid

Electrorheological fluid was suspension of solid particles of the order of 1-100 μm in an electrically insulating fluid such as silicone oil, mineral oil and kind of paraffin's (Block and Kelly, 1988). The viscosity and yield stress which were

rheological properties of these fluids could be changed when imposed to external electric fields. Based on the phenomena of dielectric polarization mechanism, the dispersed particles were aligned in line in the direction of the electric field, thereby fluid flow between the two electrodes was restricted as shown in Figure 2.17.

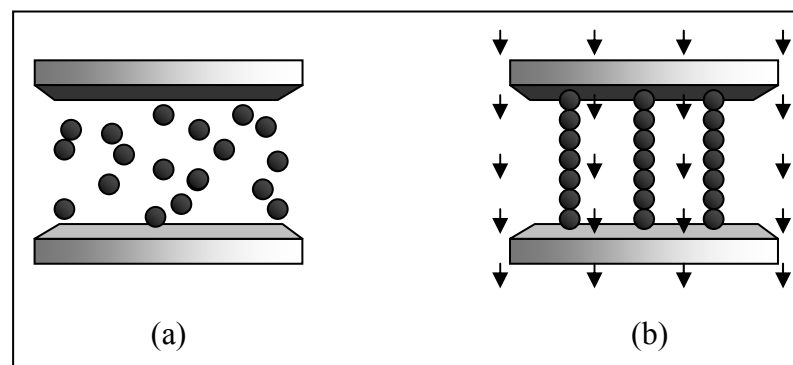


Figure 2.17 Forming of electrorheological fluid (a) without applied electrical field and (b) with applied electrical field.

According to Fricke (1993) and Garner (1996), a tactile display which utilized ER fluid to activate the tactile dot had a structure as shown in Figure 2.18 (a). The ER fluid which was stored in a sink was transported by a low pressure pump into the supply manifold. In normal state, the ER fluid flowed continuously into the dot actuator chamber from the supply manifold through the flow restricting orifice, and downward to the passageway through the exhaust orifice. The area of the exhaust orifice which was formed by a common ground electrode and a conductive dot electrode was used to apply a voltage to restrict the ER fluid resulting in increasing of the pressure inside the dot actuation chamber. An elastic diaphragm which was attached to the upper surface of a nonconductive plate would be deflected used as a tactile dot. Another embodiment based on ER fluid was shown in Figure 2.18 (b). An uppermost plate which had a hole extending with a spring-load pin inside was positioned above, and mounted on an elastic diaphragm. With actuation

as described above, the pin was extended above the upper surface of the uppermost plate to be sensed by the reader, and the spring provided a downward force to the pin to ensure that it returned to normal position.

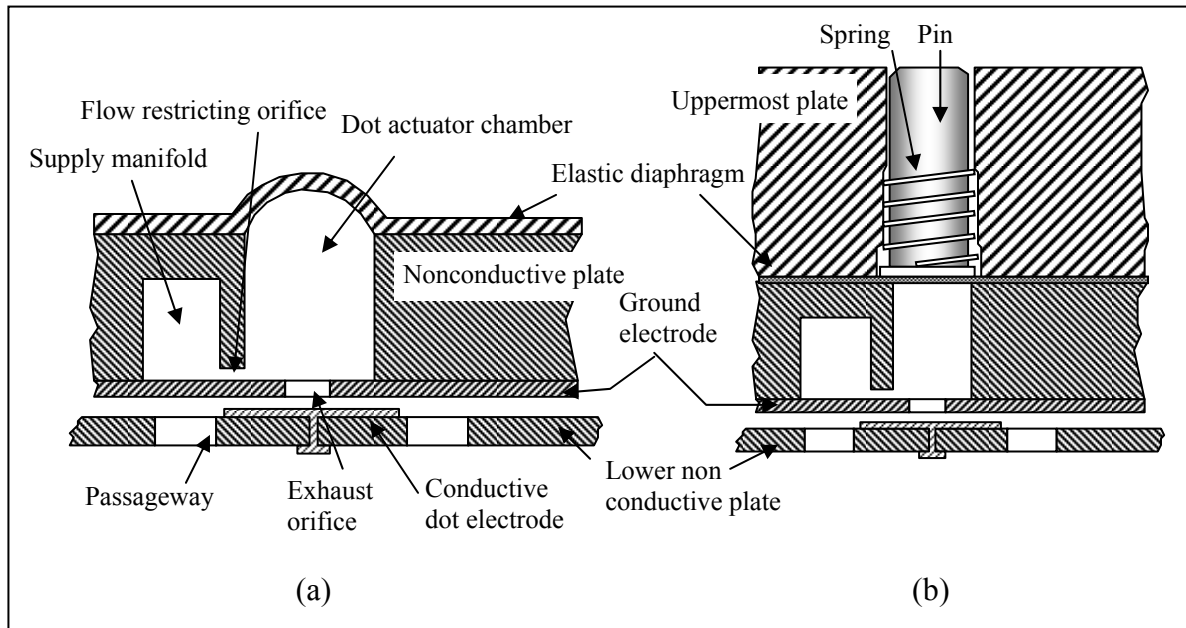


Figure 2.18 A tactile display utilized ER fluid (a) cross-sectional view and (b) a spring-load pin inside the uppermost plate.

2.5.2.8 Pneumatic Braille display

Pneumatic Braille display was performed by external pressure to raise the tactile dot. The housing of the tactile dots provided actuator chamber to keep sufficiently large internal pressure which could develop pressure difference across the Braille screen. The pneumatic tactile dot concept depicted in Figure 2.19 could perform with the principle of raising individual pins or dome shapes out of the surface. Figure 2.19 (a) shows the tactile dot in the early principle with the raising individual pins (Sutherland, 1972). The pneumatic mechanism consisted of movable pins which were placed in cylindrical tubes and arranged in 2×3 array configuration of Braille cell. A plurality of pneumatic channels connected to the bores through a small passage at the central body part.

Each pin could be selectively raised to projecting positions by pneumatic signals. Each Braille cell could operate to lock the pins in their positions.

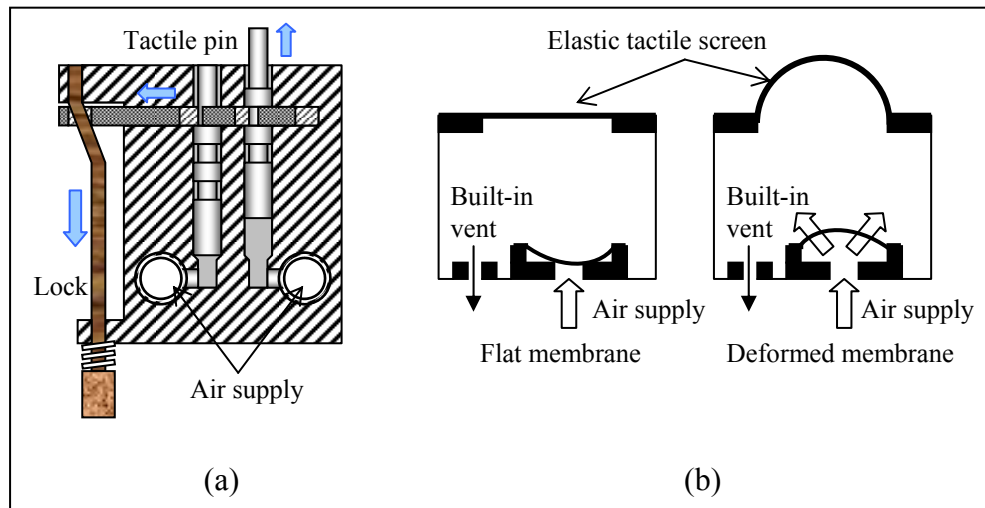


Figure 2.19 Pneumatic Braille displays (a) using raising individual pins in the early principle and (b) using an array of actuators and an elastic membrane.

Another mechanism for the pneumatic Braille display as shown in Figure 2.19 (b) showed the basic concept of raising dome shapes using a pneumatic actuator and an elastic membrane (Yobas et al., 2003). This method prevented the actuator that might be damaged from the mechanical load of the touch, and increased the stroke length and force of the actuated dot. In this work, sufficiently large pressure in the open state of the actuator could be developed across the screen and the membrane was elastically deformed out of the surface. To get back to a flat status of the Braille screen, the actuator was closed and the pressure trapped inside the actuator was vented out through the built-in vent.

2.5.2.9 Shape memory alloy (SMA)

Shape memory alloy was an alloy that remembers its shape in the original state after the metal was bent into a variety of new shapes. The two phases occurred in SMA which were Martensite and Austenite could be transformed through a

solid state phase change of a molecular rearrangement. The molecular in Martensite phase was twinned in its cold state, cubic structure as shown in Figure 2.20, which was the relatively soft and easily deformed phase of SMA. If SMA was deformed to any shape, the phase structure would be changed to the deformed martensite in which the structure was not cubic and hold that shape until it was heated above the transition temperature. At high temperature, the SMA was recovered to its original shape with the cubic structure like as the martensite phase, but it was stronger than the martensite phase. That was the austenite phase. This phase at high temperature occurred by electric current which directly flows in the SMA without any heater. When the SMA cooled down to normal temperature, it remained in the hot shape until deformed again. This property of SMA had been used to drive many movable mechanisms of actuator including the tactile dot actuation. If SMA straight wire was deformed as a micro-coil, it could be used as an actuator to keep the up or down state in linear motion by a control of applied current.

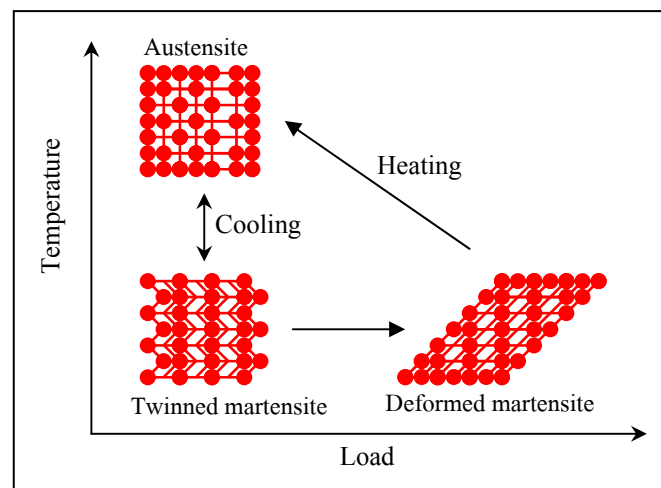


Figure 2.20 Microscopic diagram of the shape memory effect.

The Braille dot mechanisms with SMA are shown in Figure 2.21 (a) by Haga et al. (2004). SMA was deformed in micro-coil actuators that were fixed between two printed circuit boards. Each SMA coil was inserted with insulated metal pins and was

compressed from the length of the memorize shape, and the middle of SMA was grounded for current flow to the upper or lower half of the SMA coil. The upper section of pin provided a magnetic tube for holding position to the permanent magnet, which could be attracted and fixed the position with magnetic force greater than the SMA spring force in the normal state. In the normal state without dot display, the SMA coil stayed in the lower half of the SMA coil result in recovering to the memorized shape with the recovering force greater than the magnet force as shown in Figure 2.21 (a). The magnetic attraction happened to the magnetic tube in upper position of the pin although the driving current was already cut off. In a contrary manner, when the electrical current was applied in the upper half of the SMA coil, the pin was driven up by the recovering memorized of SMA, as shown in Figure 2.21 (b). The pin could be held in position even if the driving current was cut off.

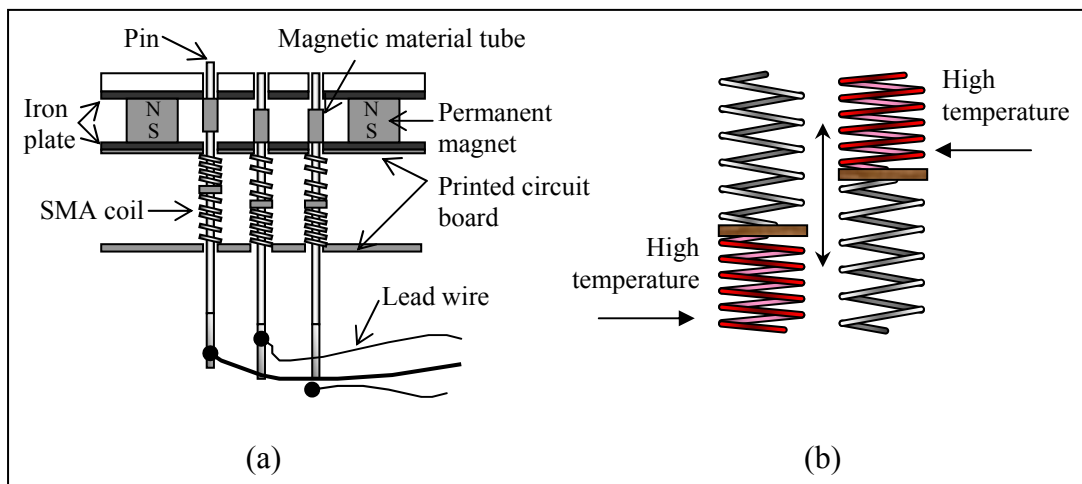


Figure 2.21 SMA based Braille display (a) structured view and (b) contraction energizing of the SMA coil.

2.5.2.10 Lateral skin deformation

Lateral skin deformation was realized exclusively as flexible elements in comb structure as shown in Figure 22 (a), which had teeth of flexible slabs arranged in line with narrow space. Some of the sensation could be generated by moving element of the teeth at mid length. By lateral running under the index finger, the resulting sensation could give the feeling to fingers that implied the Braille dot characteristic. This simple experimentation was a concept for tactile display device using distributed lateral skin stretch which had different mechanism from the conventional tactile display. The material which was used to create a deformable structure was based on the piezoelectric material with bimorph structure as shown in Figure 22 (b). It could achieve substantial displacement by mean of bending of cantilever under electrostatic filed. The resulting motion could be directly used to stretch the skin without requiring for extra motion amplification mechanism and operated over a large bandwidth to vibrate for the sensation (Pasquero and Hayward, 2003).

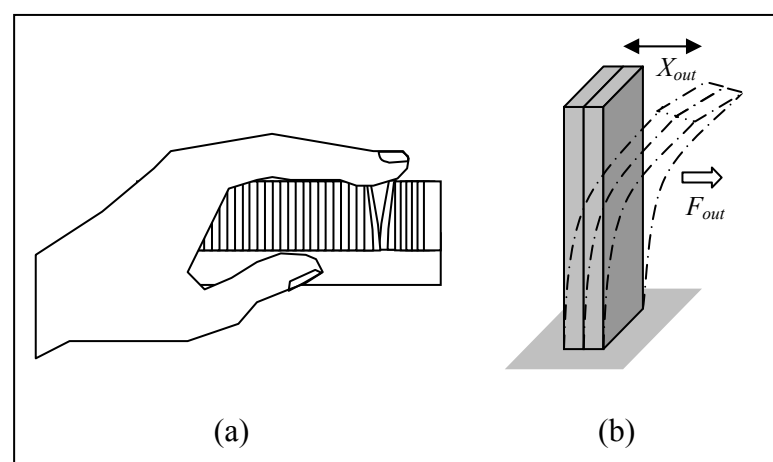


Figure 2.22 Braille display based on lateral skin deformation (a) reading the dot by skin sensation and (b) a lateral displacement to the load of piezoelectric bimorph.

Thick piezoelectric bender plates were arranged in stack which their base were separated by insulated polymers (Levesque et al., 2005) and clamped between two rigid endplates as shown in Figure 2.23 (a). The actuators were driven separately by the voltage applied between electrodes to generate the vibro-tactile to the fingertip as shown in Figure 2.23 (b). Although the lateral skin deformation could create Braille dot sensation, only one line of actuated contactors could be used at a time. Levesque et al. (2007) extended this work to the display of complete 6 Braille dots using a general purpose 2-D tactile transducer called STReSS² which had an array of 10-by-6 independent skin contactors to apply lateral skin deformation.

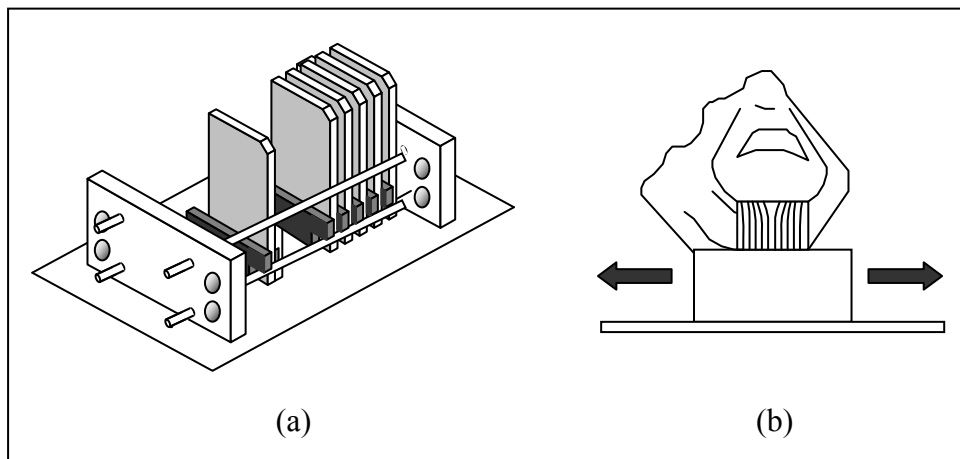


Figure 2.23 Thick piezoelectric bender plates (a) assembly of the virtual Braille display and (b) strain applied during finger contact.

2.5.2.11 Servo motor

Servo motor was used to vertically actuate a 6×6 array of mechanical pins based on the Braille character (Wagner et al., 2003) as shown in Figure 2.24. The steel piano wires of one millimeter diameter were utilized to invent the mechanical pins. Each pin was connected at the end closest to the servo through a hole in the plastic arm that was configured in a Braille cell. The commercially available radio-

controlled (RC) small servomotors were used to actuate an array of mechanical pins. Each servo motor was tightly packed and arranged in the servo block. The corresponding servo was controlled by the duty cycle of a PWM voltage signal which was generated by logic implemented on Xilinx programmable gate array. The height of each pin was set by the rotational motion of the servo which in turn translated into vertical motion. However, a drawback of this Braille display was the large number of servos result in a package that was too large for real applications.

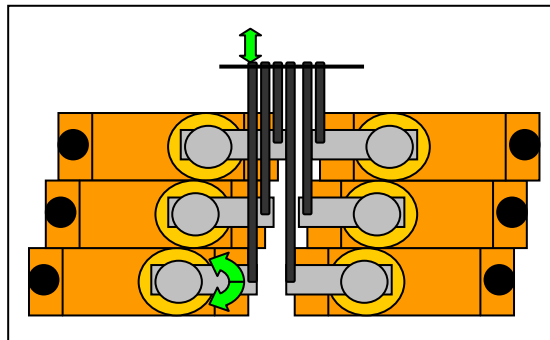


Figure 2.24 Driving mechanism of servo motor based Braille dots.

2.5.2.12 Bimetallic strip

Bimetallic strip was a cantilever of metal which consisted of two different sheets that had been bonded together. Difference between the coefficients of thermal expansion (CTE) of each sheet was a key factor causing one side of the strip to lengthen more than another when heat was applied (Cohen, 2003). A stress created on the strip bent the beam with the highest deformation at the center. This motion was utilized for a large displacement with linear motion by the changes in temperature. The tactile display mechanism was constructed in a simple block with a hole position for a plastic rod that is attached on top of a bimetallic strip as shown in Figure 2.25 (a).

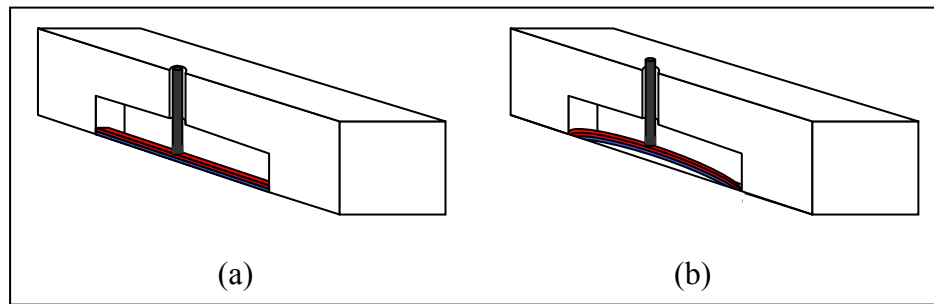


Figure 2.25 A Braille dot based on a principle of bimetallic strip

(a) unheated and (b) heated with raised rod.

The bimetallic strip was fixed at bilateral ends, so that it could not move around. To obtain the changes in temperature on the strip, three heating wires with coated insulation were put together as a heating element. The maximum deformation of the bimetallic strip achieved as the strip was heated, so that the pin was raised over the screen display as shown in Figure 2.25 (b). The normal state could be attained when the power to the bending elements was switched off. However, this method did not provide enough mechanical loads for the touch sensation. The vibration with a very fast refresh rate was needed in order to ensure that the rod can make a sufficient sensation against the fingertip of the readers.

2.5.2.13 Electrocutaneous

Electrocutaneous was a method to provide a sensation of feeling by passing electric pulse through the skin (Ostrom et al., 1999; Kajimoto et al., 2001). By activating via array of electrode to the fingertip, a nerve axon that was connected to mechanoreceptors in the human skin generated an Activating Function (AF) which was related to nerve activity. When electrical current was applied from electrode to the skin surface with the three stimulation modes as shown in Figure 2.26, three types of mechanoreceptors were stimulated by different polarity of the electrodes in three modes including SAI, RAI and RAI modes, respectively. The SAI mode was depth-selective

stimulation by adding anodic current around a central cathodic current resulting in stimulation of the shallower region of the Merkel cell (SAI). If the cathodic current was added around the central cathodic current on the contrary, a deeper region of Pacinian corpuscle can be stimulated for RAI mode. The RAI mode was performed by adding anodic current around the central cathodic current to stimulate the Meissner corpuscle.

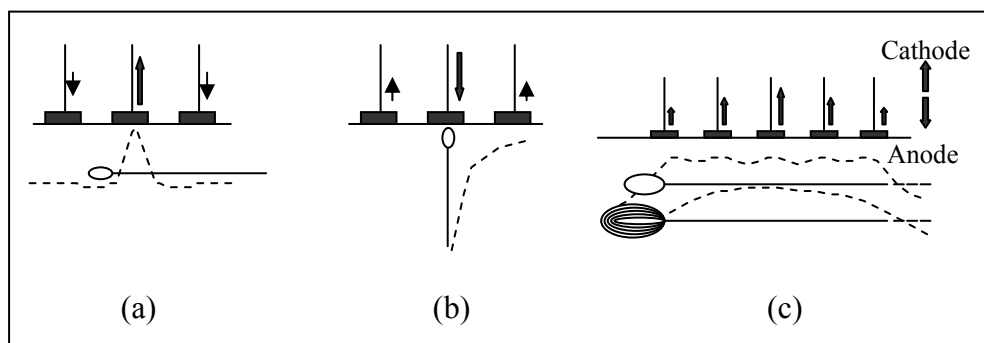


Figure 2.26 A Braille dot based on electrocutaneous stimulation (a) anodic-current stimulation for SAI mode (b) cathodic-current stimulation for RAI mode and (c) deeper-region stimulation or RAII mode.

The tactile display consisted of a 2D array of rod electrodes and each stimulation mode was defined as in Figure 2.27 which was controlled by the interference of the current between electrodes.

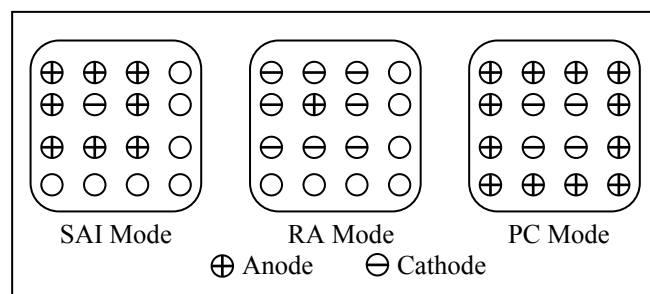


Figure 2.27 Stimulation modes of an electrocutaneous Braille dot in a 2D case.

2.5.2.14 Air jet tactile display

Air jet tactile display was a stimulator relied on air jets compress the skin locally without mechanical contact (Asamura et al., 1998). By controlling air pressure in the caves between the skin and stimulator with two kind of stimulation as shown in Figure 2.28 (a) and (b), the tissue of mechanoreceptors lie beneath the skin as shallow receptors and deep receptors could be stimulated. The air pressure only stimulated shallow receptors, while the vibration stimulated both shallow and deep receptors. Therefore, the vibrator was a method of selective stimulation. The device provided a rigid display surface and depression as shown in Figure 2.28 (c). The fingertip had a close contact on the display surface. Air pressure was passed through a small valve which was driven at low frequencies to generate the vibration stimulation. The resulting sensation felt on the skin similar to a creeping of a small bug.

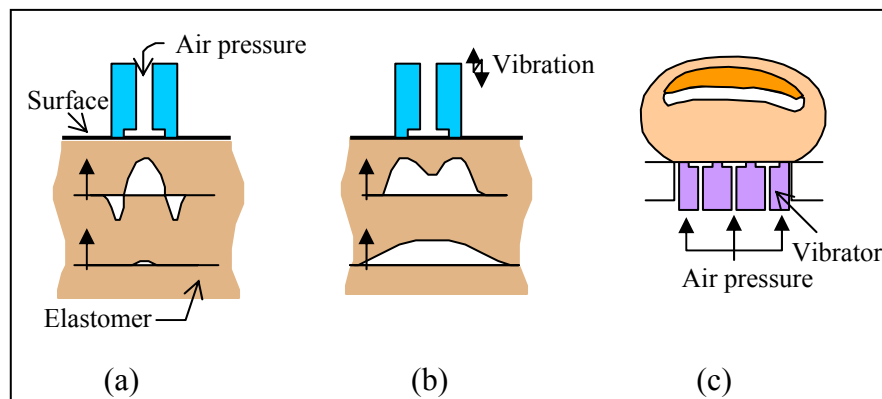


Figure 2.28 Air jet tactile display (a) the air pressure stimulation (b) the vibration stimulation and (c) schematic diagram of air jets stimulator.

2.6 The Braille Display Utilizing MEMS Technology

At the same time, many alternatives designed for multiline RBDS have been demonstrated in publications. All of them have shared the process of raising tactile dot with desired characteristics including with efficiency, low cost, light weight, low power and

integration capability. These kinds of systems would be almost impossible if MEMS technologies have not emerged. MEMS technologies revolutionize every product category with micromachining technique, supporting the realization of complement system-on-a-chip with the development of smart products. As a batch fabrication process, the technique similar to be used for the integrated circuit, MEMS can be used to make a large number of miniaturized devices at a time.

An example of MEMS technologies that have been commercially applied to Braille display is the refreshable Braille display with integrated microvalves at the iACTIV Corporation (<http://www.iactivcorp.com>). The refreshable Braille cell is assembled in the Braille module to show character on the screen. Figure 2.29 shows schematic example of a Braille cell of pneumatic actuation. The cell has three main parts including an elastomeric polymer, orifices, and micro-electro-mechanical actuators. The operation of this device based on the pneumatic Braille display has been discussed as described in Section 2.5.2.8.

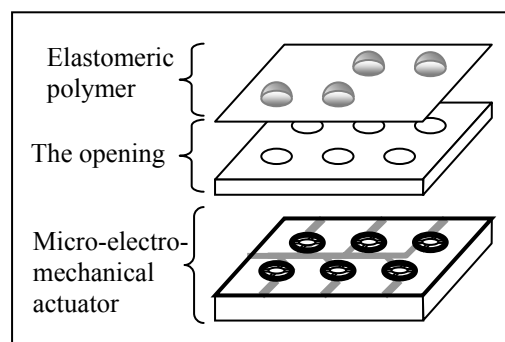


Figure 2.29 Schematic of the commercial refreshable Braille display of the iACTIV corporation.

Nevertheless, some applications of MEMS to tactile display were encountered several limitations. First, microstructures in actuating mechanism may be damaged from mechanical load touch because MEMS actuators are miniaturized devices. Second, the linear

motion or stroke length and force of the actuation may not be large to stimulate touch sensation. Moreover, the total cost of tactile system is still high although it has been promising for tactile display system.

2.7 Motivations for LIGA Braille Display

As mentioned in Section 2.5 and 2.6, the fabrication process of the refreshable Braille display has been mainly based on IC technology. Many of them have been fabricated with special techniques such as piezoelectric and solenoid actuation, which require specific material resulting in high cost, high technology, and difficulty of maintenance. Therefore, the simpler technique of dot raising have to be invented in order to deliver low cost and valid performance of touch sensation. In this thesis, fabrication techniques based on synchrotron X-ray lithography have been developed to meet such requirement.

LIGA (Lithographic Galvanoformung Abformung) process is the effective technology based on synchrotron radiation to fabricate thick and high-aspect-ratio microstructures. By exposing X-ray radiation through an X-ray mask onto a thick photoresist film, desired photoresist microstructures can be formed and used as electroplating mold to obtain corresponding complement any metallic version. Such photoresist and metallic microstructures can be replicated into a large amount by means of casting hot embossing or mold injection techniques using materials including plastic, ceramics or other materials. Figure 2.30 illustrates fabrication steps of the LIGA processes.

This research concentrates on application of LIGA technique in realization of the refreshable tactile dot for Braille display which is done at the beamline BL-6 of the Synchrotron Light Research Institute (Public Organization), Ministry of Science and Technology, Thailand. The Braille mechanism is designed to fabricate for two types of Braille dot actuation. The first one is the polymer Braille dot which is generated by

applying a different pressure inside the cavity across the tactile screen to deform an elastic membrane. The second one is the piston Braille dot which carries out a moving part of rigid element against the fingertip. All of these are based on the X-ray lithography process to enable the repeated fabrication and non-complicated technique to bring out a new system that invents tactile display as a new interface for visually impaired people.

2.8 Chapter Summary

In this chapter, overview of the state-of-art in tactile display modalities and Braille display applications has been investigated. Basic knowledge of tactile perception of human with mechanoreceptors under cutaneous skin has been given in order to understand the relationship between human sensation and the tactile dot stimulation. The tactile mechanisms have been described with the principle of raising individual pins or dome shape in presenting for text and graphics applications. However, the majority of research and developments have experienced several restrictions which limit their possibility to become commercial products. Although MEMS technologies have been shown significant role with high efficiency integrated tactile display, some limitations still exist in some application areas. To breakthrough various problems with special techniques of fabrication, X-ray LIGA process has been proposed to deliver the performance of the repeated fabrication by micro-molding and electroforming technique. It is possible that batch fabrication and non-complicated aspects of X-ray LIGA lithography will bring out new system that invents tactile display as a new interface in every day life for the visually impaired.

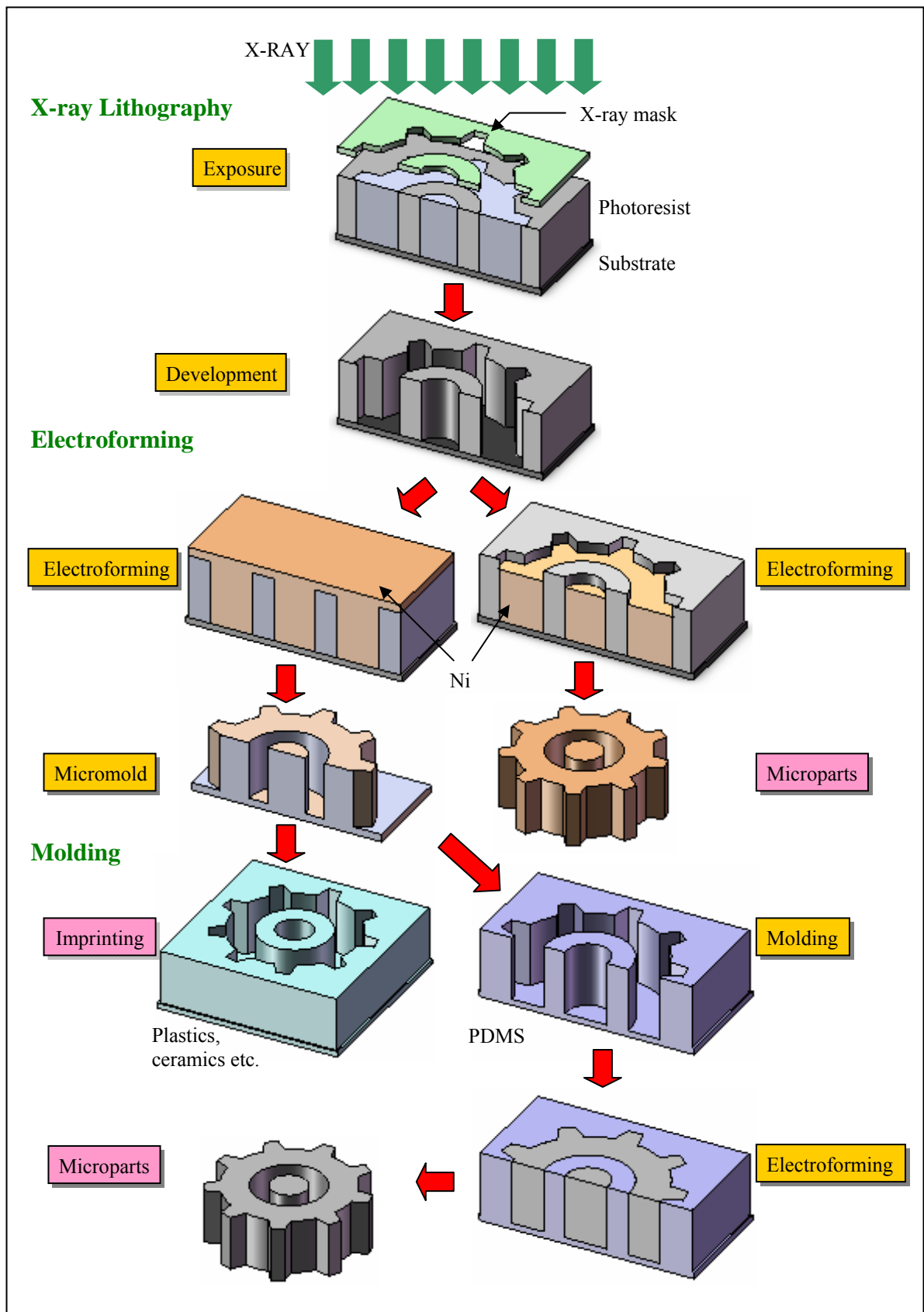


Figure 2.30 LIGA fabrication sequences.

CHAPTER III

DEVELOPMENT OF 3D X-RAY LIGA PROCESS

3.1 Introduction

In order to accomplish pneumatic tactile display by using X-ray lithography, specialized micromachining process must be developed. Four processes for the realization of 3D X-ray LIGA are discussed in this chapter. Transparent X-ray masks with silver absorber which is a key feature for transferring patterns into the thick film photoresist are described in the upcoming section. Section 3.3 describes a new construction concept of 3D complicated microstructures. A method to control final film thickness is introduced, and fabrication of 3D complicated test structures is demonstrated. Section 3.4 proposes a method to create the bonding between a PDMS and SU-8 which is becoming a useful tool for a pneumatic tactile display. Section 3.5 describes a fabrication process of micro-piston by etching of silver sacrificial material. This process is used to fabricate moving-part for a single tactile mechanism and control separation between piston and cylinder for single dot display. To realize the capability of the repeated process, the application of LIGA process for the multilayer gear is proposed in Section 3.6. This process helps to reduce the cost and ease of fabrication by using the simple process of micro-machining. Finally, the summary of this chapter will be presented.

3.2 X-ray Masks on a Transparent Substrate

X-ray lithography is the first step of LIGA fabrication based on synchrotron radiation to applying for the three-dimensional photoresist structures. For mask fabrication, patterns have been designed and transferred by UV lithography onto the mask for imaging

of the absorber patterns. The X-ray lithography mask consists of two major parts, the absorber and the membrane as shown in Figure 3.1. The membrane must be transparent to X-ray, and it should have dimension stability and have mechanical strength for handling. Material with low atomic number and low densities such as silicon (Si), silicon nitride (SiN), silicon carbide (SiC), titanium (Ti), beryllium (Be), polyamine (PI), and graphite (C) are frequently used to make X-ray mask membrane. For X-ray absorption, the material must efficiently absorb X-ray to provide image contrast on the photoresist. Materials with high atomic number and high density such as gold (Au), silver (Ag), tantalum (Ta), tungsten (W), and lead (Pb) are employed in this role.

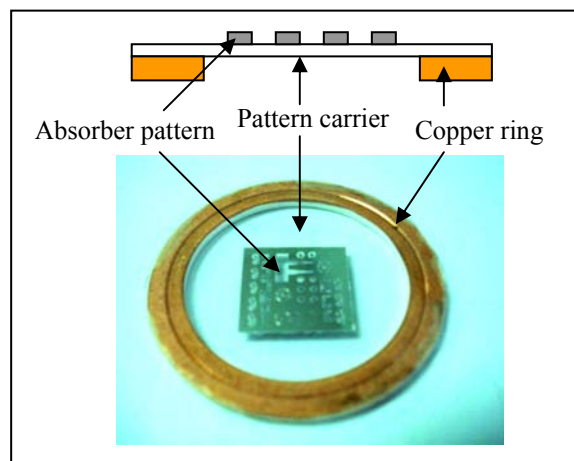


Figure 3.1 Components of an X-ray mask.

3.2.1 Power spectrum through various filters

For those different material membranes, Ti and Si compound membranes are highly transparent to X-ray for a thickness of few microns. However, they are expensive and difficult to handle. Be is the most favorable material due to the same reasons, but toxicity and cost are limitations. Moreover, graphite sheet is opaque to visible light, and difficult to apply in fabrication of multilayer LIGA structures. In the same way of absorber material, gold has been used as standard absorber of X-ray mask but its electroplating bath

solution is considered very expensive. However, Wanburee et al. (2007) have studied possibility of substituting gold absorber with silver whose electroplating bath solution costs about three-time lower. This technique is an alternative tool for development of a low-cost X-ray mask.

In order to improve the performance of X-ray mask but still remain the pattern resolution, the process which uses a transparent sheet of polyester (PET or Mylar[®]) and polyimide (PI) as the membrane, and silver as the absorber material is developed. To prove the characteristic of these materials, X-ray Oriented Programs (XOP) for X-ray calculation is used to compare the power spectrum between traditional materials (Au, graphite) and proposed materials (PET, Ag) as shown in Figure 3.2.

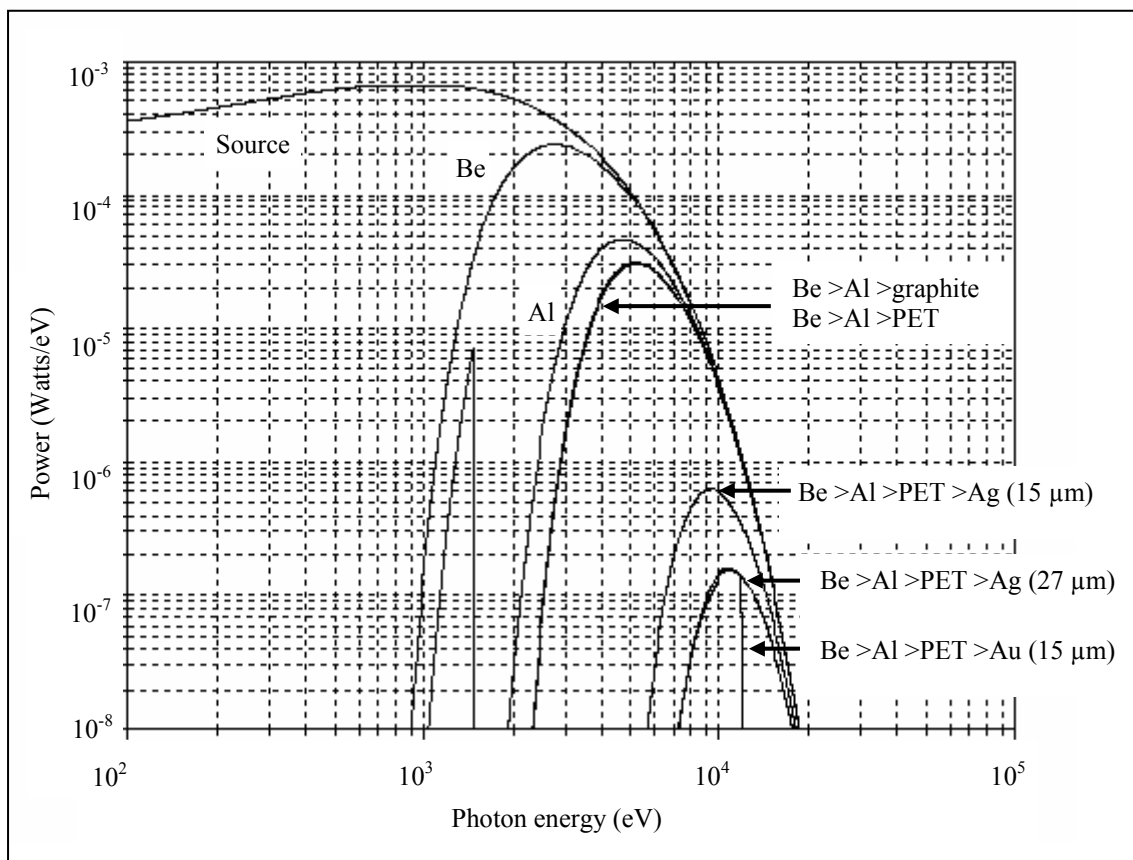


Figure 3.2 Power spectrum of lithography beamline BL-6 through various filters.

In X-ray lithography, synchrotron light has passed various filters before exposing on the photoresist. In place of gold absorber, comparable thickness of silver is used to selectively absorb the radiation for this research. PET sheet which is a common plastic material used in copier is used as a mask blank instead of graphite. From the simulation results, it could be observed that a 100 μm -thick PET filter has a power spectrum at the same level as graphite. This confirms that it can be used as a membrane material in place of graphite.

The next consideration is on absorber materials between gold and silver. As shown in Figure 3.2, a 15 μm -thick gold absorber which can absorb X-ray irradiation for 300 μm thick film photoresist is simulated to be the base curve. Silver absorber with a thickness of 15 μm is first simulated, but the result implies that its thickness has to be increased. By increasing the silver thickness to 27 μm , the spectrum curve of silver is decreased and arranged in line with gold curve. This result provides good expectation of substituting gold absorber with silver. Therefore, silver absorber and PET membrane show high potential to be used in X-ray lithography, especially for the multilayer X-ray LIGA fabrication.

3.2.2 X-ray mask fabrication

A scheme of the fabrication process is shown in Figure 3.3. The transparent films such as copier transparency and PI sheet is tightly attached to a copper frame which serves as a mechanical support as shown in Figure 3.3 (a). The seed layers of Ti/Ag are evaporated on the substrate, followed by deposition of AZ P4620 positive photoresist as shown in Figure 3.3 (b). The coating is then exposed to UV light to transfer 2D patterns onto the photoresist layer as shown in Figure 3.3 (c). After pattern development, silver material is electroplated with minimal thickness of 27 μm by using DC current as shown in Figure 3.3 (d). To keep the silver patterns from etchant solution, a 0.5 μm thick protective layer of nickel is electroplated on the top of silver patterns. The photoresist mold is

removed by acetone as shown in Figure 3.3 (e). The mask is released and rendered transparent by etching the seed layer of Ag and Ti in 3 : 1 NH_4OH : H_2O_2 and 3%v HF solution as shown in Figure 3.3 (f), resulting in the transparent X-ray masks membrane as shown in Figure 3.4 (a) for PET sheet and PI sheet as shown in Figure 3.4 (b).

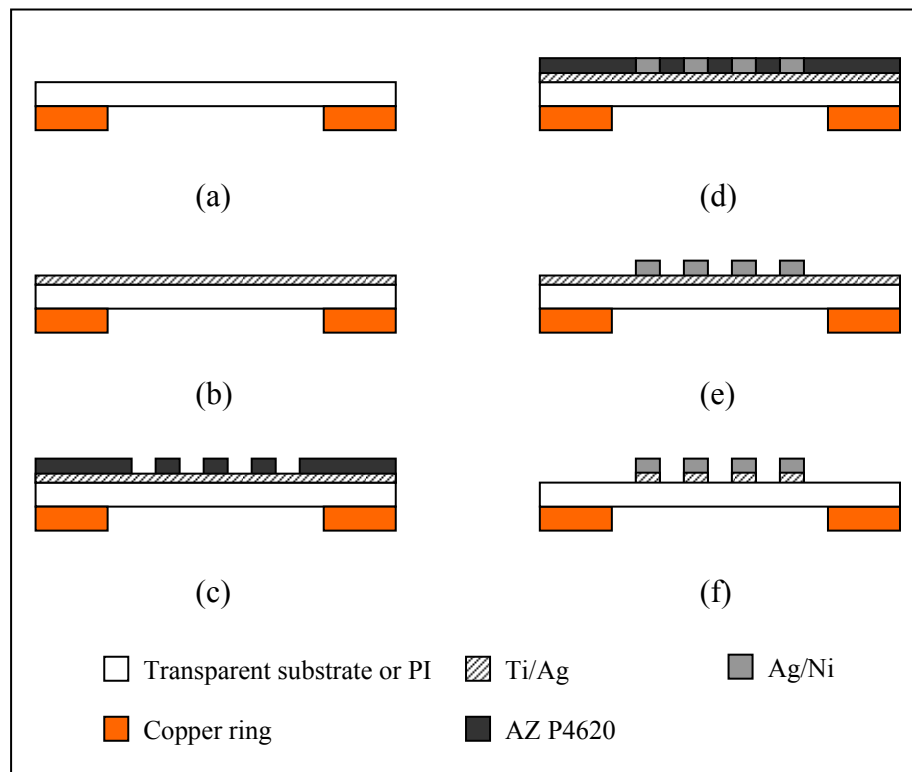


Figure 3.3 Fabrication sequences of the transparent X-ray mask.

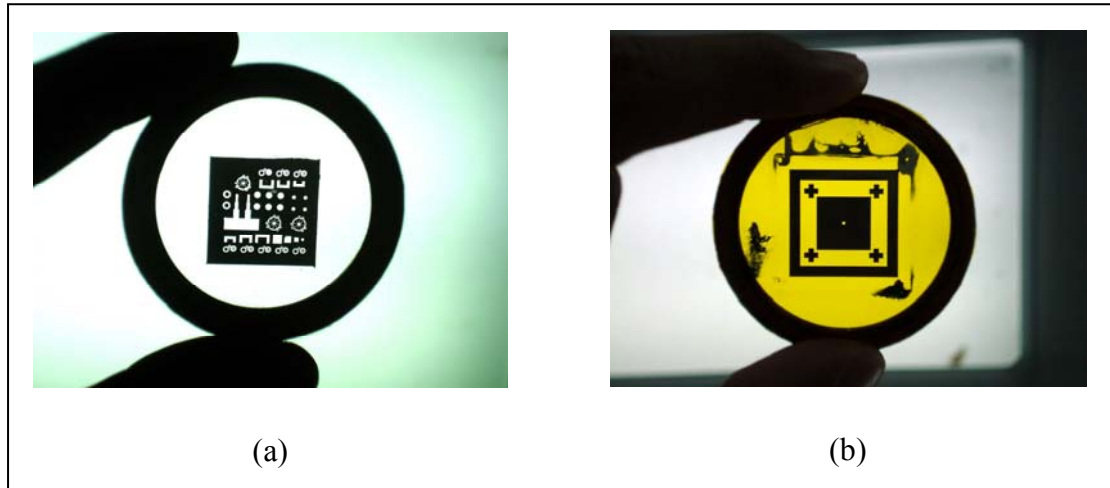


Figure 3.4 X-ray mask with silver absorber (a) on copier transparency and (b) on PI sheet.

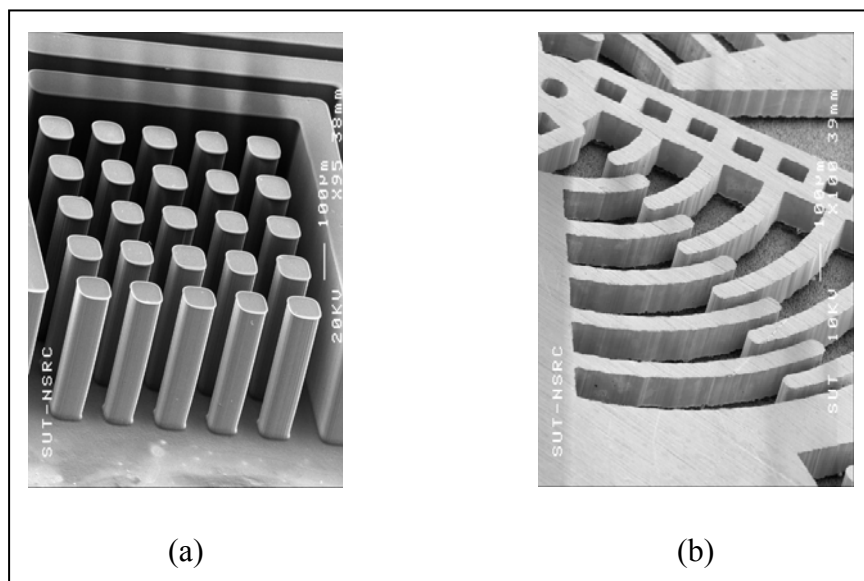


Figure 3.5 Samples of X-ray microstructures (a) The SU-8 300 μm -thick photoresist and (b) nickel microstructures with thickness of 150 μm .

3.2.3 X-ray lithography experiments

The transparent membrane mask with a thin silver absorber is used to pattern the thick film photoresist as LIGA microstructures which are prepared by using

SU-8 powder casting in the vacuum chamber that is discussed in Section 3.3. After X-ray exposure with suitable energy, the sample is post-exposure baked and developed to construct microstructures and it has been inspected using a scanning electron microscope as shown in Figure 3.5 (a). Furthermore, some photoresist molds have been filled with nickel material by electroplating, and SU-8 photoresist is removed by O₂/CF₄ plasma to obtain only metallic structures as shown in Figure 3.5 (b).

Silver material has been tested successfully to be used as X-ray mask absorber material include the transparent membrane of copier transparency and PI sheet. Obviously, the membrane mask has been transparent to X-ray with high mechanical strength support to the absorber. These deliver a positive outcome in fabrication of LIGA microstructure. Fabrication of multilayer polymer micro-parts will be demonstrated in the next section.

3.3 Three-Dimensional X-ray Lithography

X-ray lithography is a method which has been adopted in fabrication of MEMS devices, mainly in the fields of microfluidics and LIGA application. A microstructure of vertical side walls with a height ranging up to several millimeters can be obtained. However, fabrications of complicated 3D microstructures in polymer MEMS devices are difficult to achieve in X-ray lithography. Because the spin-coating is a standard method for photoresist preparation, the specific high thickness controls for multilayer are difficult and suffers from a large amount of spilled-away photoresist waste and long soft baking. In addition, fabrication of multilayer 3D microstructure may require that each layer is fabricated onto non-planar surface where microstructures from previous layer already exist. To avoid problems in spin coating that may give undesired results, a casting method from SU-8 powder with solvent content of 7% has been proposed by Charles et al. (2003).

In order to reduce photoresist waste, Chathirat et al. (2007) have proposed the method to control final film thickness by using the least weight of SU-8 powder in reflow casting. The mass of photoresist is needed to give the SU-8 layer with thickness slightly over that of the target is calculated from SU-8 density and an experimental correction factor. Then, excessive reflow casted SU-8 is polished by a finest standard abrasive paper to obtain the target film thickness with a mirror like top surface. In this section, mathematical models for thickness control which are used to sequentially prepare by multi-step powder casting and X-ray lithography are proposed. Three-layer all-polymer 3D microstructure is demonstrated to validate the model as shown in Figure 3.6 which is defined on three thickness levels as 500 μm , 300 μm and 300 μm , respectively.

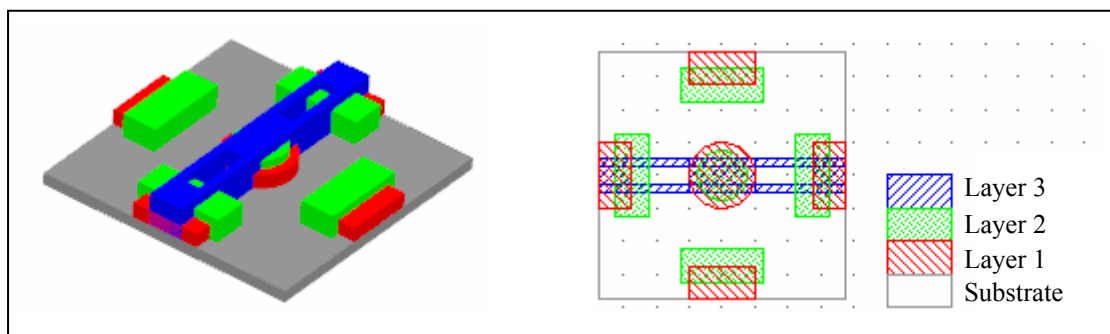


Figure 3.6 A model of multilayer powder casting of SU-8 thick film.

3.3.1 SU-8 powder preparation

SU-8 powder is prepared from SU-8 2100 in liquid form (MicroChem Co., Newton, MA) with a solvent content of 25%. Liquid SU-8 is poured onto a polyimide sheet laminated on an aluminum disc with an area of 400 cm^2 . The photoresist is spread over the polyimide sheet by extra slow speed spinning to prevent SU-8 waste from spilling out. The weight of wet SU-8 ($W_{initial}$) is measured excluding that of polyimide sheet and aluminum disc. During soft-baking at 95°C, the weight of SU-8 (W_{final}) is monitored and the remaining solvent content inside the photoresist film is calculated from $W_{initial}$, W_{final} and solid content

of the photoresist at 75% (MicroChem Corp.). A formula for solvent content calculation is given by Equation (3.1) (Charles et al., 2005). Soft baking time for solvent evaporation based on the initial weight is illustrated in Figure 3.7.

$$\text{Solvent content} = \left(1 - 0.75 \frac{W_{\text{initial}}}{W_{\text{final}}} \right) \times 100\% \quad (3.1)$$

The polyimide sheet is used to simplify peeling of dried SU-8 film off the aluminum disc. The peeling breaks dried SU-8 photoresist into small chips. In order to obtain more uniform photoresist layer, SU-8 chips are further broken into powder before reflow casting. All steps of SU-8 powder preparation are done in a clean room with yellow ambient light. The resulting powder is loaded into an opaque bottle and stored in a vacuum desiccator. Overall step of SU-8 powder preparation is shown in Figure 3.8.

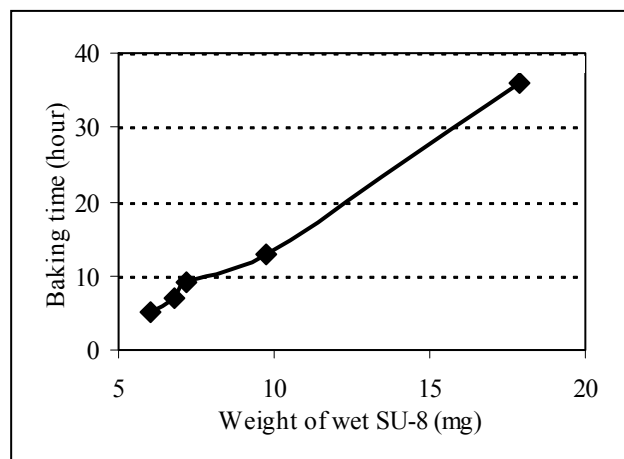


Figure 3.7 Duration time for soft bake of SU-8 powder preparation.

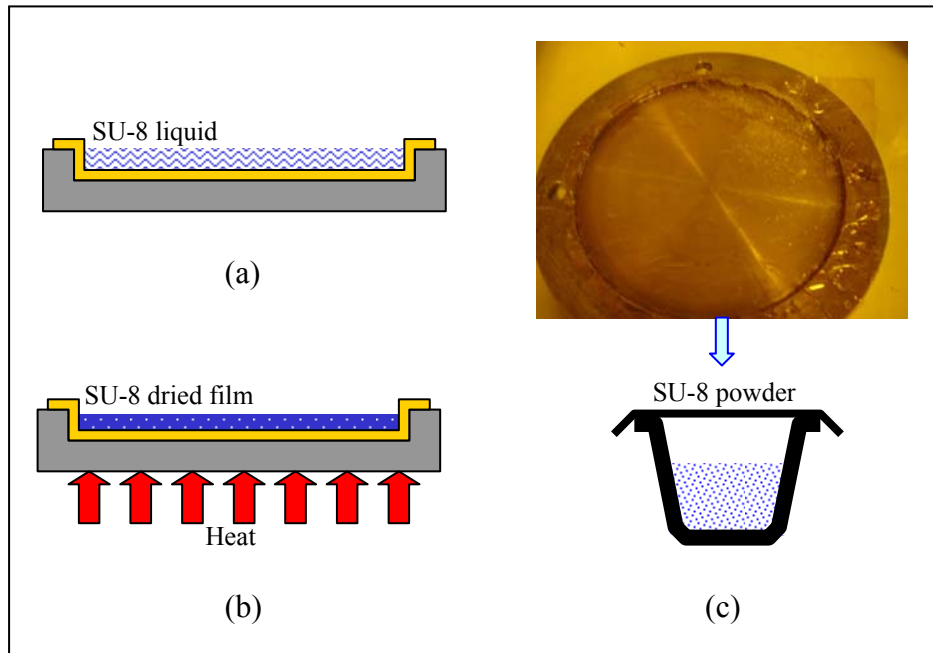


Figure 3.8 Sequence process for SU-8 powder preparation (a) SU-8 liquid content on PI tape laminated on aluminum disc (b) soft bake to reduce solvent content and (c) dried SU-8 photoresist into powders.

3.3.2 Single-layer reflow casting

Single layer of thick SU-8 photoresist is prepared by reflow casting in an area confined by a square polydimethyl-siloxane (PDMS) frame which is clamped on top of the substrate and pressed by aluminum clamp as shown in Figure 3.9 (a). Then, SU-8 powder is loaded into PDMS frame as shown in Figure 3.9 (b). Based on SU-8 density d of 1.2 g/cm^3 , PDMS frame area A of 4 cm^2 , correction factor f_c , the weight of SU-8 powder W_n (g) can be calculated to form a photoresist layer of the desired thickness t_n (cm) by Equation (3.2). The correction factor f_c accounts for error in density value of SU-8 powder and additional weight loss of SU-8 film during reflowed casting.

$$W_n(g) = f_c \cdot d \cdot A \cdot t_n(cm) \quad (3.2)$$

Then, the sample is placed on the heater located inside the vacuum chamber at a pressure of 30 mtorr to remove air bubbles that may be trapped in powder grains as shown in Figure 3.9 (c). The heater is turned on and the sample temperature is ramped to 120°C. During temperature ramping, SU-8 powder is melted and reflowed to form a continuous photoresist film. The molten SU-8 is allowed to reflow at 120°C until the absence of apparent air bubbles. The sample is then removed from the vacuum chamber and naturally cooled down to room temperature as shown in Figure 3.9 (d).

Resulting SU-8 film is allowed to further reflow by heating on hot plate at 95°C in ambient air for 10 minutes, followed by natural cooling to room temperature as shown in Figure 3.9 (e). The PDMS frame is then peeled off from the substrate and the film thickness is measured. Excessive photoresist is mechanically polished down to the target thickness which is the best solution to reduce SU-8 waste while preserving film thickness accuracy as shown in Figure 3.9 (f). The reflow casted photoresist film is now ready for X-ray lithography to form single layer microstructures.

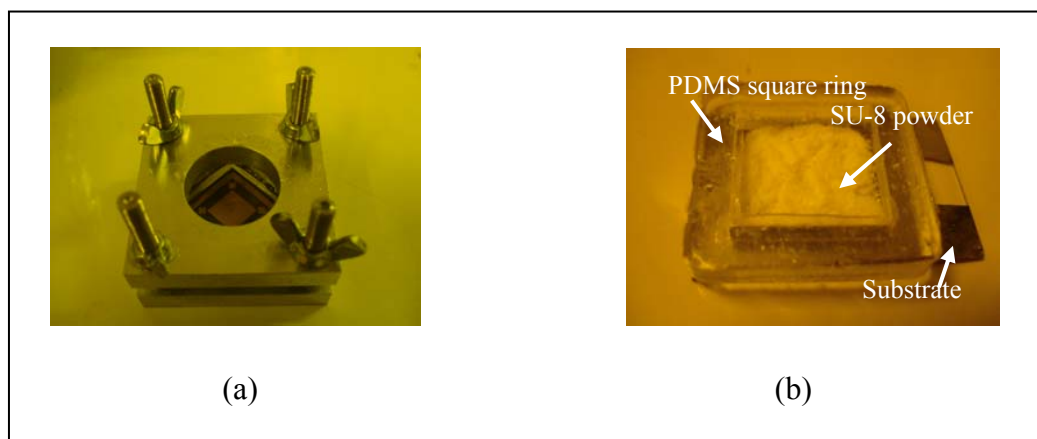


Figure 3.9 Fabrication sequences of single layer reflowed casting of SU-8 photoresist.

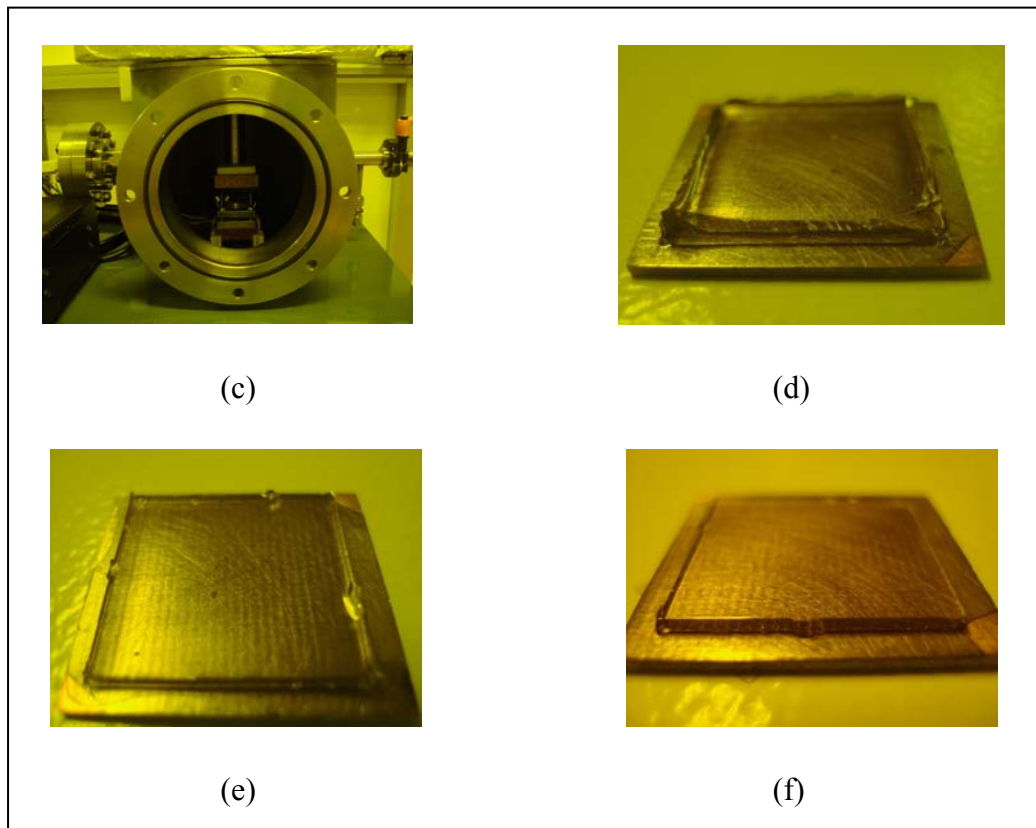


Figure 3.9 Fabrication sequences of single layer reflowed casting of SU-8 photoresist (Continued).

3.3.3 X-ray lithography of single-layer reflow casted SU-8 film

SU-8 microstructures are formed by exposing synchrotron X-ray onto the reflow casted photoresist film through the mask containing patterns of X-ray absorber. Figure 3.10 (a) shows the first X-ray masks containing 30 μm -thick Ag absorber on a 100 μm -thick transparency support.

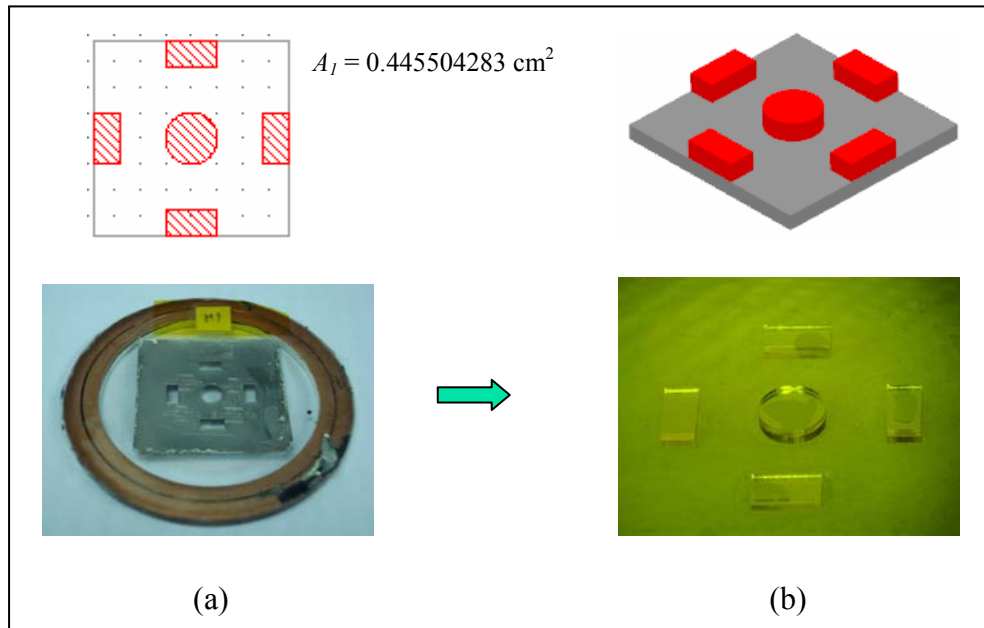


Figure 3.10 X-ray lithography of single-layer reflow casted SU-8 film (a) transparent X-ray masks and (b) the first microstructure after development.

After X-ray exposure, the sample is baked in an oven at 95°C and developed in SU-8 developer at room temperature, followed by a second wash with isopropyl alcohol (IPA) and dry with nitrogen gas. The first microstructure which is shown in Figure 3.10 (b) with thickness of $500 \mu\text{m}$ is hard baked or final cured in an oven at 95°C for 3 hours to ensure that SU-8 microstructures can sustain next reflow casting and X-ray lithography steps. The volume of existing SU-8 microstructures V_{PRI} is a multiplication of the first expose area A_I and thickness t_I as shown in Equation (3.3).

$$V_{PRI} = A_I \cdot t_I \quad (3.3)$$

3.3.4 Multilayer reflow casting

X-ray lithography sequences of the second layer reflowed casted SU-8 film are shown in Figure 3.11. To prepare next layer of SU-8 thick film, another PDMS frame of the same size is clamped on the sample and SU-8 powder of the appropriate weight is

loaded into the frame. Since some portions of the area has been occupied by existing microstructure as shown in Figure 3.11 (a), the new volume must include an empty volume of previous layer and a full volume of this layer.

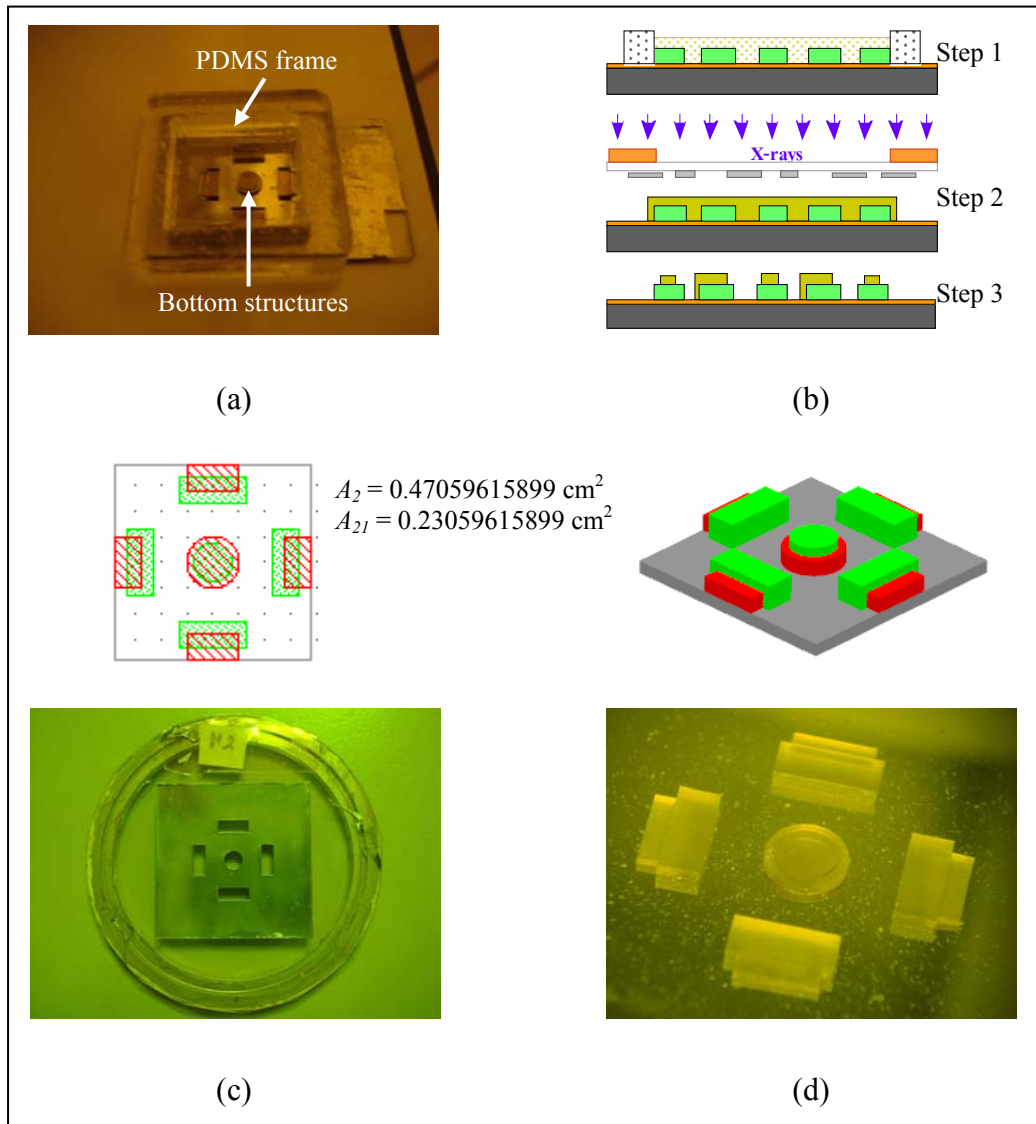


Figure 3.11 X-ray lithography of the second layer reflowed casted SU-8 film (a) SU-8 microstructures from previous layer enclosed by PDMS frame for next reflow casting (b) X-ray lithography steps for formation of multilayer complicated microstructures (c) the second X-ray mask and (d) the second microstructure.

To calculate this volume, an overall volume $A\left(\sum_{m=1}^n t_m\right)$ will be subtracted by a cumulative existing volume $\left(\sum_{m=1}^{n-1} V_{PR(m)}\right)$ of previous layer as illustrated in Equation (3.4) which is used to find the second volume in Equation (3.5). This also indicates that the appropriate weight of SU-8 powder can be achieved by Equation (3.6) which is in turn passed to Equation (3.7) for the second layer. Consequently, the SU-8 powder reflow casting will be reproduced again, followed by polishing of excessive photoresist to the desired thickness.

$$V_n = A\left(\sum_{m=1}^n t_m\right) - \left(\sum_{m=1}^{n-1} V_{PR(m)}\right) \quad (3.4)$$

$$V_2 = A \cdot (t_1 + t_2) - V_{PR1} \quad (3.5)$$

$$W_n(g) = f_c \cdot d \cdot V_n \quad (3.6)$$

$$W_2(g) = f_c \cdot d \cdot V_2 \quad (3.7)$$

After reflow casting process (step 1) as shown in Figure 3.11 (b), the second X-ray mask as shown in Figure 3.11 (c) is placed on the sample by alignment through a transparent membrane (step 2) for X-ray exposure, followed by film development (step 3). As illustrated in Figure 3.11 (d), some portions of the recent expose volume are placed on the previous layer and substrate with the thickness of 300 μm and 800 μm , respectively.

A summation volume of SU-8 micro-structures after development of n^{th} layer $V_{PR(n)}$ can be obtained by Equation (3.8) which is a summation of a cumulative volume of SU-8 micro-structures existing on the sample $\sum_{m=1}^{n-1} V_{PR(m)}$ and a total overlapping

projection volume of X-ray beam after development of n^{th} layer $\sum_{m=1}^n t_m$, and subtracted by a cumulative projection volume of SU-8 from multiple exposures $\sum_{m=1}^{n-1} A_{nm}t_m$.

$$V_{PR(n)} = \sum_{m=1}^{n-1} V_{PR(m)} + A_n \left(\sum_{m=1}^n t_m \right) - \left(\sum_{m=1}^{n-1} A_{nm}t_m \right) \quad (3.8)$$

The current expose area A_n and overlapping X-ray projection areas A_{nm} between layer n^{th} and m^{th} can be found by using layout drawing CAD with design area calculation tools such as the freeware LayoutEditorTM. Therefore, the summation volume of photoresist structures after development of the second layer is given by Equation (3.9).

$$V_{PR2} = V_{PR1} + A_2(t_1 + t_2) - (A_{21}t_1) \quad (3.9)$$

For the third layer which has the desired film thickness of 300 μm , 600 μm and 1000 μm on the second layer, the first layer, and the substrate, respectively, will be calculated the reflow volume V_3 by Equation (3.10) which is derived from Equation (3.4).

This volume conveys to the weight of SU-8 powder calculated by Equation (3.11)

$$V_3 = A(t_1 + t_2 + t_3) - (V_{PR1} + V_{PR2}) \quad (3.10)$$

$$W_3(\text{g}) = f_c \cdot d \cdot V_3 \quad (3.11)$$

$$V_{PR3} = (V_{PR1} + V_{PR2}) + A_3(t_1 + t_2 + t_3) - (A_{31}t_1 + A_{32}t_2) \quad (3.12)$$

After reflow casting and polishing process, the third X-ray mask as shown in Figure 3.12 (a) is aligned on the sample and exposed to X-ray radiation with an appropriate energy dose, followed by post-exposure baking and development. The exposed volume of the third layer is evaluated by Equation (3.12). Three experiments are carried out to define features with a total height of 1100 μm as shown in Figure 3.12 (b).

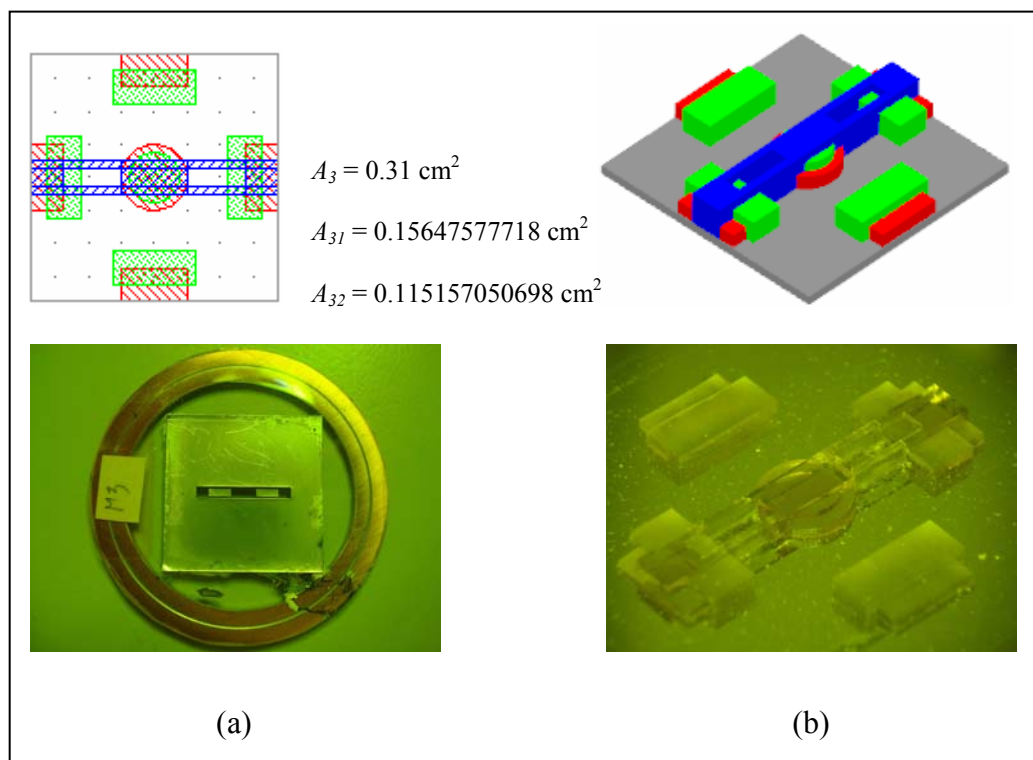


Figure 3.12 X-ray lithography of the third layer reflowed casted SU-8 film

(a) the third X-ray mask and (b) SU-8 multi-layer.

3.3.5 Experimental results

Fabrication steps of multi-step powder casting for complicated microstructure with five main processes are shown in Figure 3.13. Firstly, after the substrate is already pretreated with a suitable method, the SU-8 powder volume that is needed to fill inside PDMS frame is calculated by Equation (3.2) and (3.3). Secondly, the SU-8 powder is loaded into the frame with an appropriate weight by using Equation (3.6), and the reflow

casting process is carried out to prepare thick layer of SU-8. Then, the polishing of excessive reflow casted SU-8 is performed to obtain the target film thickness. Next, X-ray exposure is used to define SU-8 microstructures by alignment through a transparent X-ray mask. The exposed volume after development of n^{th} layer is added up to the total expose volume that can be found by Equation (3.8). Finally, if the next layer is required, the SU-8 volume for the next layer will be calculated by Equation (3.10) to find a suitable weight of SU-8 powder for the next reflow casting, and the first step will be repeated until the multi-step microstructures are completely fabricated.

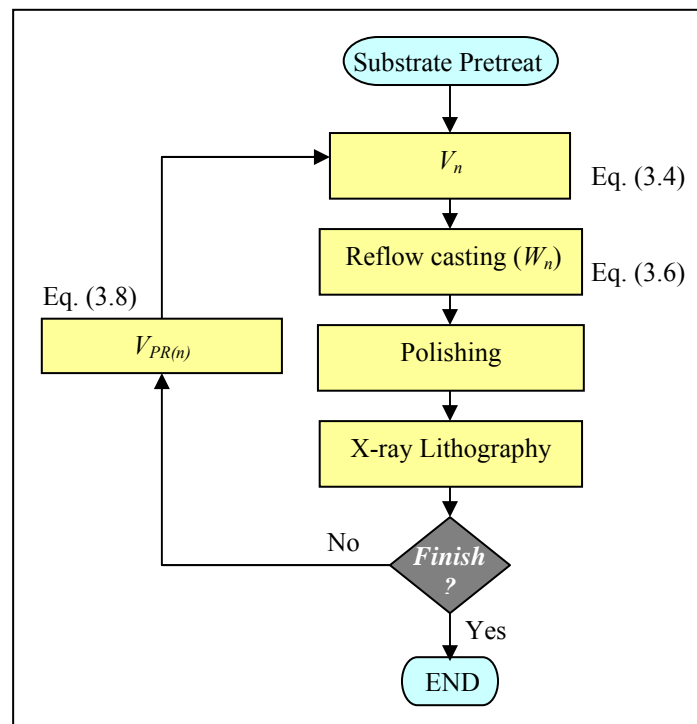


Figure 3.13 A flow chart for realization of multi-step microstructures by using SU-8 powder reflow casting technique.

In a reflow casting process, the correction factor f_c has been accounted for error in density value of SU-8 powder and additional weight loss of SU-8 film during reflow casting. The sample of 11 pieces have been sequentially tested to find a suitable f_c

value that cause only positive error as shown in Figure 3.14 (a)-(c). From the results, it could be observed that the thicknesses are increased from the dash lines to solid lines when it is placed on the hotplate for the reflow. This helps lower the correction factor to a value than 1.0 for the first and the second layer, while the value for the third layer is about 1.0 for making the thickness higher than the target film thickness. The best solution for this experiment is illustrated in Table 3.1 which causes positive errors in a range of 50-100 μm .

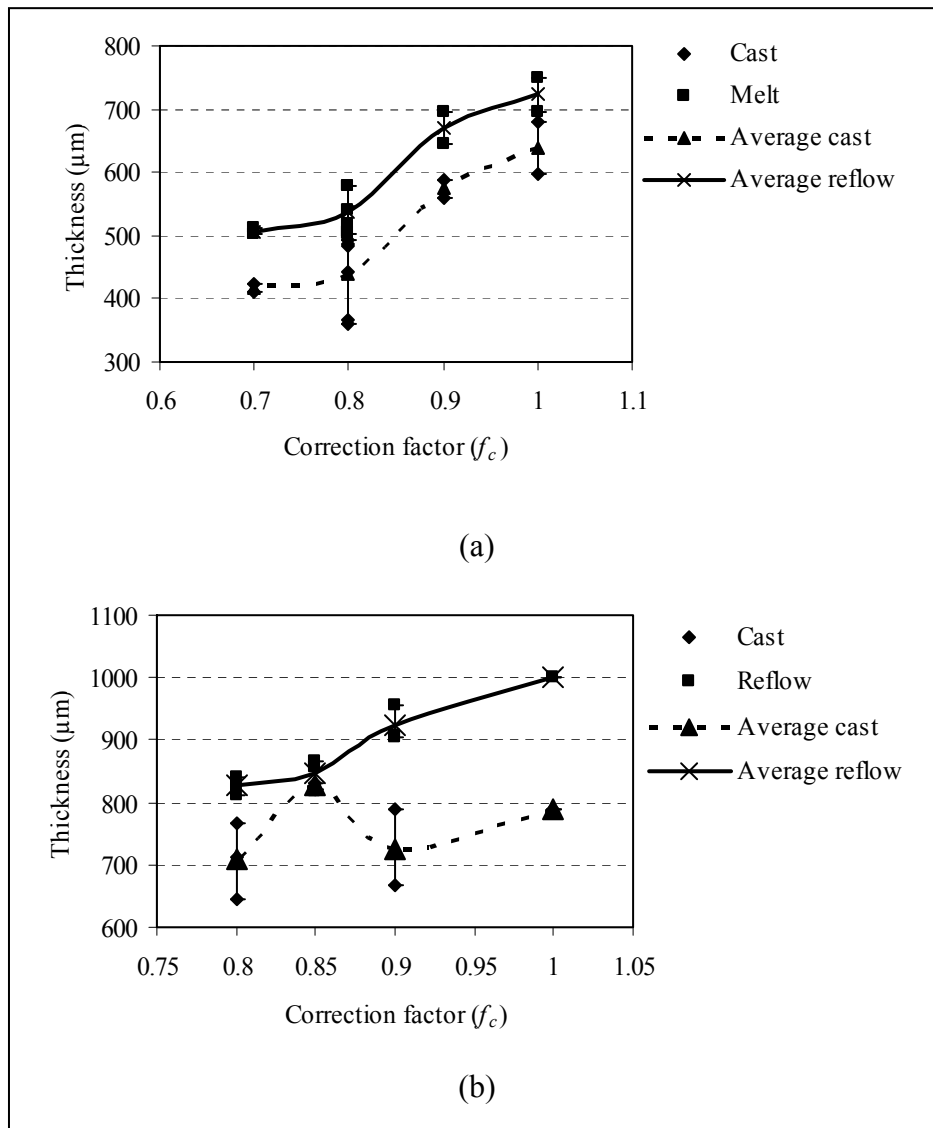


Figure 3.14 Relationship between correction factor and film thickness (a) the first layer (b) the second layer and (c) the third layer.

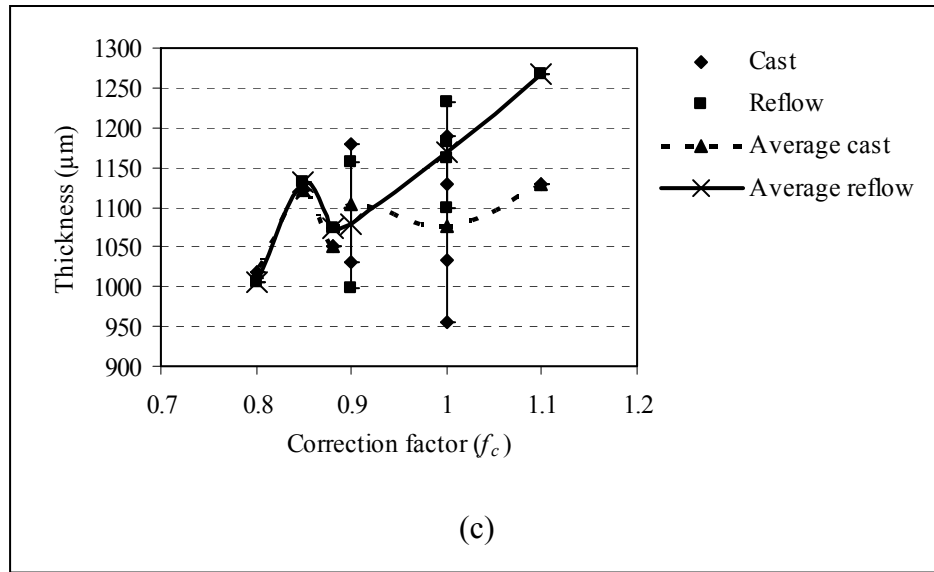


Figure 3.14 Relationship between correction factor and film thickness (a) the first layer
(b) the second layer and (c) the third layer (Continued).

Table 3.1 The suitable correction factor for reflow casting process.

Layer	Correction factor	Thickness (μm)	Target thickness (μm)	Error (μm)
1	0.8	550	500	+50
2	0.85	860	800	+60
3	1.0	1170	1100	+70

Planarization techniques by using finest standard abrasive paper have been used to obtain the target film thickness with a mirror like top surface. For this purpose, the abrasive paper number 1200 is used to eliminate non-planar surface with water as a lubricant substance during polishing process. The sample is continuously measured by a micrometer to monitor the film thickness. However, the transparent surface of photoresist

layer is damaged by scratching from abrasive paper as shown in Figure 3.15 (a). This damage causes alignment difficulty in fabrication of multilayer microstructures. Fortunately, the SU-8 photoresist at this point can be farther reflowed to region surface transparency as shown in Figure 3.15 (b). The unclear surface with average roughness of 256 nm is reduced to 78 nm after reflow treatment at low temperature as shown in Figure 3.16 (a) and (b), respectively. This technique provides small change less than 1 μm in thickness and also offers a clear and smooth surface which is suitable for X-ray mask alignment.

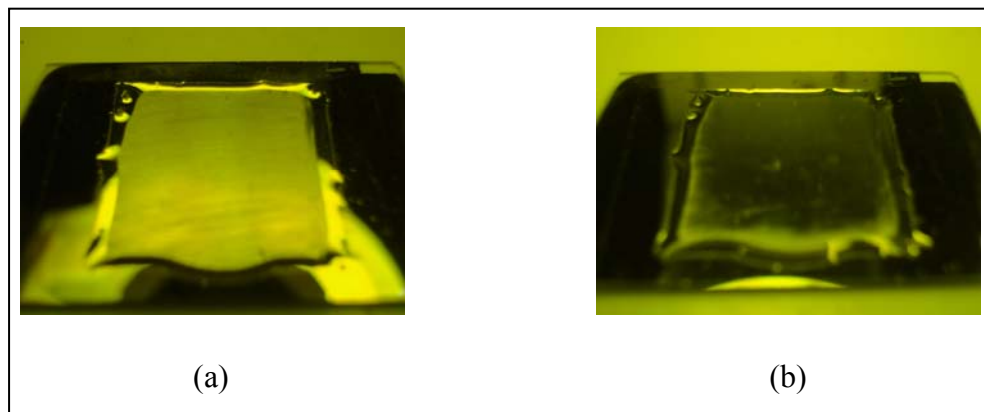


Figure 3.15 Casted SU-8 thick film (a) after polishing surface and (b) after reflow at low temperature to regain film transparency.

Three SU-8 thick layers are carried out to check thickness accuracy of the features. Scanning electron micrographs in Figure 3.17 confirm that the resulting complicated microstructures are almost the same as in the layout design. Combining both reflow casting thickness control with positive error and excessive photoresist polishing, the least amount of SU-8 is wasted. This method will greatly reduce manufacturing cost of X-ray lithography in case of thick polymeric microstructures. In addition, complicated 3D polymeric microstructures fabricated with this technique can generate wider range of applications especially in the field of precision micromold making.

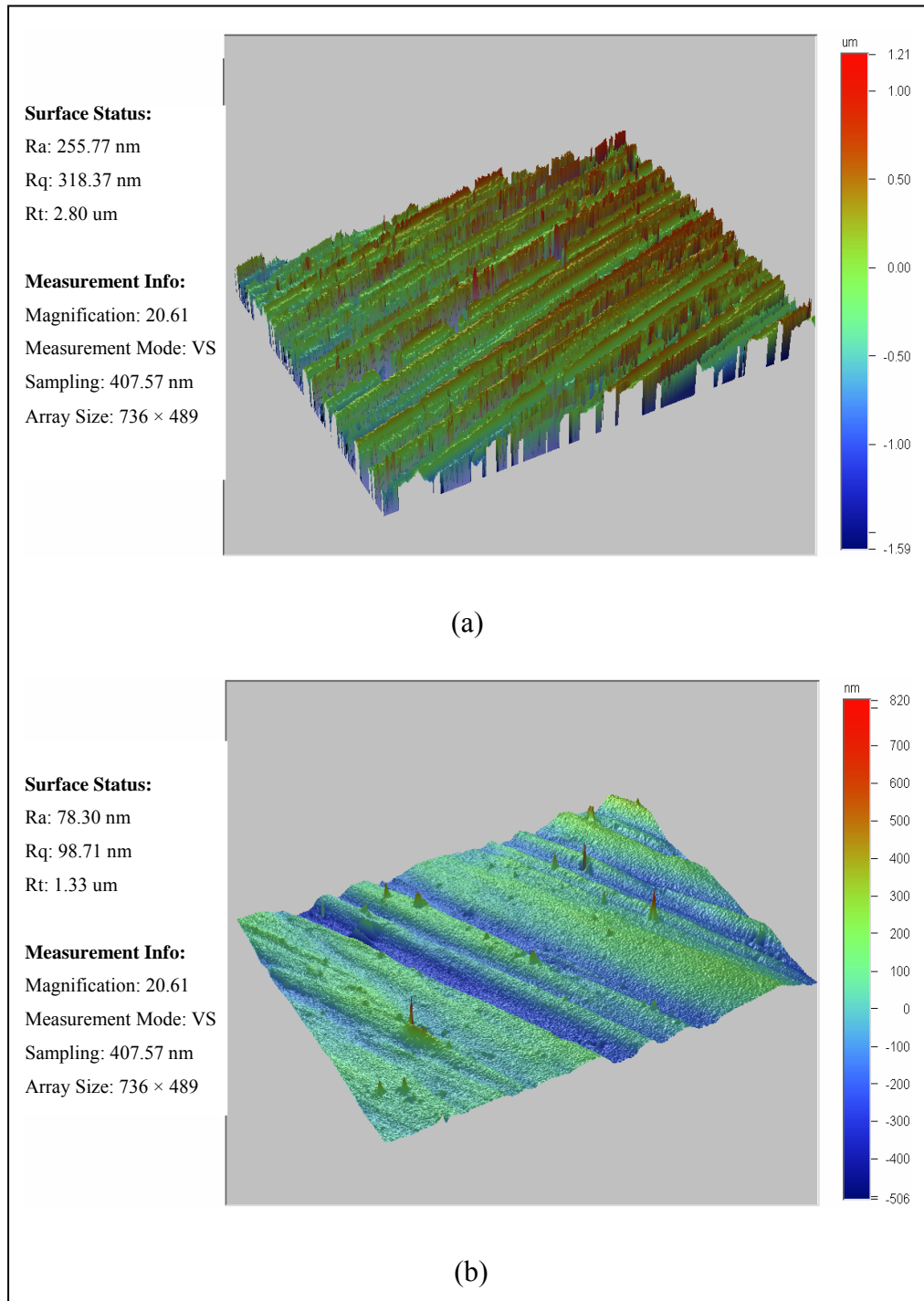


Figure 3.16 Average surface roughness of casted SU-8 thick film

(a) before reflow treatment and (b) reflowed surface.

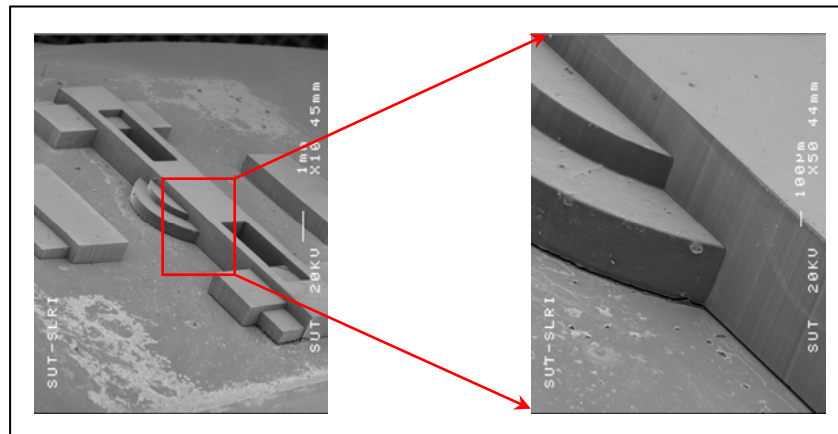


Figure 3.17 SEM images of a three-layer SU-8 microstructure.

3.4 Bonding of PDMS and SU-8 for Tactile Dot Stimulation

Novel bonding techniques of PDMS membrane and SU-8 tactile dot structure are presented in this section. These techniques which include PDMS film thickness control have been promising to achieve precise, well-controlled, and low temperature bonding of tactile dot stimulation. A thin membrane (16-90 μm) of Poly-dimethylsiloxane (PDMS) is prepared by spin-coating on a film of AZ 1512 sacrificial photoresist. Then, SU-8 structure constructed by using X-ray lithography process is placed and pressed on a wet PDMS film by a mass of 1 kg. PDMS membrane is then totally cured at 90°C for 3 hours and bonding is effectively achieved at this relatively low temperature. AZ sacrificial photoresist is subsequently removed and the sample is released from the substrate. Tensile bonding test is performed by applying nitrogen gas pressure to activate a deflection of membrane higher than 480 μm standard height designated by National Library Service for the Blind and Physically Handicapped (NLS). The tactile dot with diameter of 1450 μm arranged into a 9×9 array are successfully fabricated using this novel bonding method.

3.4.1 Thin PDMS films using sacrificial photoresist

PDMS prepolymer (SYLGARD 184 Silicone Elastomer Kit, Dow Corning) as shown in Figure 3.18 (a) is mixed with its curing agent with a volume ratio of 10 : 1. Then the mixed polymer is degassed in a vacuum chamber for 10 minutes to remove bubbles formed during mixing. Next, the mixed polymer is spin coated at different spinning speeds onto glass substrates with dimension of 1 inch \times 1 inch as shown in Figure 3.18 (b). The spinning time is 5 seconds at 500 rpm and ramp to a desired rate for 30 seconds.

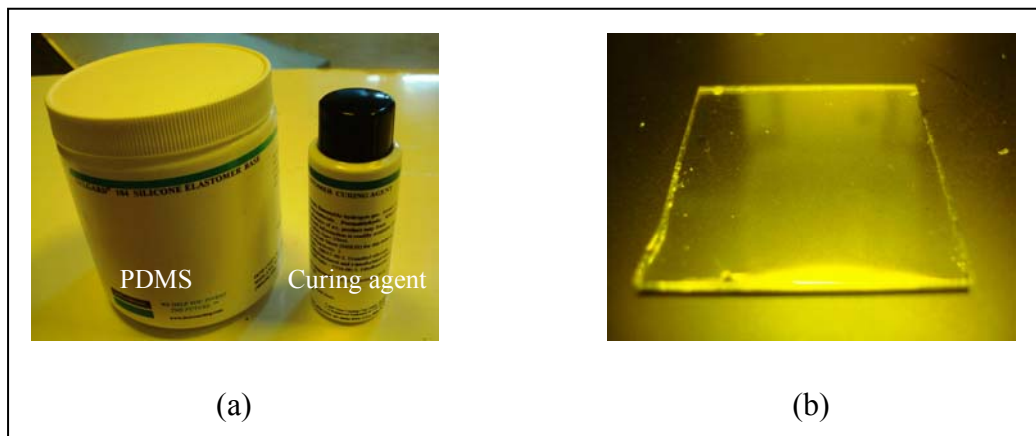


Figure 3.18 Preparation of thin PDMS films by spin coating (a) SYLGARD 184 Silicone Elastomer Kit and (b) PDMS film spin coated on a glass substrate.

The spin coated PDMS layer is pre-cured at room temperature for 20 hours to increase its viscosity and to release air bubbles that may be trapped inside. The film in which the solvent has been evaporated is very viscous and sticky. Then, the samples are heated at 90°C for 3 hours. After cooling down to room temperature, the film thicknesses are measured by Veeco[®] Optical Profiler. Figure 3.19 shows relationship between the film thickness of PDMS and spinning rate.

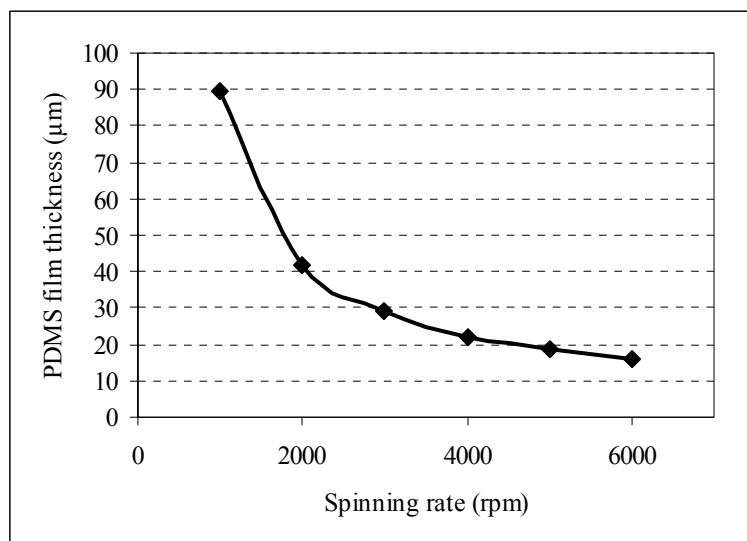


Figure 3.19 Thickness of film spin coated at various spinning rate.

After the PDMS film thicknesses have been observed, the thin film releasing technique have to be developed due to the high strength bonding of Si-O-Si between PDMS and glass, it is difficult to remove the cured PDMS film from the substrate. Therefore, sacrificial layer technique is used to make a small gap between them. Starting with spin-coating of AZ 1512 at 3000 rpm for 30 seconds to cover the area of the substrate, the sample is then immediately soft baked at 90°C for 30 minutes in an oven. After naturally cooled down to room temperature outside the oven, the sample is spin coated with PDMS pre-polymer which have been prepared with the standard volume ratio at 6000 rpm for 30 seconds. The PDMS film is pre-cured at room temperature for about 20 hours. A 16 µm thick layer of PDMS is then cured at 90°C for 3 hours. Finally, AZ photoresist sacrificial layer is removed in acetone to release PDMS film from the substrate as shown in Figure 3.20. The resulting PDMS thin membrane can be used in construction of the tactile dot in later processes without any problems.

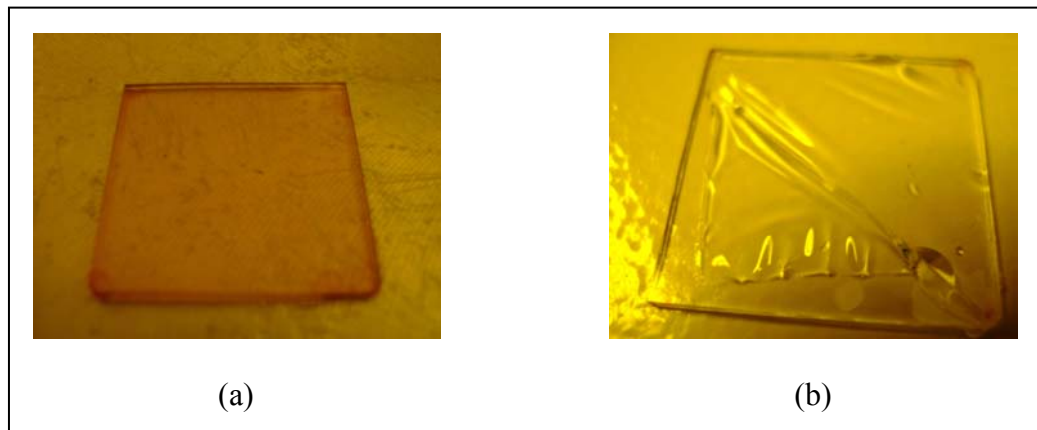


Figure 3.20 Preparation of thin PDMS film (a) AZ 1512 photoresist for sacrificial layer and (b) release of PDMS film.

3.4.2 PDMS – SU-8 bonding for construction of a tactile dot

SU-8 tactile dot structure is created by using X-ray lithography process illustrated in Figure 3.21. This process starts with preparation of an X-ray mask and a SU-8 thick film. The tactile dot pattern with diameter of $1450\ \mu\text{m}$ is designed in a 9×9 array and transferred onto an X-ray mask. SU-8 powder are reflow casted into a thick film with a thickness of $1000\ \mu\text{m}$ after polishing and reflow treatment as shown in Figure 3.21 (a). Then, the SU-8 thick film is patterned by X-ray exposure through the X-ray mask, post-exposure baking, and development to obtain an SU-8 frame of the tactile dot array as shown in Figure 3.21. Lastly, the SU-8 frame is removed from the substrate and cleaned with oxygen plasma. This SU-8 frame is then bonded with the PDMS thin membrane of form tactile dot cells.

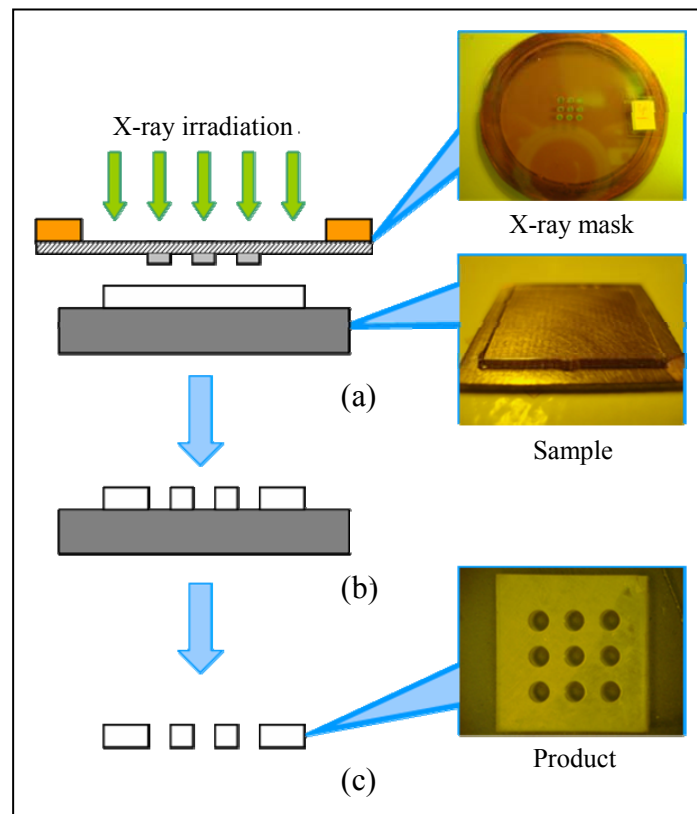


Figure 3.21 Preparation of an SU-8 frame of the tactile dot array (a) X-ray mask and SU-8 thick film for X-ray lithography (b) the sample development and (c) the tactile dot array.

Two methods for SU-8 and PDMS bonding been studied. The First one is oxygen plasma bonding which is commonly used to bond PDMS to another surface, especially for PDMS and glass. The thin layer of PDMS, that has been spin coated on a glass substrate with AZ photoresist as a sacrificial layer, along with the SU-8 frame are treated in oxygen plasma with a power of 200 W for 3 minutes. They are then bonded immediately under a pressure of 1 kg with 3 hours baking at 90°C. After naturally cooled down to room temperature, the sample is examined. It could be observed that they did not adhere well after AZ photoresist sacrificial layer is removed as shown in Figure 3.22. This problem is caused by non-uniformity of the SU-8 surface resulting from polishing process that generates small gaps between them. Moreover, the chemical compositions of SU-8 do

not support to create O-Si-O bonds by using oxygen plasma treatment, except for van der Waals attraction to each other.

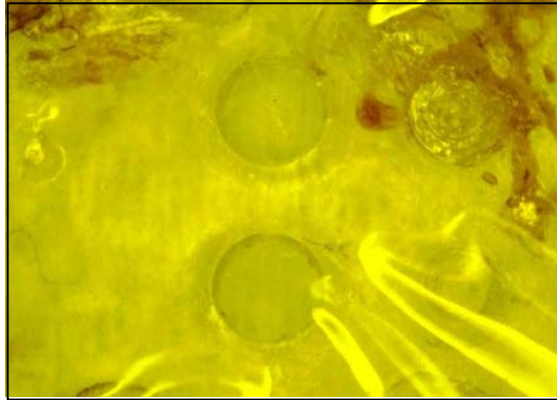


Figure 3.22 Peeling of the PDMS membrane after release of AZ photoresist sacrificial layer.

The second technique is SU-8/PDMS wet bonding which is performed while the PDMS film is still in a viscous state. After spin coating of PDMS layer, the SU-8 frame is immediately placed and pressed on the wet PDMS film by a mass of 1 kg weights as shown in Figure 3.23 (a). The sample is totally cured at 90°C for 3 hours and naturally cooled down to room temperature. Figure 3.23 (b) shows the bonded sample before release of the PDMS membrane. The resulting SU-8/PDMS tactile dot cells are shown in Figure 3.23 (c). With SU-8/PDMS wet bonding, the tactile dot cells are realized successfully at low temperature. Strong adhesion between SU-8 and PDMS is thought to be due to mechanical locks generated when the viscous PDMS fills small gaps on SU-8 surface.

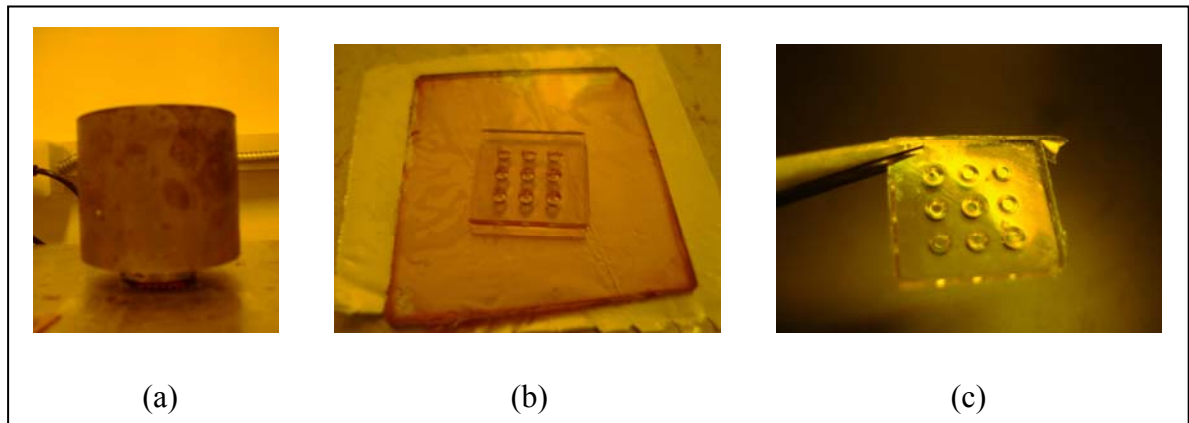


Figure 3.23 Bonding of SU-8 frame and PDMS thin membrane for tactile dot cells

(a) compress with the pressure of mass 1 kg weights

(b) SU-8/PDMS bonding before released from the substrate and (c) the result of interface bonding.

The bonding strength is tested by applying nitrogen gas pressure to deflect the PDMS membrane. By adjusting the gas regulator, a level of pressure can be selected. At a certain level of gas pressure, the deflection of PDMS membrane as high as $370\ \mu\text{m}$ can be observed as shown in Figure 3.24.

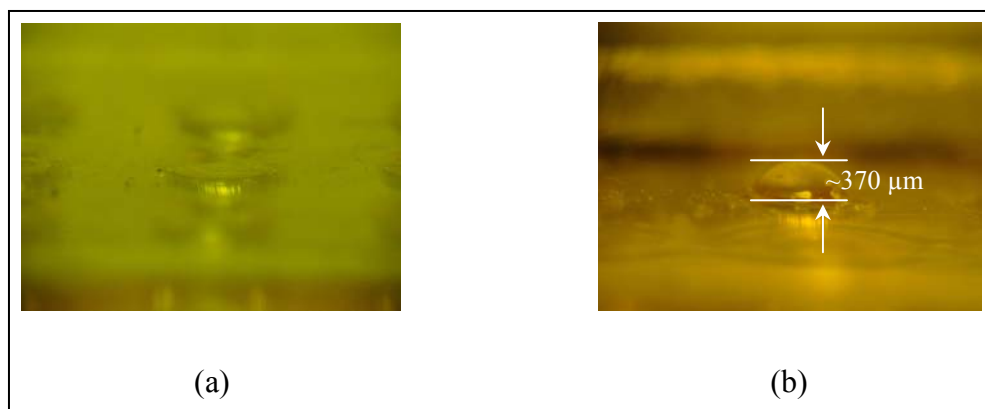


Figure 3.24 Testing of SU-8/PDMS dot cell by applying a gas pressure (a) non-deflected and (b) deflected of PDMS membrane under nitrogen gas pressure.

3.5 Fabrication of Micro-Piston Based on Release Etching of a Conformal Sacrificial Layer

A novel technique to release the moving part of a piston-like structure using a conformal sacrificial spacer is presented in this section. The nickel mold which has been fabricated by X-ray lithography and electroplating process as shown in Figure 3.25 is used as a master mold in PDMS casting.

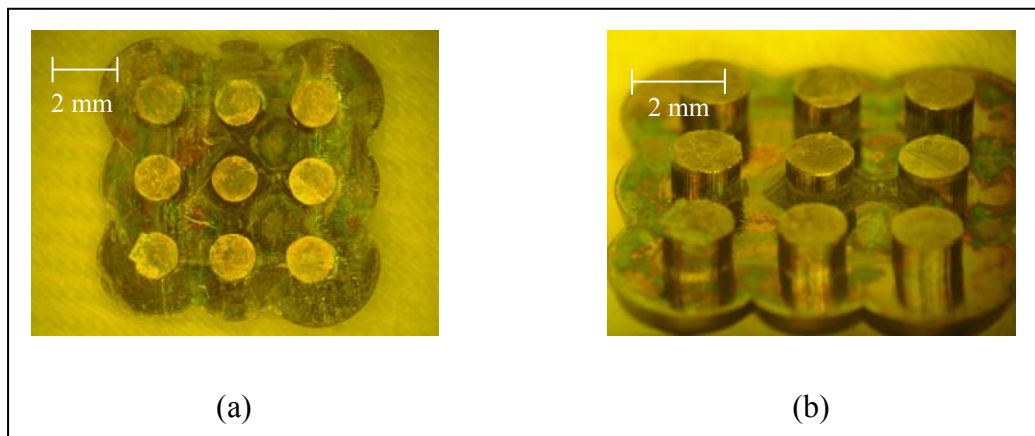


Figure 3.25 Optical micrographs of a Ni master mold (a) top view and (b) bird's eye view.

After molding and curing PDMS as shown in Figure 3.26 (a), the polymer template is peeled off and bonded on a conductive substrate by using a thin photoresist film as an adhesive layer as illustrated in Figure 3.26 (b). The photoresist adhesive film inside the mold is opened by oxygen plasma at 200 W as shown in Figure 3.26 (c) and nickel rods are electrodeposited inside the PDMS mold as demonstrated in Figure 3.26 (d). After the PDMS mold is removed, piston-like Ni rods are obtained as shown in Figure 3.26 (e). A layer of silver is then conformally grown along conductive surface of the substrate and metallic rods by electroplating as displayed in Figure 3.26 (f). This silver layer functions as a sacrificial spacer layer as well as a conductive plating base for conductive electroplating of the next Ni layer as illustrated in Figure 3.26 (g). Mechanical polishing is done to

planarize the top surface until silver rings enclosing the piston obviously appear as demonstrated in Figure 3.26 (h). The pistons are then separated from the enclosing cylinders by chemical wet etching of the silver sacrificial layer as shown in Figure 3.26 (i). Finally, the pistons are mechanically detached from the metal cylinders as shown in Figure 3.26 (j).

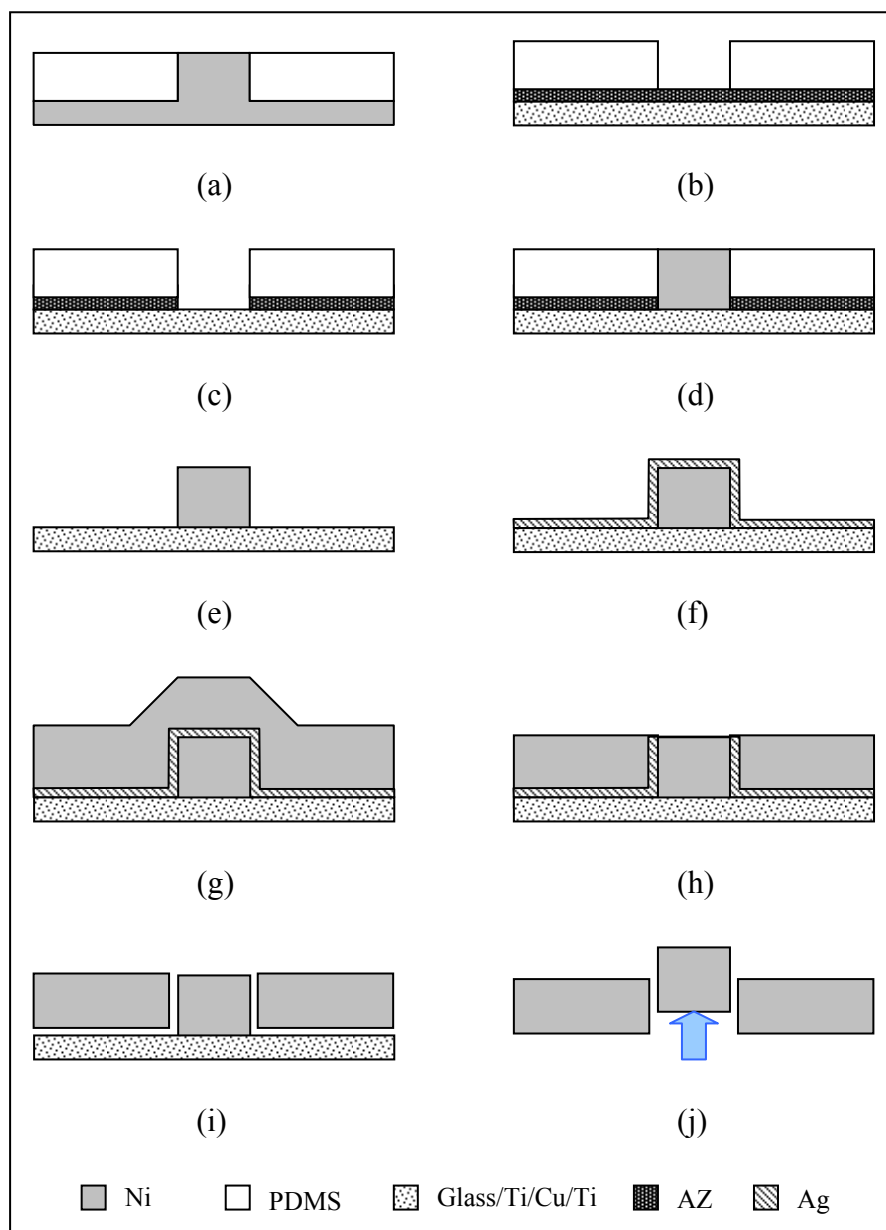


Figure 3.26 Fabrication processes of micro-pistons and complementary cylinders by using a conformal and conductive sacrificial spacer.

3.5.1 PDMS molding

PDMS pre-polymer is mixed with its curing agent in a volume ratio of 10 : 1 and degassed in a vacuum chamber to remove bubbles formed during mixing. The mixture is then carefully poured over a nickel master mold which is already placed in a PDMS square frame as shown in Figure 3.27 (a). To solidify the mixture, the sample is placed on a hotplate at 90°C for 5 minutes. After curing, the casted PDMS is cut around in a square pattern as shown in Figure 3.27 (b). The PDMS plate is then carefully peeled from the mold by using a tweezer as shown in Figure 3.27 (c).

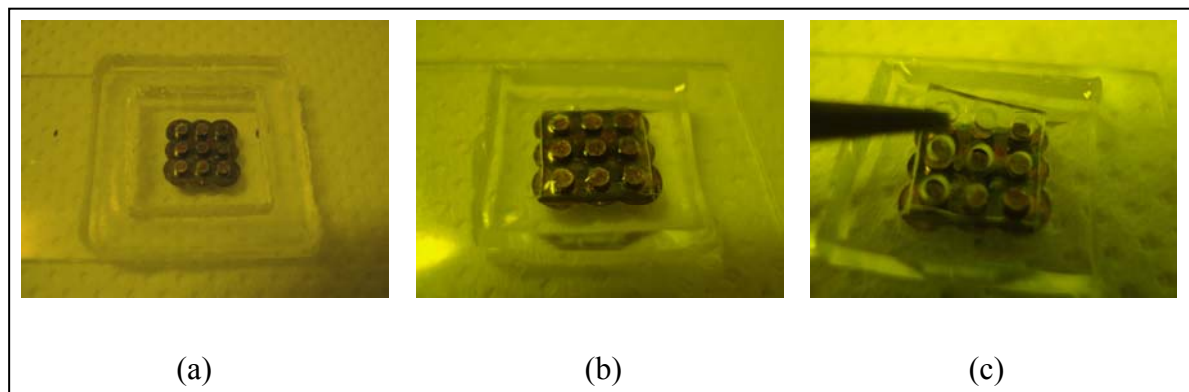


Figure 3.27 PDMS molding (a) a nickel master mold placed inside a PDMS frame (b) cutting around the casted PDMS and (c) peeling off from the master.

3.5.2 PDMS - conductive substrate bonding

Since the PDMS mold will be removed after the nickel piston is electroformed, a suitable condition of this bonding has to be investigated. The first technique is the touch and paste bonding. The mold is temporarily in touch with the wet AZ P4620 photoresist which has been spin-coated on a glass substrate at 1000 rpm for 10 seconds. Then, the mold is placed on the Ti layer as shown in Figure 3.28 (a) and stuck on the substrate by PI tape as shown in Figure 3.28 (b). Soft baking is performed to condense the film at 80°C for 8 hours on a hotplate and naturally cooled down to room temperature.

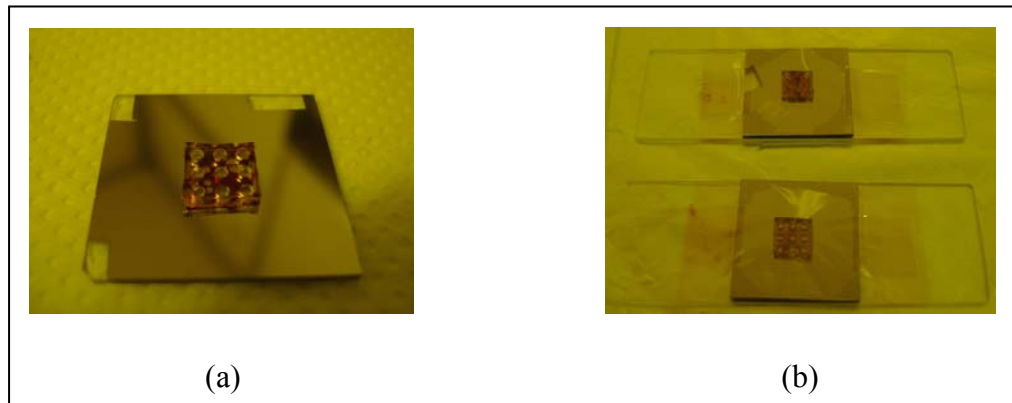


Figure 3.28 (a) Touch and paste bonding and (b) sticking with PI tape.

The experimental result show that the PDMS mold can be fixed to the substrate as illustrated in Figure 3.29 (a), but there are cumulative photoresist around the circumference of the base mold as shown in Figure 3.29 (b). This excessive photoresist causes the distortion on the piston configuration and difficult to remove from the substrate by using oxygen plasma. Therefore, another technique has to be invented to create the uniform photoresist surface after bonding.

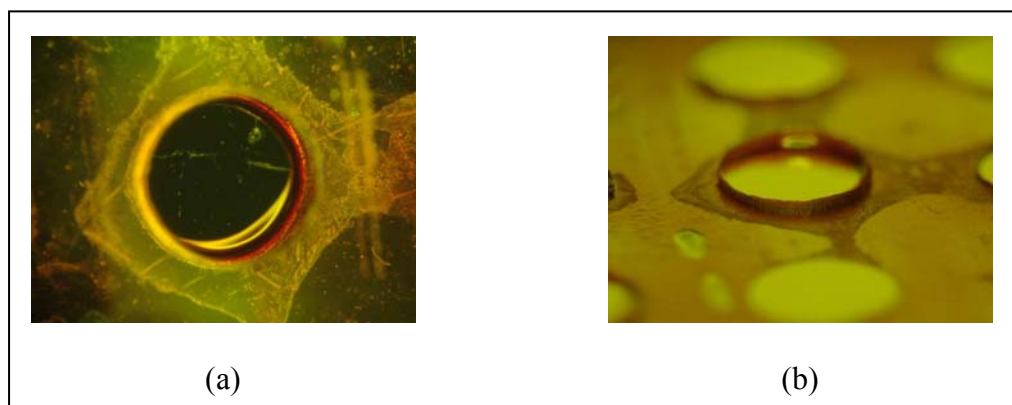


Figure 3.29 (a) The bonding of the photoresist to the substrate and (b) cumulative photoresist around circumference of the base mold.

As mentioned, the uniform photoresist layer can be obtained by the spin-coating before the PDMS mold is placed. Hence, the second technique is relied on the spin and paste bonding. The conductive substrate was coated with AZ 1512 at 800 rpm for 30 seconds. The PDMS mold is then immediately placed during the photoresist is staying in viscous state as shown in Figure 3.30 (a), and stuck on the substrate by PI tape to ensure that there do not have any small gap between them as shown in Figure 3.30 (b). The sample is soft baked on the hotplate at 90°C for 3 hours and naturally cooled down to room temperature. Figure 3.31 demonstrates the bonding result which could be observed that there are gas bubbles generated at the bottom of the mold. However, this can be eliminated by using oxygen plasma for exposing the seed conductive layer as illustrated in Figure 3.32.



Figure 3.30 (a) Bonding with AZ photoresist and (b) sticking on the substrate with PI tape.

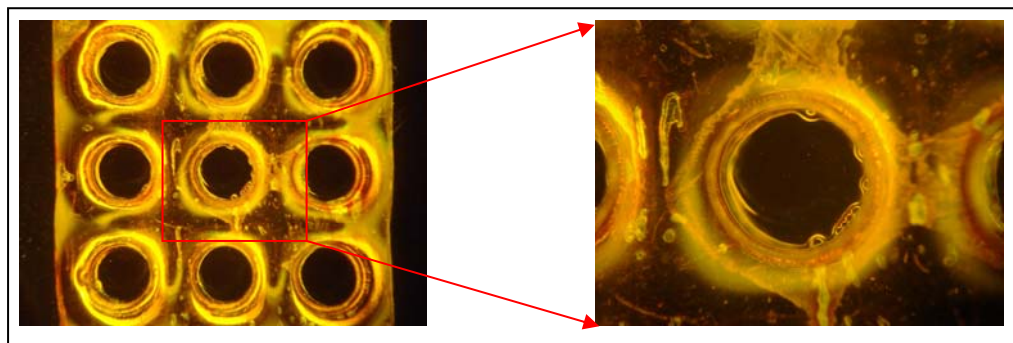


Figure 3.31 The result of PDMS-substrate bonding.

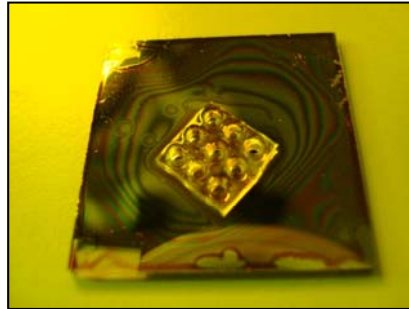


Figure 3.32 The seed layer exposed by oxygen plasma.

3.5.3 Nickel electroplating

The PDMS mold is filled with nickel material to form the piston structure. The low current density ramping is play significant role in this process since its products usually damage from the plurality of gas bubbles that are naturally generated during electroplating as shown in Figure 3.33. To avoid this problem, the current density is adjusted with a special low ramping as shown in Figure 3.34 (a). Although this technique has to be processed for a long time, it provides the satisfied result by without gas bubbles trapped inside the structure as illustrated in Figure 3.34 (b).

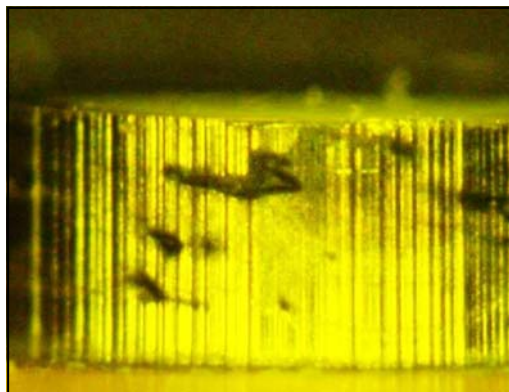


Figure 3.33 Gas bubbles trapping inside the structure

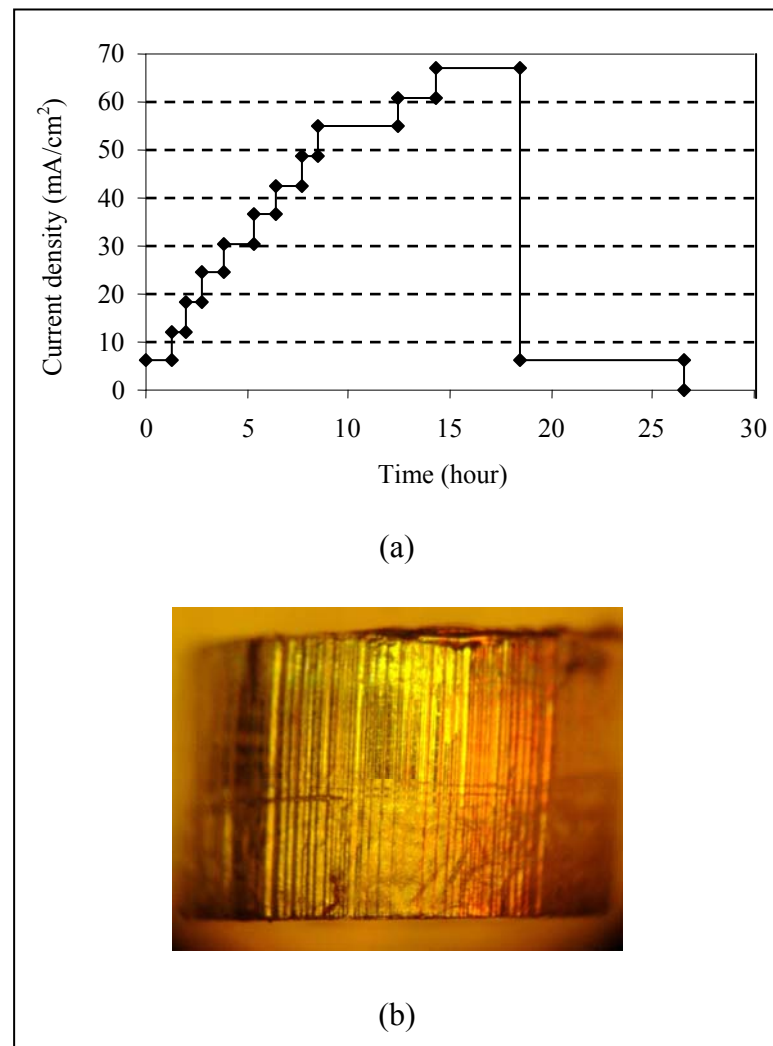


Figure 3.34 (a) Current ramping rate of nickel electroplating and
(b) the piston without gas bubbles.

Then, the temporary PDMS mold is removed and the square mold around the piston is constructed by SU-8 reflow casting and X-ray lithography process as shown in Figure 3.35 (a). Thin layer of silver sacrificial material is conformally grown over the conductive surface as shown in Figure 3.35 (b). The SU-8 mold is filled with nickel material as shown in Figure 3.35 (c), followed by the mechanical polishing to a desired thickness and the appearing of the silver ring around the piston as shown in Figure 3.35 (d).

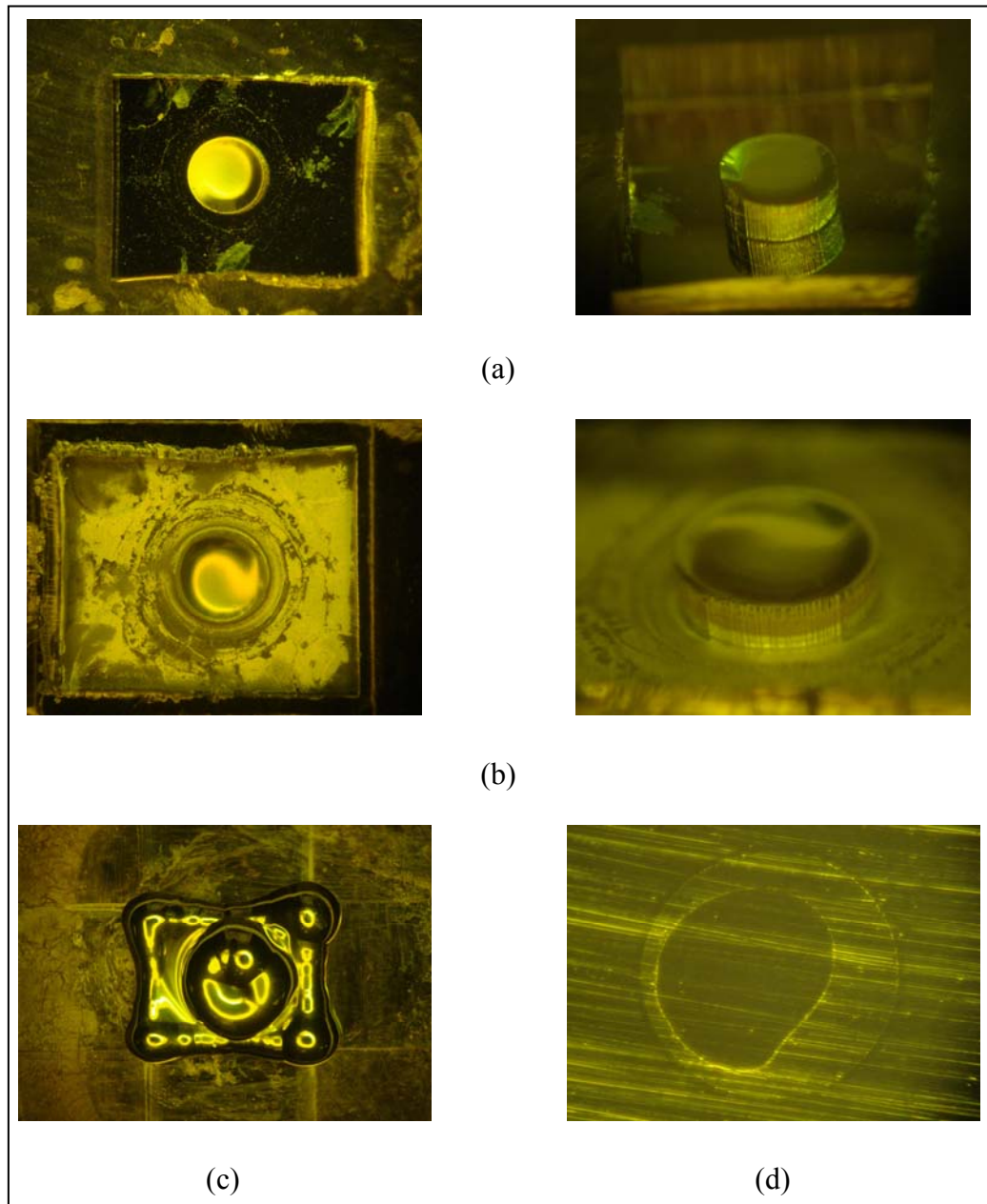


Figure 3.35 Fabrication sequences of piston (a) The SU-8 mold for the cylinder electroplating (b) growing of silver sacrificial layer (c) the cylinder electroplating and (d) the mechanical polishing to expose the silver ring.

3.5.4 The piston releasing

To separate the piston from the cylinder, the silver sacrificial is etched by chemical wet etching in a chemical mixture of a 3 : 1 $\text{NH}_4\text{OH} : \text{H}_2\text{O}_2$. This step is performed for a long time because there are limited areas for the wet etchant solution that can be

inserted into the space from the top surface as illustrated in Figure 3.36 (a). After 48 hours or more, the piston can be moved out by the mechanical force as shown in Figure 3.36 (b).

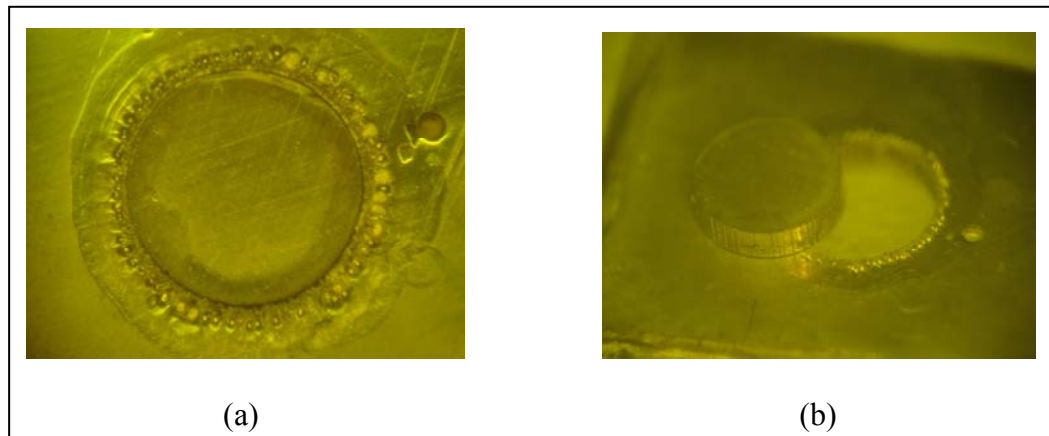


Figure 3.36 Releasing of sacrificial layer (a) small hole around the piston between wet etching and (b) the piston releasing from the cylinder.

The novel technique for creation of precise gap has been proposed. By using the temporary bond between the PDMS mold and the conductive surface, the metallic piston is simply fabricated and separated from the cylinder by the silver sacrificial layer. The current density with slow ramping rate in electroplating process has been delivered to a smooth plating structure and prevents the creating of gas bubbles. This positive result is extended to be the important technique in fabrication of multi-step of the piston structure for the tactile dot stimulation.

3.6 X-ray LIGA application

The X-ray LIGA process which has been described for the repeated structures by using the X-ray molding will be introduced for the complicated microstructures in this section. Figure 3.37 (a) shows the model of a gear which consists of 3 layers of metal structure. The specification of each layer is illustrated in Figure 3.37 (b) and (c).

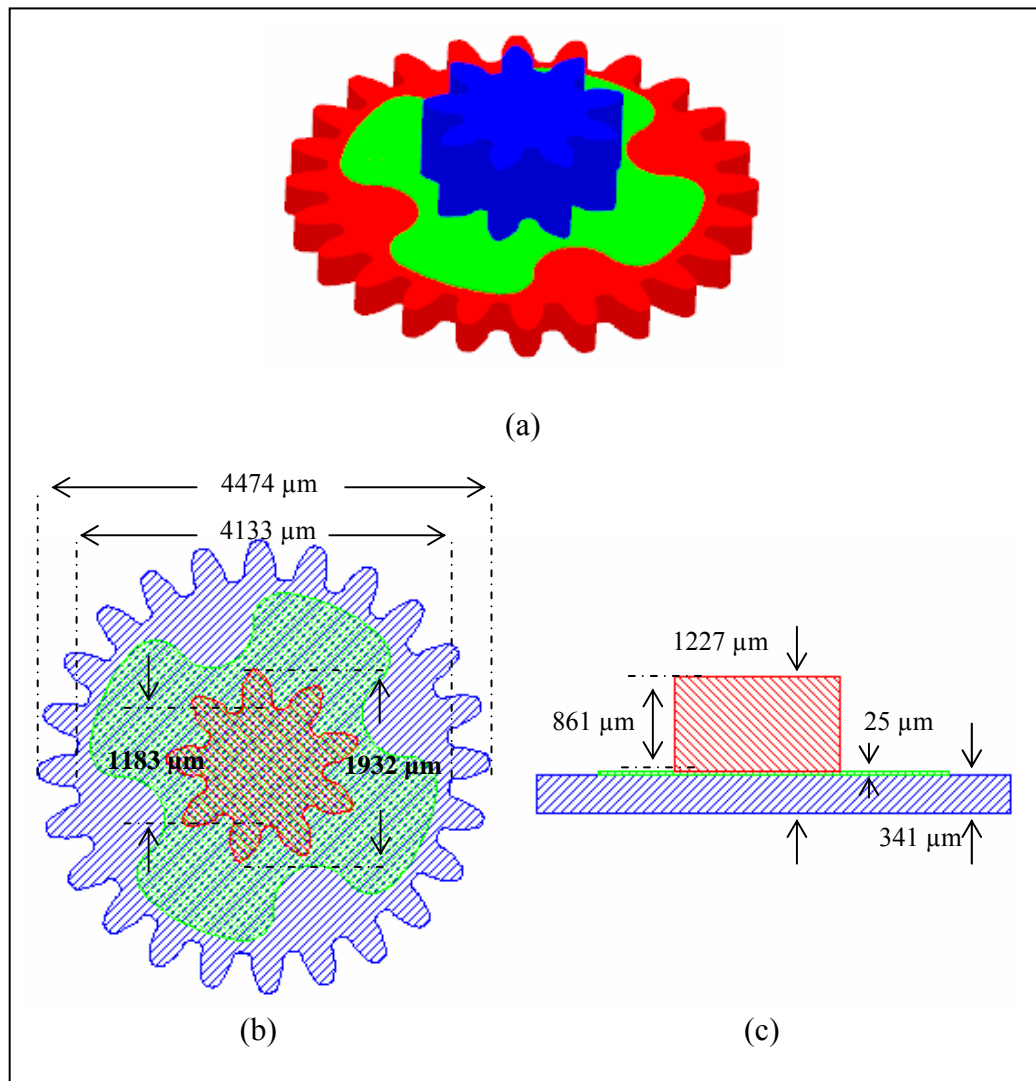


Figure 3.37 Gear structure (a) 3D model (b) top view and (c) cross-section view.

The fabrication process is divided into 3 sections consisting of master mold making, PDMS molding, and metal construction. For the first section, the X-ray mask is designed and fabricated by using UV lithography and silver electroplating process resulting in the negative silver patterns as shown in Figure 3.38. Three master molds of the gear are constructed with SU-8 photoresist with thickness of 800 μm by using X-ray lithography process as shown in Figure 3.39.

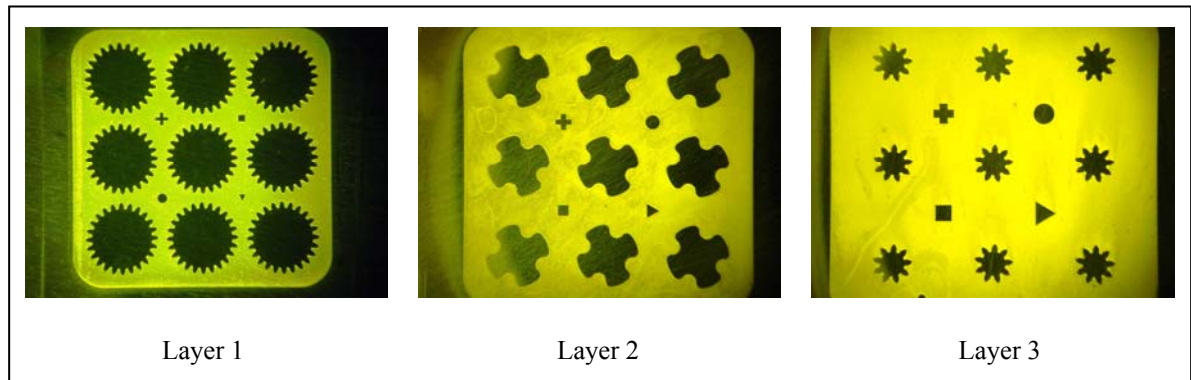


Figure 3.38 X-ray masks for the multi-layer gear.

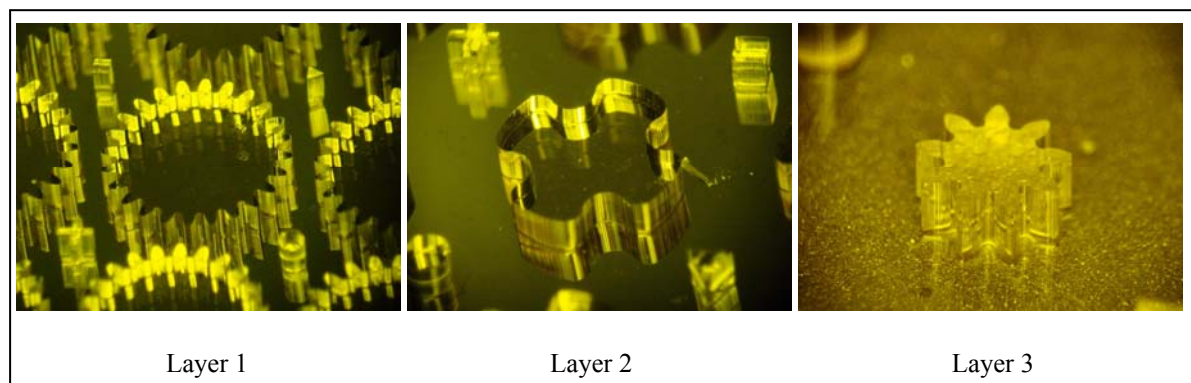


Figure 3.39 Three master molds of SU-8 photoresist.

Second, the PDMS mold is copied the patterns from the master mold. PDMS prepolymer is mixed with a volume ratio of 10 : 1 and vacuumed to remove gas bubbles. The SU-8 master mold is coated with silicone lubricants to prevent the adhesion between the mold and PDMS. The sticky PDMS is loaded into the mold by a pin that is used to fill gradually until the PDMS level is rinsed-up to the top surface of the mold as shown in Figure 3.40 (a). To condense the polymer, the sample is heated up to 90°C for 10 minutes, followed by placing on a cold stainless plate. The condensed PDMS is suddenly contracted since the rapidly decreasing of temperature, and the silicone lubricant is sprayed on the sample to separate the PDMS from the SU-8 mold. To remove the PDMS plate, the pin is

inserted under the polymer and lifted slowly from the bottom until the polymer is totally taken away from the SU-8 mold as shown in Figure 3.40 (b). All of PDMS mold are copied and suddenly placed on the clean substrate to prevent the contamination on the PDMS surface.

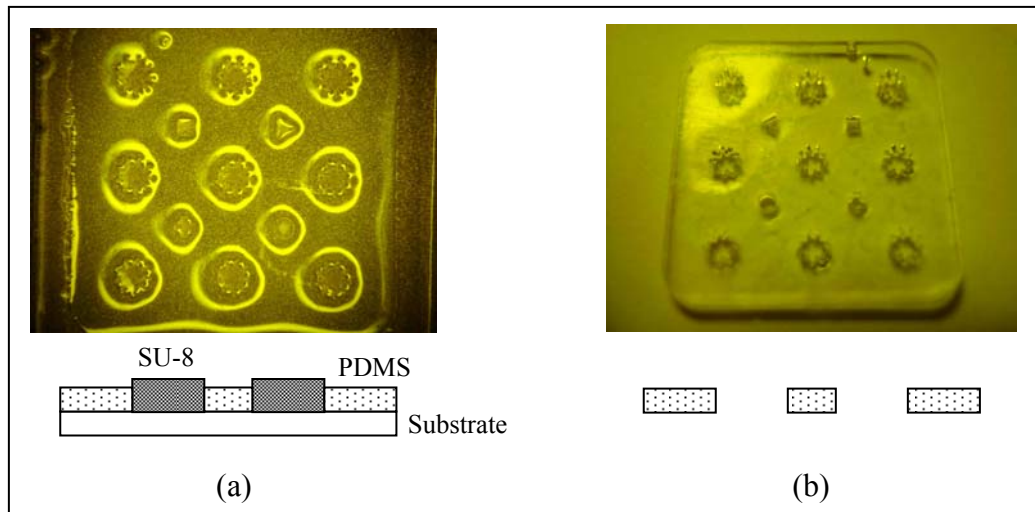


Figure 3.40 Molding of PDMS (a) PDMS loaded into the SU-8 master mold and (b) the PDMS mold removed from the mold.

Finally is the metal construction by using the electroplating inside the PDMS mold. The first gear pattern must be primary formed by placing the PDMS mold onto a conductive substrate which is a glass coated with Ti/Cu/Ti seed layer as shown in Figure 3.41 (a). Nickel structures are formed inside the mold and remained alone on the substrate after removing of the PDMS mold as shown in Figure 3.41 (b). From the desired thickness of 341 μm required by specification, the metal structure must be polished to decrease the thickness without any distortion on the structure. Un-exposure SU-8 photoresist is utilized to support the structure by using SU-8 powder reflow casting as shown in Figure 3.41 (c), following by mechanical polishing on the waterproof silicon carbide paper #1200 and DP Mol cloth as shown in Figure 3.41 (d).

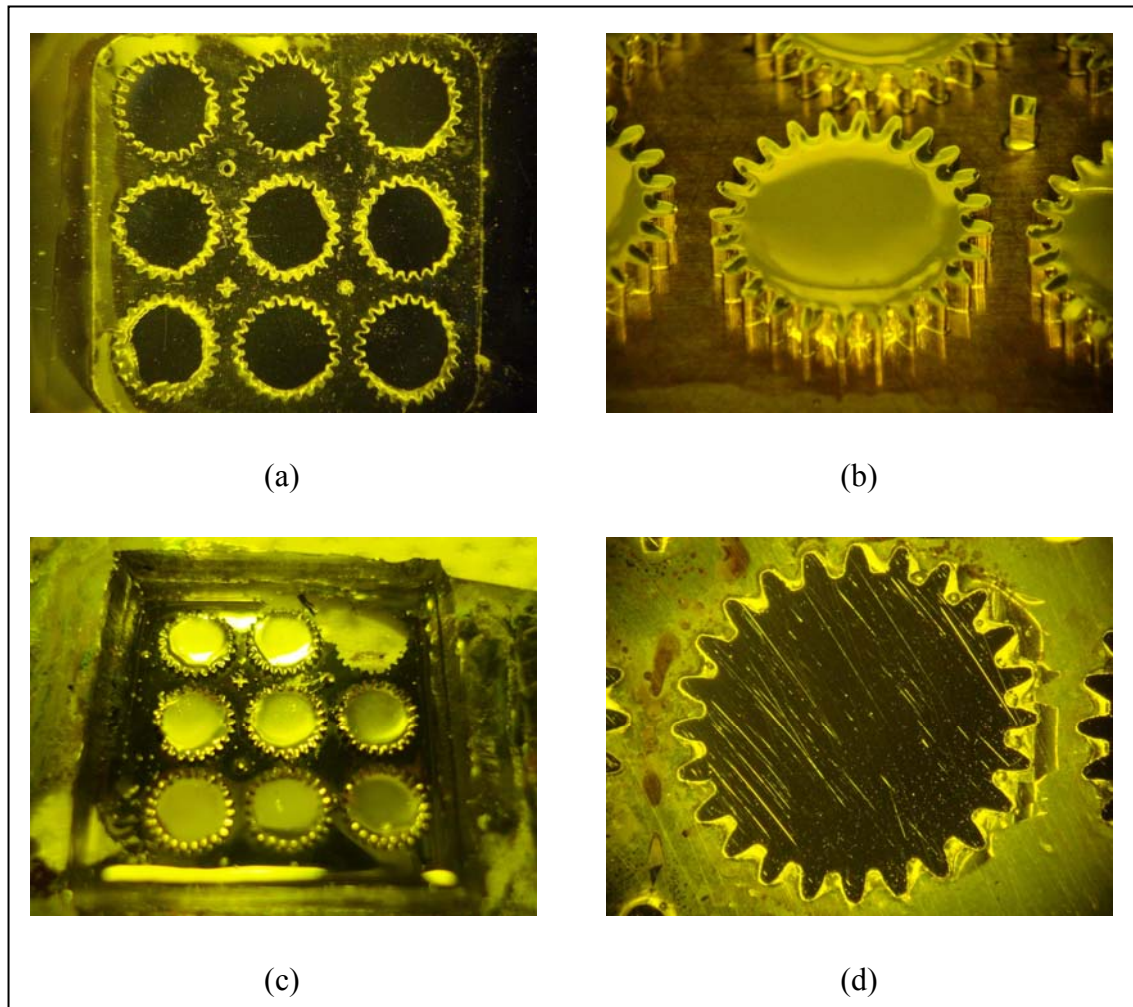


Figure 3.41 Fabrication sequences of the first gear structure.

The second gear layer is formed on the first gear layer. PDMS mold of layer 2 is aligned and placed on the metal substrate as shown in Figure 3.42 (a). The bottom PDMS surface which was peeled away from the SU-8 mold is sticky patch helped to seal between their interfaces and prevented the inserting of electrolyte under the mold. Since the desired thickness of this layer is 25 μm , the nickel electroplating has to be always monitored to avoid the higher thickness as shown in Figure 3.42 (b). After forming of the metal structure, both of the PDMS mold and the unexposed SU-8 photoresist are removed, followed by oxygen plasma cleaning before casting with SU-8 photoresist again as shown in Figure 3.42 (c). At last, the thickness is decreased to 25 μm by mechanical polishing as shown in Figure 3.42 (d).

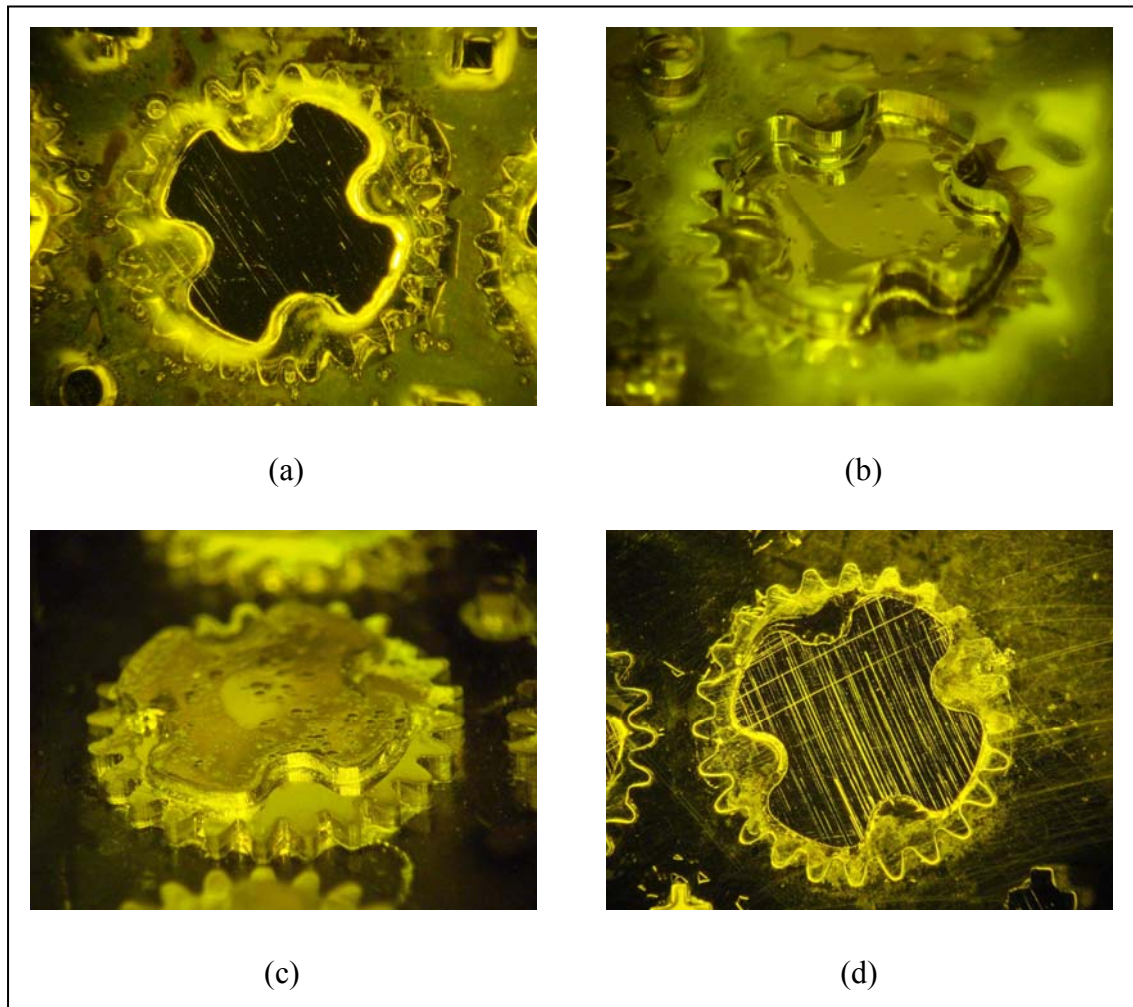


Figure 3.42 Fabrication sequences of the second gear structure.

The third gear layer is finally formed by repeating the process similar to the previous layer. The PDMS mold of layer 3 is aligned and placed on the base as shown in Figure 3.43 (a). Nickel is then formed as shown in Figure 3.43 (b) and the PDMS mold is removed, followed by the SU-8 reflow casting. The metal thickness is reduced to 1227 μm by polishing process as shown in Figure 3.43 (c). Finally, un-exposure SU-8 photoresist is totally removed and the sample is cleaned by oxygen plasma as shown in Figure 3.43 (d).

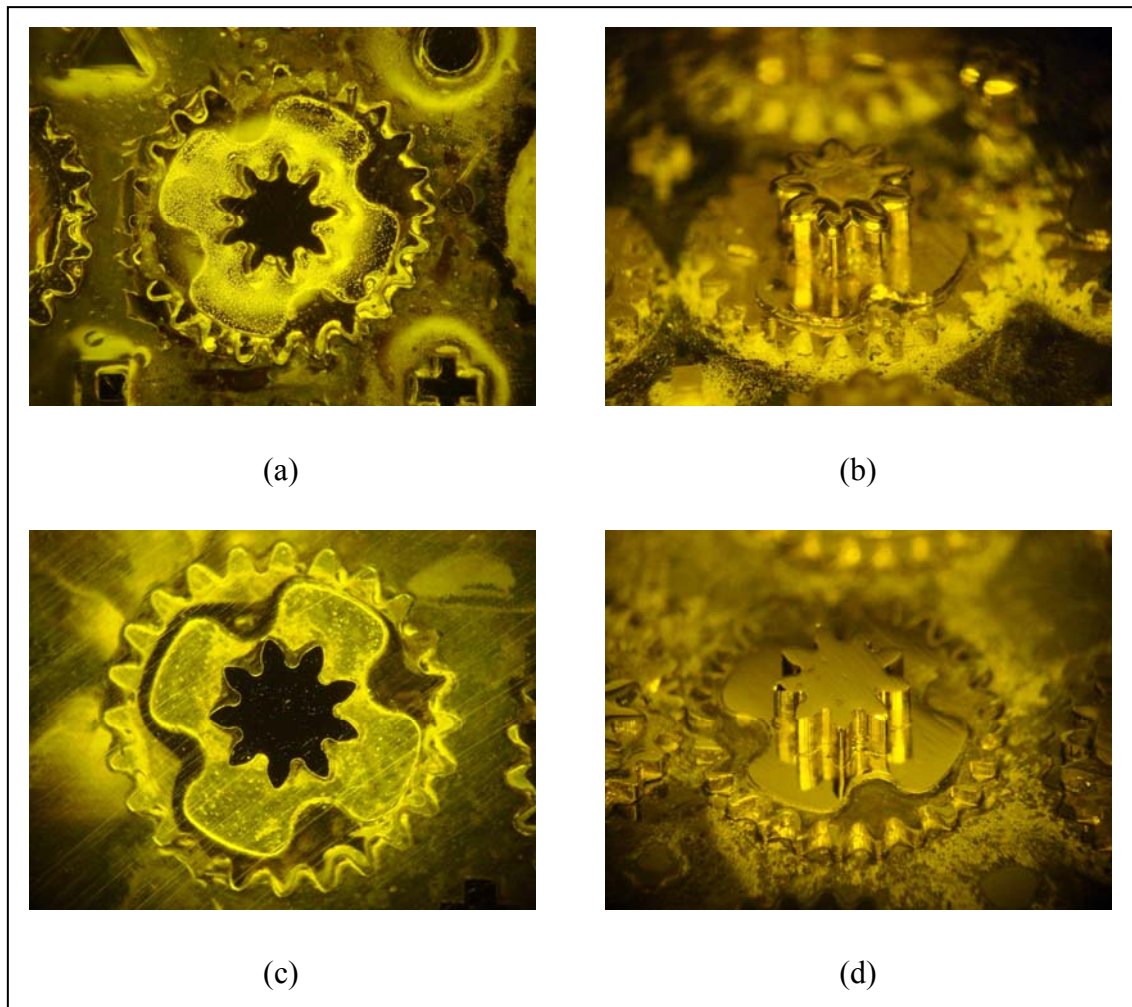


Figure 3.43 Fabrication sequences of the third gear structure.

Figure 3.44 (a) shows the SEM images of the finished structure which clearly demonstrated that the complicated structure can be performed by using LIGA process. Moreover, the connection area between the layers is also investigated as shown in Figure 3.44 (b) and (c). They have some nickel grain resulting from electroplating process. This is happened from damaged PDMS molds which can be observed on the remained PDMS at the base of the SU-8 master mold as shown in Figure 3.45 (a). Another problem is the effect of the stress of the PDMS mold between electroplating process as shown in Figure 3.45 (b). However, the overall process of LIGA fabrication has been already demonstrated to construct the complicated structure which can be improved for many applications in the further.

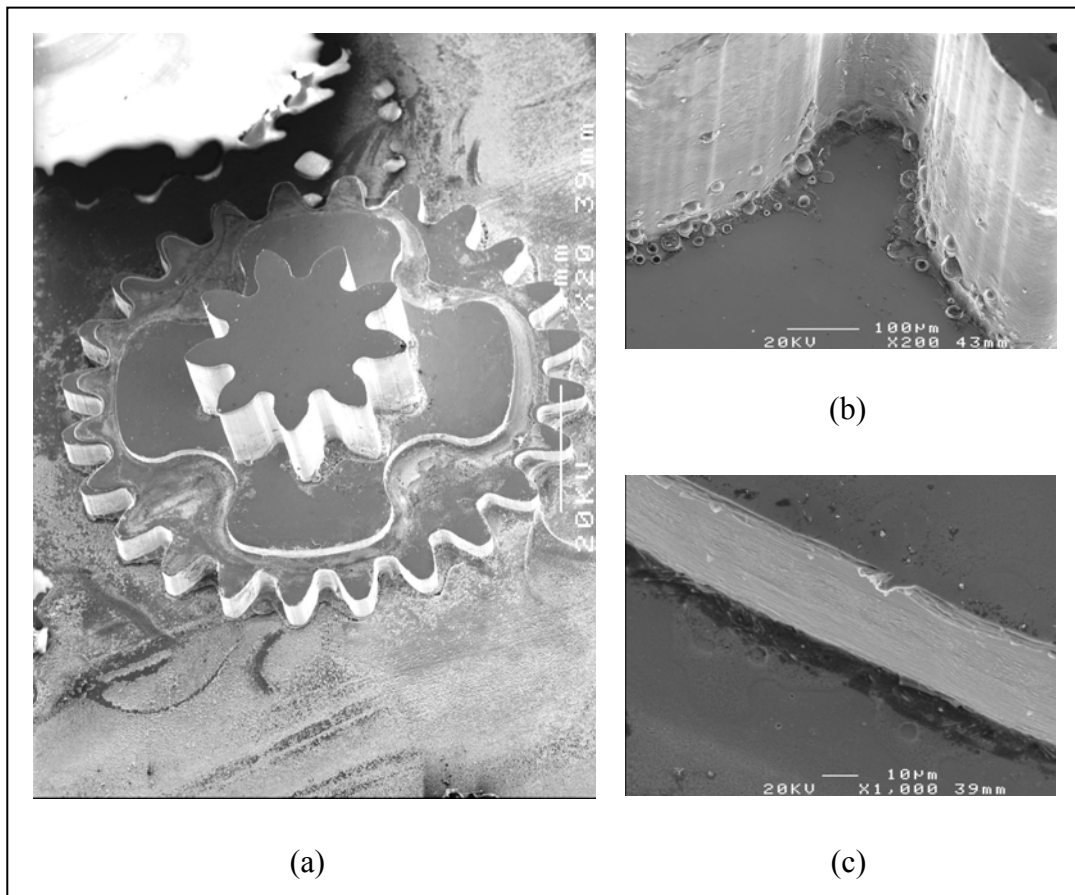


Figure 3.44 SEM image of gear structure (a) finished structure (b) the connection area between layer 2 and 3 and (c) between layer 1 and 2.

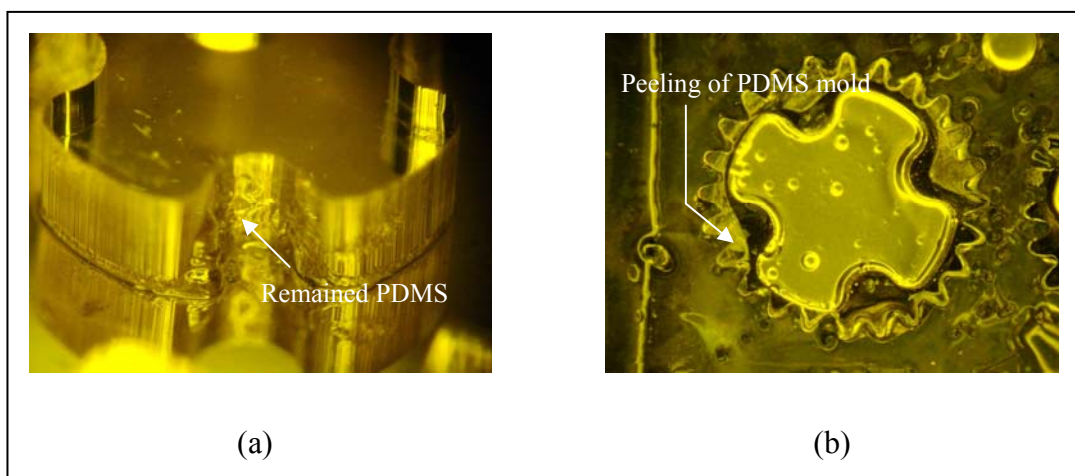


Figure 3.45 Problems of PDMS molding (a) Remained PDMS on the SU-8 master mold and (b) the peeling partially of PDMS mold between electroplating.

3.7 Chapter summary

The specialized micromachining processes have been developed in order to realize the tactile dot mechanism. Transparent X-ray mask is helps to create the complicated microstructures which are generated by using the SU-8 powder reflow casting process. At the same time of the tactile dot stimulation which has been presented to fabricate for 2 techniques. First is PDMS membrane which the pneumatic tactile actuation can be achieved from the simply bonding. Second is the novel technique for releasing the piston delivers to the fabrication of moving part with small gap. This is assisted to decrease the gas leakage while the piston is pushed up to indicate the tactile dot. Furthermore, the LIGA application for complicated gear structure is also introduced in capability of the repeated process which helps to reduce the cost and easily to fabricate by using the simple process of micro-machining.

CHAPTER IV

ELECTROSTATIC ACTUATOR FOR MICROVALVE APPLICATION

4.1 Introduction

Microvalves have found ever increasing applications in microsystems including microfluidic chemical analyzers, biological microvolume processing chips, pneumatic microactuators, refreshable Braille display systems, and several other systems. Fluids used by microvalves are categorized into two groups, liquids and gases. Microvalves used for gases have been applied to drive liquid flows in microfluidic systems, control mass flow rate in mass-flow controllers, as well as programming of tactile dots in refreshable Braille display systems. Microvalves applied for gases utilize several mechanisms to control movement of an orifice closure plate that covers the valve outlet. These include electromagnetic (Meckes et al., 1997), pneumatic (Rich and Wise, 1999), thermopneumatic (Grosjean et al., 1999), piezoelectric (Shoji et al., 1991), bimetallic (Jerman, 1991), and electrostatic actuations (Haji-Babaer et al., 1997).

Electrostatic actuator is a simple mechanism providing low-power consumption applied in portable devices. In order to switch gas flow through an electrostatic microvalve, the substrate and orifice-closure plate must be conductive and separated by an insulator. By applying sufficient voltage between the substrate and closure plate, the movable closure plate is pulled down to touch the insulator, seal the orifice and switch-off gas flow. To switch-on gas flow, the applied voltage is removed and the closure plate is pulled back to the original position resulting from spring mechanical.

Microvalves are always applied in many portable device because there provide the miniature dimension as well as small power consumptions. Oh et al. (2005) were invented multichamber micro PCR chip (Polymerase Chain Reaction) which applied microvalves in dual functions of sample injection and sealing. In drug delivery applications, microvalves were included in micro-pump for prevent the flow back of the solutions (Teymoori and Sani, 2005). For tactile display systems, Yabas et al. (2003) has been presented the concept of microvalves applications in the dot rising mechanism as shown in Figure 4.1. The microvalve is assembled inside a dot chamber which has a flexible screen tactile cover the chamber. The screen remains flat when the actuator is closed. To drive the dot up, the microvalve is applied voltage resulting in the increasing of differential pressure inside the chamber. The membrane is elastically deformed and users can sense the feeling of text display.

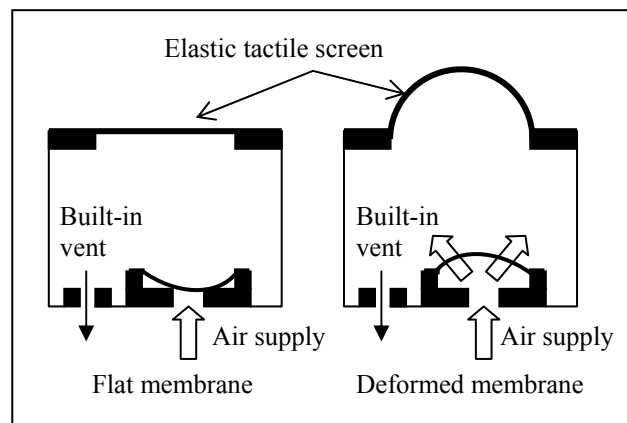


Figure 4.1 Application of electrostatic microvalve in tactile display systems.

By focusing on the applying in tactile display systems, a curled-up with polymeric/metal bimorph structure is introduced into the concept of electrostatic actuator for microvalve application in Section 4.2. The design and fabrication process is presented according to X-ray lithography for the substrate construction and UV lithography process for the closure plate fabrication in Section 4.3. Section 4.4 provides the testing setup and

results of the microvalve in experimentation. Furthermore, simulation models of the microvalve behavior based on electrostatic-fluidic-mechanical domains are proposed in Section 4.5 to estimate the microvalve characteristics. The summary of this chapter can be found in Section 4.6.

4.2 Curled-Up SU-8/Metal Closure Plate Actuator

The actuation principle of curled-up plate for valve operation is illustrated in Figure 4.2. The closure plate is fabricated on top of an orifice which is a gap path way in upward direction. Because the residual stress has been generated from different coefficients of thermal expansion during fabrication, the closure plate is curled away from the substrate as shown in Figure 4.3 (a). As voltage is applied between the ground substrate and the electrode on the curled-up plate, electrostatic force is generated between them to flat the closure plate onto the substrate, resulting in closing position as shown in Figure 4.3 (b). Pattanakul et al. (2006) have been proposed the use of SU-8 photoresist material instead of the conventional material such as SiO_2 (Haji-Babaer et al., 1997) and polyimide (Lee, 1996). The new material allows low-temperature and much more simple processes, which help to reduce the cost of microvalves.

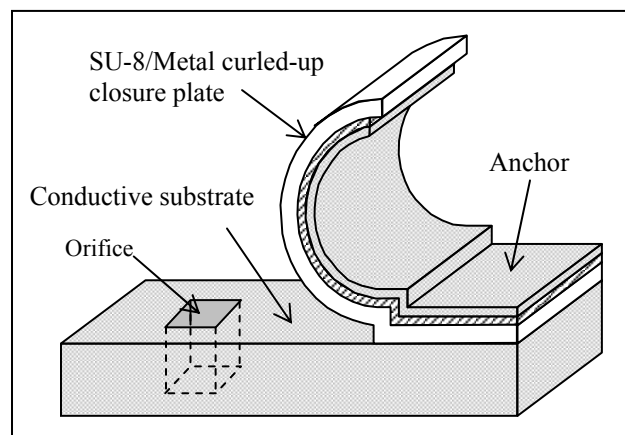


Figure 4.2 Structure of curled-up closure plate for electrostatic microvalves.

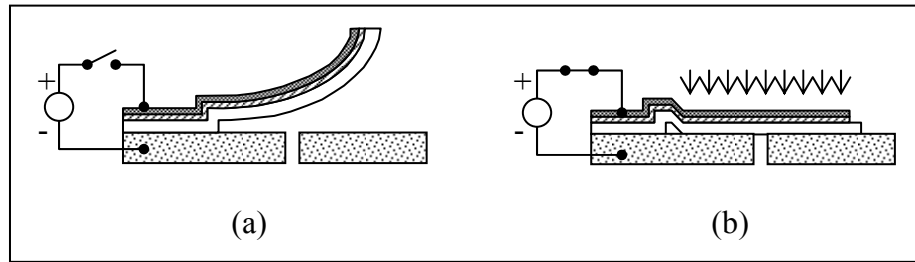


Figure 4.3 Schematic of operation principle of SU-8/metal electrostatic microvalve

(a) open configuration and (b) closed by applying voltage.

4.3 Design and Fabrication Processes

The characteristics of the curled-up closure plate microvalve are illustrated in Table 4.1 and Figure 4.4. The SU-8 photoresist is coated with thickness of $2.3 \mu\text{m}$ (t_{SU-8}) onto a $0.2 \mu\text{m}$ -thick sacrificial layer. After the SU-8 closure plate is created as a rectangular plate with size of $940 \mu\text{m}$ -lengths (L_{SU-8}) and $620 \mu\text{m}$ -widths (w_{SU-8}), the metal electrode with thickness of $0.224 \mu\text{m}$ (t_{metal}) is then formed onto the SU-8 pattern with length and width of $840 \mu\text{m}$ (L_{metal}) and $520 \mu\text{m}$ (w_{metal}), respectively. Finally, the bimorph closure plate is released from the substrate by removal of the sacrificial layer. The compressive-stressed SU-8 film expands while the tensile stressed metal film shrinks. The closure plate is therefore curled away from the substrate.

Table 4.1 Design and constant values of the curled-up closure plate microvalve.

Characteristics	L_{SU-8} (μm)	w_{SU-8} (μm)	t_{SU-8} (μm)	CTE_{SU-8} (ppm/K)	L_{metal} (μm)	w_{metal} (μm)	t_{metal} (μm)	CTE_{metal} (ppm/K)	t_g (μm)
Values	940	620	2.3	~50	840	520	0.224	~13.3	0.2

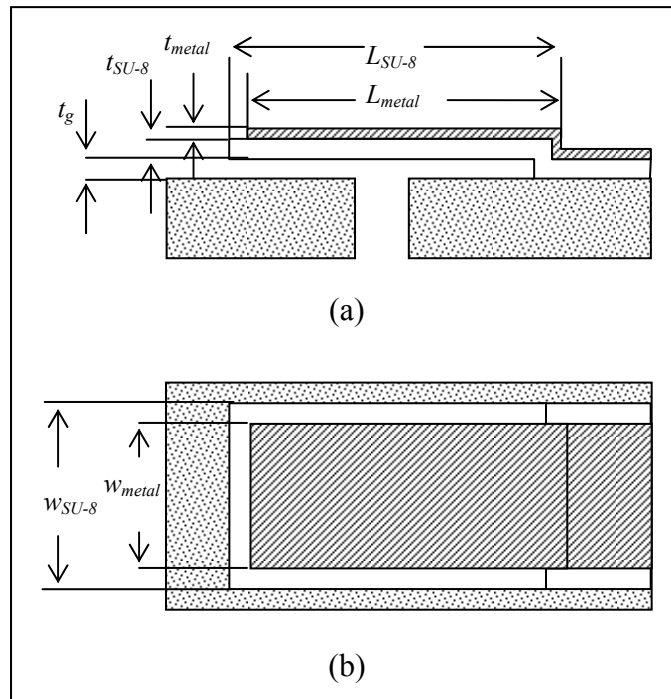


Figure 4.4 Characteristics of microvalve (a) cross-section view and (b) schematic layout.

Microvalve fabrication is planned to fabricate for two sections. The first section is the inlet orifice on the conductive substrate as shown in Figure 4.5. A print circuit board (PCB) with 25 μm -thick copper which is used for the microvalve holder is drilled a hold at the center with a diameter of 2.5 millimeter as shown in Figure 4.5 (a). The work piece is sealed on the top surface by PI tape and filled with PDMS pre-polymer on the back side. To condense the polymer, the sample is cured for 30 minutes at 90°C on a hot plate. After cooling down, the PI tape is peeled off from the sample, resulting in planar surface as shown in Figure 4.5 (b). The top surface is coated with Ti/Cu/Ti by evaporation to utilize as seed layers. Then, a 300 μm -thick film SU-8 photoresist with size of 70 $\mu\text{m} \times 70 \mu\text{m}$ is constructed by using X-ray lithography at the center of the PDMS area as shown in Figure 4.5 (c). The nickel substrate is formed by electroplating and polishing surface as shown in Figure 4.5 (d). The remained SU-8 photoresist inside the orifice is eliminated by O_2/CF_4 plasma until the light can be passed through the orifice as shown in Figure 4.5 (e). At last of this

process, the orifice is planarized by using sacrificial material such as AZ P4620 positive photoresist or un-crosslinked SU-8 negative photoresist. The back side is filled with photoresist and vacuumed through the orifice by a vacuum pump. After soft baking at 90°C for 8 hours, the nickel surface is polished on a polishing cloth to remove all of photoresist placing around the orifice as shown in Figure 4.5 (f).

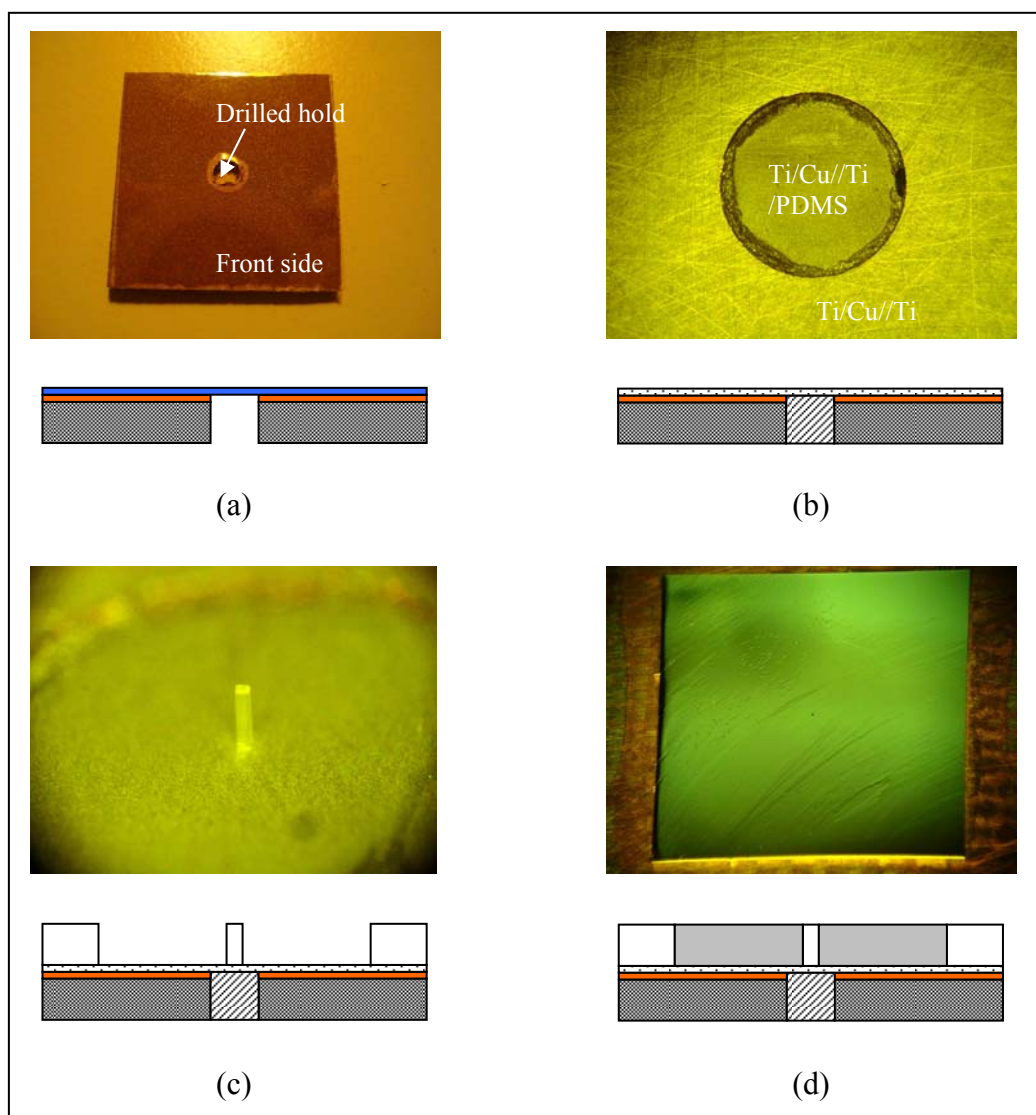


Figure 4.5 Fabrication sequences of the nickel substrate with an inlet orifice.

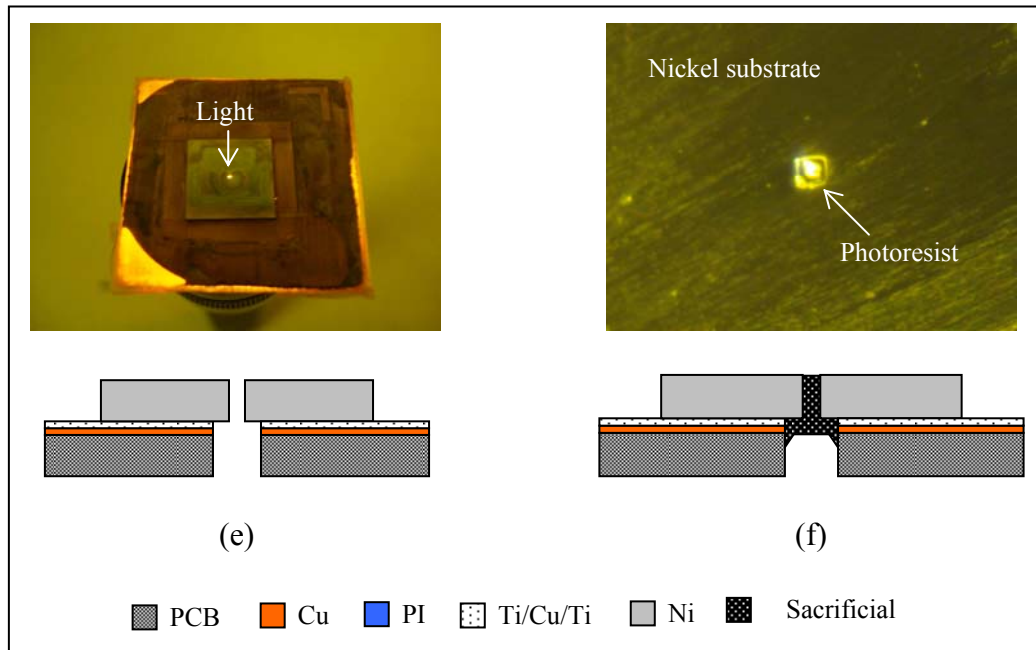


Figure 4.5 Fabrication sequences of the nickel substrate with an inlet orifice (Continued).

The second section is the curled-up closure plate of microvalve which is used to as a shutter for the applied pressure. The nickel substrate with the planarized orifice is deposited with a 0.2 μm -thick Al thin film by using evaporation. UV lithography processes are then used to create a rectangular pattern of Al as shown in Figure 4.6 (a). This Al rectangle serves as a sacrificial support for the closure plate. A layer of SU-8 2002 negative photoresist is spin-coated and patterned as the rectangular area in which one end is anchored on the glass substrate whilst another lies on top of the sacrificial Al layer as shown in Figure 4.6 (b). Metal films of 300 \AA Ti / 500 \AA Cu are evaporator-deposited and patterned as an upper electrode above the SU-8 layer to form an SU-8/metal bimorph structure. To protect Cu layer from oxidation, AZ 1512 is spin-coated and patterned on the copper as shown in Figure 4.6 (c). Nickel is grown on the copper layer as shown in Figure 4.6 (d), followed by AZ photoresist removal. Other thin films are also etched by wet solution to open the Al sacrificial layer as shown in Figure 4.6 (e). Finally, the bimorph closure plate is released from the substrate by removal of the sacrificial Al support in wet etchant. Upon release of the

composite closure plate, the compressive-stressed SU-8 film expands and the tensile stressed Ti/Cu metal film shrinks. The closure plate is therefore curled away from the substrate as shown in Figure 4.6 (f) and compared to an ant as shown in Figure 4.7.

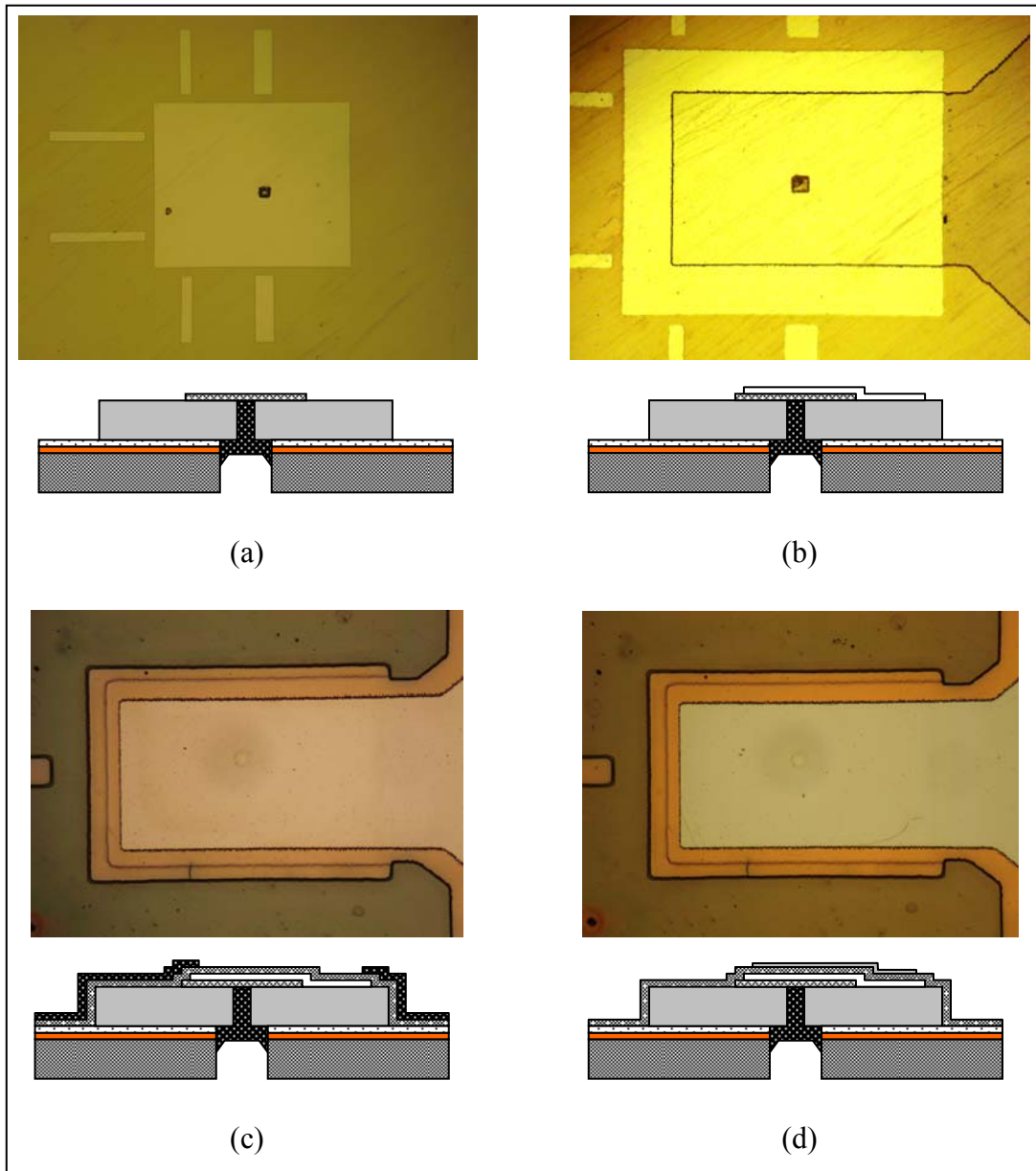


Figure 4.6 Fabrication process of the curled-up closure plate of microvalve.

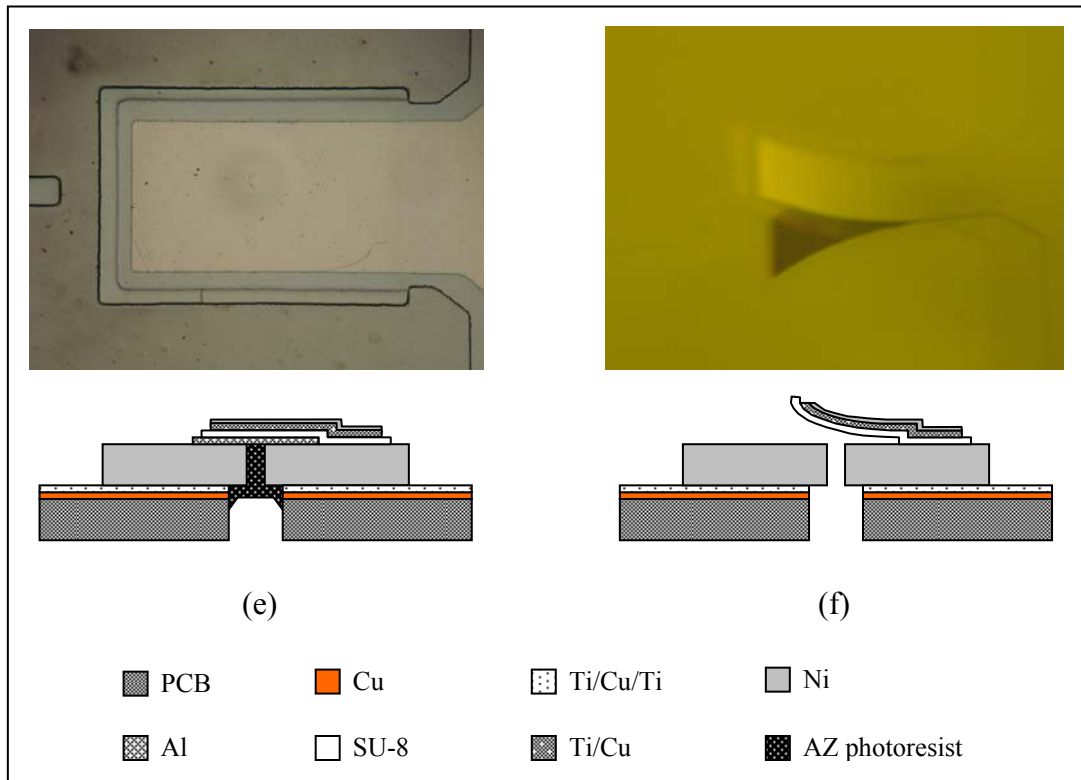


Figure 4.6 Fabrication process of the curled-up closure plate of microvalve (Continued).

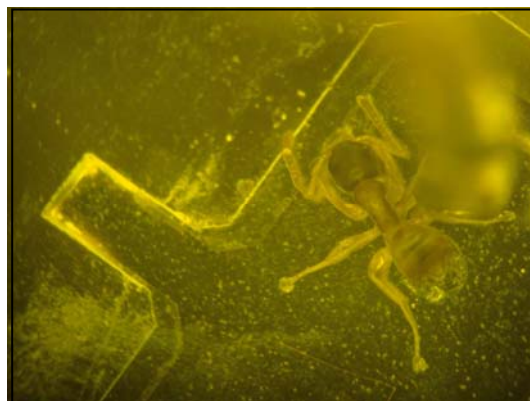


Figure 4.7 The finished curled-up closure plate microvalve compared to ant.

4.4 Experimental Setup and Results

The closure plate is made of $2.3 \mu\text{m}$ SU-8 layer with $0.224 \mu\text{m}$ adhesive layer of Ni by neglecting the thickness of Ti/Cu composite layer. A distance from substrate to free end of closure plate is measured by Veeco[®] interferometric surface profiler NT1100 which give

the deflection of $138\ \mu\text{m}$ from the substrate and $3.2\ \text{mm}$ of radius curvature as shown in Figure 4.8. Assuming the beam is flat before deposited metal layer, the residual stress in the metal film can be calculated using Stoney equation which achieves a stress value of $1.773\ \text{MPa}$. The mathematic model of the bimorph structure which is estimated the beam characteristics will be described in Section 4.5. Applying a positive voltage to the composite metal layer on the closure plate and a ground to the nickel substrate, a voltage of $115\ \text{V}$ is needed to pull down the closure plate in absence of gas flow through the orifice as shown in Figure 4.9.

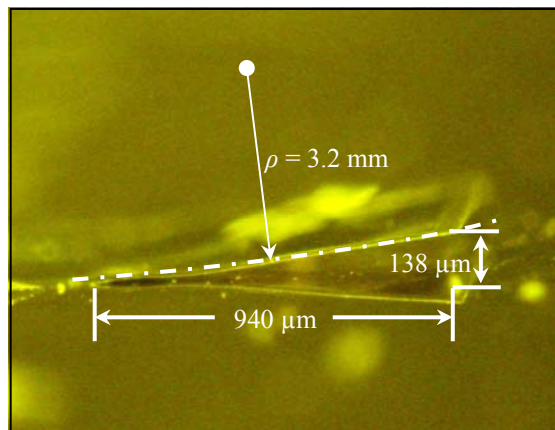


Figure 4.8 Bird's eye view optical micrographs of the curled-up closure plate microvalve.

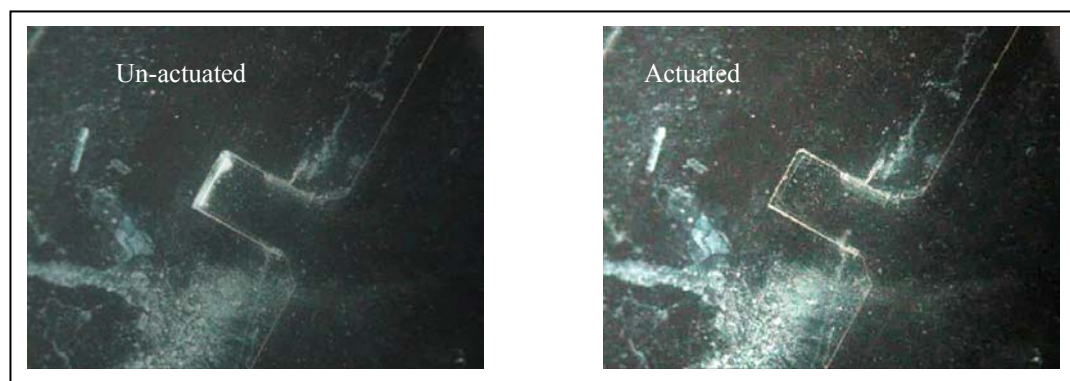


Figure 4.9 Experimental testing of the curled-up plate of microvalve.

After testing in normal state, microvalve is contained in an acrylic package which is fixed with two pneumatic tubes on each side as shown in Figure 4.10 (a). Two PDMS square frames are used to seal the gas leakage of the applied pressure on both side of the microvalve and tightly compressed by four screws as shown in Figure 4.10 (b). The top and bottom electrodes of microvalve are connected with copper wires and linked to the external for applying high DC voltage. The gas pressure is applied at the bottom through the inlet orifice of microvalve operated as the normally open valve.

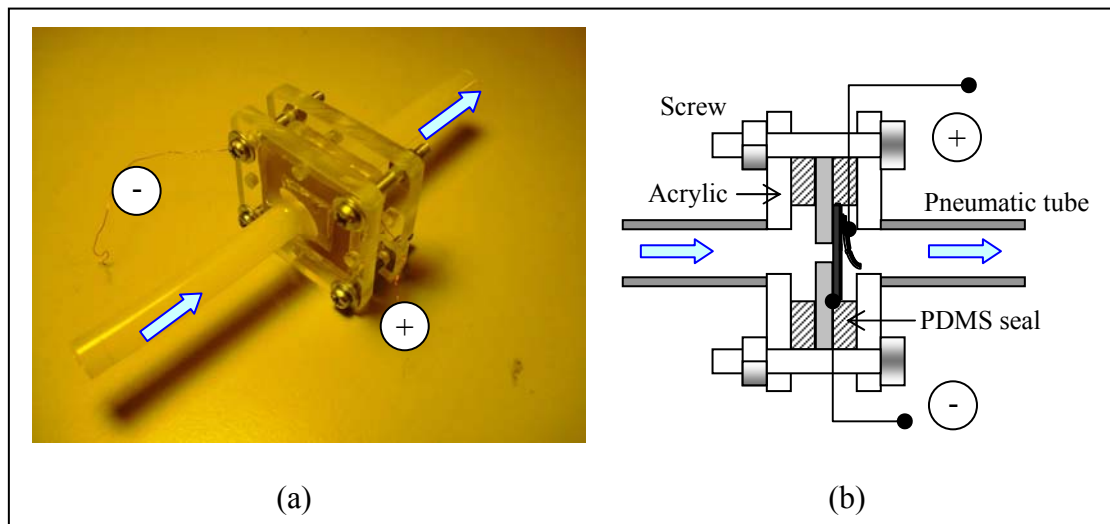


Figure 4.10 Setup of microvalve (a) inside the acrylic package and (b) cross-section.

After the microvalve was contained in the package, the volume flow rate experimentation is set up as shown in Figure 4.11 (a). The applied gas pressure is monitored at input port by using a pressure gauge and the volume flow rate is measured at output port by connecting the mass flow controller series to the microvalve. The high voltage DC generator, ranging from 0 V to 1 kV, is connected between the electrodes of microvalve to actuate the closing state. As shown in Figure 4.11 (b), the pressure sensor, MPX5700 series piezoresistive transducer, is connected to input port and displayed the results on the pressure gauge. The mass flow controller, Fofloc 8300, which is connected in

series to the microvalve is measured in unit of sccm or ml/min. Figure 4.12 illustrates the microvalve operation consisting of 3 states. No applied pressure is the first state as shown in Figure 4.12 (a). Then, the nitrogen gas is applied by feeding nitrogen gas pressure through the inlet hole, resulting in a small deflection of the closure plate as shown in Figure 4.12 (b). At last, the actuated voltage is applied to the microvalve and pulls the closure plate collapse to the substrate as shown in Figure 4.12 (c).

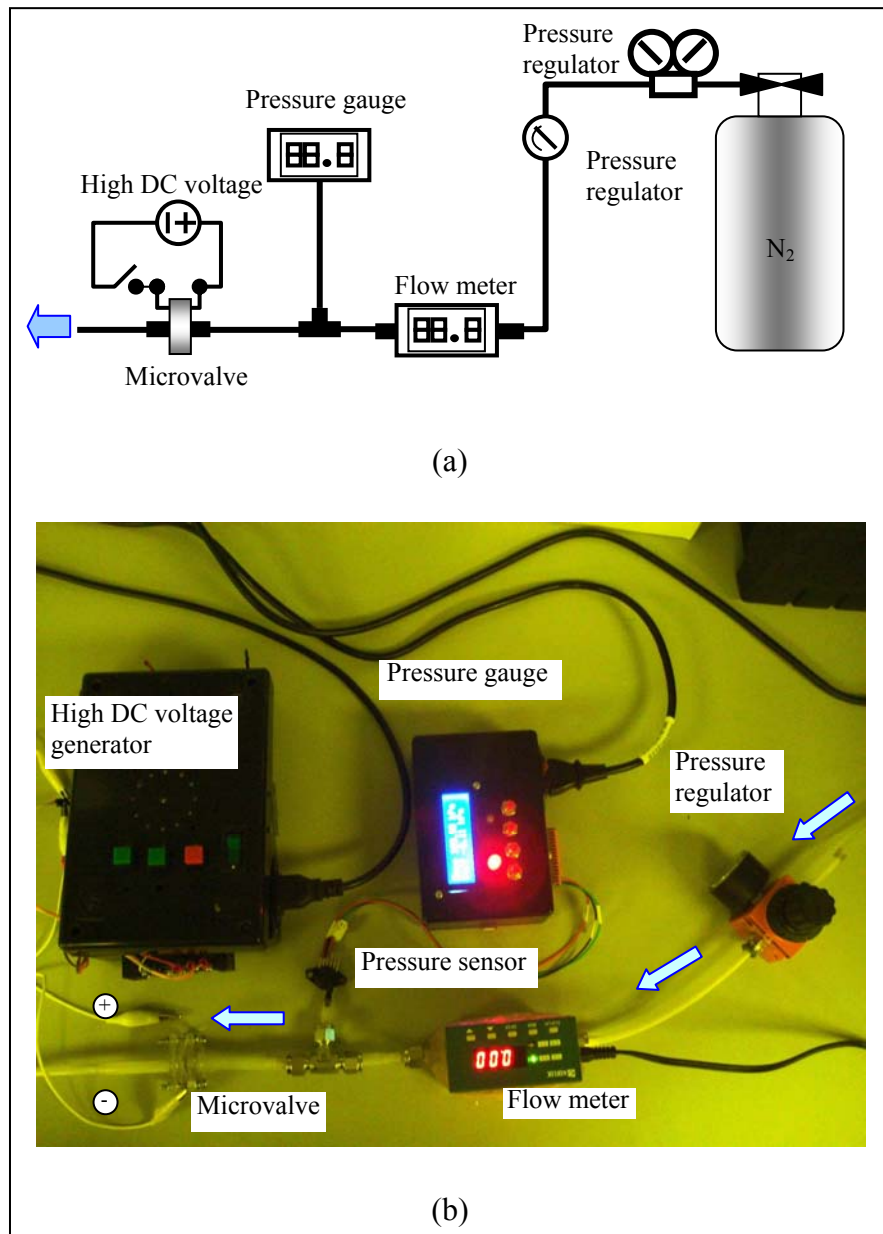


Figure 4.11 Experimental setup for the microvalve.

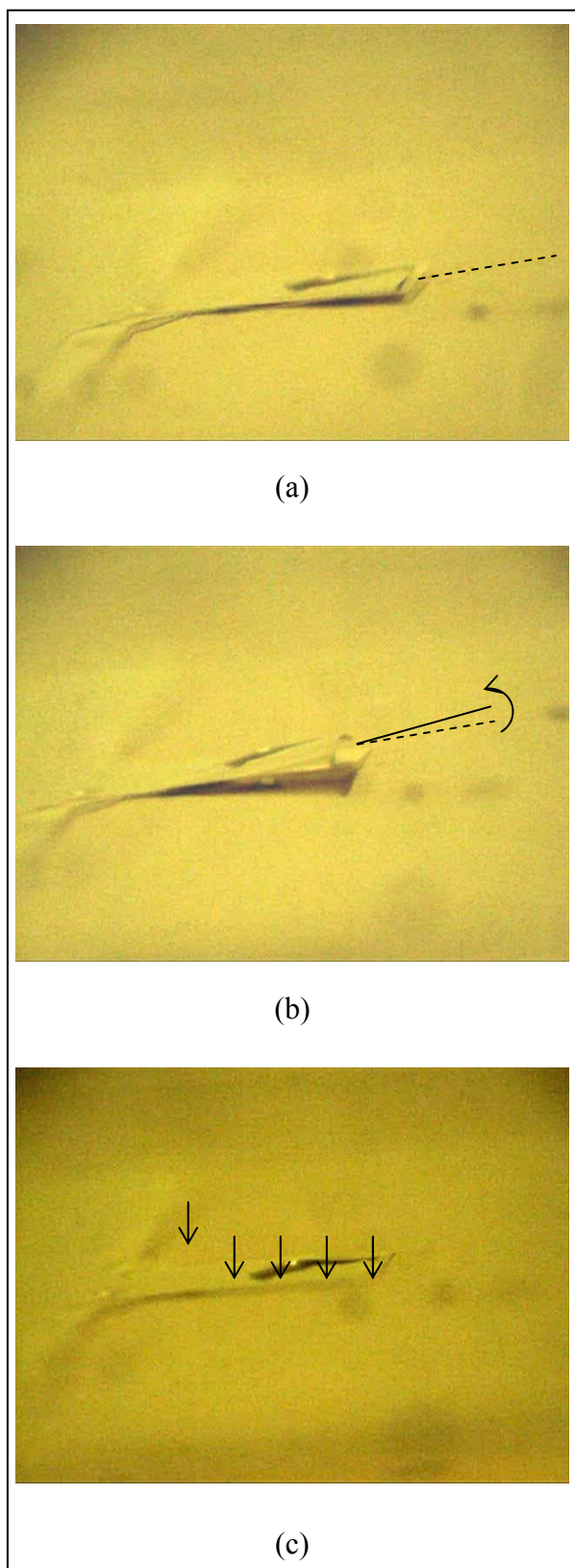


Figure 4.12 Experimental testing the microvalve (a) no voltage potential
(b) applied gas pressure and (c) applied closing voltage.

The volume flow rate as a function of the applied voltage is shown in Figure 4.13. The initial rate is set up for 5 values and the actuated voltage is increased until the volume flow rate is reduced to a constant value. At these points, the behaviors of closure-plate are pull-in state to close the orifice, but there are not absolutely closed and percent of leakages are also illustrated in the figure.

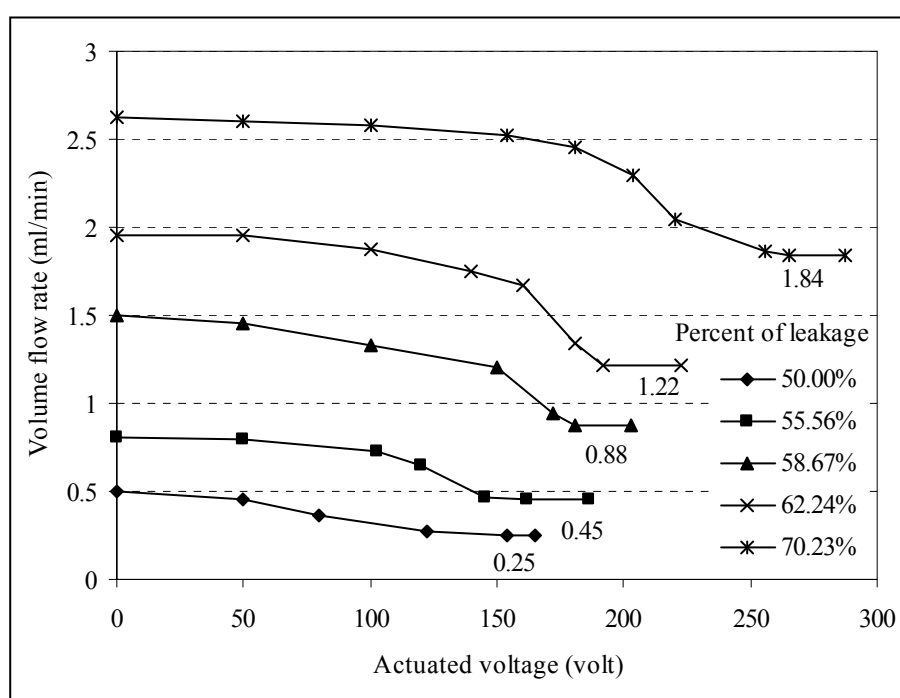


Figure 4.13 Volume flow rate as a function of the applied voltage.

The valve characteristics are investigated as demonstrated in Figure 4.14. The volume flow rates vary according to the differential pressure inside the pressure chamber as shown in Figure 4.14 (a). The increased volume flow rates require higher closing voltage since the pneumatic force is raised the closure plate higher as shown in Figure 4.14 (b). Furthermore, the volume leak rates when the valve is closed are also investigated as shown in Figure 4.14 (c).

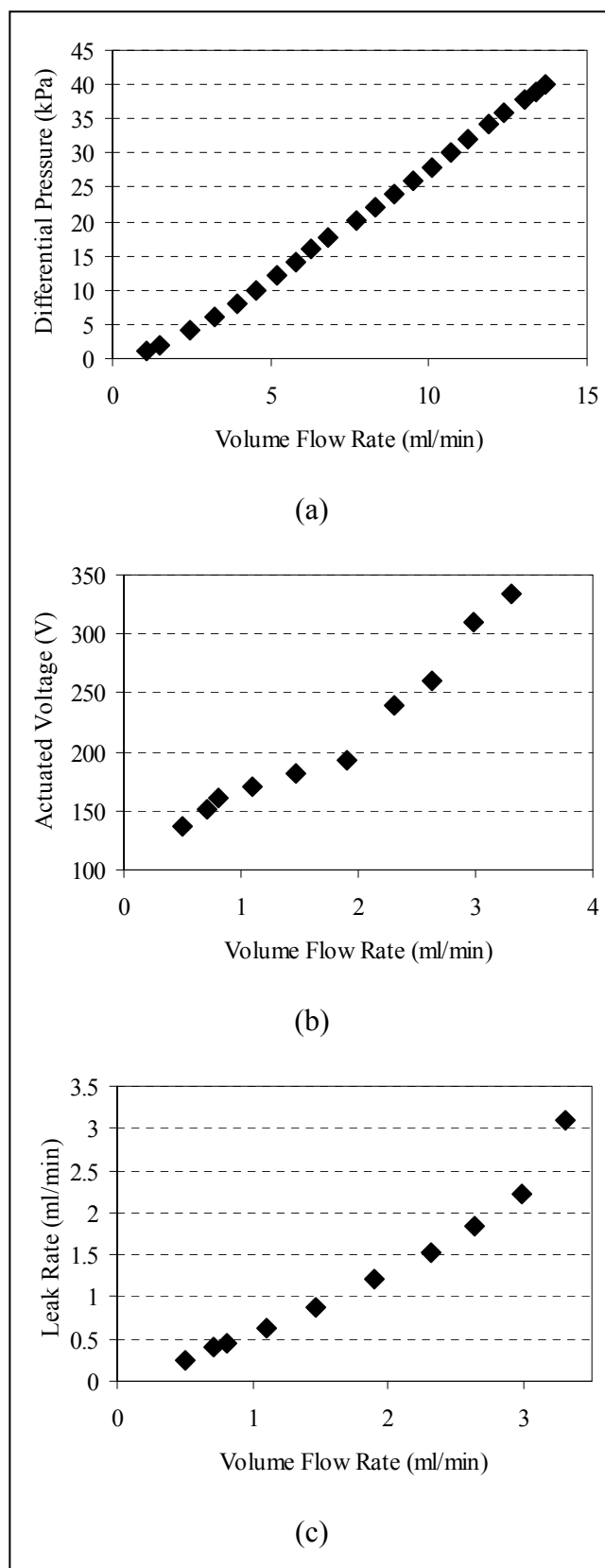


Figure 4.14 The characteristics of curled-up electrostatic microvalve.

The leakages of microvalve are resulted from the roughness of the nickel substrate cause by the polishing process as shown in Figure 4.15 (a). Although the nickel surface when scanning through the microscope does not appear the obvious abrasion, it can be clearly seen in the bird eye view as shown in Figure 4.15 (b). This make the closure plate of microvalve can not be closed perfectly.

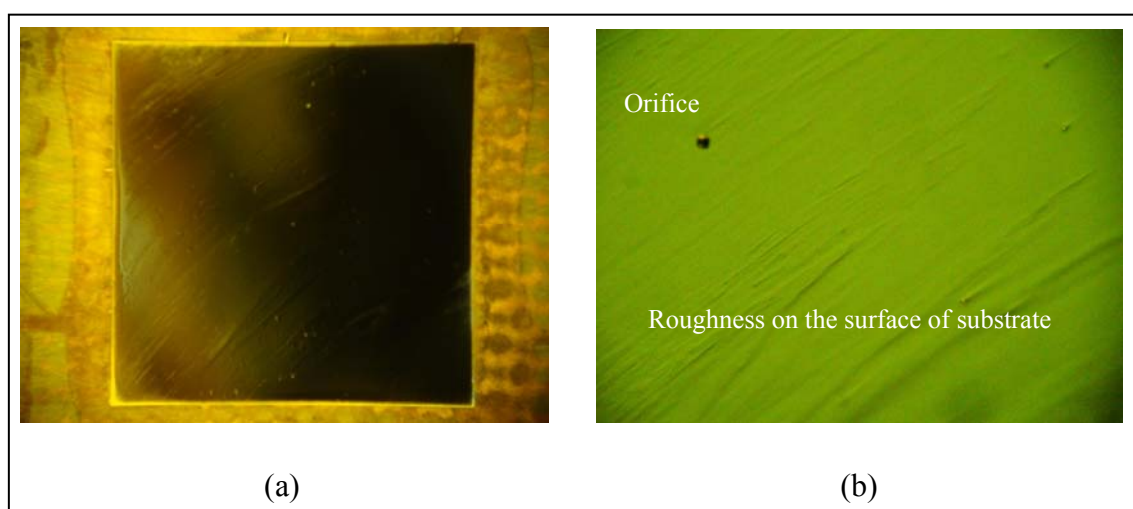


Figure 4.15 (a) Top view of the polished nickel substrate and (b) bird eye view.

Moreover, the irregular residual stress between the bi-material structure, SU-8 and metal upper electrode, induce the distorted curve on the closure plate as shown in Figure 4.16. However, this problem can be solved by improving of the polishing technique. The polishing machine with the cloth abrasive can be used to clear these roughnesses. In addition, spin-coating of thin polymer film on the substrate before the closure plate is fabricated will be helped to reduce the plurality of gaps under the substrate.

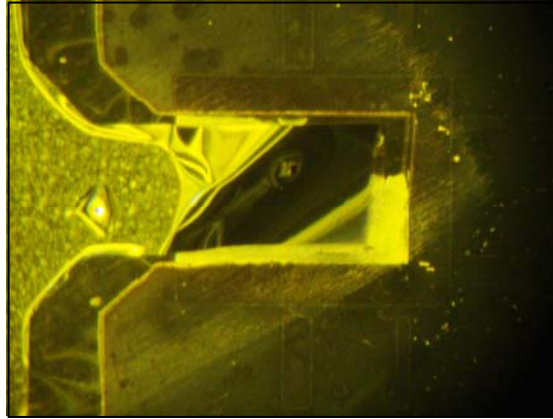


Figure 4.16 The distorted curve on the closure plate of microvalve.

4.5 Mathematical Models

4.5.1 Mathematic models of the curled-up closure plate

Figure 4.17 shows schematically the composite plate which is composed of two materials with different residual stresses, σ_1 and σ_2 , as well as different Young's modulus, E_1 and E_2 . The two materials also have difference thickness, t_1 and t_2 and likewise the width, w_1 and w_2 . This device has the mechanical behaviour similar to the bimetallic strip used in thermostats (Timoshenko, 1925). With difference residual stress and thermal expansion inside each layer, the composite beam is bent up. Assuming the axial forces, P_1 and P_2 , act at the center of their cross section, a force and moment will be balanced at the interface between two materials as shown in Equation (4.1) and (4.2).

$$P_1 = P_2 = P(\text{equilibrium}) \quad (4.1)$$

$$P\left(\frac{t_1 + t_2}{2}\right) = M_1 + M_2 = M \quad (4.2)$$

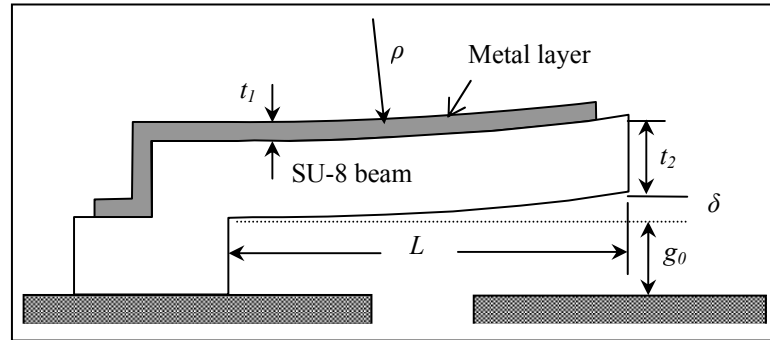


Figure 4.17 Dimensions of the curled-up closure plate.

where $M_1 = E_1 I_1 / \rho$ and $M_2 = E_2 I_2 / \rho$ are moment of SU-8 and metal beam, respectively, ρ is a radius of curvature of the closure plate. The moments of inertia of top and bottom material are given by $I_1 = w_1 t_1^3 / 12$ and $I_2 = w_2 t_2^3 / 12$, respectively. The strain is developed from 4 components: residual stress, axial force, the force due to curvature, and thermal expansion (Edmonds et al., 2004) which leads to Equation (4.3).

$$\alpha_1(\Delta T) + \frac{\sigma_1}{E_1} + \frac{P_1}{E_1 t_1 w_1} + \frac{t_1}{2\rho} = \alpha_2(\Delta T) + \frac{\sigma_2}{E_2} + \frac{P_2}{E_2 t_2 w_2} + \frac{t_2}{2\rho} \quad (4.3)$$

where, α_1 and α_2 are the coefficient of thermal expansion (CTE) of material of two layer, and ΔT is the change in temperature.

Axial force, P , from Equation (4.2) is substituted into Equation (4.3). And for the initial radius of curvature of ρ_0 , the change in radius of curvature is given by Equation (4.4).

$$\frac{1}{\rho} - \frac{1}{\rho_0} = \frac{(\alpha_2 - \alpha_1)\Delta T - \frac{\sigma_1}{E_1} + \frac{\sigma_2}{E_2}}{\frac{t}{2} + \frac{E_1 t_1^3 + E_2 t_2^3}{6t} \left(\frac{1}{E_1 t_1} + \frac{1}{E_2 t_2} \right)} \quad (4.4)$$

Assuming that the SU-8 closure plate is planar at room temperature, the curvature radius due to residual stress in metal film is $\rho = L^2/2\delta$, and the residual stress can be calculated using the Stoney formula is given in Equation (4.5) (Stoney, 1909). The initial deflection of the closure plate along the length, $z(x)$, is given by Equation (4.6) (Musolt and Khol, 2003).

$$\sigma_1 = \frac{E_2 t_2^2}{6(1-\nu_2)t_1} \left(\frac{1}{\rho_0} - \frac{1}{\rho} \right) \quad (4.5)$$

$$z(x) = \frac{x^2}{2} \left(\frac{1}{\rho} - \frac{1}{\rho_0} \right) \quad (4.6)$$

where L , t are length and thickness of beam, δ and ν_2 are deflection of the end of the beam and Poisson's ratio of SU-8, respectively.

For activation microvalve, applying a voltage between the substrate and the closure plate provides electrostatic force that pulls the movable plate down. For simulation of deflection behaviour of closure plate under this condition, electro-mechanical model with a first-order fringing-field correction is included in electrostatic to simulate with Equation (4.7) (Osterberg, 1995). Because of SU-8 photoresist is dielectric layer and main structure of the closure plate, the model included the dielectric term (t_2, ϵ_2) in this calculation for optimal solution. The factor in parentheses on the right of equation is the fringing-field correction.

$$(\tilde{E}I)_{eqv} \frac{d^4 g}{dx^4} = -\frac{\epsilon_0 w_1 V^2}{2(g + t_2 / \epsilon_2)^2} \left(1 + 0.65 \frac{(g + t_2 / \epsilon_2)}{w_1} \right) \quad (4.7)$$

where $(\tilde{E}I)_{eqv} = \tilde{E}_1 I_1 + \tilde{E}_2 I_2$, is an equivalent beam strength which is used (Hopcroft, 2002). For diaphragms ($w \geq 5t$), the effective modulus \tilde{E}_1 and \tilde{E}_2 are $E_1/(1-\nu_1^2)$ and $E_2/(1-\nu_2^2)$,

respectively. And $g = g_0 + z$, is the height of beam from substrate as a function of distance, x , along the length of the beam from the fixed end, $x = 0$. Permittivity of SU-8 and applied voltage are ϵ_2 and V , respectively.

For gas flowed through the orifice is assumed to be compressible based on theory of ideal gases in nozzle as shown in Figure 4.18 (a) and (b). Yobas (2003) has been presented the couple fluidic-mechanical model which the mass flow rate through the microvalve (m), the orifice (m_o) and the gap (m_{gap}) must be identical with Equation (4.8).

$$m = m_o = m_{gap} \quad (4.8)$$

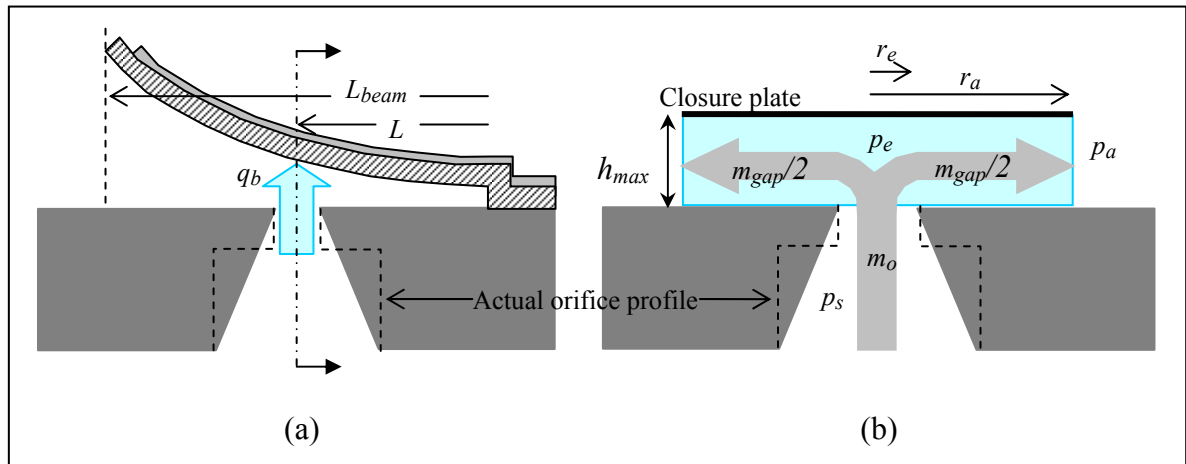


Figure 4.18 Structure parameter in a nozzle of microvalve.

The model covers the full range of flow conditions. Meanwhile, pressure ratio of outlet pressure p_e and inlet pressure p_s greater than critical value $(p_e/p_s) > (2/(\gamma+1))^{\gamma/(\gamma-1)}$, the mass flow rate, m_o , through the square orifice can be approximated with subsonic flow by Equation (4.9).

$$m_0 = C_i A_{eff} p_s \sqrt{\frac{2\gamma}{(\gamma-1)RT} \left[\left(\frac{p_e}{p_s} \right)^{\frac{2}{\gamma}} - \left(\frac{p_e}{p_s} \right)^{\frac{(\gamma+1)}{\gamma}} \right]} \quad (4.9)$$

where C_i is discharge coefficient, A_{eff} is the effective valve area approximated by $A_{eff} = 2\pi r_e h_{max}$, p_s and p_e are absolute supply pressure of the microvalve and absolute pressure under the gap entrance, respectively. γ is ratio of specific heats of air (1.4), R is universal gas constant/molecular weight, T is temperature in Kelvin (K).

The mass flow through the gap can be approximated by using analytical of Reynolds differential equation (Gross, 1980; Yobas, 2003) in Equation (4.10). Based on this approximation, the closure plate and orifice are presumed circular and aligned well at the center. The supply pressure p_s is applied under the orifice, resulting in the pressure under the closure plate p_e while the atmosphere pressure p_a staying around the closure plate. The pressure variation underneath the closure is assumed to act only in radial direction and any disturbance of the beam is neglected. r_a and r_e are radius of the closure plate and orifice, respectively.

$$m_{gap} = \frac{\pi h_{max}^3 (p_e^2 - p_a^2)}{12\mu RT \ln\left(\frac{r_a}{r_e}\right)} \quad (4.10)$$

The gap height h_{max} in Equation (4.10) is the maximum deflection at the center of the closure plate which is a summation of the initial gap resulting from naturally curled-up beam h_o and the deflection of the beam under the applied pressure h_p . As shown in Figure 4.19, the fixed-end beam with point load method is used to estimate the deflection at point L applied by net load F_p as a result of constant applied pressure under the closure plate. The maximum deflection and the force under the closure plate (F_b) due to gas film pressure (Hamrock, 1991) can be estimated by using Equation (4.11) and (4.12), respectively.

$$h_{\max} = h_o + h_p = h_o + \frac{F_b L^3}{3EI} \quad (4.11)$$

$$F_b = \frac{\pi(p_e - p_a)(r_a^2 - r_e^2)}{2 \ln\left(\frac{r_a}{r_e}\right)} \quad (4.12)$$

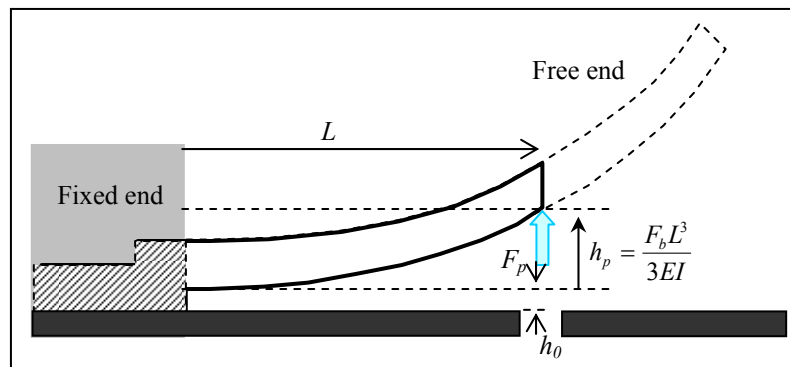


Figure 4.19 The fixed-end cantilever free body diagram.

By substituting Equation (4.12) in (4.11), the maximum deflection of the model is only based on p_e for movement calculation which can be obtained as:

$$h_{\max} = h_o + \frac{\pi(p_e - p_a)(r_a^2 - r_e^2)L^3}{6EI \ln\left(\frac{r_a}{r_e}\right)} \quad (4.13)$$

Since the mass flow through the microvalve can be measured by using the mass flow meter in the experimental, the maximum gap in Equation (4.13) is substituted in Equation (4.10) and the absolute pressure at the film entrance p_e is iterated until they results have an error less than 0.0001. Therefore, p_e and h_{\max} are solved and substituted in Equation (4.9) to calculate the discharge coefficient C_i for this curled-up closure plate microvalve. By definition, the discharge coefficient is the ratio of actual flow rate to the theoretical rate of

flow through the orifice. The value of C_i is less than 1 because the theoretical flow rate is always greater than the experimental measurement depending on the microvalve structure. After calculating C_i , the volume flow rate through the microvalve can be calculated by Equation (4.14) which should be the same as the experimental value.

$$Q = \frac{m_o}{\rho} = m_o \left(\frac{RT}{P_s} \right) \quad (4.14)$$

4.5.2 Modelling results

For closure plate behavior simulation, the initial deflection of curled-up closure plate is achieved by using the deflection model in Equation (4.5) and (4.6). The initial tip deflection of the beam is 138 μm (zero applied voltage) as shown in Figure 4.20 (a). Continuous deflection is occurred up by a bias voltage of 107 V which the deflection of the beam is 99.3 μm . Applying voltages beyond this point, the closure plate is suddenly pulled down and made contact with the substrate. Figure 4.20 (b) shows simulation results by using Scilab for the tip deflection under the applied voltage which agrees with the experimental results.

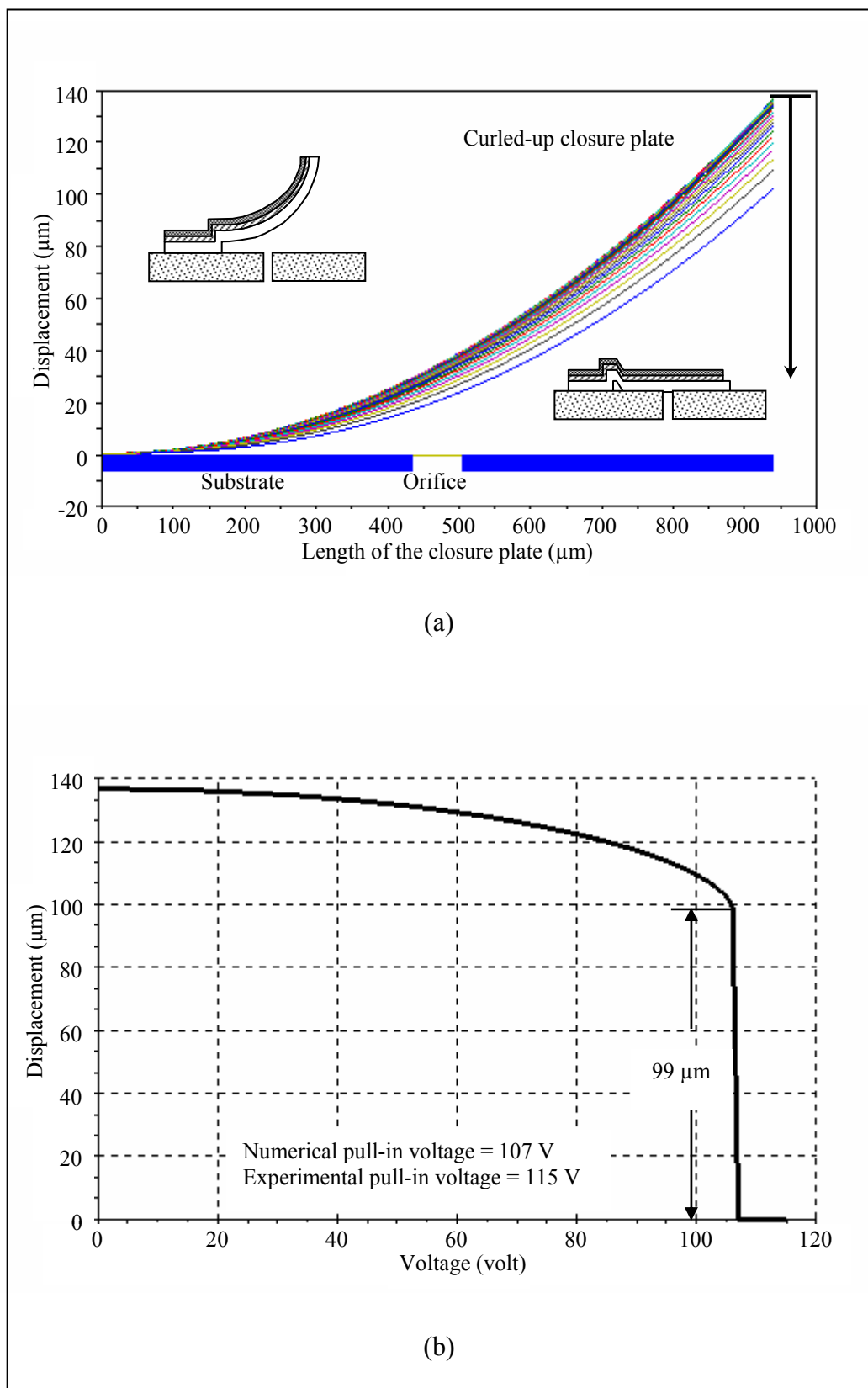


Figure 4.20 Simulation results (a) moving of closure plate and (b) deflection-voltage behavior.

The solution, $g(x)$, of the fourth order nonlinear differential equation can be solved by apply following boundary condition: no deflection at the fixed end of the beam ($g(x = 0) = g_0$), slope of the deflection at the fixed is zero ($dg(x = 0)/dx = 0$), no moment acting on the free end ($d^2g(x = L)/dx^2 = 0$), and no shear force acting on the free end ($d^3g(x = L)/dx^3 = 0$). A finite-difference iterative relaxation method is performed in Scilab to solve for pull-in voltage of curl-up closure plate in normal state without the applied pressure.

For the couple fluidic-mechanical model which is used to calculate three unknown values, p_e , h_{max} and C_i , is illustrated the results in Figure 4.21. Figure 4.21 (a) shows the estimated values of C_i as a function of the pressure ratio p_e/p_s for the curled-up closure plate. The valve with the orifice size of $70 \mu\text{m} \times 70 \mu\text{m}$ and the curled-up closure plate require small discharge coefficient which implies an increase in the pressure losses when the applied pressure is increased. Form the C_i results, this mass flow model can be used for the subsonic flow that have a pressure ratio greater than the critical value of 0.5283. Base on the mathematic model, this microvalve can be supported with the maximum supply pressure of 85 kPa at a pressure ratio of 0.5436. The pressure at the gap entrance is 0.03 kPa resulting in the deflection of the closure plate of $74 \mu\text{m}$. The maximum volume flow rate based on this estimation is 5.2 ml/min and the mass flow rate is 0.19 mg/sec. The discharge coefficient which is calculated by this model is a result of the pressure at the gap entrance p_e as shown in Figure 4.21 (b). The p_e values are very small when compare with the applied pressure. These imply that the pressure losses greatly happen at the gap entrance since the actual profile of orifice is not the nozzle which is used to calculate in the model. Furthermore, the gap height at the center of the curled-up closure plate is estimated under constant pressure as shown in Figure 4.21 (c). The initial separation h_o over the orifice is $33 \mu\text{m}$ and can be deflected up to $101 \mu\text{m}$ depending on the applied pressure.

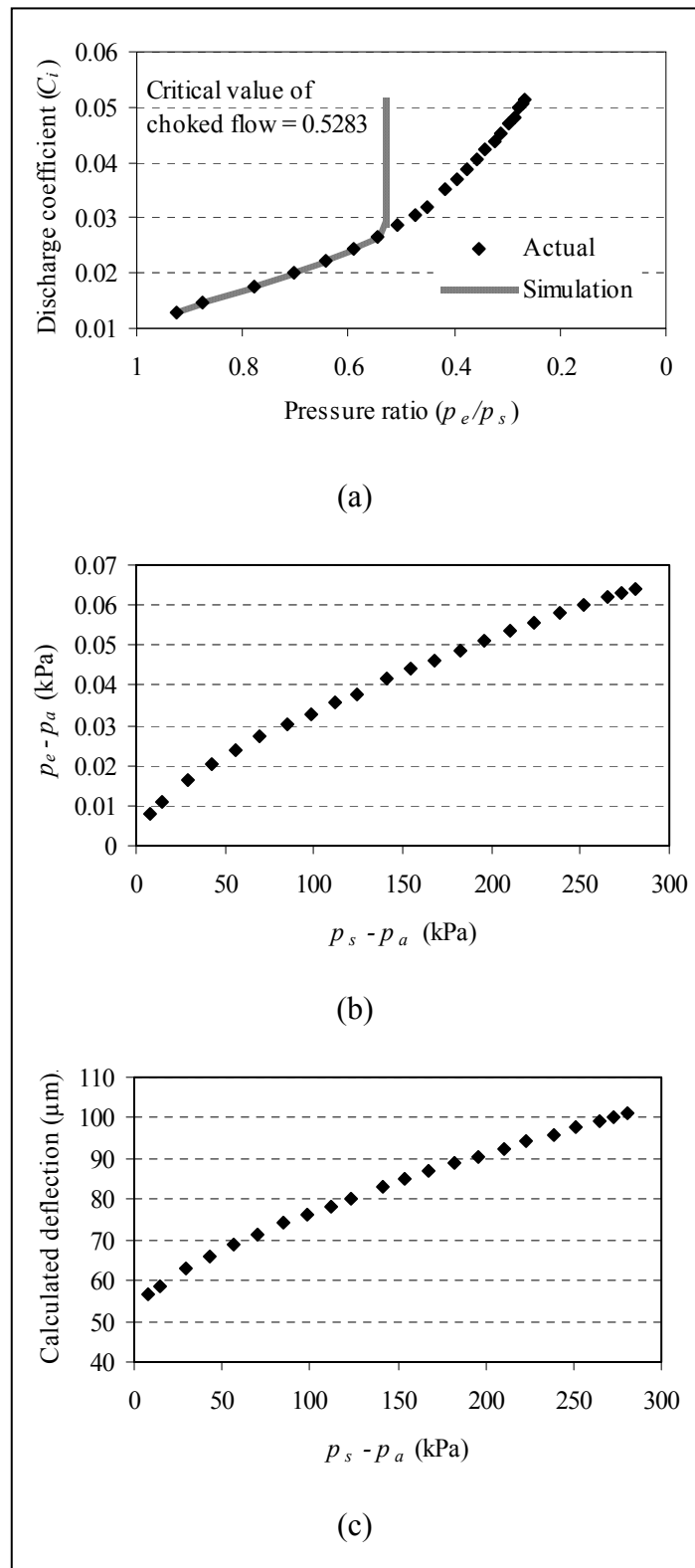


Figure 4.21 The modelling results of the SU-8 curled-up closure plate microvalve.

From the gap deflection simulation, the results are utilized to estimate the actuated voltage of the curled-up closure plate as shown in Figure 4.22. The simulated gap height is used to be references in the mechanical-electrical model in Equation (4.7). The stress of the SU-8 closure plate is searched by using bi-section method until the deflection of the beam close to the simulated gap height. Finally, the closed voltage is calculated by using the finite different method and plotted in the figure.

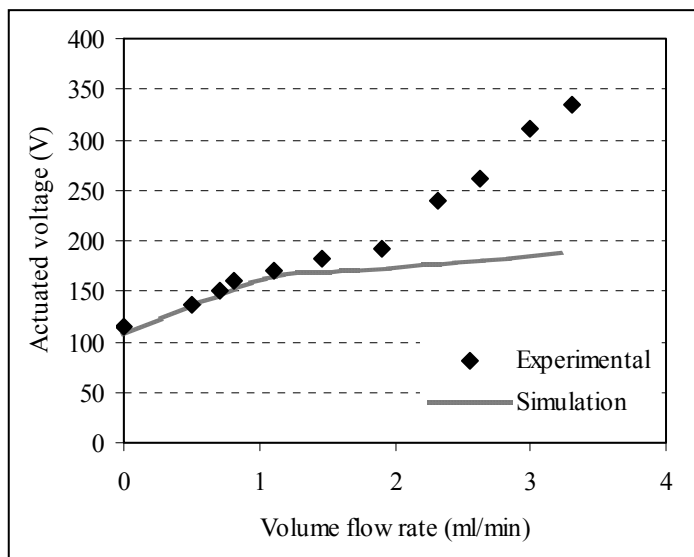


Figure 4.22 The actuated voltage simulation compare with the experimental results.

From the simulation results, the estimated values are significantly lower than the experimental testing which is the function of the volume flow rate. The maximum deflection from the model is calculated at $66.17 \mu\text{m}$ which give the closed voltage at 188 volt while the tested voltage was 334 V at the same volume flow rate. These inconsistencies are the consequence of the model estimation resulting from the gap height function. The actual deflections under the supplied pressure are always greater than the model results and require the higher actuated voltage. These imply that the force at the gap entrance resulting from the model cannot be perfectly used to estimate the actual load on the closure plate. However, the

fluidic-mechanical model can be utilized as the fundamental concept for the microvalve estimated results in the fabrication which needs to know for the structure optimization.

4.6 Chapter summary

The SU-8/metal curled-up closure plate microvalve has been designed and fabricated to perform as the shutter of the tactile dot display system which is available by using MEMS technology. The microvalve consists of the orifice and the closure plate. The orifice which is the nickel substrate is fabricated by using X-ray LIGA and electroplating process. After polishing and planarization on the substrate, the closure plate is constructed on the orifice based on UV lithography fabrication. Using the wet etchnat of sacrificial material, the closure plate is curled away from the substrate resulting from the stress gradient between the bi-material. The microvalve is then experimentally measured the characteristics, including the volume flow rate, actuated voltage, and leak rate. Moreover, the electrical-mechanical model is introduced to estimate the actuated voltage of the closure plate, and the fluidic-mechanical model is also applied to evaluate the flow characteristics of the microvalve based on the system in a steady state. The pull-in voltage model has the results agree with the actual testing, but the other one have to be improved about the fluidic model for optimization of the microvalve design.

CHAPTER V

DEVELOPMENT OF A PNEUMATIC TACTILE DISPLAY

5.1 Introduction

Development of the tactile dot stimulation based on pneumatic actuation is presented in this chapter. In the standard six-dot Braille display module as illustrated in Figure 5.1, a Braille dot with a diameter of 1.45 mm and a height of 480 μm is formed in two columns each of which contains three dots. This implies that the developed tactile display must be in this configuration.

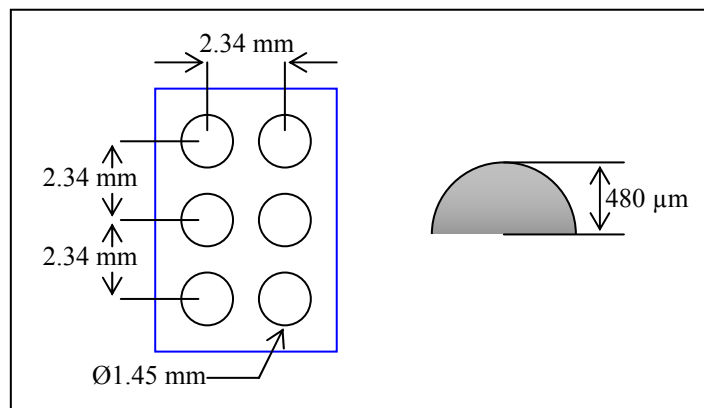


Figure 5.1 The nominal Braille specifications as set by the National Library Service for the Blind and Physically Handicapped (NLS).

The main objective of this chapter is a working prototype of the novel pneumatic tactile dot stimulation based on X-ray LIGA technology. The development of elastic polymer tactile display, polymethylsiloxane (PDMS, known commercially as Sylgard), is the first presentation in Section 5.2. Three bonding methods between PDMS membrane and SU-8 tactile structure are proposed to utilize in the tactile dot under the applied pressure.

Deflection of the membrane is measured and analyzed to calculate in the load-deflection model. Section 5.3 introduces SU-8 tactile dot structure fabricated by X-ray LIGA which is developed and driven as rigid tactile dot stimulation. Multilayer construction of SU-8 photoresist is performed and created as a small piston inside a display panel, resulting in obvious sensation of the dot rising. Section 5.4 presents two prototypes of the refreshable tactile display. The SU-8 tactile display placing on PDMS membrane is the first proposed, followed by the SU-8 dot stimulation placing on the curved spring segment. The summary of this chapter can be found in Section 5.5.

5.2 Tactile Dot Display with a PDMS Membrane

PDMS is one of polymer material that is always used in micro-fluidic application. Flexible structure with compatibility at low cost including convenient preparation and organization is the advantage in consideration this material for many applications. Micro-channel construction is continuously performed in the basic structure of medicine and biotechnology through the molding and bonding technique (Mokkapati et al., 2008). At the same time, the repeated structure by using PDMS mold has been greatly adapted to micro-part commercial in order to reduce the cost and improve the performance (Kim et al., 2002). Moreover, other research is illustrated this material compatibility with smart device such as micro-pump (Jeong and Konishi, 2005), and tactile display (King et al., 2008; Pappas et al., 2009).

5.2.1 PDMS – SU-8 bonding

After the PDMS membrane and SU-8 tactile structure have been fabricated as described in Chapter 3, the next step in driving to the complete Braille display is the dot demonstration under the applied pressure. The main process in this section presents techniques to create the suspended PDMS membrane on the orifice of the SU-8 tactile structure.

The basic knowledge of PDMS bonding is the creation of the hydroxyl group (OH) on the surface by exposure to oxygen plasma. The materials which have the composition of silicon can be treated to permanently fix them together. However, the cross-linked SU-8 does not support on this principle. Although PDMS membrane and SU-8 surface are altogether exposed to 100% oxygen plasma at 300 mTorr and 200 W RF power for 2 minutes and suddenly fixed them together as shown in Figure 5.2 (a), the permanent fix resulted from OH group is not created between them. The PDMS membrane can be peeled away from the substrate (SU-8 structure) when the sample is held at the applied pressure of 16.38 kPa as shown in Figure 5.2 (b). This implies that only the Van der Waals force is generated between the interface bonding as a temporary bonding which is hard to resist the applied pressure.

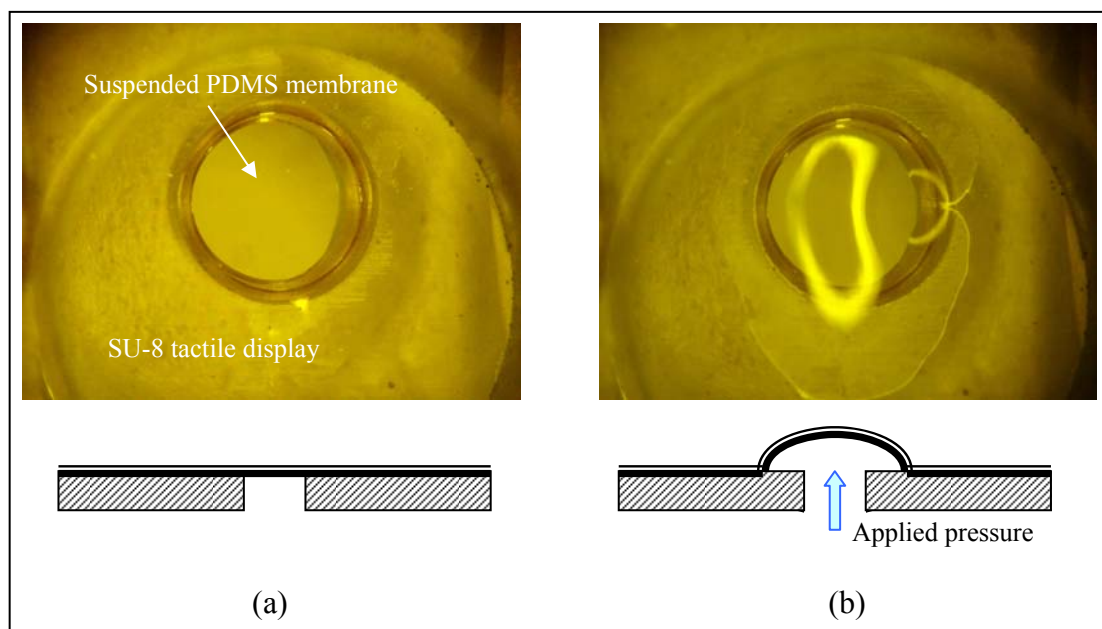


Figure 5.2 Plasma bonding (a) PDMS membrane fixing on the SU-8 tactile structure and (b) peeling of PDMS membrane under the applied pressure of 16.38 kPa.

Therefore, the new method has to be investigated to meet this goal. Three methods of bonding techniques are presented for the tactile display based on the bonding between PDMS membrane and the SU-8 structure.

5.2.1.1 PDMS – PDMS/SU-8 Plasma bonding

The conventional method for PDMS bonding to another smooth surface such as glass, silicon, and PDMS is oxygen plasma which creates a tight seal caused by Si-O-Si bond between them. The initial state of PDMS surface is the hydrophobic which does not support the flow of water as shown in Figure 5.3 (a).

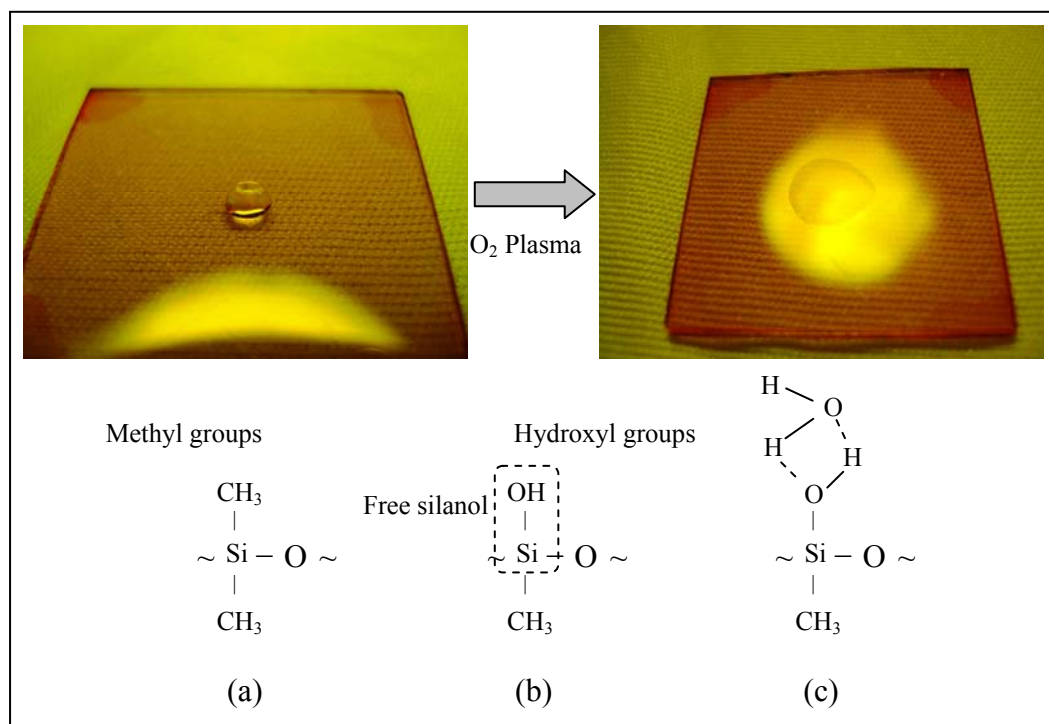


Figure 5.3 (a) Hydrophobic state before oxygen plasma (b) oxygen plasma treatment on the PDMS surface and (c) hydrophilic state after oxygen plasma.

One unit chemical structure of PDMS consists of one atom of silicon and oxygen, and 2 molecules of methyl group (CH₃) which are bonded to the silicon atom, and they are formed the repeat unit in the polymer (Hillborg and Gedde, 1999).

Oxygen plasma treated on the PDMS surface with sufficient power changes the upper methyl group to hydroxyl group (OH) which is combined to create a free silanol group (Si-OH) with silicon atom as shown in Figure 5.3 (b). The surface property of PDMS is changed to hydrophilic that allows the water flow on the surface by the bonding of oxygen and hydrogen atom as shown in Figure 5.3 (c). In the same way of water, two PDMS surfaces can be bonded together by creating of hydrophilic on both surfaces under the oxygen plasma treatment which produces the bond of Si-O-Si at the interface of polymer and release the water when the process is finished as shown in Figure 5.4.

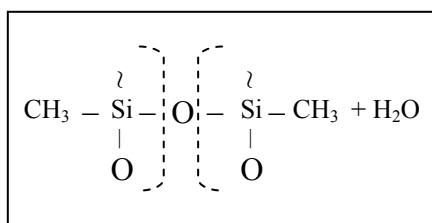


Figure 5.4 Chemical structure of PDMS-PDMS bonding by oxygen plasma.

Because the PDMS membrane cannot be bonded on the crosslinked SU-8 surface by using oxygen plasma, the bonding method of PDMS – PDMS/SU-8 is developed and presented in this section. Figure 5.5 illustrates the fabrication sequences of this bonding method which begins by the spin-coating and curing of PDMS membrane on the SU-8 tactile display as shown in Figure 5.5 (a). Partial PDMS coated on the surface flow down into the orifice and coat on vertical sidewall of SU-8 which is helped to catch the cured PDMS to the wall as the mechanical lock. At the same time, PDMS membrane that has been prepared on AZ sacrificial layer is brought to bond with the PDMS/SU-8 structure by mean of exposing in 100% oxygen plasma at 300 mTorr and 200 W RF power for 1.30 minutes as shown in Figure 5.5 (b). After compression by a mass of 1 kg weights, the

sample is released from the substrate by removing of the sacrificial layer, resulting in suspended PDMS membrane as shown in Figure 5.5 (c).

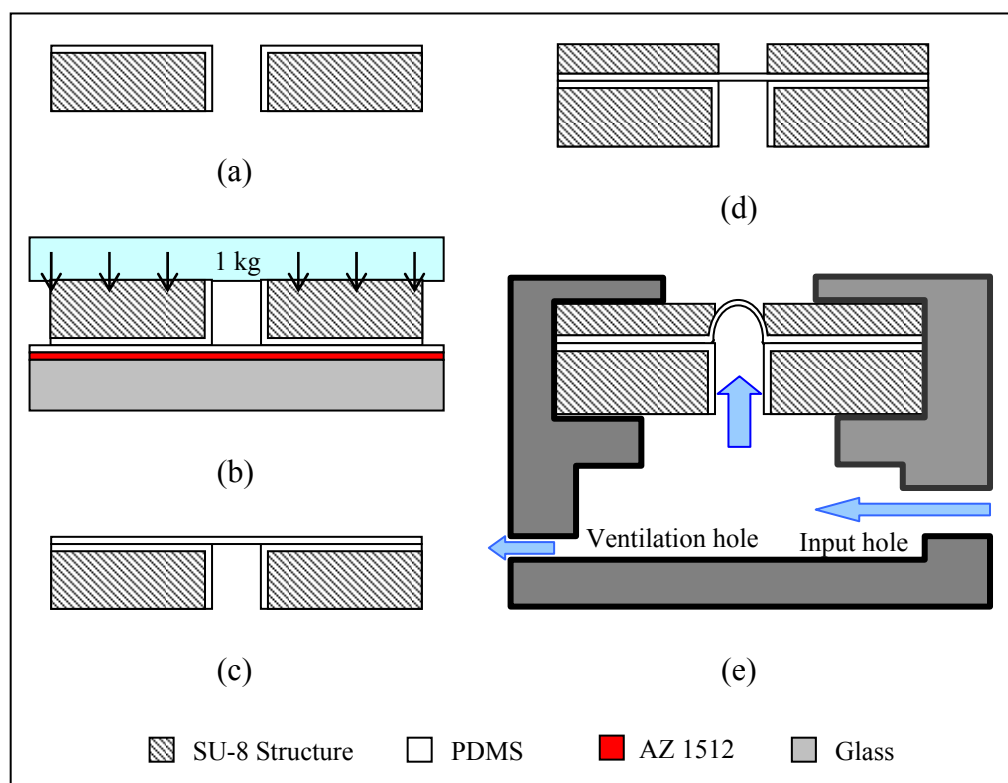


Figure 5.5 Fabrication sequences of the tactile dot by using PDMS-PDMS/SU-8 plasma bonding.

The sample which has been suspended with the PDMS membrane is initially tested the load-deflection to evaluate the sealing performance. Because this method is based on the reaction caused by oxygen plasma which naturally gives the permanent bonding between the surfaces, the deflection of the membrane is gradually applied to the reference differential pressure of 27.6 kPa (Yobas et al., 2003). Although the suspended PDMS membrane can be fixed strongly on the other one, it cannot suffer from this applied pressure. As demonstrates in Figure 5.6, the upper PDMS membrane is peeled from the other one resulting from the non-uniform on the interface. Even though the spun PDMS membrane is resulted from spin-coating process at high rotation speed, SU-8 tactile

panel does not provides flat bonding surface like as the surface of glass or silicon wafer. This roughness reduce the interface area between them result in the peeling on partial area of the upper PDMS membrane.



Figure 5.6 Peel-off damages of the PDMS membrane after testing.

To solve this problem, the area of PDMS membrane will be limited in a display area of a standard tactile dot display by covering with the SU-8 tactile panel as shown in Figure 5.5 (d) and 5.7 (a). The sample is mounted on a holder as shown Figure 5.5 (e) and applied by the constant differential pressure of 27.6 kPa. The suspended membrane is rapidly raised up as shown in Figure 5.7 (b) without any damage on the sample. Then, the resultant deflection at the center of the membrane under various applied pressures is measured by the optical profiler which reports the load-deflection characterization as demonstrated in Figure 5.8. The deflection is increased when the differential pressure is gradually applied. The applied pressure is increased until the deflection at the center of the membrane equal or higher than the standard deflection of 480 μm which obtain at the differential pressure of 27 kPa for a spun PDMS at 5000 rpm. The maximum differential pressure is applied to 388 kPa which give the highest deflection at 618 μm for spun PDMS at 4000 rpm.

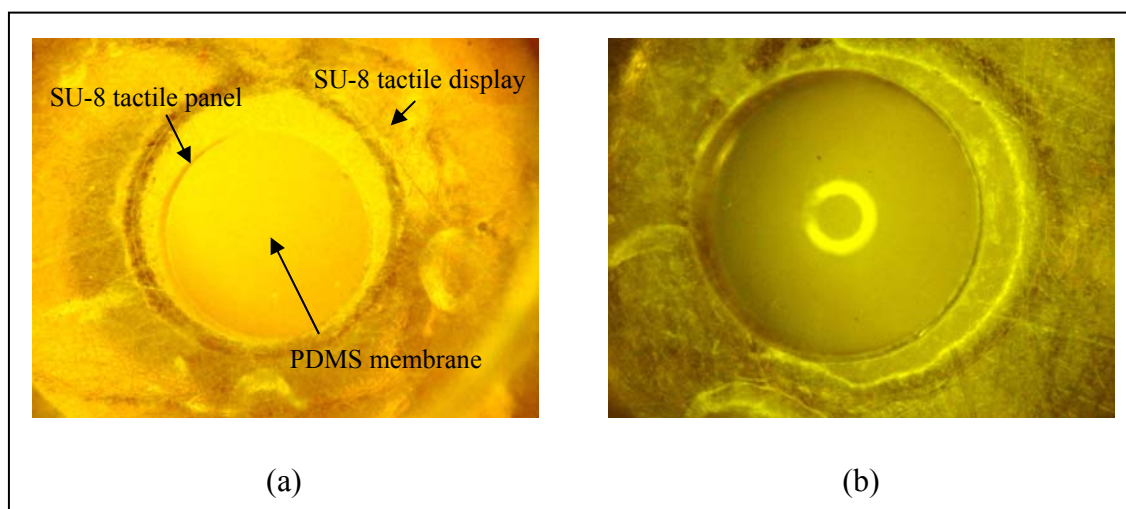


Figure 5.7 Optical micrograph of the PDMS dot (a) OFF position and (b) ON position with deflected membrane under 27.6 kPa differential pressures.

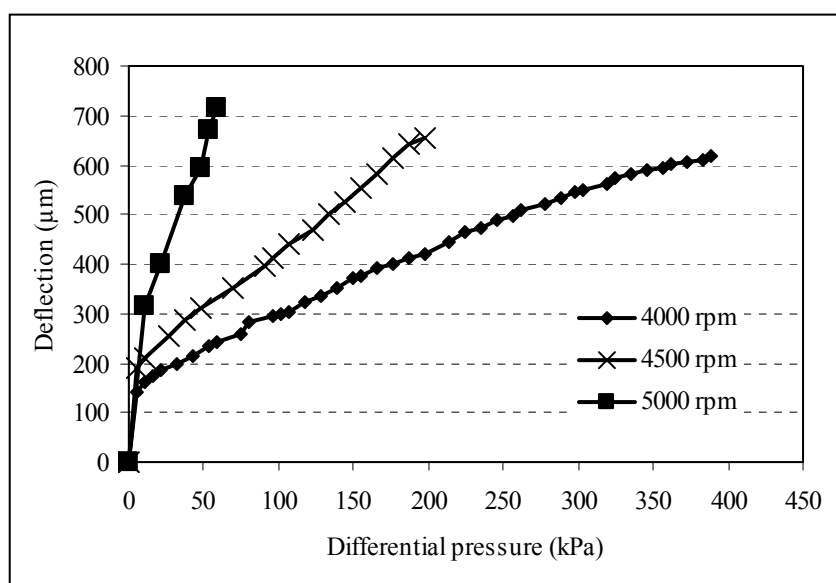


Figure 5.8 Measured deflections of PDMS membranes prepared by various spin coating speeds.

Although the oxygen plasma method did not provide perfectly bonding between the PDMS interface since the problem of the roughness area of SU-8 structure, there are the way to utilize from the sample by limiting the display area using the

standard dot panel. However, the experimental result proves that the oxygen plasma bonding is difficultly applied to the PDMS surface which does not smooth enough. Therefore, another bonding method which does not depend on the smooth surface has to be developed to avoid this problem.

5.2.1.2 PDMS – SU-8 wet bonding

This method is performed during the PDMS membrane is staying in viscous state. After spin coating of PDMS membrane at 6000 rpm on AZ 1512 sacrificial layer as shown in Figure 5.9 (a), the SU-8 tactile structure is immediately placed on the wet PDMS film and compressed into the sticky PDMS by mass of 1 kg weights as shown in Figure 5.9 (b). The sample is totally cured at 90°C for 3 hours and allows them to cool down naturally. Figure 5.9 (c) shows the sample when the mass is moved out, and the sample is released from the substrate result in the effective bonding at this relatively low temperature. This can be described that the PDMS in viscous state are easily to insert into the plurality of small gap of SU-8 surface. The mechanical lock between them is produced and adheres well to SU-8 tactile structure when it was heated to condense the polymer film. The bonding strength test is performed through applying of nitrogen gas pressure to activate the deflection of membrane. The experimental result is shown in Figure 5.9 (d) which is tested controlling of the gas pressure regulator.

The experimental results of the PDMS - SU-8 wet bonding is illustrated in Figure 5.10 (a) which shows the back side of the sample that demonstrates the membrane of PDMS consisting of thin and thick PDMS layer. As described above mention, this method is based on wet bonding which have SU-8 holes act as tubes place in the viscous PDMS. The consequent phenomena that happen naturally are capillary action which creates a concave meniscus at the lower end of the vertical SU-8 tube. The viscous PDMS is pulled up at the wall by surface tension (Batchelor, 2000). For this reason, the thickness of PDMS membrane inside the SU-8 orifice is slope down from the vertical

sidewall to the center. The diameter of PDMS membrane which can be supported for the dot display is decreased from 1450 μm to 720 μm as shown in Figure 5.10 (b).

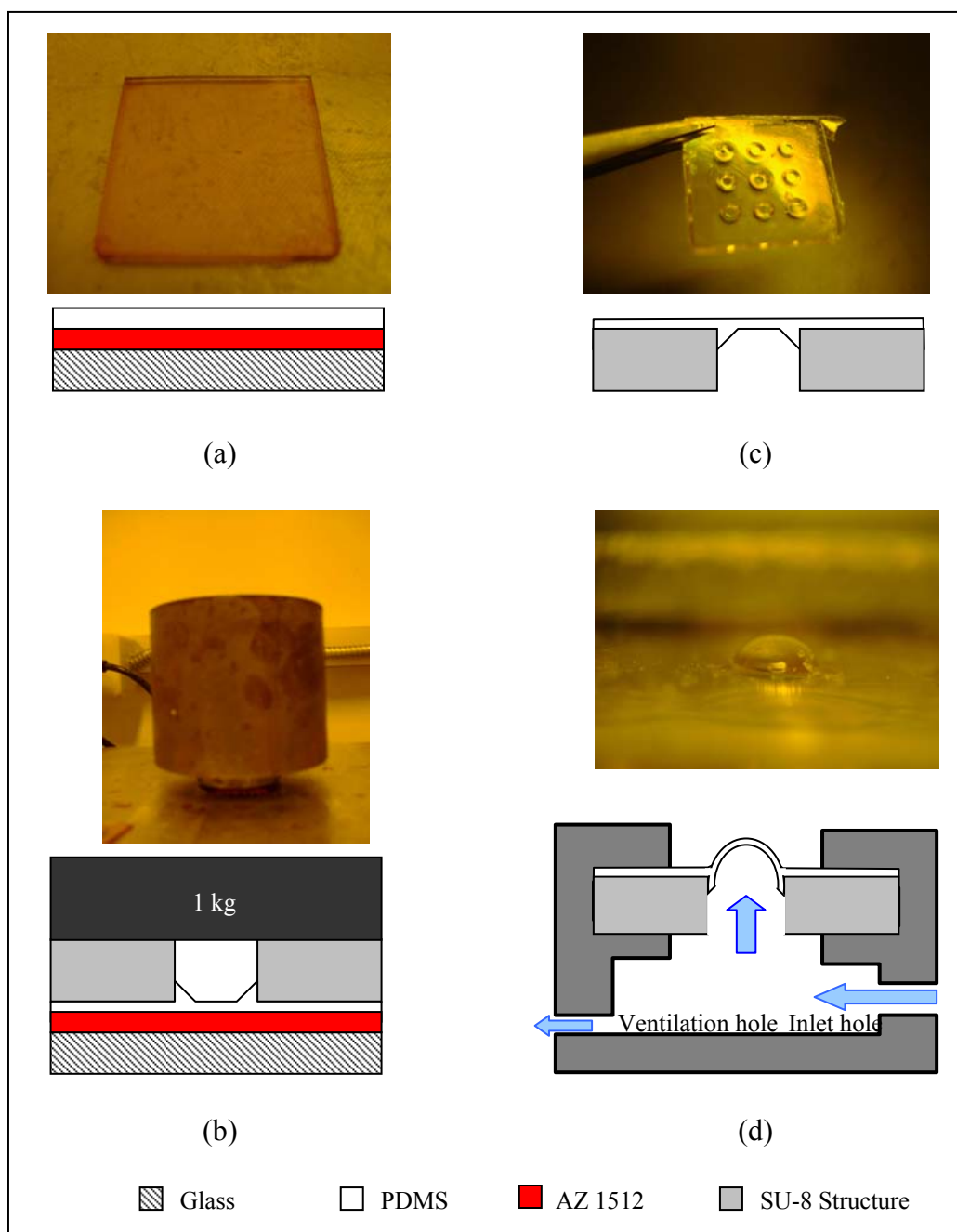


Figure 5.9 Fabrication sequences of PDMS tactile dot by wet bonding (a) spin-coating PDMS on AZ photoresist sacrificial layer (b) placed SU-8 frame and press with a mass of 1 kg (c) release from the substrate and (d) test under an applied pressure.

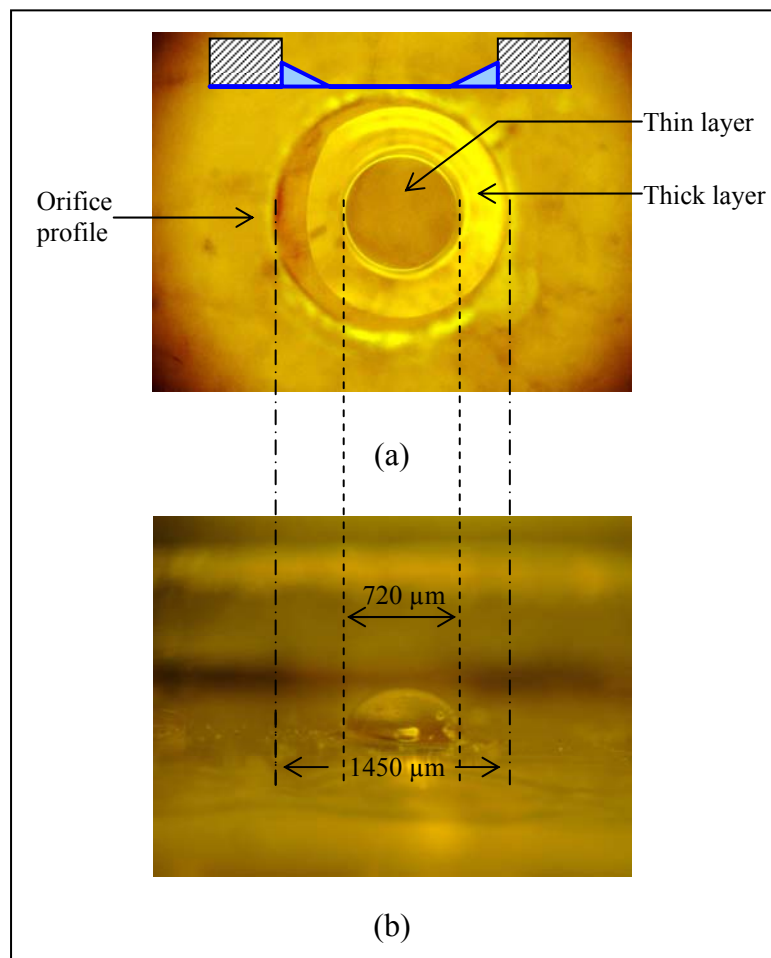


Figure 5.10 The PDMS dot display resulting from wet bonding (a) bottom view and (b) side view with deflected membrane under applied pressure.

Figure 5.11 shows the deflection of PDMS membrane under various differential pressures. The first pressure which can be detected by pressure sensor is 16.37 kPa resulting in the deflection of 203 μm. The applied pressure is gradually increased until reach the maximum differential pressure of 96.25 kPa that give the deflection of the membrane at 368 μm. Since PDMS membrane at the center is very thin and easily deformed, the applied pressure have to be controlled carefully until the deformation reaches to the standard Braille display at 480 μm. However, the applied pressure damages the thin PDMS membrane which is extremely thin by surface tension caused by the capillary action as shown in Figure 5.12. Therefore, this bonding technique is not appropriate for the PDMS tactile fabrication.

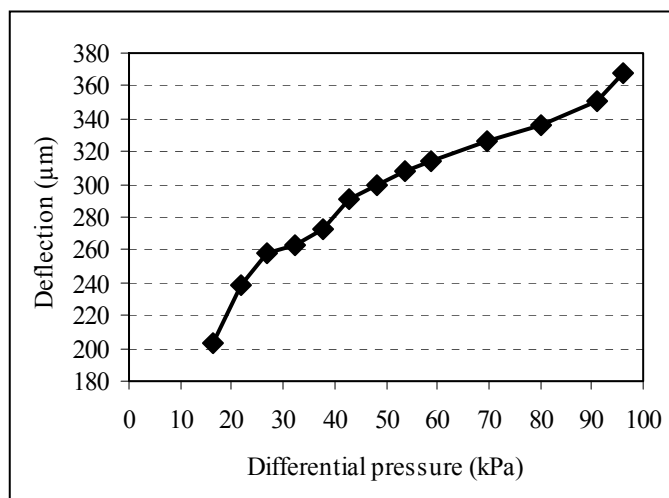


Figure 5.11 Measured deflection of the PDMS membrane in PDMS – SU-8 wet bonding Braille dot.

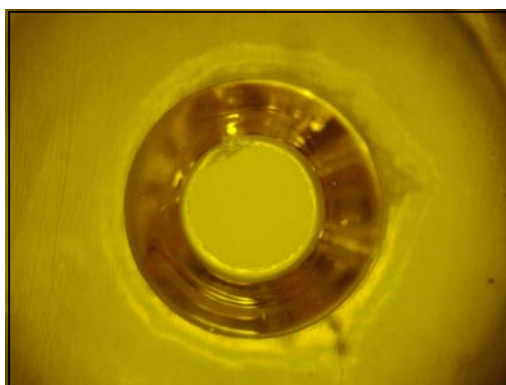


Figure 5.12 Damaged PDMS membrane under an applied pressure.

5.2.1.3 PDMS tactile display by using SU-8 sacrificial material

PDMS membrane is fabricated on the un-crosslinked SU-8 sacrificial material which is planarized in a SU-8 hole by the reflowed casting and polishing process as shown in Figure 5.13 (a). Mixed PDMS is then spun on the surface as shown in Figure 5.13 (b). The membrane is cured in the oven at 45°C for 5 hours to avoid the reflow of SU-8 photoresist which can create the roughness on the PDMS membrane. After cooling down, the SU-8 photoresist is removed in the developer and rinsed in IPA and DI water,

resulting in the suspended membrane on the orifice as shown in Figure 5.13 (c). After drying in the oven at 60°C for 30 minutes, the membrane is covered by the SU-8 tactile panel as shown in Figure 5.13 (d). The tactile display is experimented in various differential pressures by setting the sample on the holder as shown in Figure 5.13 (e).

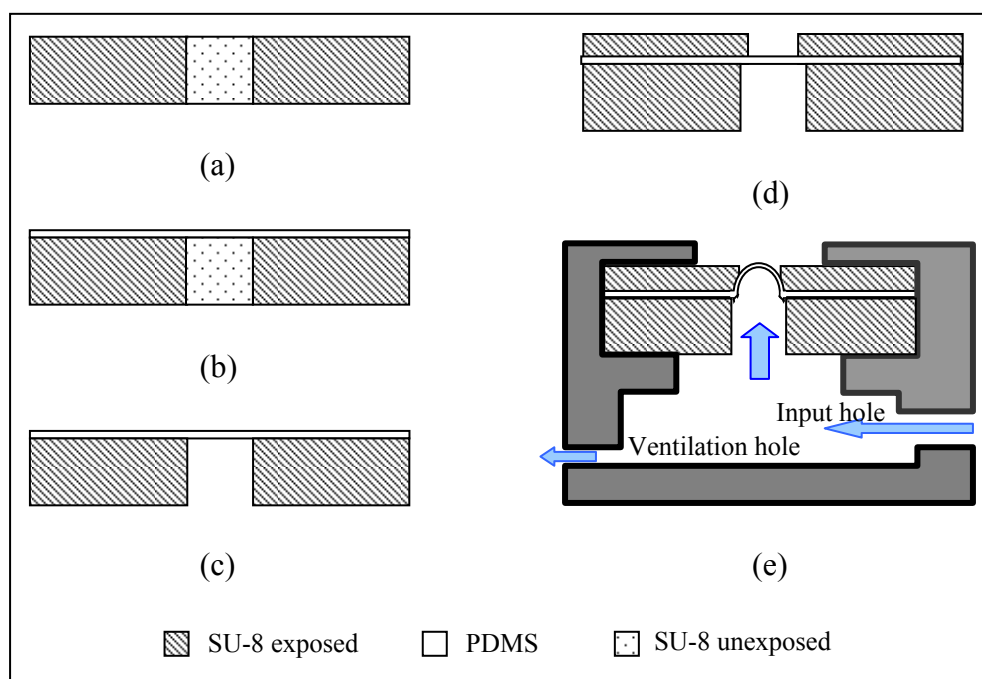


Figure 5.13 Fabrication sequences of a PDMS tactile dot by using SU-8 sacrificial material

(a) planarized with SU-8 photoresist sacrificial (b) spin-coated PDMS membrane (c) released sacrificial (d) cover with SU-8 tactile panel and (e) test under an applied pressure.

Figure 5.14 (a) shows the PDMS membrane is suspended on the SU-8 orifice after releasing of SU-8 sacrificial material. The SU-8 tactile panel that is placed on the membrane is applied to create the tactile dot as shown in Figure 5.14 (b). This panel is used to limit to size of the PDMS tactile dot into the standard display while the gas pressure is applied to the sample. Various spin-speeds are performed to create thin PDMS membranes which are used to evaluate the load-deflection behavior. Figure 5.15 shows the

results of the load-deflection characterization according to changing of PDMS spin speed coating. The deflection at the center of PDMS membrane is measured and collected for curve fitting of mathematical equation which will be described in the next section. The minimum differential pressure which can be detected by the pressure sensor is 0.06 kPa resulting in constants values at y axis.

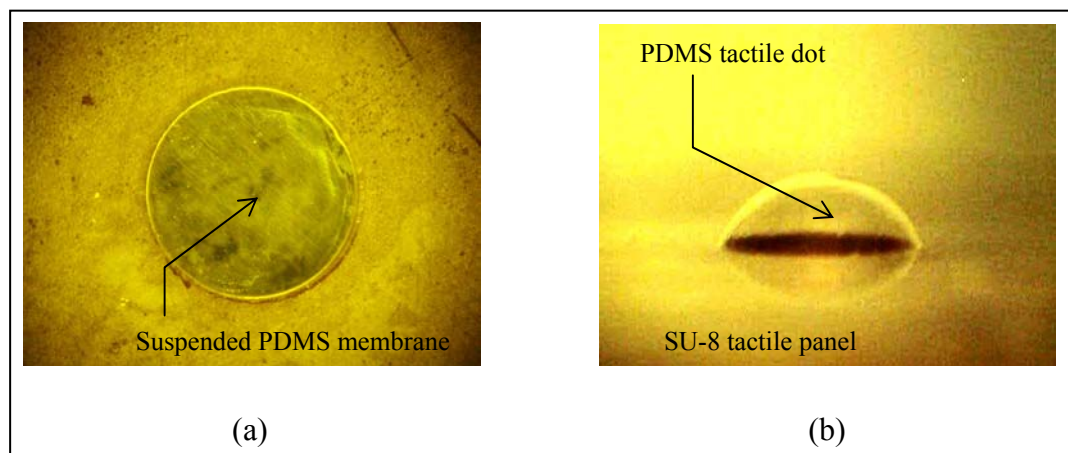


Figure 5.14 (a) The PDMS membrane covering the SU-8 orifice and
(b) SU-8 tactile panel placing on the membrane.

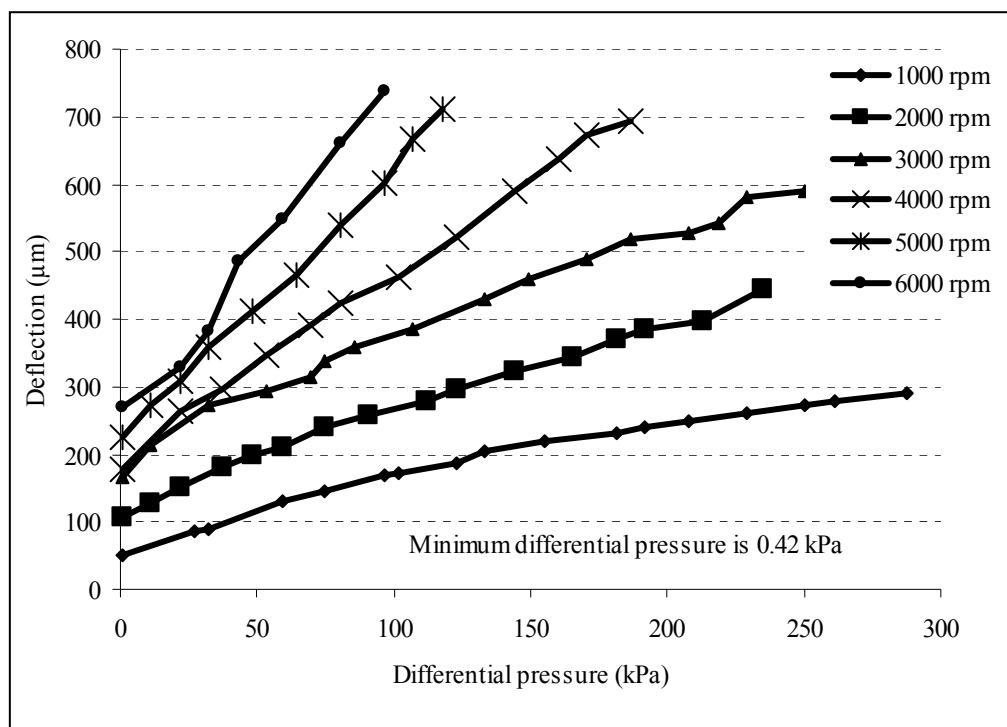


Figure 5.15 Load-deflection characterizations according to PDMS spin speed coating.

5.2.2 Load-deflection of circular PDMS membrane with a uniform pressure

The mathematic equation which is used to estimate the deflection of PDMS membrane in response to the applied pressure has been developed from the load-deflection method. For membranes with diameter of 300 μm or larger were based on a hemispherical shape as illustrated in Figure 5.16. The model for the membrane behavior which was proposed by Allen (1986) and Pan et al. (1990) is given by Equation (5.1).

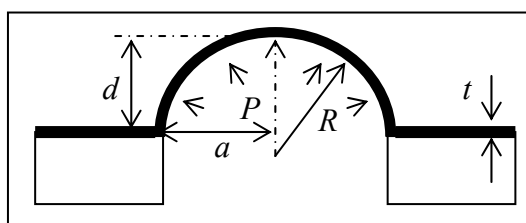


Figure 5.16 Deflection of a suspended PDMS membrane in reaction to an applied pressure.

$$P = \frac{C_1 t}{a^2} \sigma_o d + \frac{C_2 f(v) t}{a^4} \frac{E}{1-\nu} d^3 \quad (5-1)$$

where P is the applied pressure, d is the center deflection, a the radius of membrane (725 μm), t is the PDMS film thickness, E is the Young's modulus, ν is the in-plane Poisson Ratio of PDMS (0.5), σ_o is the residual stress, and $E/(1-\nu)$ is the biaxial modulus. The geometrical coefficients C_1 , C_2 , and $f(\nu)$ for the circular membrane are 4, 2.67, and $(1.026 + 0.233\nu)^{-1}$, respectively.

The fabrication of PDMS membrane is performed on a smooth surface and condensed in the oven with low temperature. The residual stress is naturally generated in the membrane and the Young's modulus of spin-coating PDMS is changed by mixing ratio and curing temperature. Because E and σ_o of PDMS material do not based on the standard value, they are unknown that have to be estimated from the experimental result by the load-deflection method. Dividing both side of equation (5.1) by the center deflection of the membrane, resulting in the linear equation of $Y = AX + B$ as shown in equation (5.2). The Young's modulus can be calculated by equation (5.3), and the residual stress is achieved by equation (5.4). A is a slope value of the straight line and B is a intersect value on the P/d axis.

$$\frac{P}{d} = \left(\frac{C_2 f(v) t}{a^4} \frac{E}{1-\nu} \right) d^2 + \frac{C_1 t}{a^2} \sigma_o \quad (5.2)$$

$$A = \frac{C_2 f(v) t E}{(1-\nu) a^4} \quad (5.3)$$

$$B = \frac{C_1 t}{a^2} \sigma_o \quad (5.4)$$

Figure 5.17 demonstrates the curve fitting by using linear regression method in estimation for the slope and linear equation of each data. The plot P/d vs. d^2 are used to calculate the Young's modulus and residual stress of the membrane by using equation (5.3) and (5.4), respectively. The coefficients of the linear equation, Young's modulus and residual stress, are demonstrated in Table 5.1

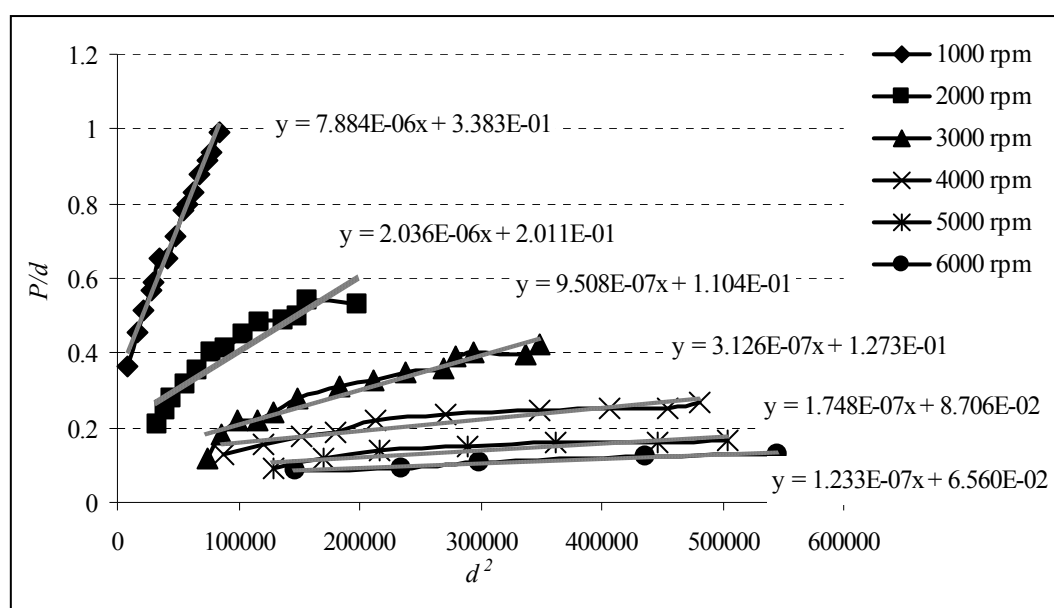


Figure 5.17 The relationship between P/d and d^2 for the calculation of Young's modulus and residual stress of the membrane.

Table 5.1 Calculated of residual stress and Young's modulus values for PDMS membranes.

Spin-speed (rpm)	Thickness (μm)	Linear Eq. $Y = AX + B$		Residual stress (kPa)	Young's modulus (kPa)
		A	B		
1000	90	7.884×10^{-6}	3.383×10^{-1}	493.941	5178.108
2000	42	2.036×10^{-6}	2.011×10^{-1}	629.186	2865.467
3000	29	9.508×10^{-7}	1.104×10^{-1}	500.250	1938.020
4000	23	3.126×10^{-7}	1.273×10^{-1}	727.305	803.393
5000	18	1.748×10^{-7}	8.706×10^{-2}	635.568	574.032
6000	16	1.233×10^{-7}	6.560×10^{-2}	538.766	455.523

By using the data of E and σ_0 which were calculated from the experimental result, the mathematic model in equation (5.1) can be used to estimate the load-deflection of the PDMS model as shown in Figure 5.18.

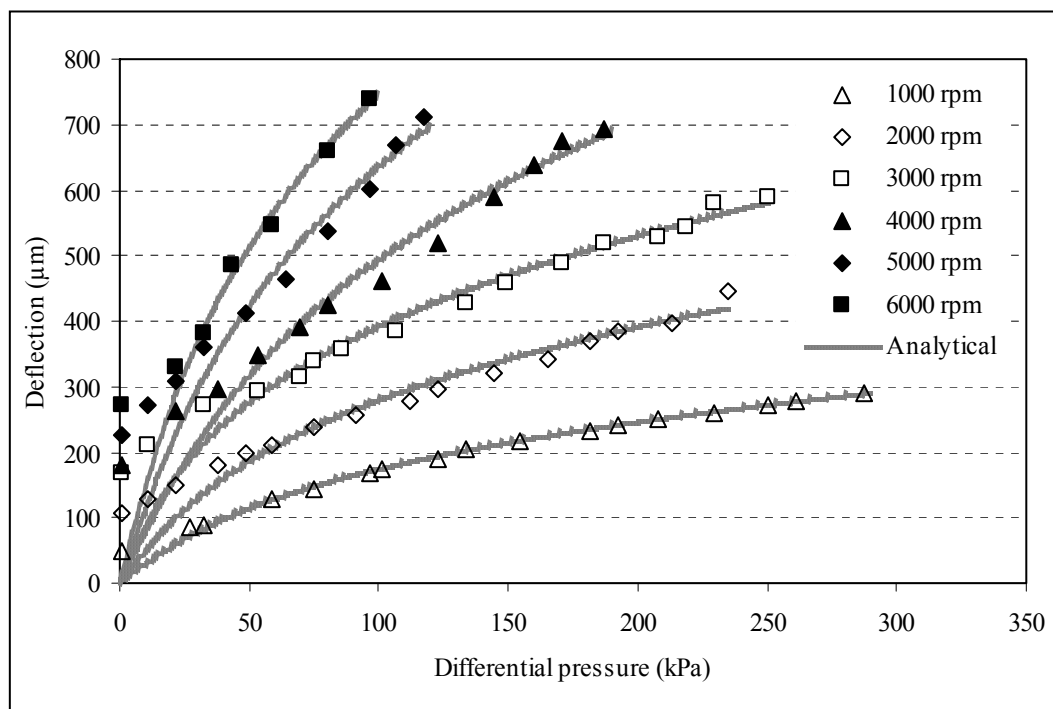


Figure 5.18 Load-deflection curve for membranes with different thickness compare with the analytical model.

5.2.3 Load-deflection experimental setup

For the large deflection study of PDMS membrane, the experimental setup is organized as illustrated in Figure 5.19. The suspended PDMS membrane is mounted on the holder and fixed to the pressure chamber which is connected to a pressure sensor. Nitrogen gas that is controlled by a pressure regulator is applied into the chamber, and the pressure sensor is operating continuously. For the deflection at the center of membrane, Veeco[®] Optical Profilors is utilized to measure and display the deflection results on the monitor.

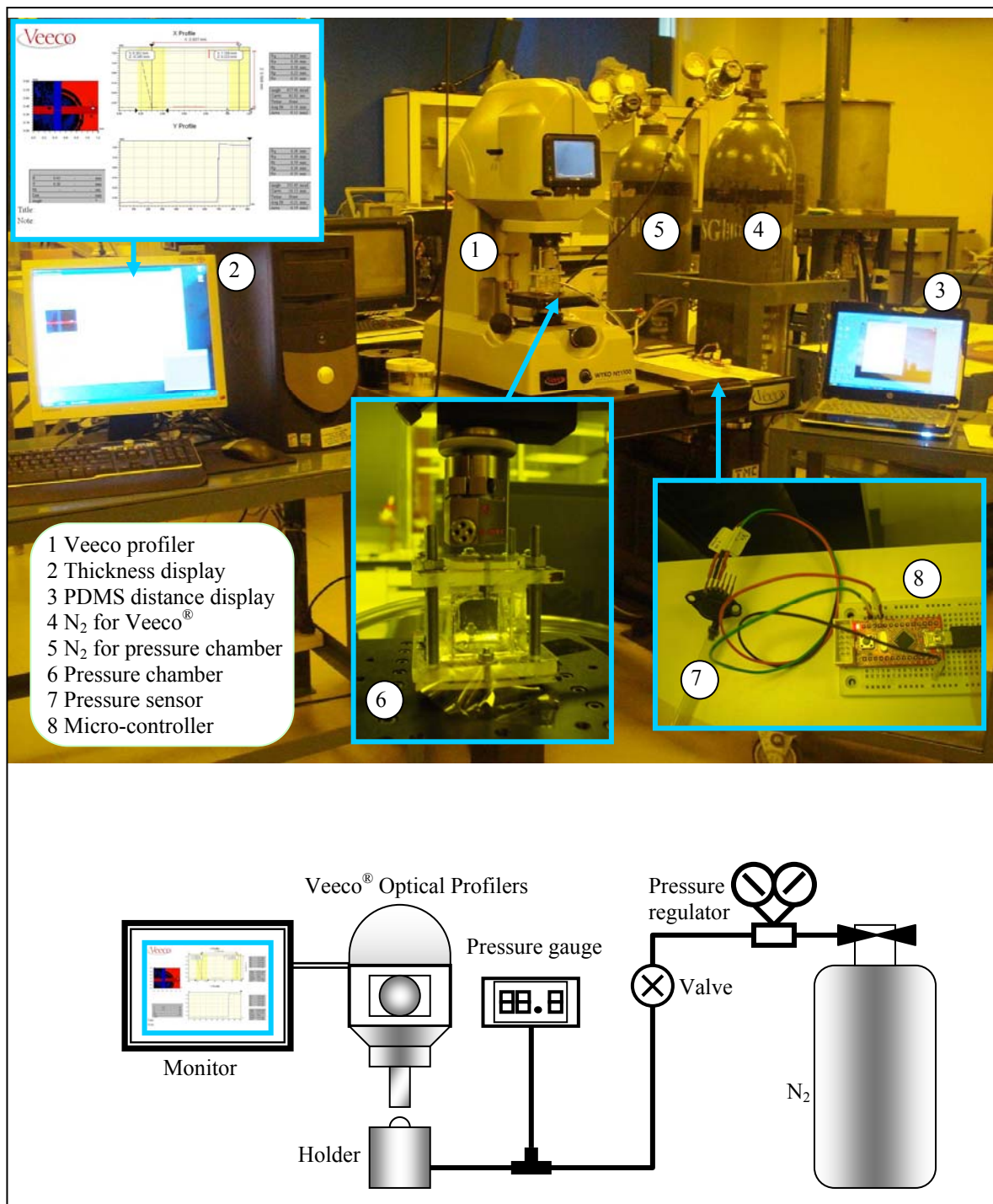


Figure 5.19 Load-deflection experimental setup.

5.3 SU-8 Tactile Display

Since the tactile dot display which is touched directly to the fingertip have to give the obvious sensation and different from the normal state. The material that is affected on the skin must strength enough to activate the perception. Although the PDMS membrane for tactile display has been successfully fabricated, the feeling of dot actuation is not clearly. Therefore, the SU-8 tactile display has to be developed to improve the strong effect of the dot activation. Figure 5.20 shows the concept operation of the piston SU-8 tactile display consisting of a movable tactile dot and a display panel (cylinder). Distance about $500\ \mu\text{m}$ inside the display panel allows the dot move up for its presentation when it is actuated by the supplied pressure.

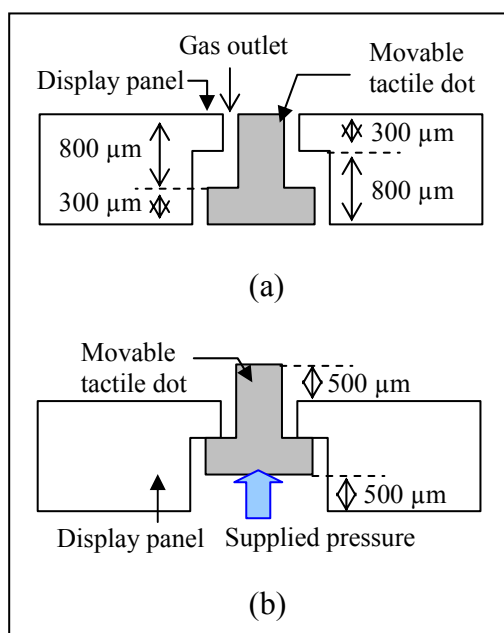


Figure 5.20 Schematic diagram of a SU-8 tactile display (a) OFF and (b) ON position.

The automatic sealing when the tactile dot is rose up to the maximum distance is the key mechanism of this designed structure. Gas leakage are always happened and increased gradually between a space of the piston and cylinder while the dot is rising up. At a

sufficient applied pressure, the gas leak will be stop since the base of tactile dot closes the gas outlet resulting in the high differential pressure that resists the load from the fingertip. The structures of them have to be vertical side wall which provides convenient movement, as well as the ultra-thick film with a narrow space in order to reduce the gas leak while the dot is lifting up. Therefore, X-ray LIGA technology is utilized for this tactile structure. Two methods of SU-8 X-ray LIGA fabrication are developed to create the small piston that acts as the tactile dot. First is the assembled SU-8 tactile display which constructs both of them simultaneously and assemble them later. Second is SU-8 tactile display by releasing of sacrificial layer. The tactile dot is only fabricated and covered with sacrificial material before forming of the display panel. Movable tactile dot will be achieved when the sacrificial material is removed.

5.3.1 Assembled SU-8 tactile display

Figure 5.21 illustrates fabrication sequences of the assembled SU-8 tactile display which consists of two layers of the tactile dot structure and the display panel. The substrate which was coated with a thin sacrificial layer is placed a 300 μm -thick SU-8 photoresist and constructed the first pattern by using X-ray lithography from synchrotron light as shown in Figure 5.21 (a). Then, the second SU-8 layer with thickness of 800 μm is reflowed to cover the previous structure and created the thick film structure by alignment through a transparent X-ray mask on the sample before X-ray exposure as shown in Figure 5.21 (b). After development, all of them are removed from the substrate by etching of sacrificial layer as shown in Figure 5.21 (c). Finally, the tactile dot is inserted into the orifice of the display panel.

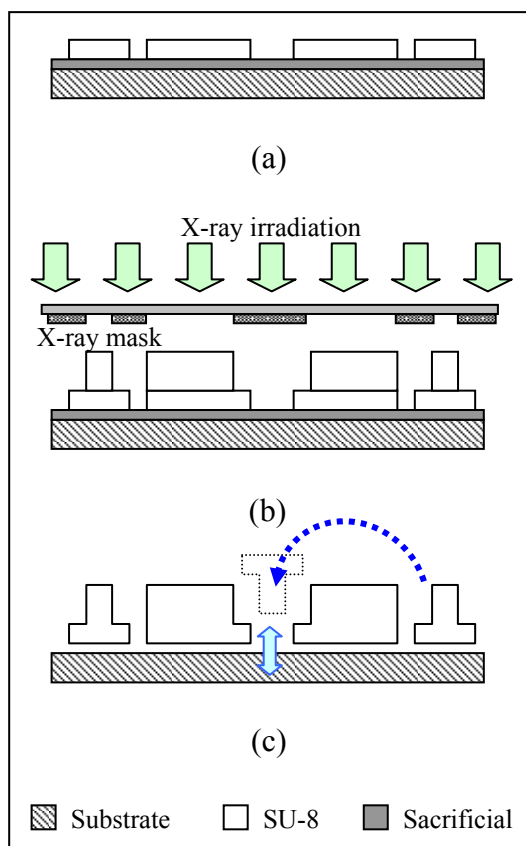


Figure 5.21 Fabrication sequences of an assembled SU-8 tactile display.

Figure 5.22 (a) shows top view of the two layers of SU-8 tactile display before removing from the substrate. At the center of the display panel as shown in Figure 5.22 (b) is provided a two step orifice that allows the tactile dot insert a small SU-8 pin into a small orifice, while a large orifice is used to support a large SU-8 pin that need to limit the moving distance of the tactile dot as shown in Figure 5.22 (c). Figure 5.22 (d) demonstrates the assembled SU-8 tactile display having the SU-8 tactile dot inside the orifice of the display panel.

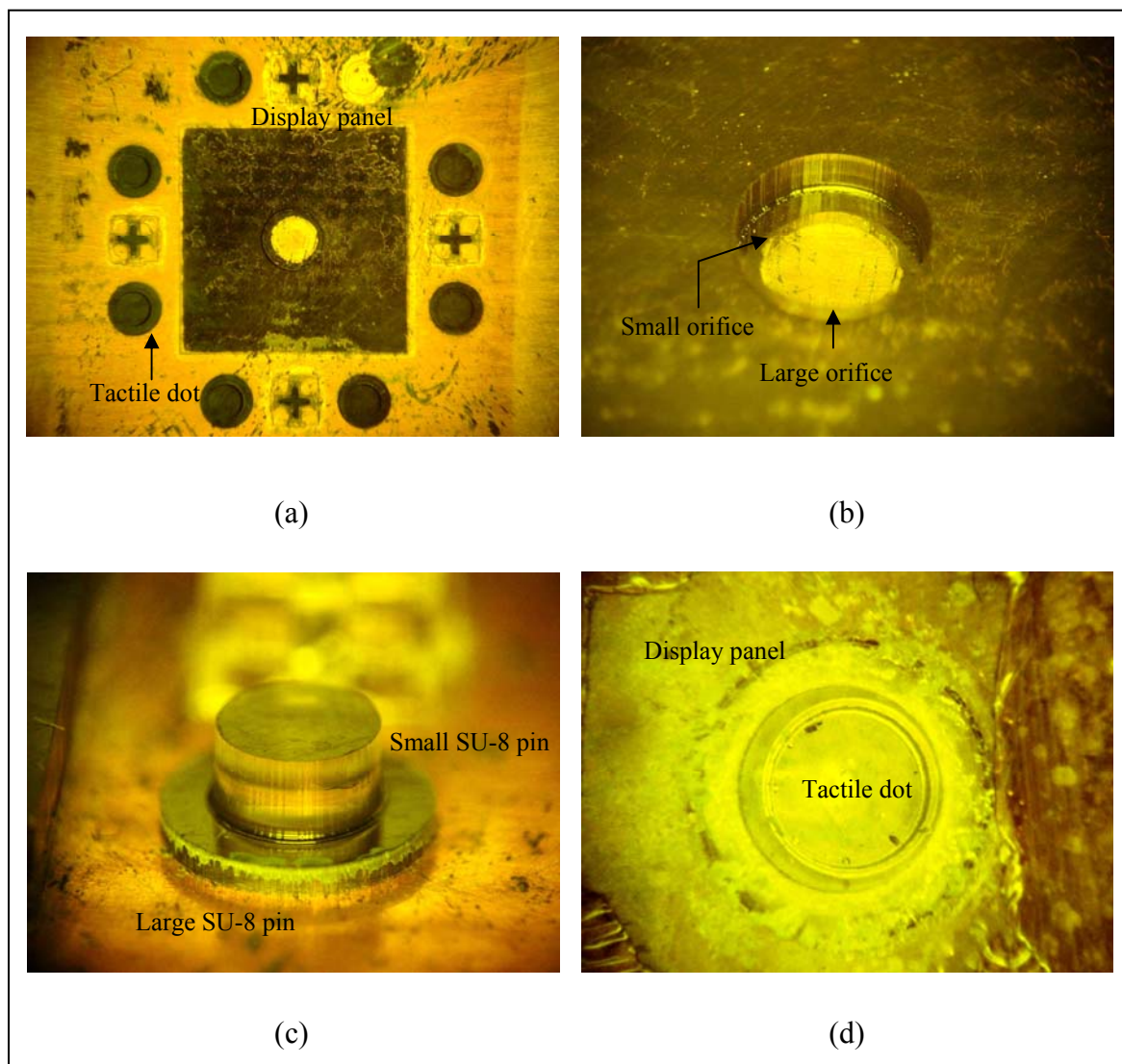


Figure 5.22 Photographs of a two layers of SU-8 tactile display.

The assembled tactile display is placed on a substrate which provides a small orifice to support the tactile dot for the applied pressure as shown in Figure 5.23 (a). Then, the gas pressure is applied into the sample as shown in Figure 5.23 (b). Gas leakage is sealed while the large SU-8 pin is reached up to the boundary of small orifice with distance about 500 μm . This demonstration is proved clearly about the difference feeling of the rigid dot display by 3 testers who wear a glove while they fingertip were touching.

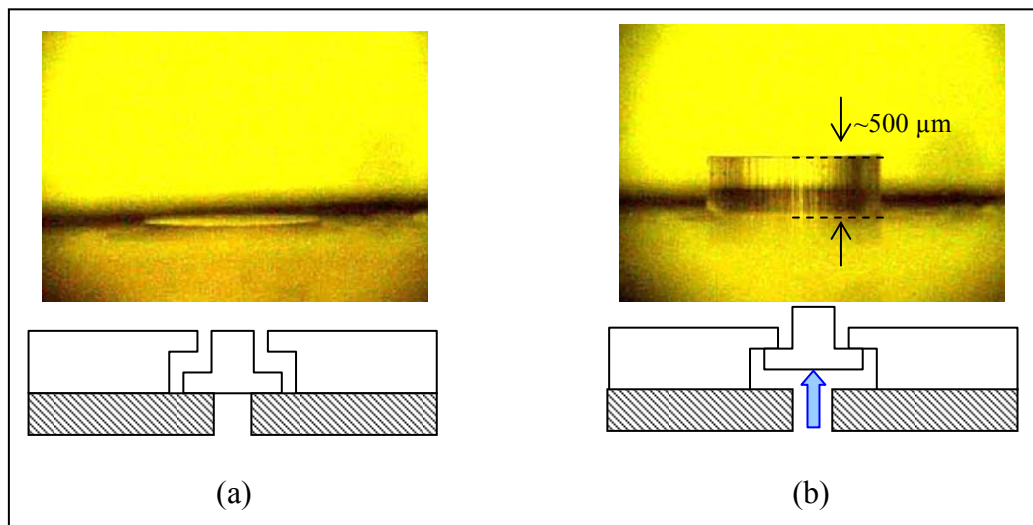


Figure 5.23 The assembled SU-8 tactile dot display on the PDMS membrane for actuation (a) OFF position and (b) ON position.

5.3.2 SU-8 tactile display by releasing of sacrificial layer

Basic idea of this process is based on the sacrificial layer between the structures which can be removed by selected wet etching as described in chapter 3 (Deekla et al., 2009). This technique is different from the assembled SU-8 tactile display because the tactile dot is only constructed on substrate and formed the tactile panel later. Fabrication sequences for the released tactile display are demonstrated in Figure 5.24. Two layers of tactile dot structure are first constructed on a graphite substrate by using X-ray lithography, and sacrificial material is then conformally covered to separate the tactile dot from the display panel as shown in Figure 5.24 (a). The SU-8 photoresist is reflowed to form the display panel as shown in Figure 5.24 (b). Top surface of the sample is polished until the sacrificial area is appeared as shown in Figure 5.24 (c). The sample is X-ray exposed to create cross-link inside the tactile panel, followed by soft-baking in the oven. After cooled down, the graphite substrate is removed by mechanical polishing until the silver area is clearly appearance as shown in Figure 5.24 (d). The piston is then released from the tactile panel by chemical wet etching of the sacrificial layer as shown in Figure 5.24 (e). Now, the

display panel which has the same thickness as the tactile dot is polished by a sand paper to decrease the thickness for 500 μm . This is provided for the high of the tactile dot when it is refilled and vertically moved in the display panel as shown in Figure 5.24 (f).

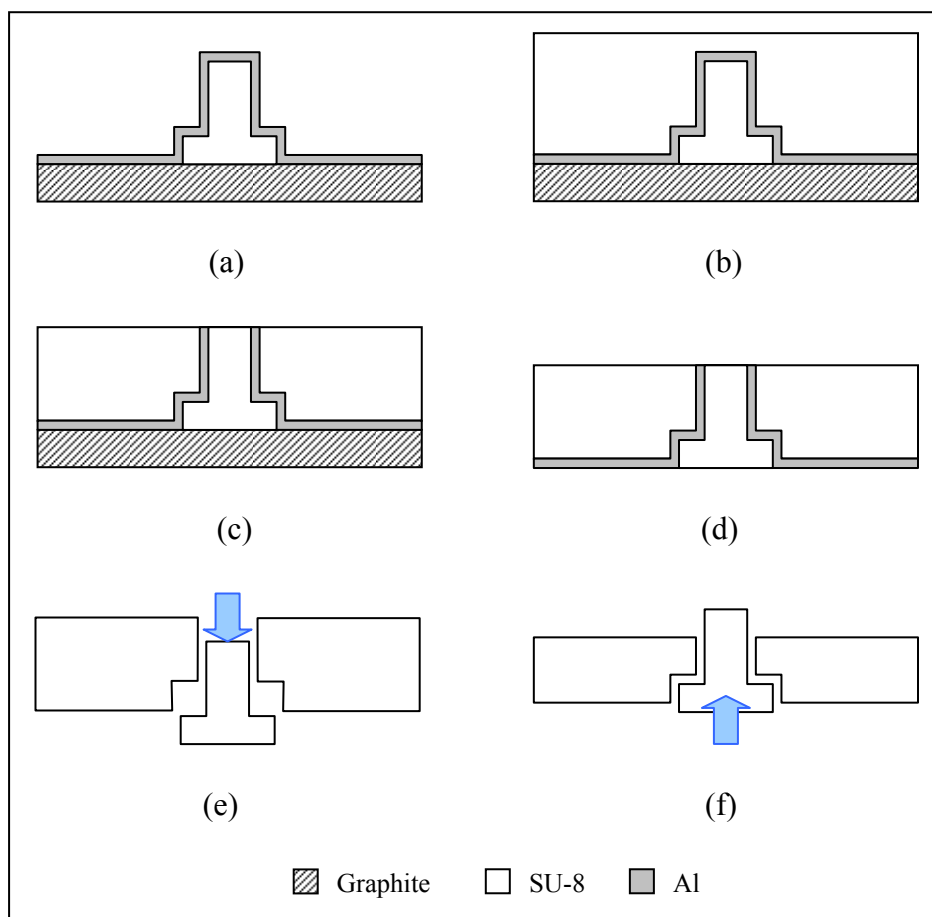


Figure 5.24 Fabrication sequences of the released tactile dot display (a) conformally coat with sacrificial layer (b) reflow SU-8 photoresist (c) polish top surface (d) polish bottom surface (e) remove sacrificial layer and (f) polish the tactile panel and insert SU-8 pin.

Two layers of tactile dot structure are constructed with thickness of 300 μm and 1000 μm on a graphite substrate by using X-ray lithography as shown in Figure 5.25 (a). The sacrificial material which is selected to cover the dot structure is aluminum from sputtering process. All surface of the dot structure is conformally coated by using rotating of

DC motor inside the DC sputtering chamber as shown in Figure 5.25 (b). Then, SU-8 powder are reflowed by heating inside the vacuum chamber to covering overall structure, followed by polishing process until the appearance of sacrificial ring as shown in Figure 5.25 (c). After removing of substrate, the tactile dot is released from the display panel by etching in wet etchant such as hydrofluoric acid (HF). The etchnat is inserted both of top and bottom area and create the narrow gap around the tactile dot as shown in Figure 5.25 (d). After etching process, the structure should automatically release from each other, but this case is not. The sacrificial material which is performed by DC sputtering at 200 W for 30 minutes give the aluminum thickness about 0.73 μm , while the vertical sidewall structure of multilayer of SU-8 structure is not perfectly smooth. Although aluminum can be coated overall surface, it is not thick enough to release the dot easily. As shown in Figure 5.26, the structure is separated by mechanical force that resulted in cracking in the tactile panel. To solve the problem, the thickness sacrificial layer must be increased by another coating method.

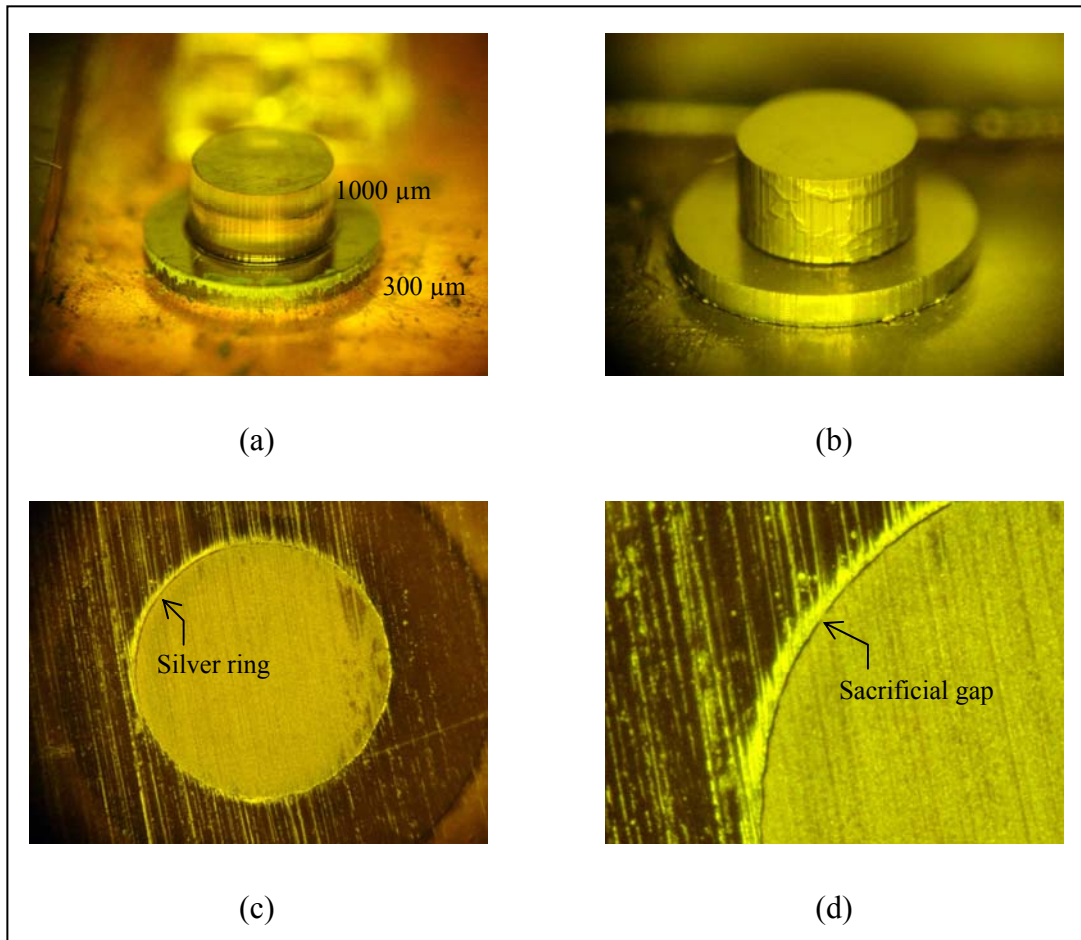


Figure 5.25 Fabrication process of the tactile display by releasing of the sputtered sacrificial material (a) construct two layers of SU-8 tactile dot (b) conformally coat Al sacrificial layer (c) polish top surface to open Al layer and (d) remove sacrificial layer.

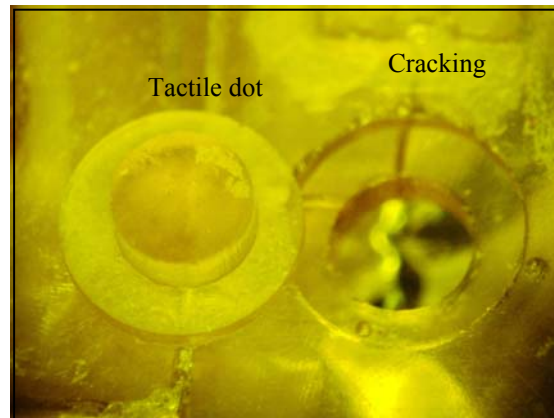


Figure 5.26 The cracked structure when the tactile dot is forced to release form the panel.

Another material which is selected to utilize as the sacrificial material have to be easily increased thickness and removed. The metal such as copper, nickel, and silver can be electroplated to increase the thickness, and they have been selectively etched in microfabrication. Therefore, silver will be used as the sacrificial material since it can be coated by sputtering and the wet etchant can rapidly remove it from the structure. As illustrated in Figure 5.27 (a)-(c), two layers of tactile dot which were constructed on the graphite substrate is conformally covered with silver sacrificial material by DC sputtering process at 200 W for 10 minutes. Then, the sample is electroplated to achieve silver thickness about 50 μm as shown in Figure 5.27 (d). The display panel is formed to cover the overall structure by SU-8 reflowed casting in the vacuum chamber, and the top and bottom surface are polished to open the area of silver material as shown in Figure 5.27 (e) and (f), respectively. To release them from each other, the sacrificial material which was opened at the top and bottom area allow the wet etchant insert into the panel and automatically separate the tactile dot from the display panel as demonstrated in Figure 5.27 (g) and (h), respectively. Finally, the thickness of the panel is only decreased for 500 μm by polishing from top surface, and the tactile dot is re-inserted into the panel having the total thickness less than the tactile dot about 500 μm .

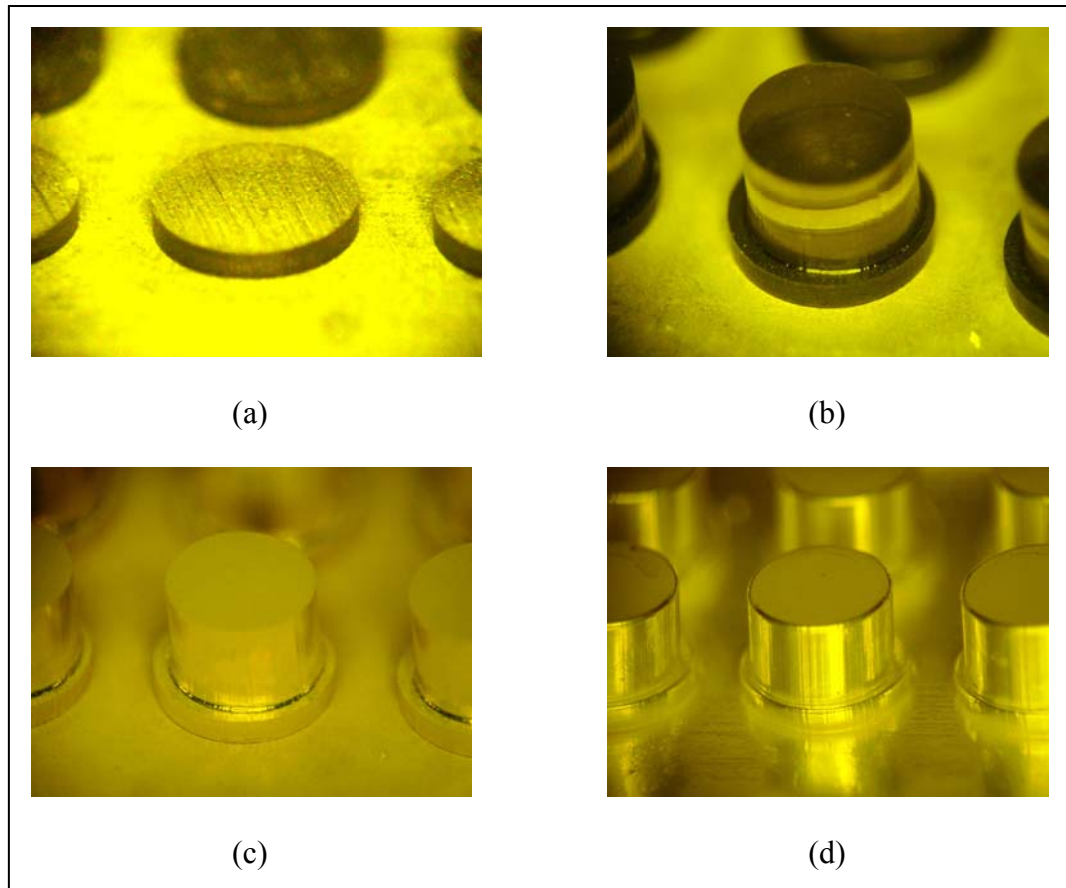


Figure 5.27 Fabrication process of the released tactile dot by silver sacrificial material

(a) construct 300 μm -thick SU-8 photoresist (b) construct 800 μm -thick SU-8 photoresist (c) coat Ag seed layer by sputtering (d) increase Ag thickness by using electroplating (e) polish top surface (f) polish bottom surface (g) remove Ag sacrificial layer and (h) polish SU-8 tactile panel and insert SU-8 tactile dot.

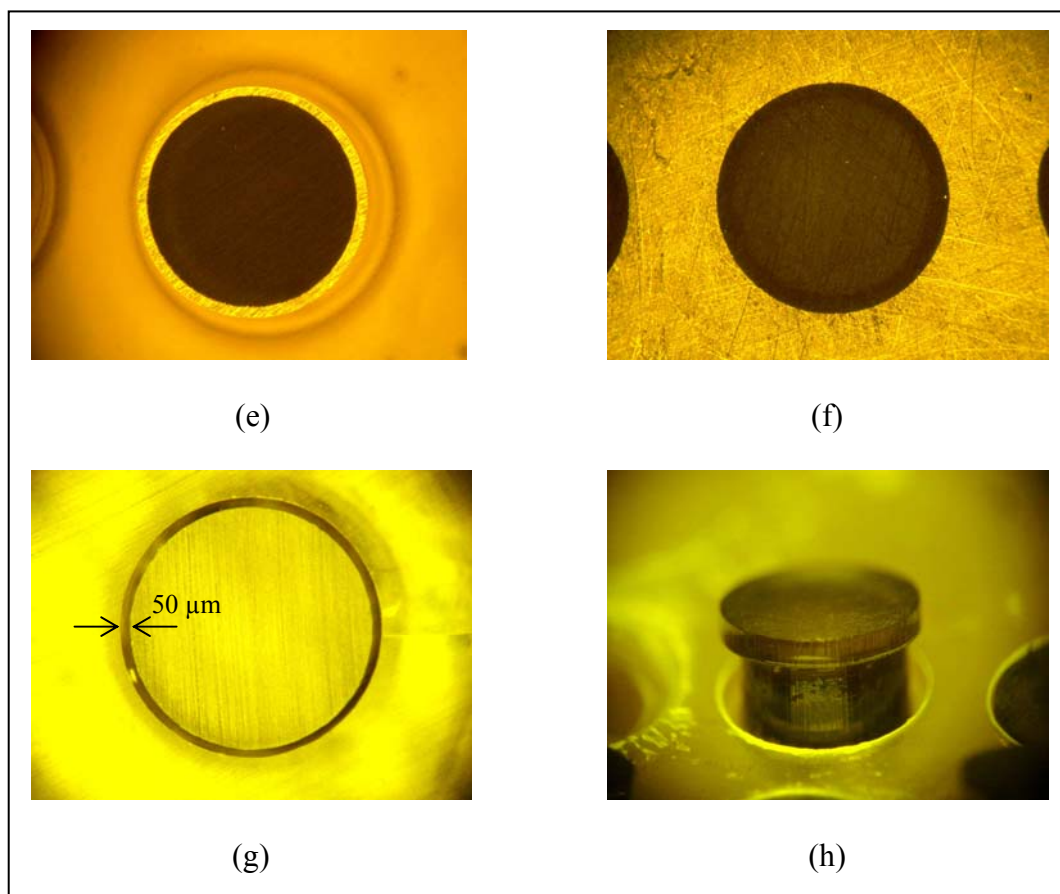


Figure 5.27 Fabrication process of the released tactile dot by silver sacrificial material

(a) construct 300 μm -thick SU-8 photoresist (b) construct 800 μm -thick SU-8 photoresist (c) coat Ag seed layer by sputtering (d) increase Ag thickness by using electroplating (e) polish top surface (f) polish bottom surface (g) remove Ag sacrificial layer and (h) polish SU-8 tactile panel and insert SU-8 tactile dot (Continued).

The next step is the assembly of the released tactile dot display. Two layers of SU-8 thick film are first prepared for a supporter of the tactile dot by using X-ray lithography as shown in Figure 5.28 (a). This SU-8 supporter is comprised of a small orifice used to support the tactile dot and the large orifice for the dot housing as shown in Figure 5.28 (b). Then, the tactile panel is covered as shown in Figure 5.28 (c) and the nitrogen gas is applied to test the tactile dot actuation as shown in Figure 5.28 (d).

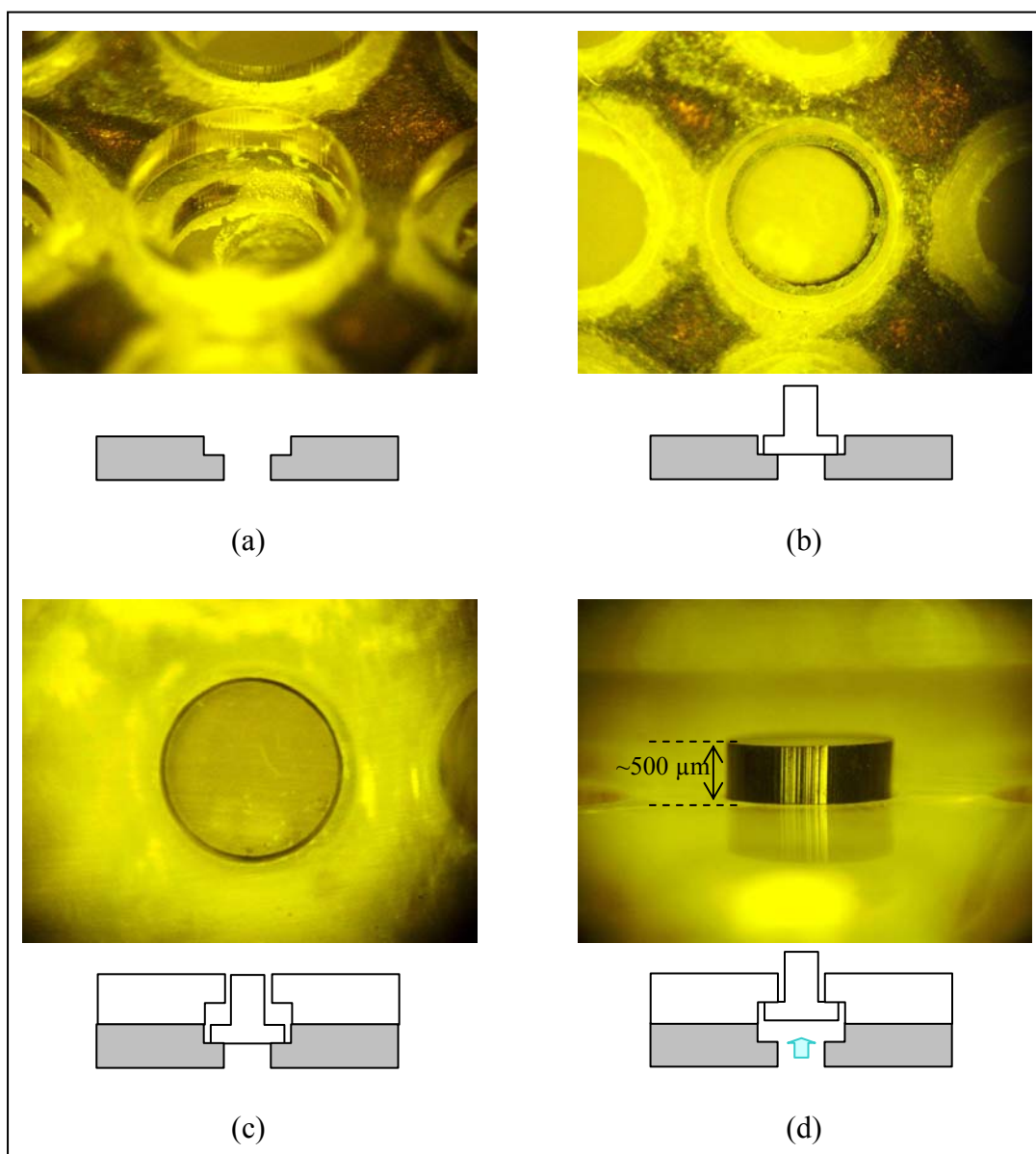


Figure 5.28 The assembly of the released tactile dot display (a) prepare a supporter of SU-8 tactile dot (b) place SU-8 tactile dot inside the supporter (c) cover with SU-8 tactile panel and (d) test under an applied pressure.

5.4 Refreshable Tactile Display

The main objective of this research is the refreshable tactile display based on repeatable mechanical function. This section will be described the development of the repeated mechanism which have two techniques on the basis of SU-8 tactile dot display.

The first technique can be worked on PDMS membrane which was suspended on the orifice and flexible in vertical direction. The second technique is improved from the SU-8 piston tactile display by adding of two spring curved segments with one support under the tactile dot. These help to pull the tactile dot back from actuating state and make them easily to perform as the pneumatic refreshable Braille display systems.

5.4.1 PDMS spring element for the SU-8 refreshable tactile display

To increase the effective display of the tactile dot, the suspended PDMS membrane and the SU-8 tactile display are combined together by placing the SU-8 tactile dot on the PDMS membrane. The SU-8 dot is fixed on the membrane by the SU-8 2002 photoresist, resulting in refreshable display of the tactile dot. PDMS membrane is used as a spring element pulled the tactile dot back to the normal state.

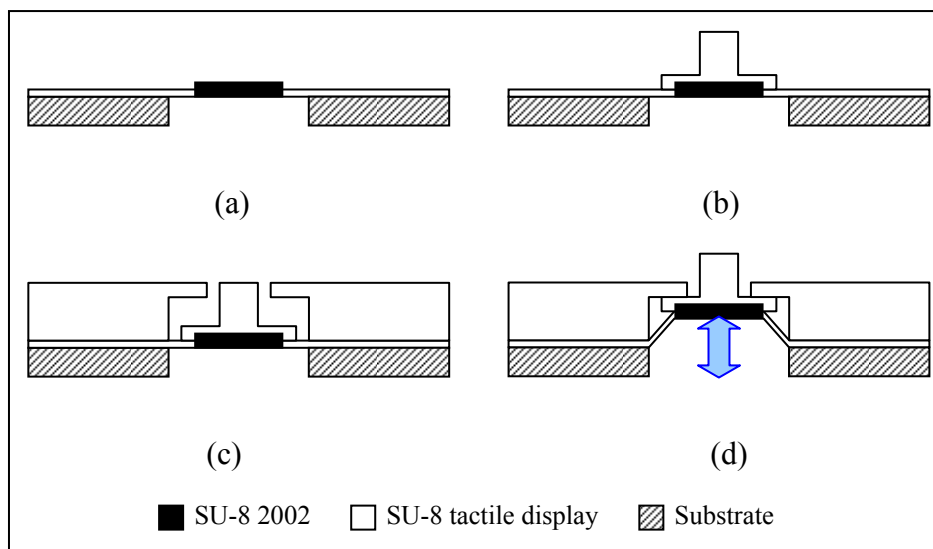


Figure 5.29 Fabrication sequences of the PDMS/SU-8 refreshable tactile display (a) paint glue at the center of suspended PDMS membrane (b) place SU-8 tactile dot on the membrane (c) cover with SU-8 tactile panel and (d) test under an applied pressure.

Figure 5.29 demonstrates fabrication sequences of the refreshable tactile display which has the PDMS membrane suspended on the SU-8 orifice. The glue used to attach them together is SU-8 2002 photoresist which is not naturally allow to flow on the PDMS membrane resulting from the hydrophobic state. To make the liquid SU-8 attaching on the membrane, the PDMS membrane is first treated in 100% oxygen plasma at 200W for 1.30 minutes, and the SU-8 is then painted at the center of the membrane by a pin as shown in Figure 5.29 (a). The SU-8 dot is manually aligned and placed at the center of the membrane as shown in Figure 5.29 (b) and 5.30 (a). The sample is baked in the oven at 70°C for 1 hour and cooled down naturally. The fixed SU-8 dot is covered with the SU-8 panel as shown in Figure 5.29 (c) and 5.30 (b). The sample is mounted on the holder and applied the gas pressure with various frequencies to evaluate the repeatable tactile display.

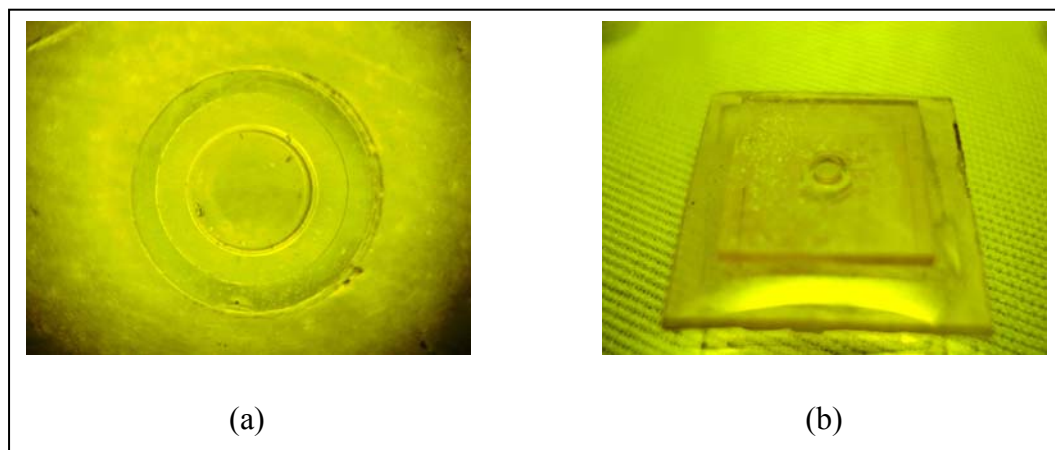


Figure 5.30 (a) The SU-8 tactile dot attaching on the PDMS membrane and
(b) covering the tactile dot with the SU-8 panel.

Figure 5.31 (a) shows the normal state of the tactile dot that is hided in the display panel. The sufficient differential pressure can push the PDMS membrane up resulted in the raising of the tactile dot upon the panel with a high of 500 μm as shown in Figure 5.31 (b). The applied pressure which is used to actuate the tactile display can be

estimated from the load-deflection behavior as described in Section 5.2.2. Furthermore, the refreshable display can be performed with various frequencies.

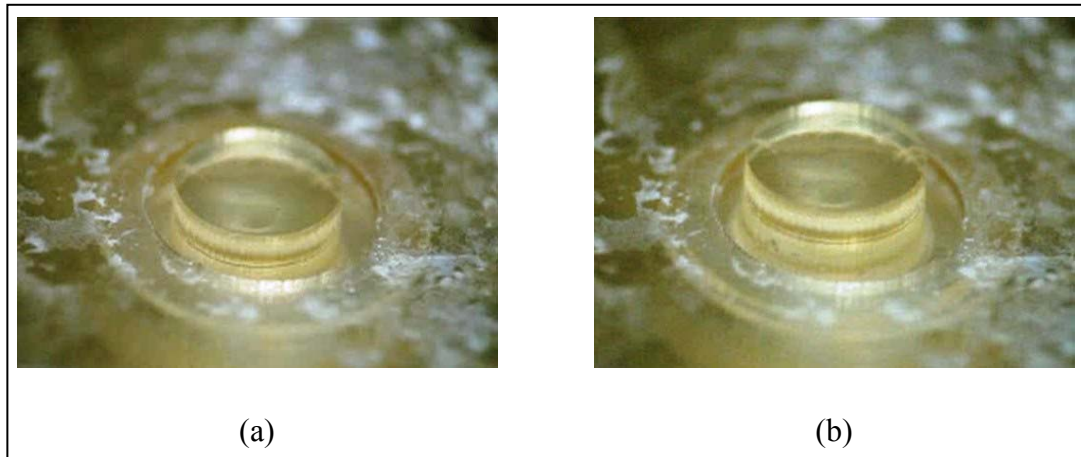


Figure 5.31 (a) The normal state and (b) the actuated state of the SU-8 refreshable tactile display with PDMS spring element.

5.4.2 Curved spring segments for the SU-8 refreshable tactile display

Since the SU-8 piston does not provide the restoring part of the tactile dot display, spring curved segments are added under the piston to pull the tactile dot back to the normal state. Figure 5.32 illustrates the schematic of two curved segments with one support which has a span angle θ of 174° and a radius R $1000 \mu\text{m}$. A beam width of the metal spring w is $100 \mu\text{m}$ and the thickness t is $30 \mu\text{m}$ based on the nickel electroplating process. The metal mesh at the center of the curved segment is used to support the SU-8 tactile dot structure which is constructed by X-ray lithography. The dimensions and the nickel properties corresponding to this structure are listed in Table 5.2.

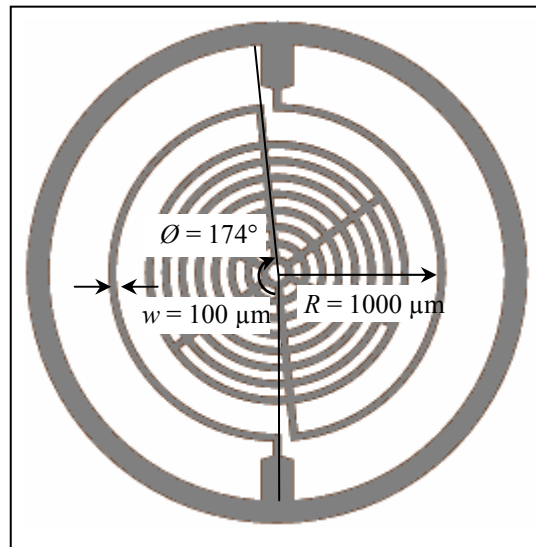


Figure 5.32 Schematic layout of the curved spring segment with one support.

Table 5.2 The dimensions and the nickel properties of the curved spring segment.

Characteristics	Details
Beam radius, R	1000 μm
Beam width, w	100 μm
Beam thickness, t	68 μm
Span angle, \emptyset	174°
Young's modulus of electroplated Ni, E	205 GPa (Luoa et al., 2004)
Poisson's ratio of Ni, ν	0.31

The spring is fabricated by electroplating of nickel material which is formed in AZ P4620 photoresist mold as shown in Figure 5.33 (a). After removing of the mold as shown in Figure 5.33 (b), the first 400 μm -thick SU-8 photoresist is constructed on the center

of the metal mesh by using X-ray lithography as shown in Figure 5.33 (c). Then, 900 μm thick SU-8 is next built at the center to perform as the tactile dot as shown in Figure 5.33 (d).

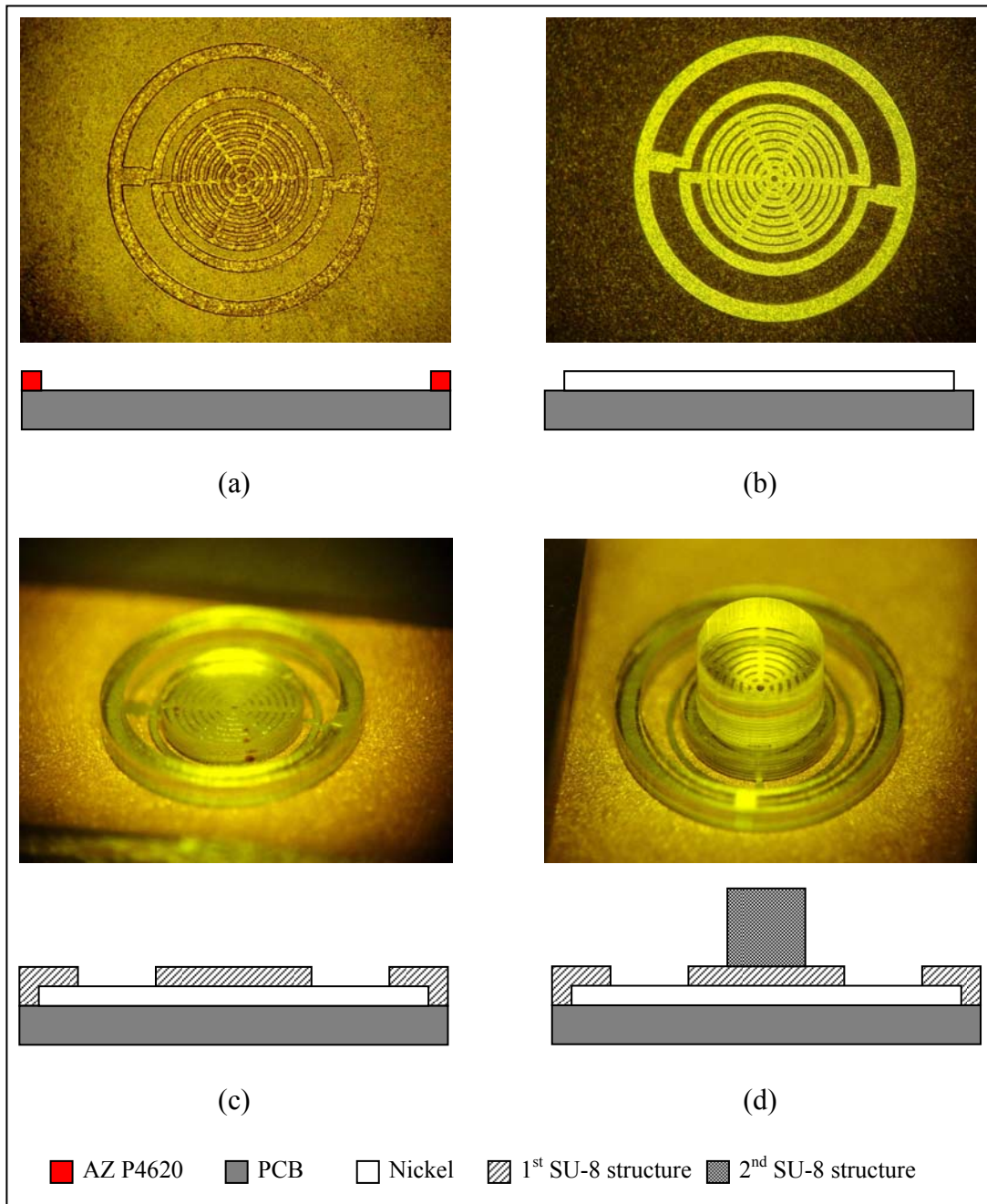


Figure 5.33 Fabrication sequences of the spring SU-8 tactile dot display.

At the same time, the tactile panel is simultaneously fabricated with the tactile dot as shown in Figure 5.34 (a). The panel with size of $1\text{ cm} \times 1\text{ cm}$ is constructed at the center of the substrate by using multi-layer X-ray lithography. The first layer which is an orifice with diameter of $1500\ \mu\text{m}$ perform as the display panel for the moving path of the SU-8 pin, while the second layer provides the orifice for the moving of the metal spring and a mechanical lock of spring structure as shown in Figure 5.34 (b).

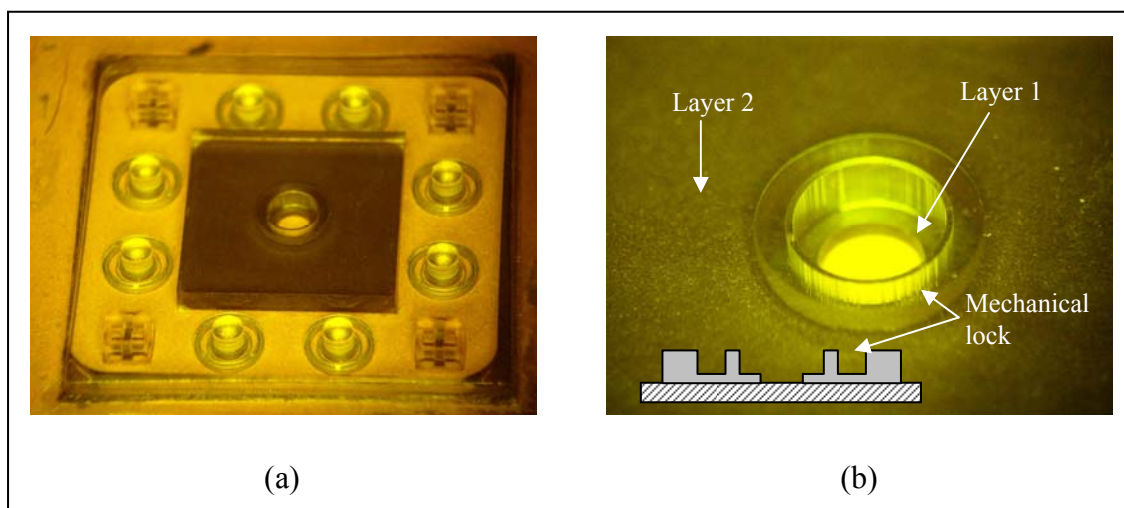


Figure 5.34 (a) The display panel with the tactile dot on the substrate and (b) two layers of the display panel.

The spring/SU-8 tactile dot and display panel are removed from the substrate by etching of sacrificial layer as shown in Figure 5.35 (a). The dot is flipped and placed in the panel by manual alignment. The SU-8 ring which is the part the metal spring is inserted into the arc-hole of the tactile display and fixed by epoxy glue as shown in Figure 5.35 (b). Figure 5.36 (a) illustrates the moving of the tactile dot resulting from the mechanical force by pressing of a pin under the tactile dot causing the display distance of $500\ \mu\text{m}$ upon the panel as shown in Figure 5.36 (b). The restoring force from the metal spring can pull the dot back to the normal state of the refreshable tactile display.

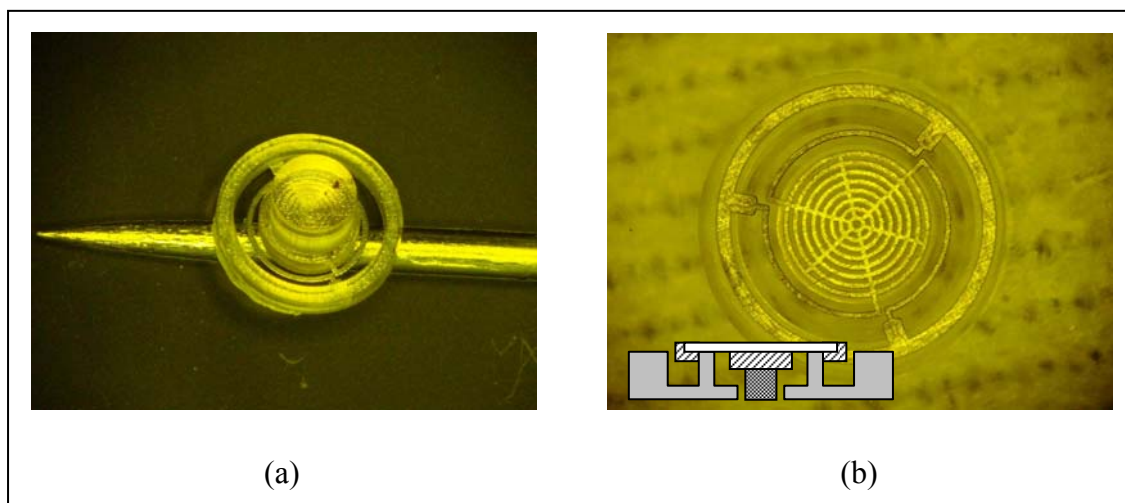


Figure 5.35 (a) The SU-8/spring tactile dot and (b) the assembly of the tactile dot display.

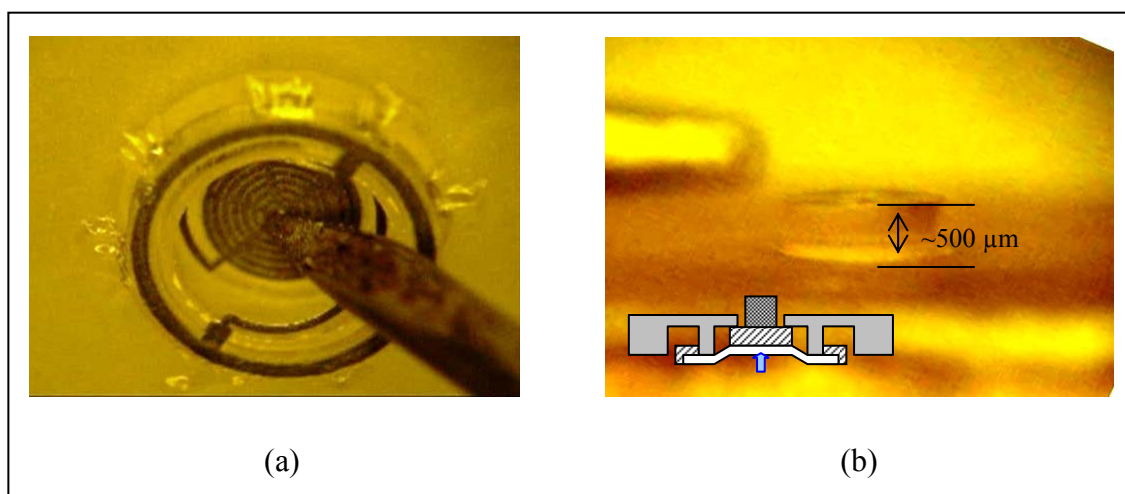


Figure 5.36 (a) Moving of the dot resulting from the mechanical force and (b) the rising of the tactile dot on the display panel.

5.4.3 Deflection of curved segments with one support

The metal spring configuration of the refreshable tactile dot is the curved segment having the span angle θ and the radius R as shown in Figure 5.37. The spring is fixed at one side while the other one is free end which is deflected by a constant force F from the external source. The bending, torsion, and direct shear are created at the fixed end

and any section of the beam. Based on the energy method, the simple approach for deflection calculation is analyzed by the Castigliano's theorem which is depended on the total strain energy.

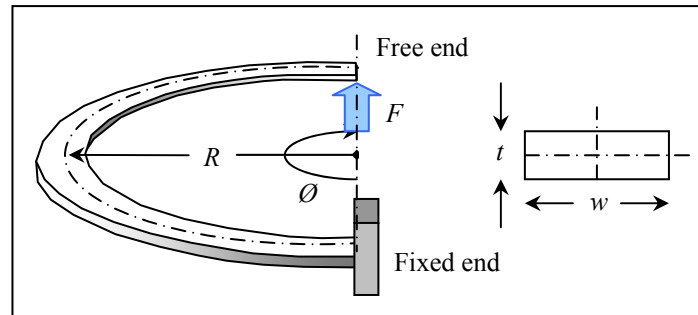


Figure 5.37 Curved segment of span angle loaded by force to the plan of the curve.

Equation (5.5) is the general expression of the Castigliano's theorem which is equal to the partial derivative of the total strain energy with respect to the direction of force (Shigley, 2004). The moments and torques at the fixed end and any section of beam can be calculated by Equation (5.6) and (5.7), respectively.

$$\delta = \frac{\partial U}{\partial F} \quad (5.5)$$

$$M = FR \sin \theta \quad (5.6)$$

$$T = FR(1 - \cos \theta) \quad (5.7)$$

where U is the total strain energy stored in structure, δ is displacement of the applied point of force in the direction of F . M and T are the moments and torques on the span angle θ on the beam having a radius of R , respectively.

To obtain the deflection at the free end, the small direct shear effect is neglected resulting in the total strain energy in Equation (5.8).

$$U = \int_0^\phi \frac{M^2 R d\theta}{2EI} + \int_0^\phi \frac{T^2 R d\theta}{2GJ} \quad (5.8)$$

Therefore, the deflection δ at free end in the direction of F is calculated by Equation (5.9) which is substituted by the partial derivative of M and T in Equation (5.10) and (5.11), respectively.

$$\delta = \frac{\partial U}{\partial F} = \frac{R}{EI} \int_0^\phi M \frac{\partial M}{\partial F} d\theta + \frac{R}{GJ} \int_0^\phi T \frac{\partial T}{\partial F} d\theta \quad (5.9)$$

$$\frac{\partial M}{\partial F} = R \sin \theta \quad (5.10)$$

$$\frac{\partial T}{\partial F} = R(1 - \cos \theta) \quad (5.11)$$

where E is Young's modulus, I is second moment of area ($wt^3/12$), G is modulus of rigidity ($E/2(1+\nu)$), w is beam width, t is beam thickness, ν is poisson's ratio, and J is polar second moment of rectangular section which is calculated by Equation (5.12).

$$J = \frac{wt^3}{A} \quad (5.12)$$

where $A = 3 + 1.462 \frac{t}{w} + 2.976 \left(\frac{t}{w}\right)^2 - 0.238 \left(\frac{t}{w}\right)^3$

The term after solving Equation (5.9) - (5.11) can be arranged the solution in Equation (5.13). The coefficients α and β are dependent on the span angle ϕ in radians and defined in Equation (5.14) and (5.15), respectively.

$$\delta = \frac{FR^3}{2} \left(\frac{\alpha}{EI} + \frac{\beta}{GJ} \right) \quad (5.13)$$

$$\alpha = \phi - \sin \phi \cos \phi \quad (5.14)$$

$$\beta = 3\phi - 4 \sin \phi + \sin \phi \cos \phi \quad (5.15)$$

The spring constant k of one curved segment with one support can be estimated by using the relationship between force and deflection by Equation (5.16).

$$k = \frac{F}{\delta} = \frac{2}{R^3 \left(\frac{\alpha}{EI} + \frac{\beta}{GJ} \right)} \quad (5.16)$$

Since there are two curved segments, the spring constant of the tactile dot k_t given by Equation (5.16) is two times the curved segment, the spring constant and deflection can be modified as giving in Equation (5.17) and (5.18), respectively.

$$k_t = 2k = \frac{4}{R^3 \left(\frac{\alpha}{EI} + \frac{\beta}{GJ} \right)} \quad (5.17)$$

$$\delta = \frac{FR^3}{4} \left(\frac{\alpha}{EI} + \frac{\beta}{GJ} \right) \quad (5.18)$$

The SU-8 piston is experimented under the applied pressure and measured the deflection by using the Veeco[®] profiler. Differential pressure is monitored in unit of Pascal (Pa) which is equal Newton/square meter (N/m²). To evaluate the differential pressure into force, the unit of Pascal is converted to Newton. The bottom area of the piston is 2402229.44 μm^2 or $2.402 \times 10^{-6} \text{ m}^2$. Therefore, Newton unit can be obtained from Pascal unit by Equation (5.19).

$$Force (N) = [2.402 \times 10^{-6} (m^2)] \times [Differential Pressure (Pa)] \quad (5.19)$$

Figure 5.38 shows comparison of analytic curved spring segment (solid line) with the experimental results (points). The analytic deflection calculated by Equation (5.18) is greater than the experimental results. The single spring constant obtained by Equation (5.16) is 82.193 N/m while the total spring constant having two curved segments is 164.385 N/m achieved by Equation (5.17).

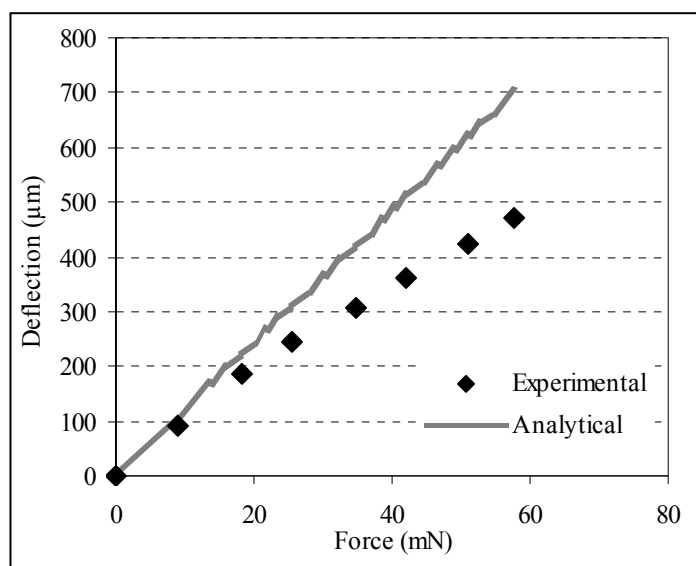


Figure 5.38 Comparison of analytic curved spring segment (solid line) with the experimental results (points).

5.5 Chapter Summary

Many fabrication methods for the tactile dot stimulation have been proposed in this chapter. The first is the PDMS dot which is fabricated by using spin-coating technique and the suspended membrane of PDMS on the orifice of the SU-8 tactile panel. Although it is easily to apply for the pneumatic refreshable tactile display, the sensation on the fingertip is not given clearly enough. To solve this problem, the rigid SU-8 tactile structure is generated by using X-ray lithography. This method is based on the SU-8 powder reflowed casting which is helped to construct the thick photoresist layer, and the polishing technique is used to control to the final film thickness. Multi-layer X-ray exposure is basically performed through the transparent X-ray mask to create the tactile dot with the vertical side wall. However, these tactile do not provide the repeated mechanism which is not appropriate for the refreshable Braille display systems. Therefore, the spring mechanism is combined into the tactile dot rising for two methods. First, the SU-8 tactile dot is placed on the suspended PDMS membrane and repeated under various applied pressure. Second, the spring curved segment is fixed at the bottom of the tactile dot to pull the dot back to the normal state after the applied pressure is gotten away. Both of refreshable tactile displays are suitable to apply for the refreshable Braille display systems which will be tested for the force actuation under the applied pressure in next chapter.

CHAPTER VI

EXPERIMENTAL OF REFRESHABLE TACTILE DISPLAY

6.1 Introduction

The SU-8 refreshable tactile displays which have been fabricated by using X-ray LIGA process are combined with the experimental setup to evaluate the tactile dot sensation and the tactile force. Experimental setup of the refreshable tactile display is described in Section 6.2. The testing setup and experimental diagram are presented to utilize in the force-pressure characteristics estimation. Section 6.3 demonstrates the force-pressure characteristics of the tactile display with PDMS spring element and curved spring segments. These can be used to evaluate the possibility of the tactile display based on the standard actuation. Section 6.4 presented the refreshable tactile display system by controlling of microvalve which has been fabricated in Chapter 4. Integrated microvalve is combined with the tactile display to play significant role in the refreshable Braille display system. Finally, the chapter summary is presented.

6.2 Experimental Setup of the Refreshable Tactile Display

Refreshable tactile displays with PDMS spring element and curved spring segments are arranged to test the force-pressure characteristics. The tactile display is held on a tactile display holder which is fixed on the pressure chamber as shown in Figure 6.1. Two pneumatic pipes are fixed on side walls of the pressure chamber for the applied pressure and the input of a pressure sensor.

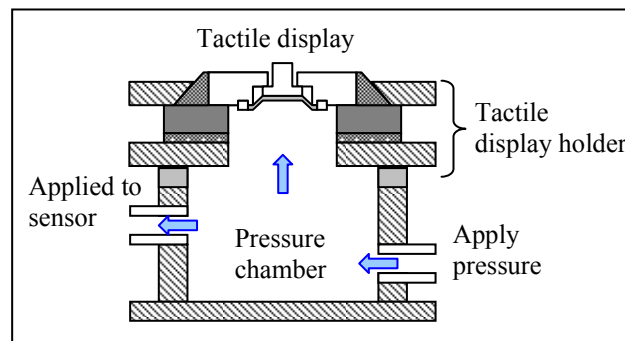


Figure 6.1 Chamber pressure with the tactile display holder.

The assembled sequences of the tactile display with pressure chamber are shown in Figure 6.2. The refreshable tactile display is fixed on a tactile display support by epoxy glue sealed around the tactile panel as shown in Figure 6.2 (a). The tactile display support which was drilled at the center with diameter of 5 mm is placed on a thin PDMS layer used for leakage protection. The upper acrylic polymer of the pressure chamber drilled at the center is performed as a base of the tactile support as shown in Figure 6.2 (b). To pack them together, other thin acrylic polymer is used to compressed and tightly fixed with four screws to form the tactile display holder as shown in Figure 6.2 (c). At last, the chamber pressure is covered with the tactile display holder and firmly packs by four screws as shown in Figure 6.2 (d).

After the tactile display was assembled with the pressure chamber, the experimental setup for the pneumatic refreshable tactile display is next consideration. The characteristics of the tactile display are measured via the testing setup illustrated by a diagram in Figure 6.3. Nitrogen tank supplies a constant pressure of gas through an 8 mm-diameter of pneumatic pipe to the pressure chamber. The 2nd pressure regulator is connected in series between the 1st pressure regulator and a solenoid valve to precisely control of the applied pressure. To switch on-off the tactile display, the solenoid valve is controlled by a programmable micro-controller in the control box. The differential pressures inside the chamber is employed a pressure sensor while the force of tactile dot is measured through a force sensor.

Monitoring results of sensor are displayed on the gauge display which can be changed display mode between differential pressure mode and force mode.

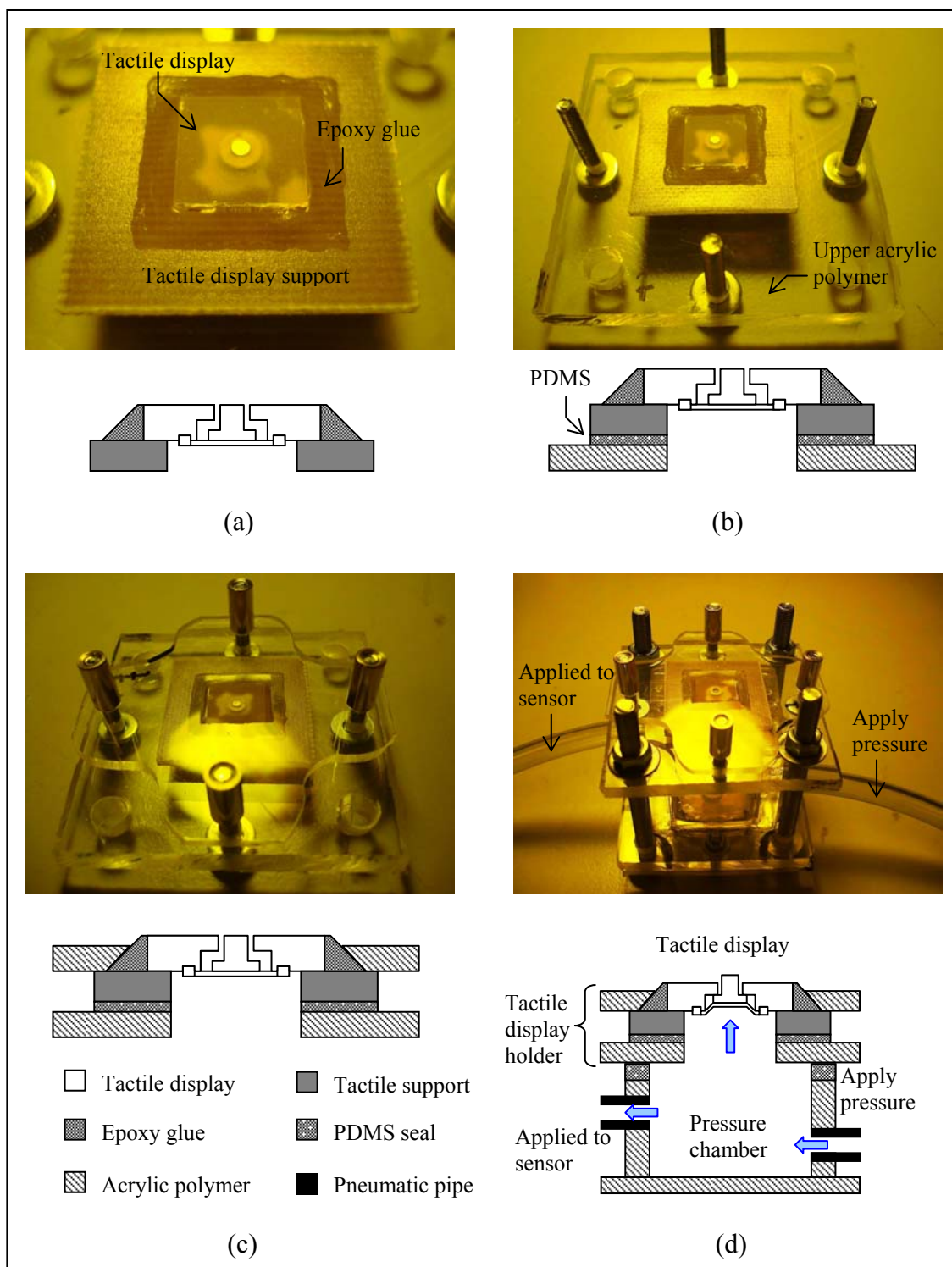


Figure 6.2 Assembled sequences of the tactile display with pressure chamber.

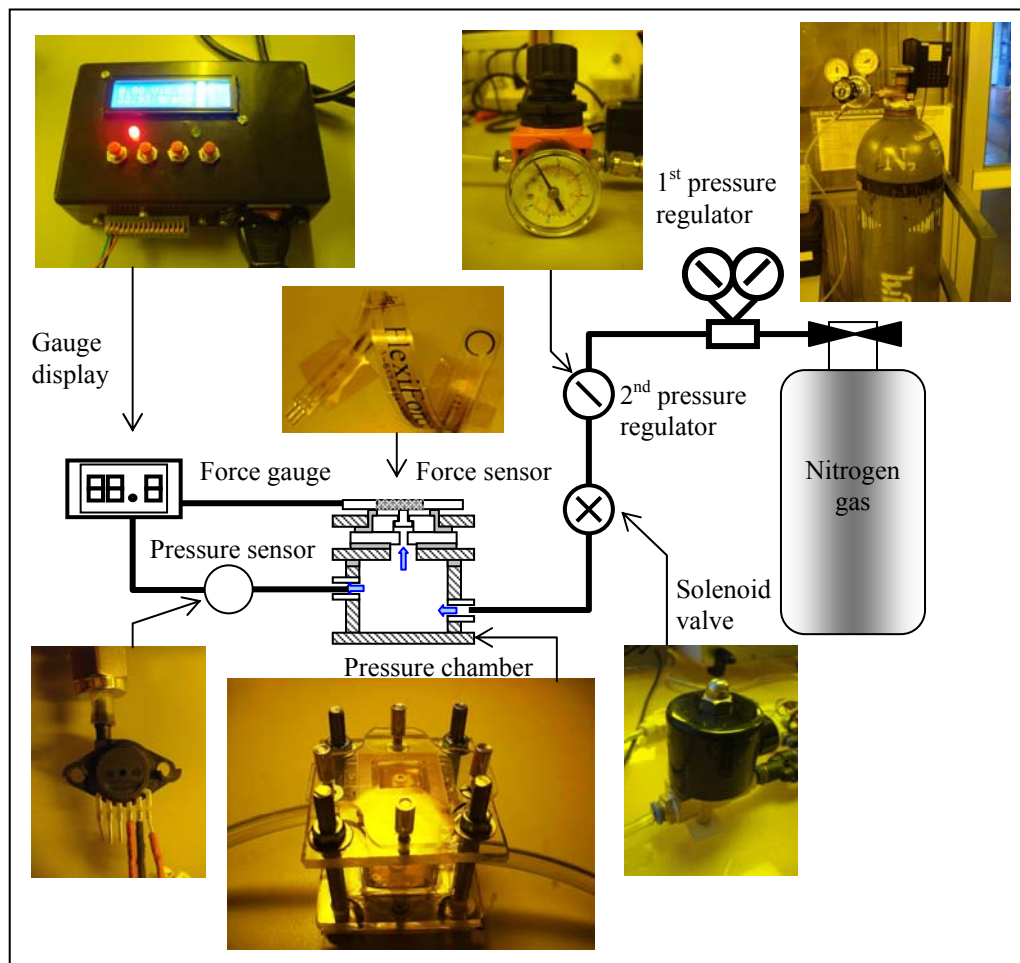


Figure 6.3 Experimental diagram of the tactile display.

The objective of this testing is force-pressure characteristics of the tactile display. Because the touching sensation is based on the strength of the load resistance against the fingertip, the force of the tactile dot rising has to be investigated to ensure that the force actuating is reached to the standard of general tactile specification. Based on Kato et al. (2007), an actuation force of the tactile dot at least 1.5 gram-force (gf) has to be guaranteed for the tactile display. To measure the force against the fingertip, individual FlexiForce[®] A201 sensor is placed on the tactile display as shown in Figure 6.4 (a). The 2nd pressure regulator gradually increased the applied pressure cause the raising up of the tactile dot, resulting in the force detection which is based on the amplitude of the applied pressure. Figure 6.4 (b) illustrates the force-pressure experimental setup consisted of the tactile display with force sensor, force calibration, pressure sensor, and gauge display.

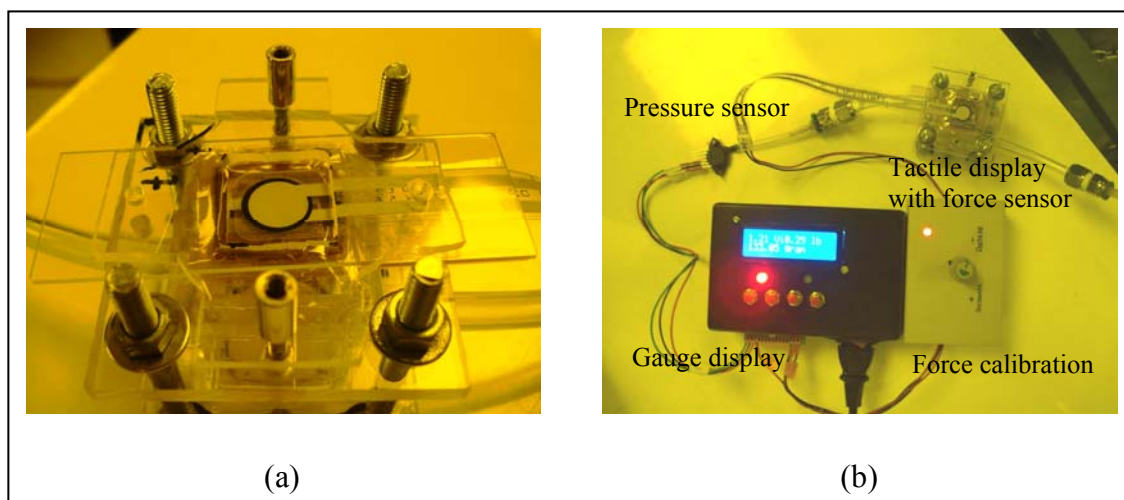


Figure 6.4 (a) Force sensor placing over the tactile display and
(b) force-pressure experimental setup.

6.3 Force-Pressure Characteristics of the Refreshable Tactile Display

The refreshable tactile display will be set up and experimented to find the force that corresponds with applied pressure as described in Section 6.2. Their results are recorded and plotted for the force-pressure curve to evaluate the tactile display performance. The tactile display with PDMS spring element is first experimented, followed by the tactile display with curved spring segments.

6.3.1 Force-pressure of the tactile display with PDMS spring element

To assemble the tactile display in experimental setup, the tactile dot is first fixed permanently on a 16 μm -thick PDMS membrane by the SU-8 3025 photoresist. This make the device is easily portable as shown in Figure 6.5. The PDMS membrane and the bottom of the tactile panel are treated in 100% oxygen plasma at 200 W for 1 minute. Then, the SU-8 3025 photoresist is painted around the tactile dot, followed by placing of the display panel and baking at 90°C for 1 hour in the oven. After cooled down naturally, the portable tactile display is assembled into the tactile display holder.

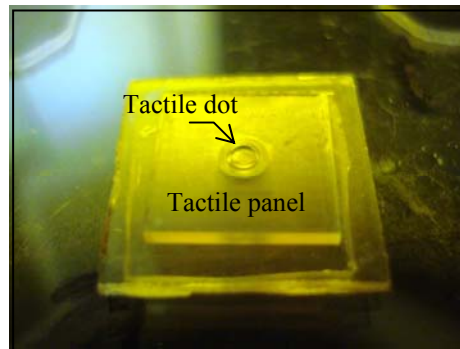


Figure 6.5 Portable tactile display.

This portable tactile display with elastic PDMS membrane is set up on the force-pressure experimentation as shown in Figure 6.6. Since this tactile display does not provide built-in ventilation, the pressure chamber must supply the small gas vent under its chamber to recover the flat tactile surface after the applied pressure is closed. To create a single tactile dot, the solenoid valve is switched on and the 2nd pressure regulator is gradually increased until there is sufficient differential pressure across the tactile display. The PDMS membrane is elastically deformed and raises the tactile dot up which user can perceive this exciting as the single tactile dot. To recover the flat surface, the solenoid valve is closed and the trapped gas inside the pressure chamber discharge through the gas vent. Figure 6.7 (a) and (b) show the normal state and actuation state of the tactile display, respectively.

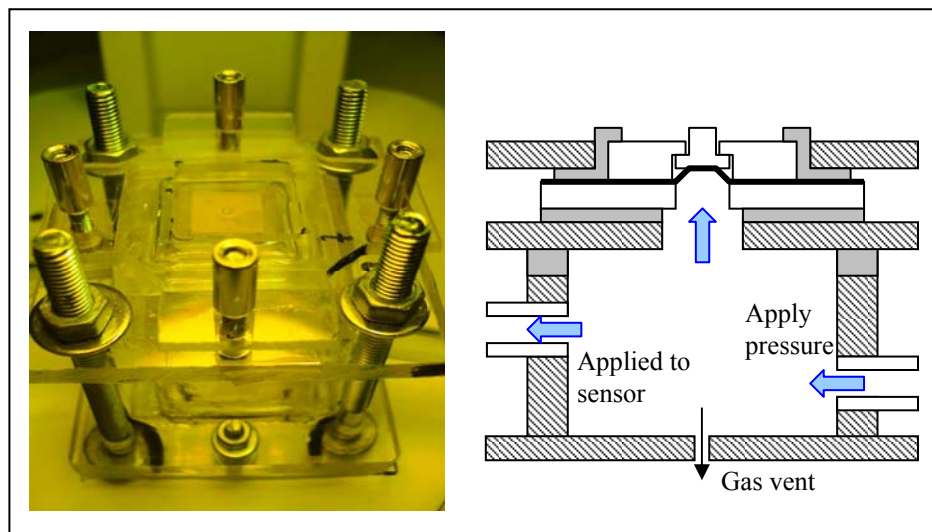


Figure 6.6 Experimental setup for the tactile display with PDMS spring element.

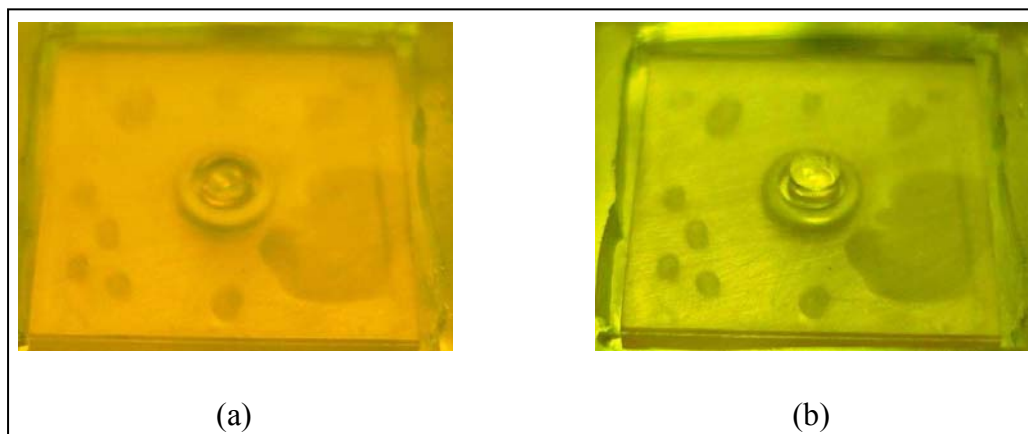


Figure 6.7 (a) The normal state and (b) the actuation state of the tactile display with PDMS spring element.

Force-pressure characteristics are observed and demonstrated the experimental result in Figure 6.8. The force sensor can sense the first actuation force when the differential pressure reaches to 3.78 kPa. The maximum tactile force of the 16 μm -thick PDMS membrane under the maximum applied pressure of 16.87 kPa is 76.71 gf which is higher than the minimum requirement of the reference tactile force of 1.5 gf.

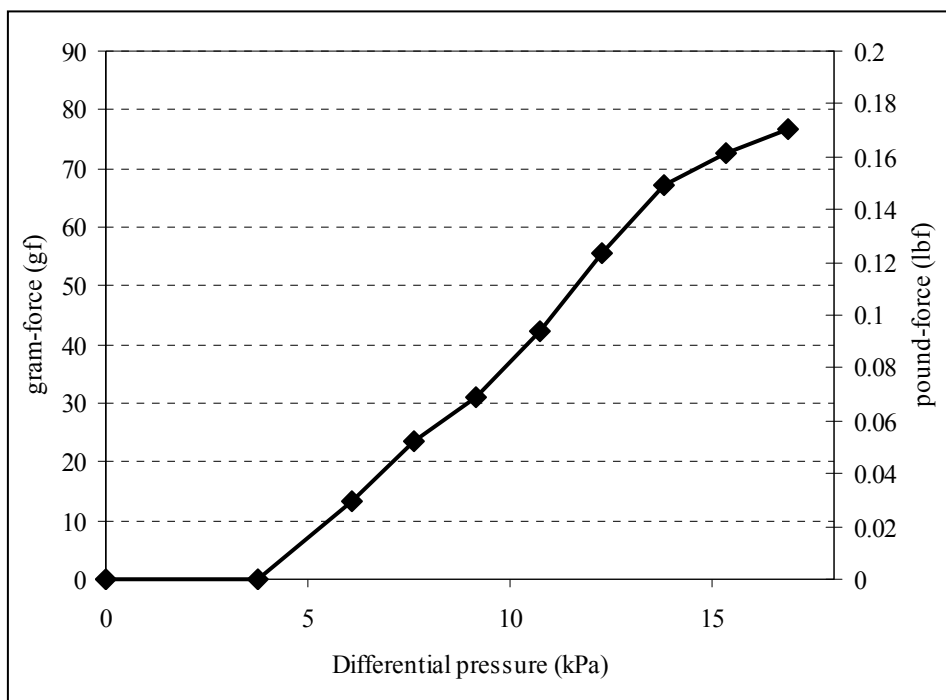


Figure 6.8 Force-pressure characteristic of the tactile display with PDMS spring element.

6.3.2 Force-pressure of the tactile display with curved spring segments

The tactile display with curved spring segments is set up in the pressure chamber of the force-pressure experimentation. This tactile display is naturally provided built-in vent which is a gap between the tactile dot and its cylinder. Therefore, the small gas vent under the pressure chamber is closed. In normal state, there are no differential pressures across the tactile display, resulting in hiding of the tactile dot inside the tactile panel as shown in Figure 6.9 (a). After the solenoid valve is switched on and the 2nd pressure regulator feeds the applied pressure, the large pressure can develop across the tactile display and tactile dot is strongly stood. User can sense this actuation as a single tactile dot via their fingertip as shown in Figure 6.9 (b). To get back flat surface, the solenoid valve is switched off, resulting in decreasing of the pressure inside the chamber. The restoring force from the curved spring segments is strong enough to pull the tactile dot back to original state.

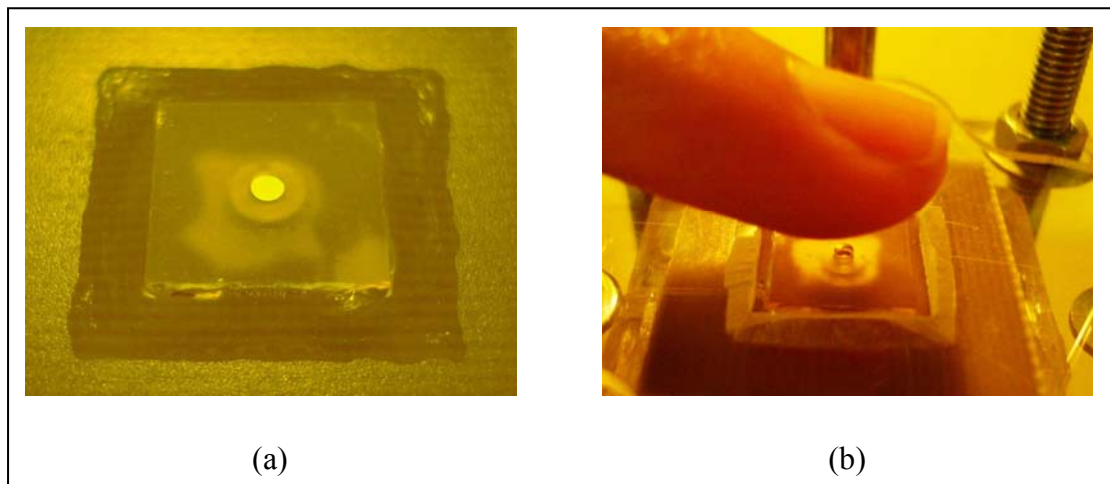


Figure 6.9 (a) The normal state and (b) the actuation state of the tactile display with curved spring segments.

The force-pressure experimental results of the tactile display are demonstrated in Figure 6.10. The applied pressure is increased and the excited force is recorded. The maximum differential pressure is 68.46 kPa result in an actuation force of 82.76 gf which higher than the minimum requirement of the reference tactile display of 1.5 gf. However, the force sensor is separated from the tactile dot with distance of 300 μm while the display distance of the tactile dot is 500 μm . The remained distance of 200 μm is the leakage hole of the applied pressure. Therefore, the total force that acts on the force sensor is summation of the gas leakage force and the tactile dot force resulted from the applied pressure. The force-pressure curve of this experimentation cannot indicate the exact characteristics of the tactile display.

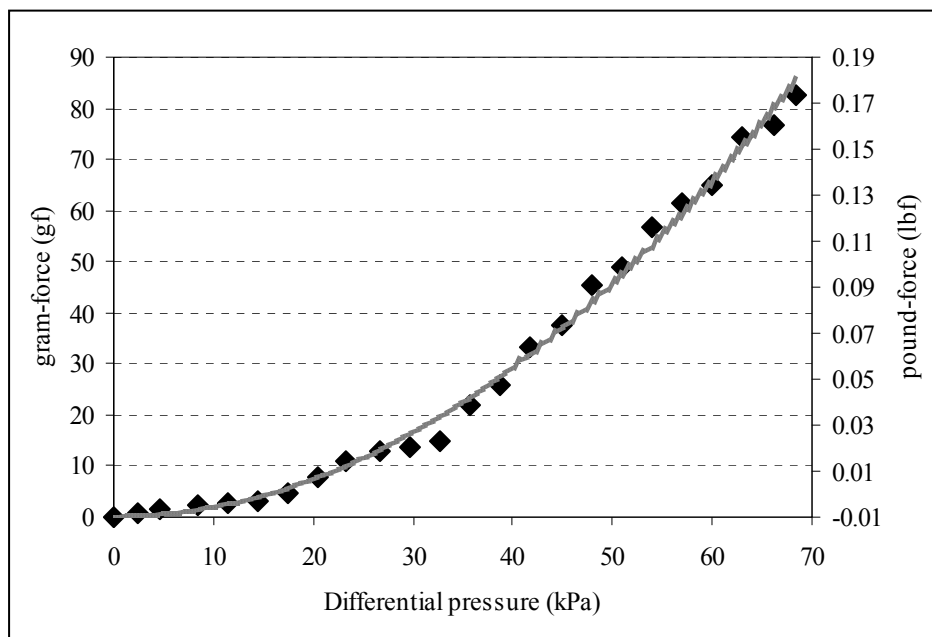


Figure 6.10 Force-pressure characteristics of the tactile display with curved spring segments.

To estimate the accurate load-pressure characteristic, another testing technique which can indicate any amount of load correspond with the applied pressure has to be performed. Figure 6.11 illustrates the weight-pressure experimental diagram that uses the tested weights indicator instead of the force sensing. Thin PDMS membranes are used as the tested weights which are placed on an aluminum disc placed on the tactile display. To find the real force of this tactile display correspond with the applied pressure, the tested PDMS weights in the range of 0.25 g to 10 g is placed on the aluminum and the applied pressure is increased until the tactile dot is rinsed to the maximum distance without any gas leakage. The applied pressure is recorded and reports the experimental data in Figure 6.12. The minimum different pressure which can raise the tactile dot up without any load and leakage is 33.92 kPa. The maximum weight of 10 g requires the applied pressure of 109.48 kPa to absolutely seal the gas leakage.

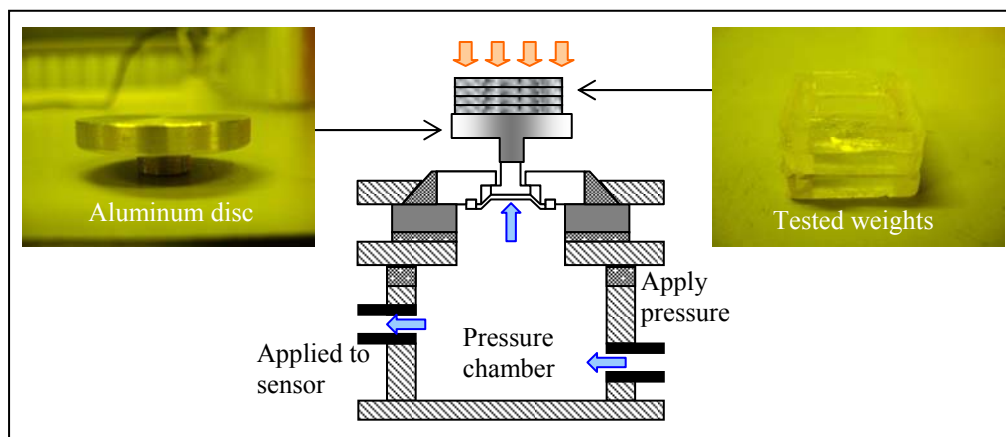


Figure 6.11 Weight-pressure experimental setup.

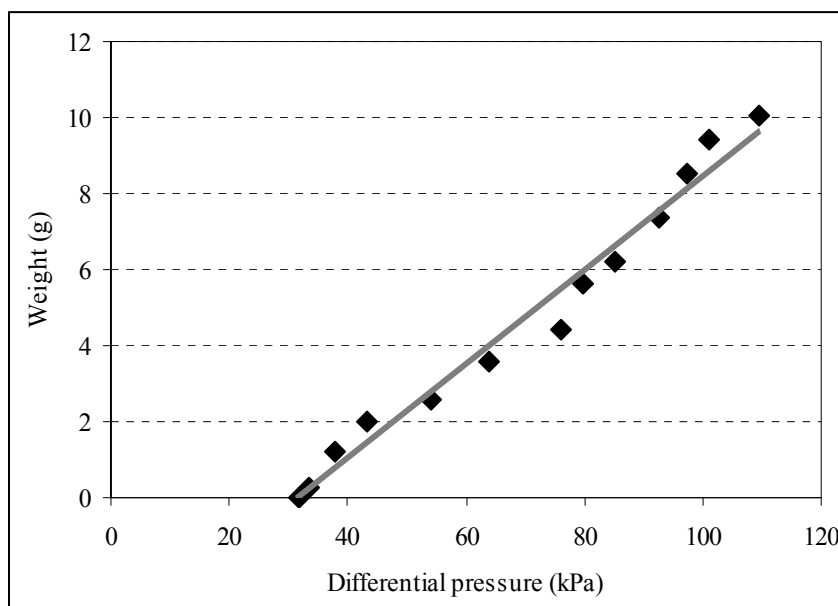


Figure 6.12 Weight-pressure characteristics of the tactile display with curved spring segments.

Moreover, this tactile display is also tested by the fingertip of the human to evaluate the minimum sensation of user as shown in Figure 6.9 (a). The minimum applied pressure of 60.06 kPa can resist the pressing from the fingertip without any gas leakage. The experimental results can be used to guarantee this tactile display for the refreshable Braille display systems which perform as the interface device for the visually impaired.

6.4. Refreshable Tactile Display by Controlling of Curled-Up Closure Plate Microvalve

Microvalve which has been fabricated in Chapter 4 is combined with the tactile display with PDMS spring element. Figure 6.13 illustrates the assembled sequences of the refreshable tactile display with microvalve that use multipart of acrylic polymer as the holder and the pressure chamber. The portable tactile display is sandwiched by PDMS frames and compressed with parallel plates of acrylic polymer as shown in Figure 6.13 (a). At the same time, the microvalve which was bonded with copper wires on the ground electrode and the top electrode is placed on a PDMS membrane to prevent any gas leakage at the bottom, while the top surface is covered with a PDMS square frame provided a gas ventilation hole in discharging of the trapped pressure inside as shown in Figure 6.13 (b). The tactile display holder and microvalve are overlapped by placing the holder on the microvalve and fixed them together with screws as shown in Figure 6.13 (c). The applied pressure is fed into the pressure which is constructed as a rectangular box with a PDMS square frame placing on the top side wall as shown in Figure 6.13 (d). Finally, the holder is placed on the pressure chamber and tightly fixed with screws to ensure that there is minimum leakage. The completed setup of the refreshable tactile display with microvalve is shown in Figure 6.13 (e).

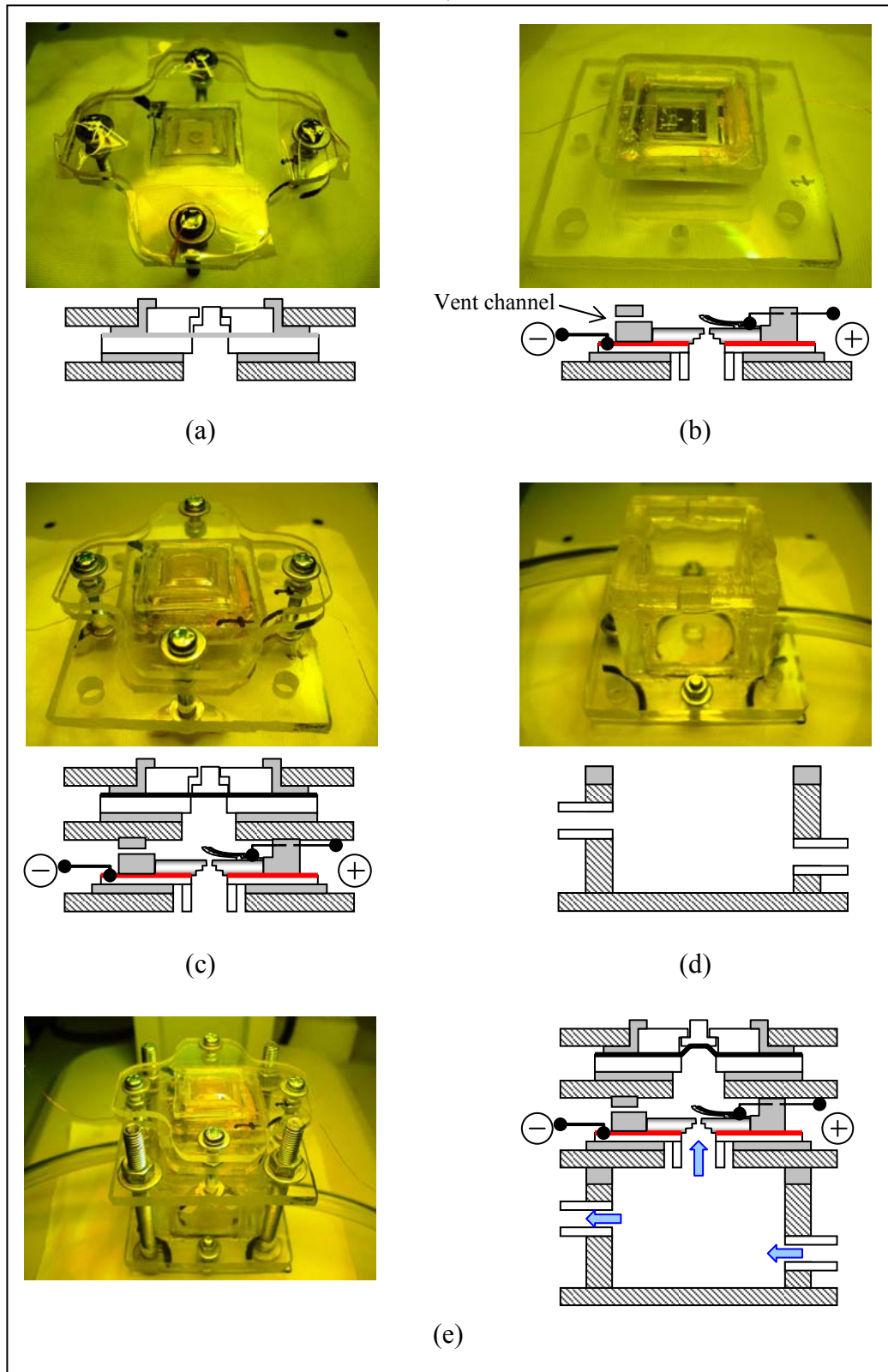


Figure 6.13 Assembled sequences of the refreshable tactile display with microvalve.

For experimental set up, the high DC voltage source is connected to the microvalve while the pressure chamber is linked to the pressure regulator through the solenoid valve as demonstrated in Figure 6.14. The supply pressure is applied a constant pressure into the pressure chamber and monitored by the pressure sensor. The pressure inside the chamber is increased gradually by controlling of the 2nd pressure regulator until the tactile dot is raised up that can views through the microscope as shown in Figure 6.15 (a). Then, the high dc voltage is applied to the microvalve and increased gradually until the tactile dot is maximally downward as shown in Figure 6.15 (b).

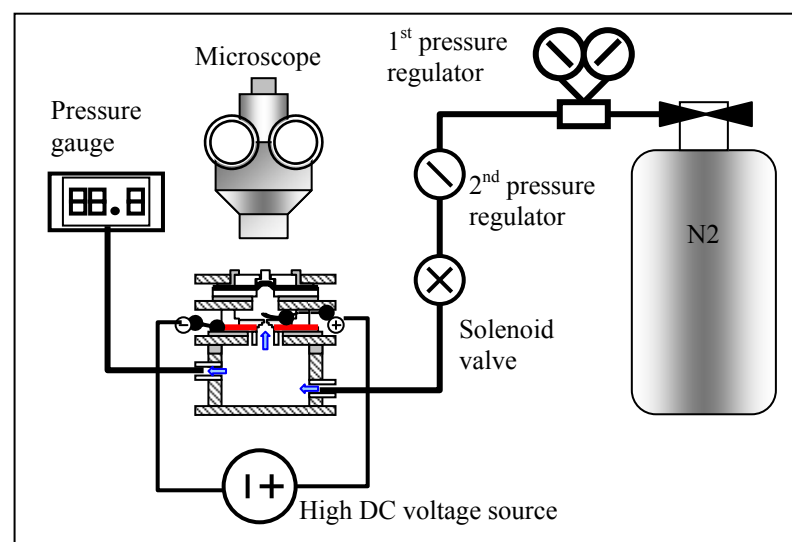


Figure 6.14 The experimental setup for the refreshable tactile display.

As shown in Figure 6.15, the gas pressure which is applied to drive the tactile dot up to the maximum deflection is 42.98 kPa, resulting in the distance of 485 μm based on the deflection of the PDMS membrane with thickness of 16 μm . Then, the dc voltage is gradually increased until the tactile dot is maximally moved down with distance of 120 μm . The dc voltage of 150 V can be used to close the microvalve in this situation. The tactile dot is not absolutely flattened with the remained deflection of 365 μm cause by the leakage of the closure plate and the conductive substrate of microvalve as described in Chapter 4.

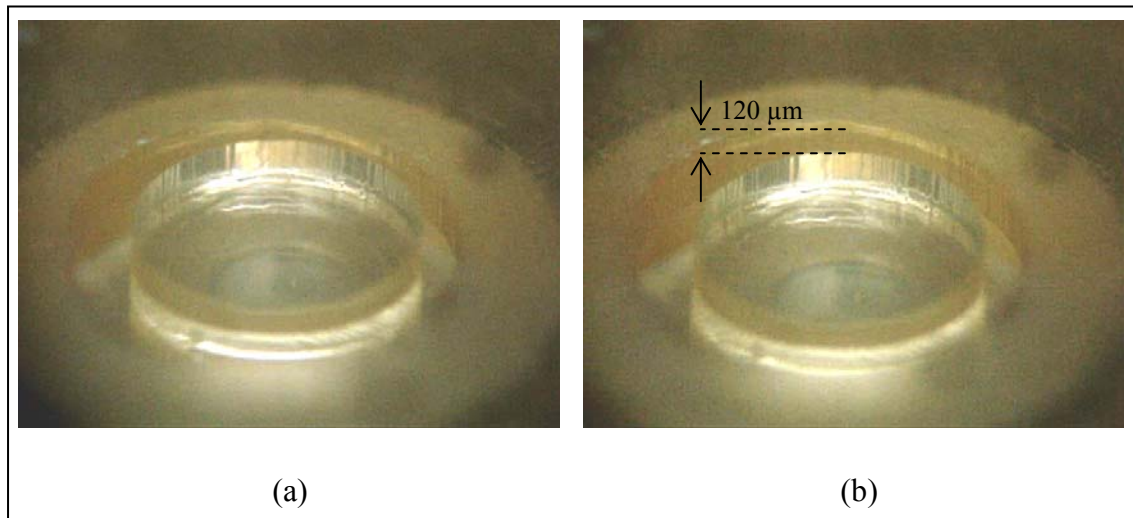


Figure 6.15 (a) Rising of tactile dot under the applied pressure and (b) the maximum downward distance after closing of microvalve.

6.5 Chapter Summary

Three types of the tactile display are set up to verify as the refreshable tactile display. They are combined with the tactile holder and the pressure chamber, and sealed by many parts of PDMS frame. The tactile display with PDMS spring element is first presentation. The obvious sensation of the tactile display can be achieved by the applied pressure of 16.87 kPa resulting in the force of 76.71 gf. The second is the tactile display with curved spring segments. The minimum differential pressure which can raises the tactile dot up without any load and leakage is 33.92 kPa. The maximum weight of 10 g requires the applied pressure of 109.48 kPa to absolutely seal the leakage. Finally, the tactile dot with PDMS spring element is combined with the curled-up closure plate microvalve to operate as the refreshable tactile display. The applied voltage for closing the microvalve is 150 V for the applied pressure of 42.98 kPa, resulting in the maximum downward distance of 120 μm . Since the closure plate of the microvalve is not absolutely close, the leakage is generated and the tactile dot is not flattened smoothly. However, the experimental results show the hope to utilize the microvalve for refreshable tactile display in the sensation device for the impaired people.

CHAPTER VII

CONCLUSIONS AND FUTURE STUDIES

7.1 Conclusions

In this thesis, X-ray LIGA technology was investigated for the realization of a tactile display to attain a novel refreshable Braille display systems (RBDS). Among numerous RBDS, the pneumatic tactile display was concentrated on this research. This selection can be supported by advantage of pneumatic actuation which did not based on specific material or complicated fabrication. Just apply pressure under the tactile dot structure; a single visible dot can be actively managed for the position of a tangible refreshable Braille dot. Fast response time and low power consumption were achieved because the applied pressure can be suddenly switched on-off by controlling of a conventional valve.

The tactile display prefer a rigid tactile dot more than a dome shape of elastic membrane. Although both of them can be displayed with a deflection of 480 μm -heights based on the Braille standard, the obvious sensation was mostly preferred on the rigid tactile display. Elasticity of the tactile membrane was a one major problem of a dome shape actuation. Polymer membrane provided large elongation with smooth surface but not robust and obvious enough to resist the mechanical load from a touch for a long time. Moreover, the excessive applied pressure can damage the elasticity of tactile membrane that does not provide the restricted deflection mechanism. Therefore, mostly of the RBDS always based on the rigid tactile dot mechanism as a pin shape forming in a tactile display for text and picture.

Many of tactile display had to be fabricated with special technique such as piezoelectric and solenoid actuation, which require specific material resulting in high cost, high technology, and difficult in maintenance. Therefore, the simple technique of tactile dot rising have to be invented to deliver the better solutions but still remain the performance of the touch sensation. Base on this requirement, if a lot tactile devices can be produced as commercial, the RBDS will be manufactured with the lower unit cost and delivered reasonable market price. To attain these requirements, X-ray LIGA technology which was applied from commercial IC technology is proposed to high-aspect-ratio microstructure and suggested to mass-produce micro-components at a low-cost production.

This thesis concentrates on realization of tactile dots for RBDS utilizing X-ray LIGA process which is performed at the beamline BL-6 of the Synchrotron Light Research Institute (Public Organization), Ministry of Science and Technology, Thailand. Two specific tactile display mechanisms were formulated regarding the design of X-ray LIGA based on the pneumatic RBDS. The first mechanism that the tactile display can actively raise the tangible dot up with a thin PDMS membrane had been evaluated through the strength of suspended PDMS membrane on the X-ray LIGA structure. PDMS tactile display suspended by using SU-8 sacrificial material proposed the best suspended solution including the restoring force, the load-deflection characteristics and estimated mathematic models under the applied pressure. However, some disadvantages such as non-obvious sensation, dirty easily, and not durable under the excessive applied pressure, made it difficult to improve for the refreshable tactile display. The second mechanism that the single tactile dot can perform similar to the conventional tangible dot had been considered through a complicated X-ray LIGA structure. The tactile dot as a piston inside a cylinder had been successfully fabricated, resulting in the robust and obvious perception under the applied pressure. Nevertheless, the moving part without any repeated mechanism was a serious problem to apply it into the refreshable tactile display.

Consequently, the refreshable tactile display improved from two mechanisms was realized by combining them together for the first X-ray LIGA tactile display. The tactile dot was placed on the suspended PDMS membrane to create the spring element. It can operate as the rigid tactile display with the maximum applied pressure of 16.87 kPa resulting in the actuated force of 76.71 gf. Furthermore, the second X-ray LIGA tactile display was improved by adding two curved segments of metal under the tactile dot. These curved members act as the spring mechanism that hold the tactile dot inside the tactile panel and get back flat surface. It was operated as the refreshable tactile display with the maximum load of 10 g required the applied pressure of 109.48 kPa.

To increase the performance of the refreshable tactile display systems, the curled-up closure plate microvalve was combined instead of the conventional valve to attain the convenient RBDS of the blind community. The microvalve was positioned under the tactile display with PDMS spring element and controlled by high dc voltage. In the repeat operation as the RBDS, the tactile dot can be move upward and downward at the actuated voltage of 150 V with maximum distance of 120 μm and 42.98 kPa applied pressure. The tactile dot was not absolutely flattened with the remained deflection of 365 μm cause by the leakage between the closure plate and the conductive substrate of microvalve. However, this innovation was demonstrated the possibility to bring out a new system that invents tactile display device as a new interface for visually impaired people.

7.2 Future Studies

In the future, X-ray LIGA technology will be realized the mass-product of the tactile display into a Braille cell. Both of the tactile display with PDMS spring element and curved spring segments can be formed in a rectangular shape containing 3×2 dots as shown in Figure 7.1 (a). The tactile dot display can be actuated by using the conventional valve or assembled with the microvalve as shown in Figure 7.1 (b).

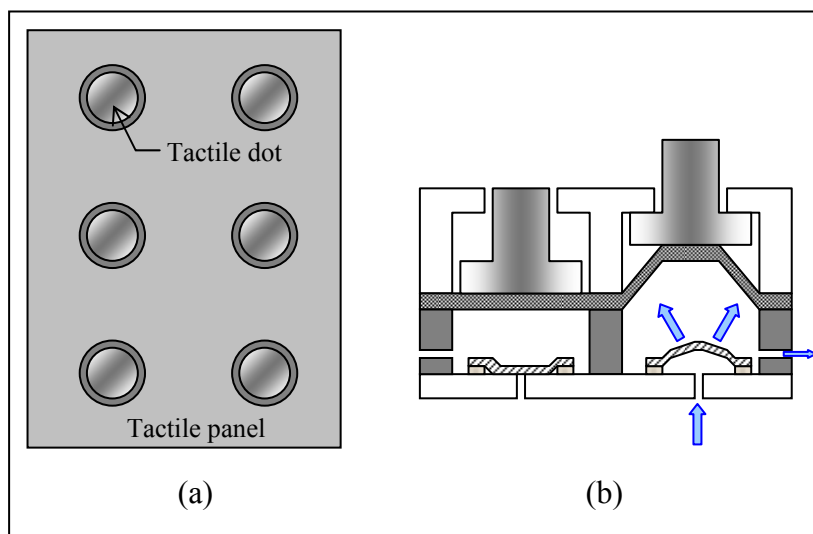


Figure 7.1 (a) Braille display by combining of 6 LIGA tactile dots and (b) the tactile display controlled by microvavle.

To supply the pneumatic pressure into the tactile display, the portable pneumatic supplier has to be invented to make the portable RBDS device. Figure 7.2 illustrates the schematic tactile display with the pressure supplier which consists of 2 sections. First, the pneumatic supply pressure box composes of an air pump, pressure tank, pressure sensor, and pressure controller. They are formed into an aluminum box and utilized to feed the applied pressure into the tactile display. The supply pressure is defined to provide the maximum pressure as 50 kPa and precisely controlled by a pressure regulator before apply through a solenoid valve that is switched by programming of a controller. The actuated pressure is always checked by a pressure sensor to protect the excessive applied pneumatic actuation.

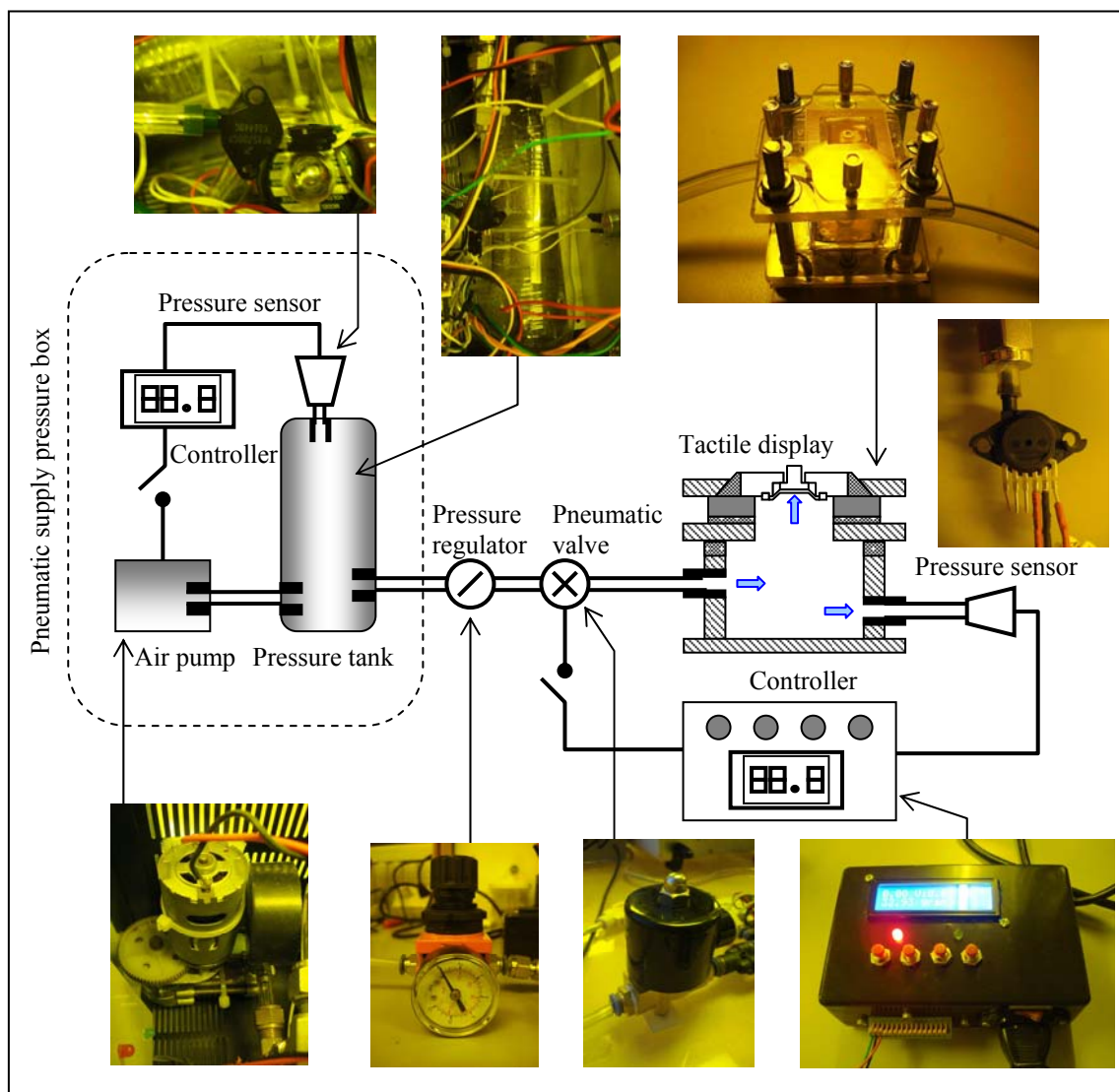


Figure 7.2 The schematic tactile display with the pressure supplier.

The tactile displays which are formed into the Braille cell will be controlled to display a Braille character by using a microcontroller as shown in Figure 7.3. Microcontroller such as AVR-ATMEGA168 which is combined in the Arduino single board microcontroller is programmed to classify Braille codes. Artificial neuron network is built in the microcontroller by using a weight $[w]$ and bias $[b]$ training in Braille code classification. Keyboard transmits inputs in ASCII codes which are converted into 8 bits binary for inputs $[p]$ of neuron network before classifying the Braille codes into 6 bits binary $[y]$. Outputs of microcontroller correspond with 6 dots of Braille characters that are

controlled by solenoid valve on each tactile dot. Drive circuit accepts output signal with logic voltage of 5 Vdc to be a supply voltage of photo-transistor (TLP521) as shown in Figure 7.4 (a). After the transistor is switched-on, a direct current from 12 Vdc supply voltage flows from pin #4 to #3, resulting in a supply voltage (V_{GS}) of a power MOSFET (IRFZ44N). Direct current I_{DS} can flows by connecting of pin D to pin S, and the solenoid valve is then turned on. The air pressure is fed through the valve into the RBDS and the tactile dot is raised up to display the Braille character.

In case of RBDS with microvalve, a drive circuit of microvalve corresponds with the input logic from microcontroller is illustrated in Figure 7.4 (b). High voltage solid state relay (LH1540) is used as a switch to support high voltage of power supply for microvalve actuation. The output signal activate pin #1 of the relay that allow a connection between pin #6 and #4. Therefore, high voltage can be applied to the upper electrode of microvalve while the bottom electrode is connected to ground in the drive circuit.

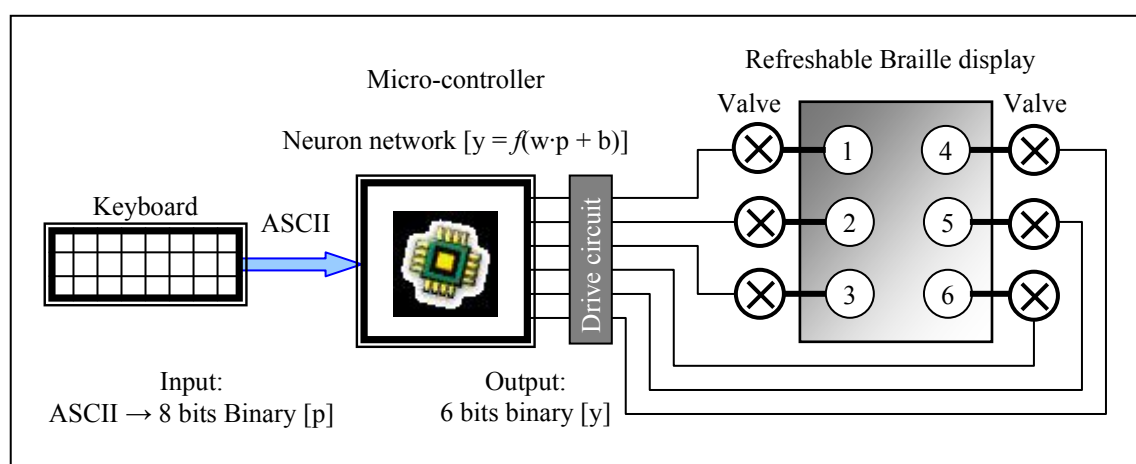


Figure 7.3 Braille display drive circuit with microcontroller.

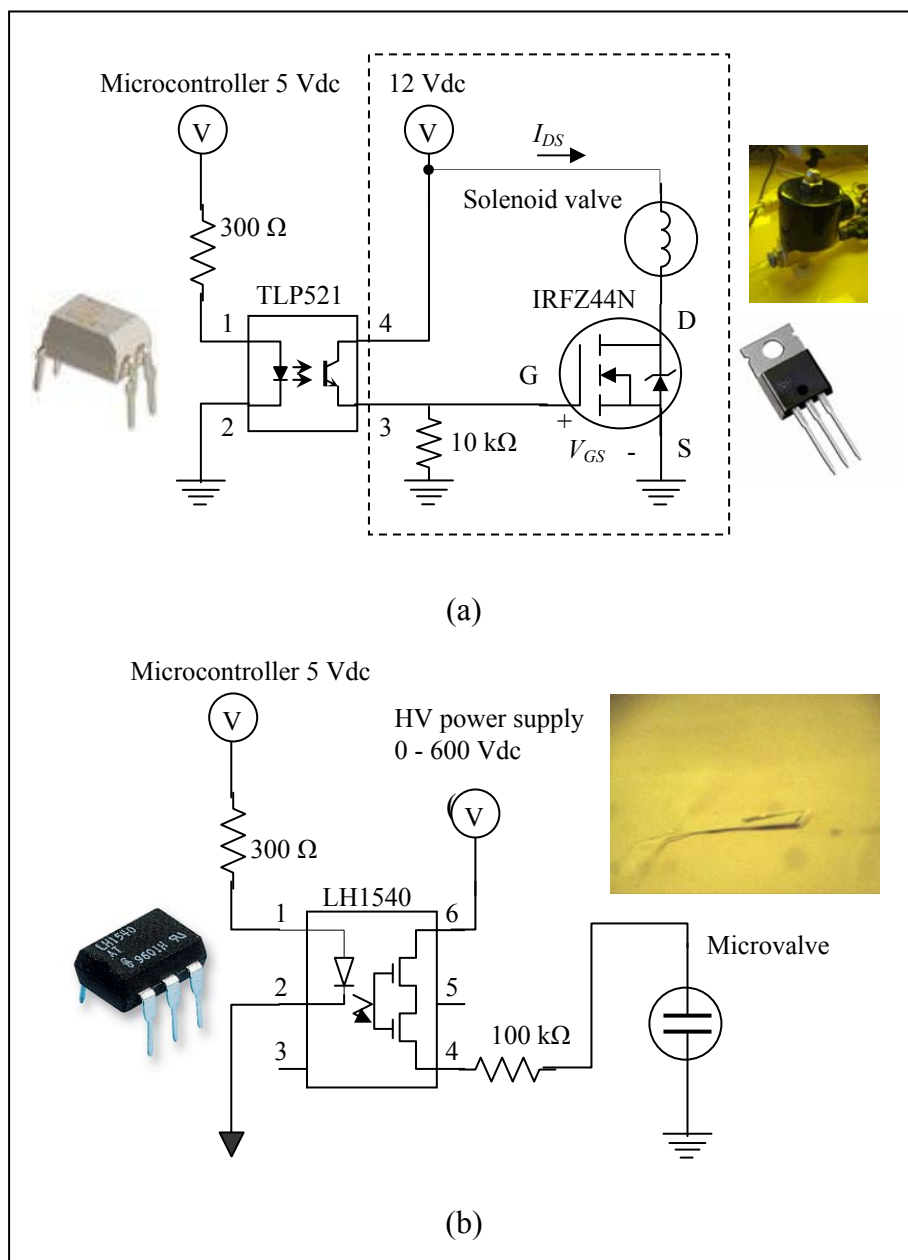


Figure 7.4 Drive circuits of (a) solenoid valve and (b) microvalve.

In addition, the microvalve can be improved to reduce the actuated voltage by using X-ray LIGA technology. As described in Chapter 4, the curled-up closure plate microvalve has a thin film of SU-8 membrane as the main closure plate structure that can be easily deflected away from the substrate under the applied pressure, resulting in the high voltage actuation. Increase the thickness with high aspect ratio microstructure as shown in Figure 7.3, the vertical deflection of the closure plate can resist the pressure load under the gap

entrance. The separation between electrodes is always small resulted in the high electrostatic forces which pull the closure plate down and close the inlet orifice. The actuated voltage is reduced by decreasing of spring stiffness with tetragonal square spiral structure. The gas flow through the microvalve can be adjusted and utilized in many applications.

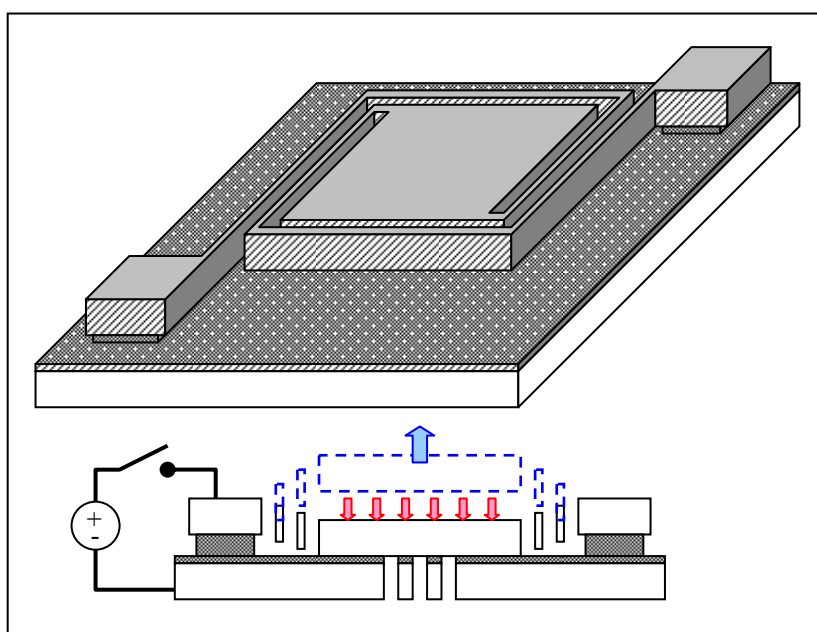


Figure 7.5 Vertical actuator for microvalve application.

REFERENCES

- Allen, A.J. (1986). Measurement of Mechanical Properties and Adhesion of Thin Polyimide Films. **M.S. Thesis**, Department of Chemical Engineering, Massachusetts Institute of Technology.
- Asamura, N., Yokoyama, N., and Shinoda, H. (1998). Selectively Stimulating Skin Receptors for Tactile Display. **IEEE computer Graphics and Applications**: 32-37.
- Batchelor, G.K. (2000). An introduction to fluid dynamics. **Cambridge University Press**.
- Beebe, D.J., Hymel, C.M., Kaczmarek, K.A., and Tyler, M.E. (1995). A Polyimide-on-silicon Electrostatic Fingertip Tactile Display. **Annual Conference of Engineering in Medicine and Biology Society**, vol. 2: 1545-1546.
- Bliss, J.C., Katcher, M.H., Roger, C.H., and Shepard, R.P. (1970). Optical-to-tactile image conversion for the blind. **IEEE Trans Man-Machine Syst.**, vol. MMS 11, no.1: 58-65.
- Block, H., and Kelly, J.P. (1988). Electrorheology. **J. Phys. D:Appl. Phys.** 21: 1661-1677.
- Charles, B., Yohannes, D., and Kevin, K. (2005). Ultra-deep x-ray lithography of densely packed SU-8 features: I. An SU-8 casting procedure to obtain uniform solvent content with accompanying experimental results. **J. Micromech. Microeng.** 15: 1242-1248.
- Chathirat, N., Songsiriritthigul, P., Klysubun, P., and Chomnawang, N. (2007). Powderization and Reflow-Casting of SU-8 Thick Photoresist for LIGA Fabrication. **Abstract at the ICMAT 2007**, Symposium N Synchrotron Radiation for Making and Measuring Materials. # N-13-OR42.
- Cho, H.C., Kim, B.S., Park, J.J., and Song, J.B. (2006). Development of a Braille Display using Piezoelectric Linear Motors. **SICE-ICASE International Joint Conference 2006**: 1917-1921.

- Cohen, X. (2003). An Innovative Approach to a Refreshable Braille Display. **Duke University Department of Electrical and Computer Engineering.**
- Deekla, P., Phatthanakun, R., Songsiriritthigul, P., Klysubun, P., and Chomnawang, N. (2009), Fabrication of High-Aspect-Ratio Complementary Micro Parts Based on Synchrotron X-ray Lithography and Release Etching of a Conformal Sacrificial Layer, **Proceedings of the International Conference on Science, Technology and Innovation for Sustainable Well-Being (STISWB 2009): 227-230.**
- Edmonds, B., Ernstberger, J., Ghosh, K., Malaugh, J., Nfodjo, D., Samyono, W., Xu, X., Dausch, D., Goodwin, S., and Smith, R. C. (2004). Electrostatic Operation and Curvature Modeling for a MEMS Flexible Film Actuator. **Statistical and Applied Mathematical Sciences Institute**, Technical Report#2004-4.
- Frick, J. (1993). Tactile graphic computer screen and input tablet for blind persons using an electrorheological fluid. **US Patent US5222895.**
- Friskin-Gibson, S.F., Bach-y-Rita, P., Tompkins, W.J., and Webster, J.G. (1987). A 64-solenoid, four level fingertip search display for the blind. **IEEE Trans. Biomed. Eng.**, vol. BME-34, no. 12: 963-965.
- Garner, H.D. (1996). Method and device for producing a tactile display using an electrorheological fluid. **US Patent US5496174.**
- Grosjean, C., Yang, X., and Tai, Y. C. (1999). A Practical Thermopneumatic Valve. **Proceedings of IEEE 12th International Micro Electro Mechanical Systems Conference: 147-152.**
- Gross, A.W. Ed. (1980). Fluid film lubrication, **Wiley**, New York.
- Haga, Y., Makishi, W., Iwami, K., Totsu, K., Nakamura, K., and Esashi, M. (2004). Dynamic Braille display using SMA coil actuator and magnetic latch. **Sensor and Actuator A 119: 316-322.**

- Haji-Babaer, J., Kwok, C.Y., and Huang, R.S. (1997). Inte-grable Active Microvalve with Surface Micro-machined Curled-Up Actuator. **Proceedings of the 12th International Conference on Solid-State Sensors and Actuators**: 833-836.
- Hamrock, B.J. (1991). Fundamental of fluid film lubrication, **NASA Reference Publication**, vol. 1255.
- Hillborg, H., and Gedde, U.W. (1999). Hydrophobicity changes in silicone rubbers, **IEEE Transactions on Dielectrics and Electrical Insulation**, vol.6, Issue 5: 703-717.
- Hopcroft, M.A. (2002). MAT-Test: A New Method for Thin-Film Materials Characterization, **MEng**, Cambridge University.
- Howe, R.D., Matsuoka, Y. (1999). Robotics for surgery. **Annual Review of Biomedical Engineering**, 01: 211-240.
- Jeong, O.C., and Konishi, S. (2005). Fabrication of all PDMS micro pump. **IEEE International Symposium on Micro-NanoMechatronics and Human Science**: 139-143.
- Jerman, H. (1991). Electrically-Activated, Normally-Closed Diaphragm Valves. **Proceedings of the 6th Inter-national Conference on Solid-State Sensors and Actuators**: 1045-1048.
- Johansson, R.S. (1978). Tactile Sensibility in the Human Hand: Receptive Field Characteristic of Mechanoreceptive Units in the Glabrous Skin Area. **J. Physiol.** **281**: 101-123.
- Kajimoto, H., Kawakami, N., Maeda, T., and Tachi, S. (2001). Electrocutaneous Display as an Interface to a Virtual Tactile World. **Proceeding of the Virtual Reality**: 289-290.
- Kato, Y., Sekitani, T., Takamiya, M., Doi, M., Asaka, K., Sakurai, T., and Someya, T. (2007). Sheet-type Braille displays by integrating organic field-effect transistors and polymeric actuators. **IEEE Trans. Electron Dev.** 54 (2): 202–209.

- Kim, K., Lee, J.B., Park, S., Manohara, H., Desta, Y., Murphy, M., and Ahn, C.H. (2002). Rapid replication of polymeric and metallic high aspect ratio microstructures using PDMS and LIGA technology. **Journal Microsystem Technologies**, vol. 9: 5-10.
- King, C.H., Culjat, M.O., Franco, M.L., Bisley, J.W., Dutson, E., and Grundfest, W.S. (2008). Optimization of a Pneumatic Balloon Tactile Display for Robot-Assisted Surgery Based on Human Perception. **IEEE Transactions on Biomedical Engineering**, vol. 55: 2593-2600.
- Kovach, M.W. (1985). Design considerations for the construction of a vibrotactile array. **M.Sc. Thesis Engineering**, The Ohio State University.
- Lee, A.P., Hamilton, J., and Trevino, J. (1996). A Low Power, Tight Seal, Polyimide Electrostatic Microvalve. **Proceedings of the 1996 ASME IMECE**, Atlanta, DSC V59, 345-349.
- Lee, J.S., and Lucyszyn, S. (2005). A Micromachined Refreshable Braille Cell. **Journal of Microelectromechanical Systems**: 673-682.
- Levesque, V., Pasquero, J., Hayward, V., and Legault, M. (2005). Display of virtual braille dots by lateral skin deformation: Feasibility study. **ACM Trans. on Applied Perception**, 2(2): 132-149.
- Levesque, V., Pasquero, J., and Hayward, V. (2007). Braille Display by Lateral Skin Deformation with the STReSS² Tactile Transducer. **Second Joint EuroHaptics Conference and Symposium on Haptic Interfaces for Virtual Environment and Teleoperator Systems (WHC'07)**: 115-120.
- Linville, J.G., and Bliss, J.C. (1966). A direct translation reading aid for the blind. **Proc. IEEE**, vol. 54, no.1: 40-52.
- Linville, J.G. (1969). Development progress on a microelectronic tactile facsimile reading aid for the blind. **IEEE Trans. Audio and Electroacoust.**, vol. AU-17, no.4: 271-274.

- Linville, J.G. (1986). Piezoelectric Polymer Transducer Arrays. **The sixth IEEE International Symposium on Applications of Ferroelectrics**: 506-510.
- Meckes, A., Bhrens, J., and Benecke, W. (1997). Electromagnetically Driven Microvalve Fabricated in Silicon. **Proceedings of the 12th International Conference on Solid-State Sensors and Actuators**: 821-824.
- Mokkapati, V.R.S.S., Piciu, O.M., Zhang, L., Mollinger, J., Bastemeijer, and J. Bossche, A. (2008). PDMS-Glass bonded Lab-on-a-chip device for Single Cell Analysis. **International Conference on Advanced Semiconductor Devices and Microsystems**: 211-214.
- Musolt, J., and Khol, P. (2003). Electrostatic actuator with intrinsic stress gradient. **United States Patent**, Patent No: 6,625,004 B1.
- Oh, K.W., Park, C., and Namkoong, K., (2005). A world-to chip microfluidic interconnection technology with dual functions of sample injection and sealing for a multichamber micro PCR chip. **Proc. IEEE MEMS 2005**.
- Osterberg, P.M. (1995). Electrostatically actuated microelectromechanical test structures for material property measurement. **Ph.D. Dissertation**, Mass. Instit. Tech., Cambridge, MA.
- Ostrom, N.P., Kaczmarek, K.A., and Beebe, D.J. (1999). A Microfabrication Electrocutaneous Tactile Display. **Proceeding of The First Joint BMES/EMBS Conference Serving Humanity, Advancing Technology**: 838.
- Pan, J., Lin, P., Maseeh, F., and Senturia, S. (1990). Verification of FEM Analysis of Load-Deflection Methods for Measuring Mechanical Properties of Thin Films. **IEEE Solid State Sensor and Actuator Workshop**: 70-73.
- Pappas, T.N., Tartter, V.C., Seward, A.G., Genzer, B., Gourgey, K., and Kretschmar, I. (2009). Perceptual Dimensions for a Dynamic Tactile Display. **Human Vision and**

Electronic Imaging XIV: 72400K-72400K-12.

- Pattanakul, R., Atiwongsangtong, N., Muanghlua, R., Titiroongruang, W., Niemchareon, S., and Chomnawang, N. (2006). Fabrication of a Curled-Up SU-8/Metal Closure Plate for Electrostatic Microvalve. **Proceedings of the 21st International Technical Conference on Circuits/Systems, Computers and Communications**, Vol.III: 485-488.
- Pasquero, J. (2003). STRESS: A Tactile Display Using Lateral Skin Stretch. **A Thesis of Master Degree of Engineering: 5.**
- Pasquero, J., and Hyward, V. (2003). STRESS: A practical tactile display with one millimeter spatial resolution and 700 Hz refresh rate. **In Proceedings of EuroHaptics 2003: 94–110.**
- Pelrine, R., Kornbluh, R., Pei, Q., and Joseph, J. (2000). High-speed electrically actuated elastomers with strain greater than 100%. **Science**, vol. 287, no. 5454: 836–839.
- Prince, T.S., Skebe, G.G., Lisy, F.J., and Schmidt, R.N. (2004). Refreshable Braille Display System with a Flexible Surface. **US Patent**, US6743021 B2.
- Rich, C.A., and Wise, K.D. (1999). An 8-bit Microflow Controller Using Pneumatically-Actuated Microvalves. **Proceedings of the IEEE 12th International Micro Electro Mechanical Systems Conference: 130-134.**
- Roberts, J., Slattery, O., and Kardos, D. (2000). Rotating-Wheel Braille Display for Continuous Refreshable Braille. **Society for Information Display '00 conference in Long Beach**, California, XXXI: 1130-1133.
- Shigley, J.E., Mischke, C.R., and Brown, T.H., (2004). Standard Handbook of Machine Design, 3rd ed., **McGraw-Hill**, New York, Chap. 16.
- Shinohara, M., Shimizu, Y., and Mochizuki, A. (1998). Three-dimensional tactile display for the blind. **IEEE Transactions on Rehabilitation Engineering: 249-256.**
- Shoji, S., Van der Schoot, V., de Rooij, N., and Esashi, M. (1991). Smallest Dead Volume Microvalves for Integrated Chemical Analyzing Systems, **Proceedings of the 6th**

International Conference on Solid-State Sensors and Actuators: 1052-1055.

Stoney, G.G. (1909). The tension of metallic films deposited by electrolysis, **Proc. R. Soc. Lond.** Ser. A 82: 172-175.

Strong, R.M., Troxel, D.E. (1970). An electrotactile display. , **IEEE Trans. Man-Machine Syst.**, vol. MMS 11, no. 1: 72-79.

Sutherland, N.B. (1972). Braille Display Device. **US Patent**, US3659354.

Taylor, P.M., Moser, A., and Creed, A. (1988). A sixty-four element tactile display using shape memory alloy wires. **Displays**, vol. 18: 163-168.

Taylor, P.M., Pollet, D.M., Hosseini-Sianaki, A., and Varley, C.J. (1998). Advances in an electrorheological fluid based tactile array. **Displays**, vol. 18: 135-141.

Teymoori, M.M., and Sani, E.A., (2005). Design and simulation of a novel electrostatic peristaltic micromachined pump for drug delivery applications. **Sensors and Actuators A** 117: 222–229.

Thompson, J.M. (1995). Braille Board with Movablr Dot Pins. **US Patent**, US5466154.

Timoshenko, S. (1925). Analysis of bi-metal thermostats, **Journal of the Optical Society of America**, 11: 233-255.

Tretiakoff, O., and Tretiakoff, A. (1977). Electromechanical transducer for relief display panel. **US Patent**, US4044350.

Vidal Verdú F., and Navas González, R. (2003). Thermopneumatic Actuator for Tactile Displays. **In Proceeding of CONFERENCE: XVIII Conference on Design of Circuits and Integrated Systems** DCIS'2003: 629-633.

Wagner, C.R., Lederman, S.J., and Howe, R.D. (2003). Design and Performance of a Tactile Shape Display Using RC Servomotor. **Haptics-e** (The Electronic Journal of Haptic Research), 3 (No. 4).

- Wanburee, W., Maturros, T., Lomas, T., Tuantranont, A., Atiwongsang-thong, N., Muanghlua, R., Titiroongruang, W., Niemcharoen, S., Songsiriritthigul, P., Klysubun, P., and Chomnawang, N. (2007). Alternative X-ray Mask Absorber for LIGA Applications, **International Conference on Materials for Advanced Technologies - ICMAT**, Singapore.
- Yang, P. (2004). Electroactive Polymer Actuator Braille cell and Braille Display. **International Application Publication Under The Patent Cooperation Treaty (PCT)**, Number WO 2004/077379 A2.
- Yobas, L., Durand D.M., Skebe, G.G., Lisy F.J., and Huff, M.A. (2003). A Novel Integrable Microvalve for Refreshable Braille Display System. **Journal of Microelectromec Syatems**, vol.12, no.3:pp.252-263.

APPENDIX A

FABRICATION PROCESSES OF CHAPTER III

Process sequences of X-ray mask with silver absorber on transparent membrane

This appendix contains the detailed process sequences used in fabrication of X-ray mask with silver absorber on transparent membrane in Chapter 3, Section 3.2.2.

1. Clean copper rings which have inner and outer diameter of 39 mm and 48.1 mm, respectively, by using the sand paper number 800, followed by washing with HCl 10%v, DI water, super sonic in DI water, DI water, and dry surface with nitrogen gas.

2. Bake the copper rings in an oven at 90°C for 1 hour, and cooled down naturally.

3. Fix copper rings on a transparent sheet by using epoxy (Epoxy Fixed[®]) mixed with ratio of 1 : 1, leaved at room temperature for 10 hours.

4. Separate fixed copper rings by a scissor and clean the transparent sheet by cotton soaked with IPA, wash the sample in DI water, dry with nitrogen gas, and baked in the oven at 70°C for 1 hour.

5. Deposit 500 Å Cr and 500 Å Ag plating base by using evaporation.

6. Spin-coat a layer of 40 µm thick AZ P4620 at 300 rpm for 5 seconds and ramp to 400 rpm for 30 seconds.

7. Soft-bake the sample suddenly in the oven at 90°C for 4.30 hours, and cooled down naturally on an insulator for 1 hour.

8. Expose UV light on AZ layer with 5460 mJ/cm² dose through mask.

9. Develop the sample in 4 g : 1 g : 200 ml KOH : H₃BO₃ : H₂O, wash the sample in DI water, and dry the sample with nitrogen gas.

10. Electroplate a 20 µm thick Ag with current density of 5 mA/cm², wash the sample in DI water without drying.

11. Electroplate a 0.5 µm thick Ni with current density of 5 mA/cm², wash the sample in DI water and dry the sample by nitrogen gas.

12. Remove AZ P4620 mold by acetone and wash the sample in DI water.

13. Remove seed layers of Ag and Ti with 10 : 1 NH₄OH : H₂O₂ and HF 5%v, respectively, rinses in DI water and dry with nitrogen gas

Process sequences of SU-8 powder preparation

This appendix contains the detailed process sequences used in preparation of SU-8 powder in Chapter 3, Section 3.3.1.

1. Clean aluminum disc with acetone, DI water, and dry with nitrogen gas, followed by baking in an oven at 90°C for 30 minutes.

2. Laminate a PI tape onto the disc and clean with IPA, DI water. Dry PI surface with nitrogen gas and bake in the oven at 90°C for 30 minutes.

3. Pour liquid SU-8 2100 onto the PI sheet for 6 grams and spread over the PI surface.

4. Soft-bake suddenly at 95°C on a hot plate for 5 hours, and cooled down naturally.

5. Peel PI sheet from aluminum disc to break dried SU-8 film into small chips.

6. Keep SU-8 powder into an opaque bottle and store in a desiccators.

Process sequences of SU-8 single layer reflow casting

This appendix contains the detailed process sequences used in fabrication of SU-8 single layer reflow casting in Chapter 3, Section 3.3.2.

1. Fix a PDMS square frame on a substrate with an aluminum clamp.

2. Load SU-8 powder into the frame with a weight that is calculated by Equation (3.2) based on the required thickness.

3. Place the aluminum clamp on a hot plate at 120°C located inside a vacuum chamber, turn-on vacuum pump and wait until the SU-8 powder totally melt without any gas bubbles.

4. Turn-off the vacuum pump and remove the aluminum clamp from the hot plate, cooled down to room temperature.

5. Remove the substrate with PDMS frame from the aluminum clamp and place the sample on the hot plate at 95°C for 10 minute for SU-8 reflowing, removed from the hot plate and cooled down naturally.

6. Remove PDMS frame and measure the excessive thickness.

7. Polish the excessive photoresist by using mechanical polishing on a sand paper number 800 with water lubricant.

8. Reflow the top surface of SU-8 by taking the top surface near a heater until its surface is totally transparent.

Process sequences of multilayer reflowed casting of SU-8 powder photoresist

This appendix contains the detailed process sequences used in fabrication of multilayer reflow casting in Chapter 3, Section 3.3.4.

1. Construct the first X-ray LIGA structure as described in Section 3.3.1 - 3.3.2, and calculate the volume of existing SU-8 microstructure V_{PRI} by Equation (3.3).

2. Calculate the total volume that need to fill for the second layer (V_2) by Equation (3.4), and then substitute into Equation (3.7) to estimate the SU-8 powder weight for layer 2 (W_2).

3. Reflow SU-8 powder as described in Section 3.3.2, followed by polishing to achieve the desired thickness.

4. Exposure X-ray irradiation on SU-8 thick film with suitable energy through X-ray mask of the second layer.

5. Develop the second structure in Nano SU-8 developer, and rinse the sample in IPA, and dry with nitrogen gas.

6. Hard-bake the SU-8 structure in an oven at 95°C for 3 hours and clean with oxygen plasma for 3 minutes at 200 W and 300 mTorr pressure.

7. Calculate the summation volume of SU-8 micro-structure of layer 1 and 2 (V_{PR2}) after development by Equation (3.8).

8. Calculate the total volume that need to fill for the third layer (V_3) by Equation (3.4), and then substitute into Equation (3.7) to estimate the SU-8 powder weight for layer 3 (W_3).

9. Reflow SU-8 powder as described in Section 3.3.2, followed by polishing to achieve the desired thickness.

10. Exposure X-ray irradiation on SU-8 thick film with suitable energy through X-ray mask of the third layer.

11. Develop the second structure in Nano SU-8 developer, and rinse the sample in IPA, and dry with nitrogen gas.

12. Hard-bake the SU-8 structure in an oven at 95°C for 3 hours and clean with oxygen plasma for 3 minutes at 200 W and 300 mTorr pressure.

Process sequences of PDMS-SU-8 wet bonding

This appendix contains the detailed process sequences used in wet bonding between PDMS and SU-8 in Chapter 3, Section 3.4.2.

1. Clean a glass substrate with IPA, acetone, IPA, DI water. Dry the surface with nitrogen gas and bake in an oven at 90°C for 30 minutes, cooled down naturally.
2. Spin-coat a layer of 3 μm thick AZ 1512 at 500 rpm for 5 seconds and ramp to 3000 rpm for 30 seconds.
3. Soft-bake the sample suddenly in the oven at 90°C for 30 minutes, and cooled down naturally on an insulator.
4. Spin-coat a layer of 16 μm thick PDMS at 500 rpm for 5 seconds and ramp to 6000 rpm for 30 seconds.
5. Place the SU-8 dot structure on the viscous PDMS and compress with a mass of 1 kg on a hot plate heated at 90°C for 3 hours, and cool down naturally.
6. Release the PDMS layer from substrate with acetone and rinse the sample with DI water. Dry PDMS with nitrogen gas and bake at 70°C in the oven for 30 minutes.

Fabrication sequences of micro-piston based on release etching of a conformal sacrificial layer

This appendix contains the detailed process sequences used in fabrication sequences of micro-piston based on release etching of a conformal sacrificial layer in Chapter 3, Section 3.5.

1. Place Ni master mold at the center of a PAMS square frame fixed on a glass substrate.

2. Mix PDMS polymer with the volume ratio of 10 : 1 and degassed in a vacuum chamber.
3. Spray silicone lubricants on the Ni master mold and gradually fill mixed PDMS by a pin until its level is rose up to the top of Ni mold.
4. Bake the PDMS on a hot plate at 90°C for 5 minutes and place suddenly on a cooled stainless plate, followed by spraying of silicone lubricants.
5. Cut around Ni mold in a square pattern and lift PDMS slowly by a pin.
6. Spin-coat a layer of 6 μm thick AZ 1512 on a conductive substrate with seed layer of Ti/Cu/Ti at 500 rpm for 5 seconds and ramp to 800 rpm for 30 seconds.
7. Place PDMS plate onto the coated substrate and fix PDMS plate and substrate together with PI tape.
8. Soft-bake on the hot plate at 90°C for 3 hours and cool down naturally.
9. Eliminate AZ thin film staying in PDMS molds by oxygen plasma at 200 W and 300 mTorr pressure until its surface all clear.
10. Seal around PDMS mold with mixed PDMS and bake on the hot plate at 90° for 5 minutes.
11. Electroplate nickel into PDMS mold to form a piston with slow ramping rate as described in Section 3.5.3.
12. Remove PDMS mold from the substrate with acetone and rinse the Ni structure with DI water, followed by cleaning the sample with oxygen plasma at 200 W and 300 mTorr pressure.
13. Reflow SU-8 powder to enclose Ni structure and polish to achieve smooth surface.
14. Expose X-ray irradiation through X-ray mask to create a SU-8 mold for a cylinder of piston.
15. Post expose-bake in the oven at 95°C for 30 minutes, followed by development of SU-8 mold. Rinse the sample with IPA and dry with nitrogen gas.

16. Electroplate a 10 μm thick silver that is conformally grown over the metal surface with current density 5 mA/cm^2 , followed by rinsing in DI water.

17. Electroplate nickel formed as a cylinder with current density as described in Section 3.5.3.

18. Polish the top surface of the sample until a silver ring is appeared.

19. Release piston from cylinder with chemical mixture of 3 : 1 NH_4OH : H_2O_2 .

20. Latch piston from cylinder with mechanical force and rinse the pair of micro parts with DI water. Dry naturally on tissue paper.

Fabrication sequences of X-ray LIGA application

This appendix contains the detailed process sequences used in fabrication sequences of X-ray LIGA application in Chapter 3, Section 3.6.

1. Fabricate three X-ray masks with silver absorber on transparent membrane as described in Section 3.2.2.

2. Construct 800 μm -thick SU-8 photoresist on glass substrates by using SU-8 single layer reflow casting as described in Section 3.3.2.

3. Exposure X-ray irradiation on SU-8 thick film with suitable energy through X-ray mask of each layer.

4. Develop the second structure in Nano SU-8 developer, and rinse the sample in IPA, and dry with nitrogen gas.

5. Hard-bake the SU-8 structure in an oven at 95°C for 3 hours and clean with oxygen plasma for 3 minutes at 200 W and 300 mTorr pressure.

6. Mix PDMS pre-polymer with volume ratio of 10 : 1 and degases in a vacuum chamber.

7. Spray silicone lubricants on the maser mold number 1 and fill PDMS by a pin gradually until its level is rose up to the top of Ni mold.
8. Cure the PDMS on a hot plate at 90°C for 5 minutes and place suddenly on a cools stainless plate, followed by spraying of silicone lubricants.
9. Remove PDMS plate by inserting of a pin under the polymer and slowly lift the edge of PDMS until it is removed totally.
10. Place PDMS mold on a conductive substrate coated with seed layers of Ti/Cu/Ti, seal around the mold with liquid PDMS and cure on the hot plate at 90°C for 5 minutes.
11. Etch Ti upper seed layer with HF 5%v and rinse in DI water.
12. Electroplate nickel into PDMS mold to form the first gear layer with slow ramping rate as described in Section 3.5.3.
13. Remove PDMS and clean the metal surface with oxygen plasma for 3 minutes at 200 W and 300 mTorr pressure.
14. Fill 500 μm thick SU-8 photoresist to enclose the gear by using the reflow casting.
15. Polish the sample to achieve the thickness 341 μm by mechanical polishing on a silicon carbine number 1200 and polished cloth with water lubricants.
16. Copy the pattern of the gear layer 2 by using PDMS molding as described in step 6-9.
17. Place PDMS mold number 2 on the first layer by aligning at the center of the first gear, and seal around the mold with liquid PDMS, cure on the hotplate at 90°C for 5 minutes.
18. Electroplate nickel into PDMS mold to form the second gear layer with slow ramping rate as described in Section 3.5.3. Always monitor the result to prevent over the excessive thickness.
19. Remove PDMS, SU-8 photoresist and clean the metal surface with oxygen plasma for 3 minutes at 200 W and 300 mTorr pressure.
20. Fill 500 μm thick SU-8 photoresist to enclose the gear by using the reflow casting.

21. Polish the sample to achieve the thickness 25 μm for the second layer by mechanical polishing on a silicon carbide number 1200 and polished cloth with water lubricants.

22. Copy the pattern of the gear layer 3 by using PDMS molding as described in step 6-9.

23. Place PDMS mold number 3 on the second layer by aligning at the center of the second gear, and seal around the mold with liquid PDMS, cure on the hotplate at 90°C for 5 minutes.

24. Electroplate nickel into PDMS mold to form the second gear layer with slow ramping rate as described in Section 3.5.3.

25. Remove PDMS, SU-8 photoresist and clean the metal surface with oxygen plasma for 3 minutes at 200 W and 300 mTorr pressure.

26. Polish the sample to achieve the thickness 861 μm for the third layer by mechanical polishing on a silicon carbide number 1200 and polished cloth with water lubricants.

27. Remove the photoresist in SU-8 developer and clean the metal surface with oxygen plasma for 3 minutes at 200 W and 300 mTorr pressure.

APPENDIX B

FABRICATION PROCESSES OF CHAPTER IV

Process sequences of the nickel substrate with a planarized orifice

This appendix contains the detailed process sequences used in fabrication of the nickel substrate with a planarized orifice in Chapter 4, Section 4.4.

1. Prepare epoxy based PCB with size of 1 inch \times 1 inch and drill a hole at the center with a diameter of 2.5 millimeters.
2. Clean copper surface with HCl 10%v and DI water, dry with nitrogen gas and bake at 90°C in an oven for 30 minutes.
3. Seal the top surface on copper side with PI tape and fill 10:1 mixed PDMS prepolymer on the back side, followed by baking at 90°C on a hotplate for 5 minutes.
4. Peel PI tape from copper side and deposit 500 Å Ti / 500 Å Cu / 500 Å Ti by evaporation.
5. Reflow SU-8 powder by casting on a hotplate at 120°C in a vacuum chamber, followed by polishing to desired thickness of 300 μm .
6. Expose X-ray irradiation through a negative X-ray mask for a square pattern of 70 μm \times 70 μm .
7. Post-exposure bake the sample in the oven at 95°C for 60 minutes, and cooled down naturally.
8. Develop the small pillar in Nano SU-8 developer, wash the sample in IPA and dry in nitrogen gas.
9. Remove topmost Ti layer of the plating base in mixed solution of 10 : 1 of NH_4OH : H_2O_2 and electroplate nickel to fill up the mold.
10. Polish the top surface with a silicon carbide number 1200 and cloth polish with water lubricants.

11. Remove PDMS from the sample and dry etch SU-8 mold by plasma in mixed gas of O₂/CF₄ 300 mTorr and 200 W RF power.

12. Fill sacrificial photoresist such as AZP4620 or SU-8 2100 on the back side and vacuum the material through the orifice from the front side.

13. Soft bake the sample in the oven at 90°C for 8 hours by placing the back side upward, and cooled down naturally.

14. Polish nickel surface to eliminate excessive photoresist around the orifice by the cloth polish with water lubricants.

Process sequences of the nickel substrate with a planarized orifice

This appendix contains the detailed process sequences used in fabrication of the nickel substrate with a planarized orifice in Chapter 4, Section 4.4.

1. Deposit 0.2 μm Al sacrificial layer by evaporation.
2. Spin-coat a layer of 3 μm thick AZ 1512 at 3000 rpm for 30 seconds and soft-bake the sample in an oven at 90°C for 15 minutes, cooled down naturally on an insulator.
3. Expose UV light on AZ layer with 116 mJ/cm² dose through mask for a rectangular pattern.
4. Develop the AZ protective layer with a mixed solution of 4 g : 1 g 200 ml of KOH : H₃BO₃ : H₂O₂, Al outside the protective layer is simultaneously etched in this wet etch at too, followed by rinsing the sample in DI water.
5. Remove AZ photoresist with acetone and rinse in DI water. Dry the sample with nitrogen gas and bake in the oven at 90°C for 15 minutes, cooled down naturally.
6. Spin-coat a layer of 2.3 μm thickness SU-8 2002 at 3000 rpm for 30 seconds.

7. Soft-bake photoresist layer in the oven at 90°C for 15 minutes and naturally cool the sample down on an insulator outside the oven.
8. Expose UV light on SU-8 2002 layer with 40 mJ/cm² dose through mask for photoresist closure plate structure.
9. Post-exposure bake the sample in the oven at 90°C for 15 minutes, cooled down naturally on the insulator.
10. Develop the closure plate pattern in Nano SU-8 developer, wash the sample in IPA and dry in nitrogen gas.
11. Hard-bake the photoresist in the oven at 90°C for 30 minutes and naturally cool down the sample.
12. Clean the sample in 100% oxygen plasma at 300 mTorr and 200 W RF power for 2 minutes.
13. Deposit 300 Å Ti / 500 Å Cu upper electrodes by evaporation.
14. Spin-coat a layer of 3 μm thick AZ 1512 at 3000 rpm for 30 seconds and soft-bake the sample in an oven at 90°C for 15 minutes, cooled down naturally on an insulator.
15. Expose UV light on AZ layer with 116 mJ/cm² dose through mask for a rectangular pattern.
16. Develop the AZ protective layer with a mixed solution of 4 g : 1 g 200 ml of KOH : H₃BO₃ : H₂O₂ rinse the sample in DI water and dry in nitrogen gas.
17. Hard-bake the photoresist in the oven at 90°C for 15 minutes and naturally cool down the sample.
18. Electroplate a 0.224 μm thick nickel in electroplating bath by biasing the sample with a current density of 3 mA/cm² for 5 minutes, gently rinse the sample in DI water.
19. Remove planarized material inside the orifice in acetone for AZ photoresist or Nano SU-8 developer for SU-8 and rinsed it in DI water.

20. Remove the Al sacrificial layer in the mixed solution of 4 g : 1 g 200 ml of KOH : H₃BO₃ : H₂O₂ rinse the sample in DI water, suddenly dip it in methanol for 5 minutes.

21. Dry the sample in nitrogen gas by blowing both of top and bottom side through the orifice.

APPENDIX C

FABRICATION PROCESSES OF CHAPTER V

Process sequences of the PDMS-PDMS/SU-8 plasma bonding

This appendix contains the detailed process sequences used in plasma bonding of PDMS-PDMS/SU-8 in Chapter 5, Section 5.2.1.1.

1. Construct SU-8 tactile panel with thickness of 800 μm by using X-ray lithography process.
2. Spin-coat 23 μm thick PDMS pre-polymer at 4000 rpm for 30 seconds, and bake the sample in the oven at 90°C for 30 minutes and cooled down naturally.
3. Prepare glass substrate with size of 1 inch \times 1 inch and spin-coat a layer of 3 μm thick AZ 1512 at 500 rpm for 5 seconds and ramp to 3000 rpm for 30 seconds.
4. Soft-bake the sample suddenly in the oven at 90°C for 30 minutes, and cooled down naturally on an insulator.
5. Spin-coat a layer of 16 μm thick PDMS at 500 rpm for 5 seconds and ramp to 6000 rpm for 30 seconds, and bake the sample in the oven at 90°C for 30 minutes and cooled down naturally.
6. Treat PDMS surface in 100% oxygen plasma at 300 mTorr and 200 W RF power for 1.30 minutes.
7. Fix their PDMS surface together and compress them with a mass of 1 kg weights on the hotplate, and heated for 3 hours at 90°C
8. Bake the sample at 90°C for 3 hours, cooled down naturally.
9. Remove AZ sacrificial in acetone, rinse the sample in DI water, and dry in nitrogen gas.

Process sequences of the PDMS-SU-8 wet bonding

This appendix contains the detailed process sequences used in wet bonding of PDMS-SU-8 in Chapter 5, Section 5.2.1.2.

1. Clean glass substrate with IPA, acetone, IPA and DI water.
2. Spin-coat a layer of 1.5 μm thick AZ 1512 at 3000 rpm for 30 seconds.
3. Soft-bake the sample on a hotplate at 90°C for 30 minutes, and cooled down naturally on an insulator.
4. Spin-coat a layer of 22 μm thick PDMS at 4000 rpm for 30 seconds.
5. Place a SU-8 tactile structure on the wet PDMS membrane, compress the sample with a mass of 1 kg weight for 3 hours.
6. Cure the PDMS layer on a hot plate at 90°C for 3 hours, and cooled down naturally.
7. Remove the mass and cut around the sample with a cutter.
8. Release the sample from the glass substrate by dipping in acetone and wash with DI water, follow by baking in an oven at 90°C for 1 hour and cooled down naturally.

Process sequences of the PDMS tactile display by using SU-8 sacrificial material

This appendix contains the detailed process sequences used in fabrication of PDMS tactile display by using SU-8 sacrificial material in Chapter 5, Section 5.2.1.3.

1. Construct the first SU-8 photoresist with thickness of 1000 μm on a PCB/Ti sacrificial layer by X-ray lithography process for a tactile panel with diameter of 1600 μm .

2. Construct the second SU-8 photoresist with thickness of 300 μm on a PCB/Ti sacrificial layer by X-ray lithography process for a tactile dot area with diameter of 300 μm .
3. Remove SU-8 structure of step 1-2 in HF 48%v, rinse in DI water and dry in nitrogen gas.
4. Reflow SU-8 powder inside the hole of the first SU-8 panel by heating on a hotplate in a vacuum chamber at 120°C for 45 minutes, remove the sample suddenly from the hotplate and cooled down naturally on an insulator.
5. Polish excessive SU-8 photoresist on the top surface by a polish cloth with water lubricants and dry in nitrogen gas.
6. Spin-coat 10 : 1 mixed PDMS pre-polymer of 16 μm thick at 6000 rpm for 30 seconds.
7. Bake the samples in the oven at 45°C for 5 hours, and cooled down naturally on an insulator.
8. Remove planarized SU-8 photoresist in Nano SU-8 developer, rinse the sample in IPA and dry PDMS surface in nitrogen gas.
9. Place the SU-8 tactile dot area at the center of the PDMS membrane fixing on the SU-8 tactile display and clamp with the testing holder.

Process sequences of the Assembled SU-8 tactile display

This appendix contains the detailed process sequences used in fabrication of assembled SU-8 tactile display in Chapter 5, Section 5.3.1.

1. Clean PCB substrate with HCl 10%v, and rinse in DI water.
2. Deposit 500 Å Ti for sacrificial layer by evaporation.

3. Construct the SU-8 thick film by the reflowed SU-8 powder at 120°C on a hotplate in a vacuum chamber.
4. Decrease the thickness to 300 μm by polishing with a sand paper number 1200, and heat on the top surface at 90°C to clarify the surface.
5. Expose X-ray irradiation on SU-8 thick layer through X-ray mask for a small orifice of a tactile panel and a large SU-8 pin.
6. Post-exposure bake the sample in an oven at 95°C for 1.45 hours, and cooled down naturally.
7. Develop the first patterns in Nano SU-8 developer, rinse the sample in IPA, and dry in nitrogen gas.
8. Clean the SU-8 structure by O₂ plasma at 200 mTorr and 200 W RF power for 3 minutes.
9. Construct the second SU-8 thick film the reflowed SU-8 powder at 120°C in the vacuum chamber.
10. Polish the top surface to reduce the total thickness to 1100 μm , and heat on the top surface at 90°C to clarify the surface.
11. Expose X-ray irradiation on SU-8 thick layer through X-ray mask for a large orifice of the tactile panel and a small SU-8 pin.
12. Post-exposure bake the sample in an oven at 95°C for 1.45 hours, and cooled down naturally.
13. Develop the second patterns in Nano SU-8 developer, rinse the sample in isopropanol, and dry with nitrogen gas.
14. Clean the SU-8 structure by O₂ plasma at 200 mTorr and 200 W RF power for 3 minutes.
15. Remove the SU-8 structure from the substrate by etching of Ti sacrificial layer in HF 30%v, wash the sample in DI water, and dry with nitrogen gas.

Process sequences of the SU-8 tactile display by releasing of sacrificial layer

This appendix contains the detailed process sequences used in fabrication of SU-8 tactile display by releasing of sacrificial layer in Chapter 5, Section 5.3.2.

1. Construct two layers of a dot structure on a graphite substrate by using X-ray lithography process. The first layer has a thickness about 300 μm and the other is 1000 μm .
2. Deposit chromium base layer at 200 W for 10 minutes follow by a thin layer of silver to cover all of structure surface at 200 W for 30 minutes using DC sputtering.
3. Redeposit silver to increase the thickness of the sacrificial layer to 50 μm through electroplating process.
4. Reflow SU-8 powder on a hotplate in a vacuum chamber to cover the overall structure.
5. Polish the top surface of the reflowed SU-8 by using a sand paper number 1200 until the appearance of silver area around the dot profile.
6. Expose X-ray irradiation on the thick SU-8 layer to create crosslink inside the substance, and soft-bake in the oven at 95°C for 1.45 hours.
7. Remove the graphite substrate by using the sand paper until the appearance of silver area.
8. Etch the silver sacrificial material in a wet etchant which is mixed between 2 parts of ammonium hydroxide (NH_4OH) and 1 part of Hydrogen peroxide (H_2O_2), result in releasing of the dot structure from the panel.
9. Decrease the thickness of the tactile panel by polishing on the top surface for 500 μm .
10. Re-insert the dot into the panel and place the work piece on testing holder.

Process sequences of the SU-8 refreshable tactile display with PDMS spring element

This appendix contains the detailed process sequences used in fabrication of the SU-8 refreshable tactile display with PDMS spring element in Chapter 5, Section 5.4.1.

1. Fabricate the suspended PDMS membrane with thickness of 16 μm by using SU-8 sacrificial material as described in Section 5.2.3.1.
2. Construct the assembled SU-8 tactile display as described in Section 5.3.1.
3. Change PDMS surface to hydrophobic state by exposing in 100% oxygen plasma at 200W for 1.30 minutes.
4. Paint SU-8 2002 photoresist on the center of suspended PDMS membrane by a pin.
5. Place the SU-8 tactile dot on the painted SU-8, bake in the oven at 70°C for 1 hour and cooled down naturally.
6. Cover the tactile dot with the tactile panel by using SU-8 2002 and bake in the oven at 70°C for 1 hour and cooled down naturally.

Process sequences of the SU-8 refreshable tactile display with curved spring segments

This appendix contains the detailed process sequences used in fabrication of the SU-8 refreshable tactile display with curved spring segments in Chapter 5, Section 5.4.2.

1. Deposit 1000 Å Ti sacrificial material on copper layer of 1 inch \times 1 inch epoxy PCB substrate by evaporation.
2. Fix around the edge of substrate with PI tape and pre-bake in the oven at 90°C for 30 minutes.

3. Spin-coat a layer AZ P4620 at 300 rpm for 5 seconds and ramp to 400 rpm for 30 seconds, remove edge bead by peeling of PI tape.
4. Soft-bake the sample suddenly in the oven at 90°C for 4.30 hours, and cooled down naturally on an insulator outside the oven for 1 hour.
5. Expose UV light on AZ layer with 5460 mJ/cm² dose through mask for spring curved segment mold.
6. Develop the sample in 4 g : 1 g : 200 ml KOH : H₃BO₃ : H₂O, wash the sample in DI water, and dry the sample with nitrogen gas.
7. Electroplate a 68 μm thick nickel in an electroplating bath at 30°C with current density of 5 mA/cm².
8. Remove AZ photoresist in acetone, rinse in DI water, and dry the sample in nitrogen gas.
9. Construct the assembled SU-8 tactile display on the metal mesh of curved spring and release them from the substrate as described in Section 5.3.1.
10. Insert the SU-8 tactile dot into the tactile panel and bond them together with epoxy glue, leave the sample for 3 hours.

APPENDIX D

PUBLICATIONS RELATED TO THE PhD RESEARCH

International Journal Papers

1. Mongpraneet, S., Wisitsora-at, A., Phatthanakun, R., Chomnawang, N., and Tuantranont, A. (2009). Low-cost x-ray mask based on micropattern sputtered lead film for x-ray lithography. **Journal of Vacuum Science and Technology B** 27(3): 1299-1303.

2. Wisitsoraat, A., Mongpraneet, S., Phatthanakun, R., Chomnawang, N., Phokharatkul, D., and Tuantranont, A. (2010). Low Cost and High Resolution X-ray Lithography Utilizing Lift-off Sputtered Lead Film Mask on Mylar Substrate. **Journal of Micromechanics and Microengineering**, (Accepted).

International Conference Papers

1. Phattanakun, R., Mapato, M., Wanburee, W., Promwikorn, S., Chathirat, N., Songsiriritthigul, P., Klysubun, P., and Chomnawang, N. (2007). Copier Transparency As A Transparent Support for X-ray Mask Absorber. **International Conference on Materials for Advanced Technologies 2007 (ICMAT 2007)**, Symposium N Synchrotron Radiation for Making and Measuring Materials: N-13-OR39.

2. Phattanakun, R., Songsiriritthigul, P., Klysubun, P., and Chomnawang, N. (2008). Multi-Step Powder Casting and X-ray Lithography of SU-8 Resist for Complicated 3D Microstructures. **International Conference on Electrical Engineering/Electronics, Computer, Telecommunications and Information Technology (ECTI-CON 2008)**: 805-808.

3. Deekla, P., Phatthanakun, R., Songsiriritthigul, P., Klysubun, P., and Chomnawang, N. (2009). Fabrication of High-Aspect-Ratio Complementary Micro Parts Based on Synchrotron X-ray Lithography and Release Etching of a Conformal Sacrificial Layer. **International Conference on Science, Technology and Innovation for Sustainable Well-Being**: 227-230.

Low-cost x-ray mask based on micropattern sputtered lead film for x-ray lithography

S. Mongpraneet and A. Wisitsora-at

Nanoelectronics and MEMS Laboratory, National Electronics and Computer Technology Center, 112 Thailand Science Park, Phahol Yothin Rd., Klong Luang, Pathumthani 12120, Thailand

R. Phatthanakun and N. Chomnawang

National Synchrotron Research Institution, Nakorn Ratchasima 30000, Thailand and Faculty of Engineering, Suranaree University of Technology, Nakorn Ratchasima 30000, Thailand

A. Tuantranont^{a)}

Nanoelectronics and MEMS Laboratory, National Electronics and Computer Technology Center, 112 Thailand Science Park, Phahol Yothin Rd., Klong Luang, Pathumthani 12120, Thailand

(Received 12 September 2008; accepted 16 March 2009; published 26 May 2009)

In this work, a low-cost x-ray micromask is developed by sputtering a lead (Pb) film on a Mylar sheet substrate through microshadow masks and the x-ray mask is experimented for patterning an SU-8 negative photoresist on a stainless steel substrate. In addition, the required Pb layer thickness as a function of SU-8 photoresist thickness is studied and compared to that of conventional gold x-ray mask. The Pb layer and SU-8 photoresist thicknesses are varied from 8 to 19 μm and from 150 to 350 μm , respectively. Sputtering is selected for Pb thick film deposition due to its high sputtering yield. The Pb mask is used for x-ray lithography of SU-8 photoresist with 125 μm wide microchannel patterns, designing for microfluidic chip fabrication. The x-ray source for x-ray lithography is produced by synchrotron radiation at Siam Photon Laboratory, Thailand. For 180 μm thick SU-8 photoresist, Pb film thickness of around 8 μm is required to block x ray at a dose of 4200 mJ/cm^2 . This is less than twice the thickness required for a gold absorbing layer, which is about 5 μm . A similar relationship is seen for different SU-8 photoresist thicknesses. In addition, a steep sidewall angle of $\sim 89.5^\circ$ for SU-8 microchannel pattern is obtained. The results demonstrate that the Pb based x-ray mask offers high lithographic quality at a very low cost. Therefore, it is highly promising for commercial applications. © 2009 American Vacuum Society.

[DOI: 10.1116/1.3117259]

I. INTRODUCTION

X-ray lithography is the patterning process that can produce high aspect ratio three-dimensional structures with nanometer-scale resolution. It is one of the most critical processes of the lithographie-galvanoformung-abformung (LIGA) system, which has been developed for fabrication of advanced microelectromechanical system devices.¹⁻³ Microstructure products including gear wheel systems, microfluidic devices (pumps, valves), as well as microreactor systems have been successfully fabricated by x-ray LIGA method in laboratories. Despite its remarkable features, x-ray lithography has not been widely used for commercial applications due to high x-ray mask production cost and expensive x-ray source that requires synchrotron radiation.

In order to produce appropriate masks for the deep x-ray lithography step, several fabrication strategies can be employed.⁴ Functional and economic constraints determine the fabrication scheme. In principle, three different fabrication methods can be applied to produce the final LIGA mask. High accuracy can be achieved by using a soft x-ray lithography step through intermediate masks. The manufacturing

of the intermediate mask, which differs from the LIGA mask only by the height of the absorber and the mask membrane material, may be performed in two different ways: patterning by means of photolithography via a chromium mask or by direct electron beam lithography.⁵ For these x-ray masks, several-micron-thick gold (Au) x-ray absorbing layer is normally deposited on x-ray transparent substrates including silicon dioxide/nitride thin membrane on silicon, graphite, and polymer sheets. The deposition of a thick gold layer by electroplating, sputtering, or evaporation is currently very expensive.

For low-cost applications such as microfluidic chips, x-ray mask may be fabricated directly from conventional photolithographic mask and gold masking layer should be replaced with low-cost materials.⁶ Tungsten (W) and tantalum (Ta) have been proposed as alternative lower cost x-ray absorbing materials. However, they are still not practical because it is difficult and costly to deposit thick film of these refractory metals. Sn/Pb alloy thick film prepared by electroplating was reported as a very low-cost x-ray mask. However, the required thickness of Sn/Pb alloy at a given x-ray dose is about three to four times higher than the required thickness for gold.⁷ Very thick x-ray masking layer is undesirable because it would reduce lateral resolution of x-ray lithography. Thus, the proposed low-cost mask may not be

^{a)}Author to whom correspondence should be addressed; electronic mail: adisorn.tuantranont@necotec.or.th

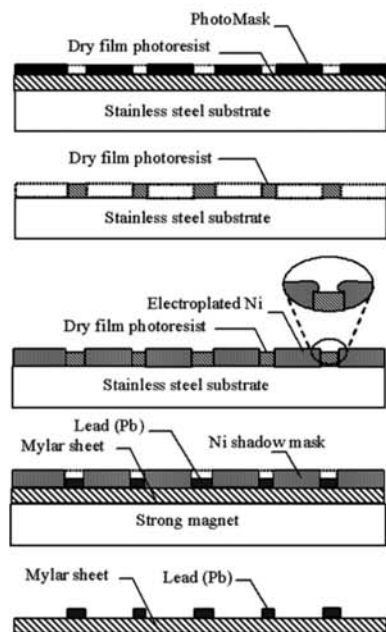


FIG. 1. Fabrication process for x-ray mask Pb patterned layer on polymer sheet via sputtering through electroplated Ni microshadow mask.

suitable for a variety of applications. In this work, pure lead (Pb) film is utilized as a novel low-cost x-ray absorbing material and low-cost fabrication of x-ray mask is developed by sputtering on a Mylar sheet substrate through an electroplated microshadow mask. The x-ray mask is utilized for patterning an SU-8 negative photoresist on a stainless steel substrate.

II. X-RAY MASK FABRICATION

The process diagram for x-ray mask fabrication is shown in Fig. 1. The process consists of two main parts, electroplating of Ni microshadow mask and pattern transfer onto polymer substrate. In the first part, the substrate for electroplating was a 2 mm thick stainless steel plate. First, a 38 μm thick dry photoresist film was laminated on the cleaned stainless steel plate by a commercial rolling-laminating machine at 80 $^{\circ}\text{C}$. It should be noted that dry photoresist film was chosen instead of wet photoresist because of its suitable thickness and low cost. Conventional photolithography was then performed to obtain desired patterns of photoresist on the substrate. In the photolithographic process, the photoresist-coated plate was exposed under 360 nm ultraviolet (UV) light from a 300 W UV source for ~ 3 s. The photolithographic mask was a thin sheet of dark film produced by a commercial pattern generator system. The pattern was a microfluidic channel system for a polymerase chain reaction device that consisted of 125 μm wide microchannels, sample mixing T junction, three reaction chambers, and input/output ports. After exposure, the photoresist was developed for 90–120 s. Next, the patterned substrate was surface

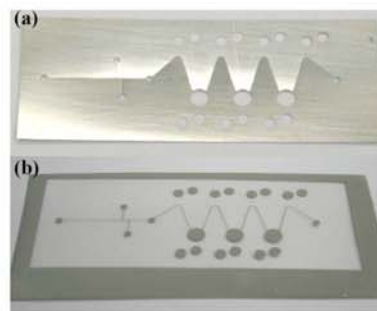


FIG. 2. (Color online) Photograph of (a) electroplated Ni microshadow mask and (b) Pb patterned layer on Mylar sheet as x-ray mask with microfluidic pattern.

treated by immersion in 20% potassium dichromate ($\text{K}_2\text{Cr}_2\text{O}_7$) aqueous solution for 3–5 min to form a very thin layer of chromium oxide on the stainless steel surface. It was necessary to form the oxide to facilitate detachment of electroplated Ni structure from the stainless steel substrate. Ni-electroplating process was then performed. In the electroplating process, the substrate (cathode) was biased at a negative potential relative to counterelectrode in nickel sulfate plating solution. The electroplating was conducted at constant current varying from 1 to 4 mA/cm^2 for ~ 4 h. Finally, the electroplated Ni microstructures are detached from the substrate by simple peeling off method. The thickness of the plated Ni film was measured to be ~ 43 μm by a white light interferometer (Polytech Inc.). It should be noted that the nickel micromask was made with overhang structure via overplating technique to reduce sidewall deposition during subsequent sputtering. As nickel was electroplated over the dry film photoresist, it grew horizontally to form an overhang structure as shown in the magnified drawing of Fig. 1. The photograph of electroplated Ni microshadow mask is shown in Fig. 2(a).

The microelectroplated structure was then used as template for pattern transfer on polymeric substrates via sputtering through shadow masking. The shadow mask was put in front of polymeric substrate (50 μm thick Mylar sheet) and strong magnets were then placed behind to attract the microelectroplated Ni templates to the substrates. The magnet was very important for pattern transfer from microelectroplated structures because the transfer of micron-scale patterns required an intimate contact between the substrates and the mask templates. The assembled structures were then loaded into a magnetron sputtering system. After a base vacuum environment of $\sim 3 \times 10^{-6}$ mbar, the substrates were cleaned by radio frequency (rf) plasma at an argon pressure of $\sim 3 \times 10^{-3}$ mbar. This cleaning was to improve adhesion of the film to the substrates by removing moisture and any organic contaminants on the surface. The 50 nm thick chromium film was then deposited by dc sputtering at room temperature under an argon pressure of $\sim 3 \times 10^{-3}$ mbar. The thin Cr layer was used as an adhesive layer between Pb film and polymer (Mylar) substrate. Pb layer was sputtered on the Cr

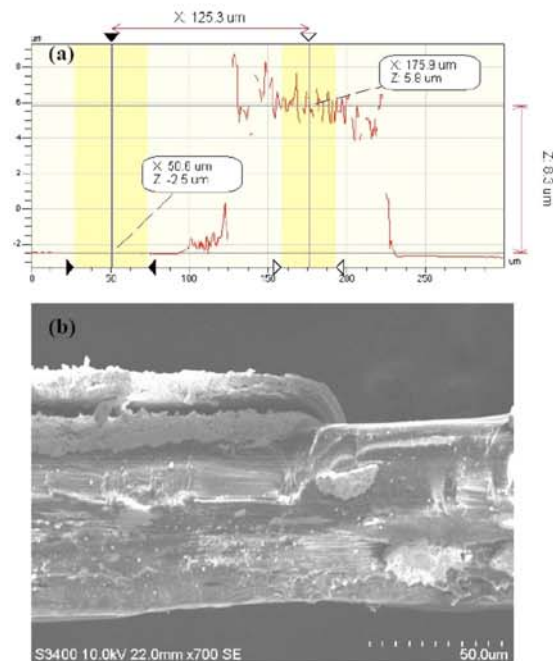


FIG. 3. (Color online) Cross-sectional (a) interferometric image and (b) scanning electron micrograph of Pb patterned layer on Mylar sheet as x-ray mask.

layer with varying thicknesses from 7 to 19 μm . Sputtering is a suitable process for Pb thick film deposition due to its high sputtering yield. To sputter a Pb thick film on a polymeric substrate, continuous sputtering time is limited to 10 min at a time and sputtering was paused for 5 min before resuming another sputtering to prevent the polymeric substrate from overheating. The sputtering cycle was repeated until desired thickness was achieved.

A typical photograph of Pb patterns on a Mylar sheet is shown in Fig. 2(b). The average linewidth of patterns was measured to be $\sim 125 \mu\text{m}$ by the interferometer. The detailed structure and dimension of the Pb layer on the Mylar sheet were measured by the white light interferometer. The cross-sectional interferometric image and scanning electron micrograph of Pb microchannel pattern is demonstrated in Figs. 3(a) and 3(b), respectively. In this case, the thickness of the Pb layer and the width of the microchannel pattern are determined to be ~ 8.3 and $\sim 125.3 \mu\text{m}$, respectively. From the interferometric image [Fig. 3(a)], it can be seen that the Pb pattern has a steep sidewall angle of $\sim 86^\circ$ and surface roughness of $\sim 1.8 \mu\text{m}$. However, the scanning electron microscopy (SEM) image [Fig. 3(b)] shows that the edge of the film is slightly round with the actual sidewall angle of $\sim 75^\circ$. The discrepancy between the two types of measurements is expected and acceptable. SEM image is considered more precise in terms of sidewall topography while interferometry can provide quantitatively accurate film thickness and surface roughness. The result demonstrates that a high sidewall

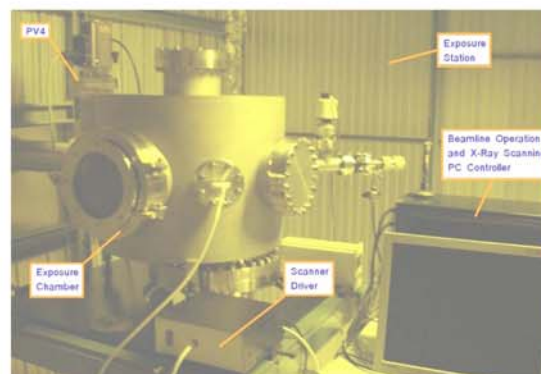


FIG. 4. (Color online) Photograph of x-ray lithographic system.

angle of 75° can be achieved by sputtering through a microshadow mask with overhang structure. The sidewall quality is satisfactory for typical x-ray lithography applications. The total sputtering time for this case is only 50 min, yielding a high deposition rate of $0.17 \mu\text{m}/\text{min}$. The main advantages of shadow masking scheme are good pattern quality, low cost, and cleanliness because it requires no wet etching process. In addition, it is suitable for mass production with physical vapor deposition techniques. However, it also has some limitations. For example, it cannot be used to form a pattern with unconnected islands and lateral resolution is limited to around a few tens of microns.

III. X-RAY LITHOGRAPHY

X-ray lithography was performed on SU-8 negative photoresist from MicroChem Co., Ltd. Before spin coating, a 2.5 mm thick, 3 in. circular stainless steel substrate was ground and precleaned by oxygen plasma treatment at 35 W rf power for 10 min. The SU-8 No. 2100 photoresist was pre-spun at 500 rpm for 5 s and then spun at different speeds from 1000 to 6000 rpm for 30 s. Next, the SU-8 film was prebaked on a hot plate at 60, 70, and 80 $^\circ\text{C}$ for 5 min at each temperature and then soft baked at 95 $^\circ\text{C}$ for 30 min, respectively. The multistep baking process was developed to minimize stress in the photoresist layer on the stainless steel substrate. After slowly cooling down to room temperature, the Pb based x-ray mask was attached in front of the SU-8 photoresist and inserted into the x-ray lithographic system of National Synchrotron Research Center (Thailand), as shown in Fig. 4. The system was a high vacuum chamber with one port connected to a hard x-ray beamline of synchrotron storage ring. The x-ray beam with 3 mm diameter was scanned over a defined area on the substrate by a motorized stage. The photoresist was exposed under x ray for different doses at a vacuum of 10^{-5} Torr. During exposure, the x-ray beam with energy density of 4000–5000 mJ/cm^2 was produced at storage ring current of 65–85 mA. The sample was then postbaked at 95 $^\circ\text{C}$ for 30 min, slowly cooled down, and

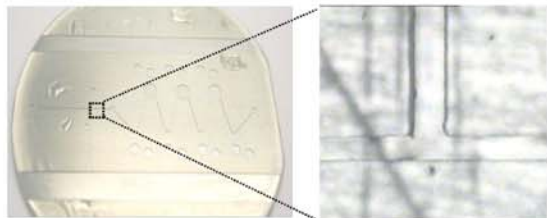


FIG. 5. (Color online) Photograph of SU-8 pattern of microfluidic channel on stainless steel substrate.

remained at room temperature for 1 h to release stress due to x-ray exposure. Finally, it was developed in SU-8 developer for ~ 30 min.

Figure 5 shows a typical photograph of an SU-8 pattern of a microfluidic channel on a stainless steel substrate. The detailed structure and dimension of the SU-8 microchannel have been measured by the white light interferometer. The three-dimensional and cross-sectional interferometric images of the T junction of the SU-8 pattern are demonstrated in Fig. 6. In this case, the thickness of the SU-8 layer, which was spun at 3000 rpm, and the width of the microchannel pattern are estimated to be ~ 180 and ~ 125 μm , respectively. In addition, it can be seen that the microchannel has a very steep sidewall with an angle of $\sim 89.5^\circ$. The result confirms the effectiveness of the low-cost Pb based x-ray mask. It has been found from a set of experiments that the lead film thickness of ~ 8 μm is required to block the x ray for 180 μm thick SU-8 photoresist that requires x-ray dose of 4200 mJ/cm^2 produced at a beam line current of 70 mA. The required thicknesses of the Pb layer for masking x ray at different SU8 thicknesses have been measured from a series of x-ray lithography experiments and the results are shown in Fig. 7. The required thicknesses of Au layer have also been measured for comparison. It can be seen that the required thicknesses of both x-ray absorber increase linearly with SU-8 thickness and the required thickness for Pb layer is approximately 1.6 times that for Au layer. Although Pb re-

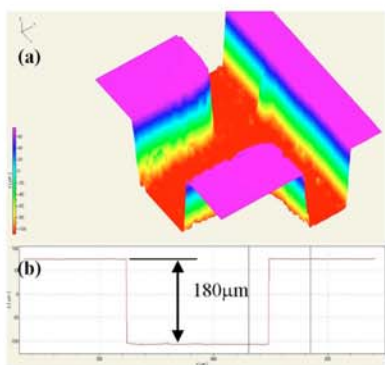


FIG. 6. (Color online) (a) Three-dimensional and (b) cross-sectional interferometric images of Pb patterned layer on Mylar sheet as x-ray mask.

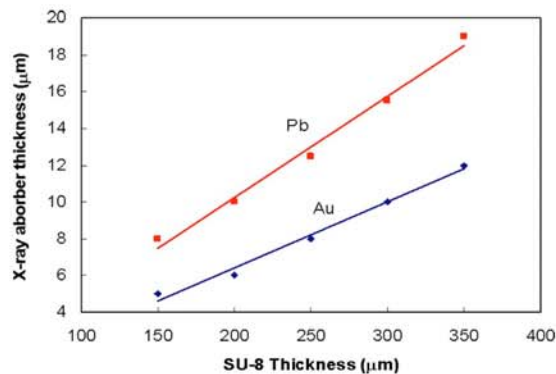


FIG. 7. (Color online) Relationship between required thickness of x-ray absorber (Pb and Au) thickness and SU-8 photoresist thickness.

quires 1.6 times more thickness than gold does, the proposed Pb based x-ray mask is more practical for commercial applications than gold x-ray mask due to the much lower material cost (Pb is about 10 000 times cheaper than Au). Although Pb may be considered a toxic material, it should not be a problem for x-ray lithography because the process is mostly conducted in vacuum environment.

IV. CONCLUSION

In conclusion, a low-cost x-ray micromask has been developed by sputtering a lead (Pb) film on a Mylar sheet substrate through Ni-electroplated microshadow masks. Sputtering is found to be a suitable process for Pb thick film deposition due to its high sputtering yield. The time required to sputter a thick Pb film is relatively short compared to other deposition processes. The lead mask has been used for x-ray lithography on the SU-8 layer by synchrotron radiation at Siam Photon Laboratory. The tested pattern is a 125 μm wide microchannel, which has been designed for microfluidic chip fabrication. At a given SU-8 photoresist thickness, it is found that the required lead film thickness to sufficiently block the x ray is only less than twice the required thickness for the corresponding gold mask. Therefore, the proposed Pb based x-ray mask is much more practical for commercial applications than gold x-ray mask because the required thickness is not significantly higher while material cost is much lower. Moreover, the process can be extended to obtain micrometer or submicrometer resolution by replacing microshadow masking with lift-off process and multistep pattern transfer.

ACKNOWLEDGMENTS

The authors would like to acknowledge the National Synchrotron Research Center (Thailand) for the use of the x ray from synchrotron radiation. This work has been funded by the National Electronics and Computer Technology Center under the Lab-on-a-Chip Development project.

1303 Monpraneet *et al.*: Low-cost x-ray mask based on micropattern sputtered lead film

1303

- ¹S. Cabrini, M. Gentili, and L. Mastrogiacomo, *Microelectron. Eng.* **53**, 599 (2000).
²Scott Hector, *Microelectron. Eng.* **41–42**, 25 (1998).
³A. L. Bogdanov and S. S. Peredkov, *Microelectron. Eng.* **53**, 493 (2000).
⁴W.-P. Shih, Y. Cheng, and G.-J. Hwang, *Microelectron. Eng.* **40**, 43 (1998).
⁵A. Schmidt, G. Himmelsbach, and H. Wolf, *Microelectron. Eng.* **57–58**, 761 (2001).
⁶B. Y. Shew, Y. Cheng, W. P. Shih, M. Lu, and W. H. Lee, *Microsyst. Technol.* **4**, 66 (1998).
⁷H. I. Smith, *Microelectron. Eng.* **53**, 77 (2000).

BIOGRAPHY

Rungureang Phatthanakun was born in Nakorn Ratchasima, Thailand, in 1981. He graduated from junior high education from Wanglang Witthayakhom School and high school level from the Benchama Rat Rangsarit Cha Choeng Sao School. He graduated with the Bachelor Degree of Engineering in Electrical Engineering in 2003 from Suranaree University of Technology, Nakorn Ratchasima, Thailand. He attended graduate program at the same institute and received a Master Degree in Electrical Engineering in 2006. With financial support from the Synchrotron Light Research Institute (Public Organization), he is currently working toward the Ph.D. degree in the School of Electrical Engineering, Institute of Engineering, Suranaree University of Technology. His research interests include X-ray LIGA application, MEMS fabrication and simulation.